

WUAV: Wooden Urban Air Mobility Vehicle

AE3200 Design & Synthesis Exercise

Group 16

Delft University of Technology



This page is intentionally left blank.

WUAV: Wooden Urban Air Mobility Vehicle

by

Group 16

Student Name	Student Number	Abbreviation
Jesse del Canho	5100380	JC
Ivor Cecelja	5484359	IC
Marc van Egmond	5499488	ME
Hubert Hakk	5283493	HH
Elisa Lazzaroli	5519640	EL
Maxim Michielsen	5233356	MM
Tsveta Radoslavova	5580897	TR
Alfonso de Rato Pueyo	5481104	AR
Filip Skrobisz	5226961	FS
Max Wilbrink	5450918	MW

Version: 2.0
Tutor: Baris Kumru
Coaches: Floyd van Steen & Sabin Anton
Teaching assistant: Igor Pszczółkowski
Institution: Delft University of Technology
Place: Faculty of Aerospace Engineering, Delft
Project Duration: 22 April 2024 - 28 June 2024

Cover image: the HAROLD, 3D render

Acknowledgements

Group 16 would like to thank all the people who helped complete this project. First of all, we would like to extend our thanks to Dr. Baris Kumru who suggested this project, and without whom this would not have been possible. His expertise in the realm of material science and his consistency helped us reach the finish line. We would also like to thank Sabin-Viorel Anton and Floyd van Steen for their tireless and consistent feedback on our work. They were always there to answer our questions and to provide a helpful hand throughout the project, and for that we are grateful. In addition, we would like to thank Dr. Julie J.E. Teuwen for her advice concerning the use of thermoplastic composites and other materials in aircraft structures. Furthermore, we would like to thank Ir. Jos Sinke for his insight on manufacturing methods and the manufacturing-cost estimation. We would also like to thank Dr. Calvin Rans for helping us approach the superposition of loads and stresses in 3D structures. Finally, we extend our gratitude to Dr. Marilena D. Pavel and Dr. ir. Leo L.M. Veldhuis, whose insight into propeller design for VTOLs proved crucial.

We would also like to thank the companies who gave us quotes, as well as all the industry professionals who advised us when it came to specifics outside our expertise. Finally, we would like to thank our friends, families, and loved ones. It was your encouragement that kept us going throughout these ten weeks.

*Group 16
Delft, June 2024*

Executive Overview

With the increasingly competitive market for personal commuter air travel, the private eVTOL (electric vertical takeoff and landing) aircraft sector is only just spreading its wings and is expected to reach great heights in the coming decade. The anticipated economic growth in this area presents opportunities for many small aircraft manufacturers to compete for their share in the rapidly expanding market.

The future of transportation will be shaped by energy-efficient and sustainable vehicles that allow people to travel conveniently while supporting a healthier living environment. The WUAV project aims to develop an environmentally sustainable eVTOL aircraft for urban and inter-city passenger transport. This project's eVTOL aircraft - **HAROLD** (Hovering Aerial paRtially woOden Lift-off Device) - seeks to achieve higher levels of environmental sustainability than its competitors by utilising wood as well as electricity generated from green hydrogen, thereby reducing the environmental impact of future flying personal travel. This initiative addresses the growing demand for sustainable urban air mobility and explores the advantages of using wood as a primary structural material.

The Market Gap

According to McKinsey, the eVTOL market is projected to reach \$1.1 billion¹, with annual revenue for an advanced air mobility (AAM) operator expected to grow to \$23.21 billion by 2028². The expected market growth in the observed sector in the United States is expected to increase as shown in Figure 1

The analysis also revealed a market gap in regional air travel for more than four passengers. At the time of the research, most electric air vehicles under development are designed for short distances of up to 100 km, accommodating two to four passengers, with numerous manufacturers focusing on this market segment [1]. The **HAROLD** aims to address the underserved market for regional air travel with a capacity of up to six passengers.

Furthermore, the WUAV **HAROLD** is designed to be cost-competitive in the current market. It is projected to cost customers a maximum of \$2.5 million. In contrast, according to independent analysts, some of the **HAROLD**'s in the 6-7 seater competitors in the eVTOL market like the Joby S4 and the Lilium jet are expected to be priced at \$1.3 million³ and \$10 million⁴ respectively.

With the cost per aircraft of \$2.2 million and a projected production series of 500 **HAROLD**s per year, the expected break-even point is predicted to be reached at the 744th aircraft produced, resulting in a time to break-even of around 1.5 years. With a programme production period of 20 years, the return on investment is evaluated to reach 1133.33% for all investors.

Project Objectives

For the purpose of defining the goals and objectives of the project, the Mission Need (MNS) and Project Objective (POS) Statements are formulated. The Mission Need Statement (MNS) of the WUAV project is:

- Design an urban passenger aircraft with a low environmental impact by means of using CO_2 -capturing wood.

Defined by the MNS, this design is intended to provide an alternative to traditional fossil-fuel-powered modes

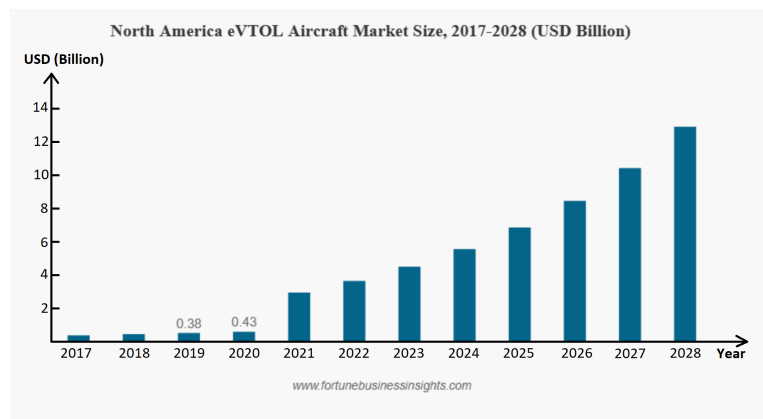


Figure 1: The expected size of the eVTOL market in according to Fortune.¹

¹<https://www.fortunebusinessinsights.com/evtol-aircraft-market-106298>, [cited 14.06.2024]

²<https://www.mckinsey.com/featured-insights/the-next-normal/air-taxis> [cited 19.06.2024]

³<https://evtol.news/joby-s4> [cited 18.06.2024]

⁴<https://www.theverge.com/2023/10/18/23920803/lilium-evtol-air-taxi-sale-us-price-emc-jet> [cited 22.05.2024]

of aerial transportation such as private jets and helicopters. The POS states the objective of the project as follows:

- Design a urban air transport system that minimises lifetime carbon emissions using wood-based materials by 10 students within a 10-week time frame.

Two primary objectives of this project follow directly from the POS:

1. *Design an eVTOL capable of intra- and intercity flight utilising wood as a structural element.*
2. *Design an eVTOL and ground station that operates safely and minimises carbon emissions from cradle to grave.*

Technical Capabilities of the Aircraft

The WUAV aims to meet the following specifications to fulfil its mission objectives, hereby providing the general expectations for the aircraft's capabilities. It is important that all of these specifications hold true simultaneously in order to count the **HAROLD**'s design as a success.

- VTOL capability.
- Construction using wood as one of the structural materials.
- A design flight range of 200 km.
- Capacity to transport a payload of six passengers, including the pilot.
- Maximum empty weight (weight without passengers) of 3000 kg.
- A maximum cruise speed of 250 km/h.

These specifications were set as guidelines for further aircraft development in terms of sizing and capabilities. The eVTOL aircraft is expected to fulfil all of these specifications by its final design.

The Preliminary and Final Designs

At this stage, the final design of the **HAROLD** has been created, provided in Figure 3. This design was reached through the intermediate sizing of the preliminary design; shown in Figure 2.

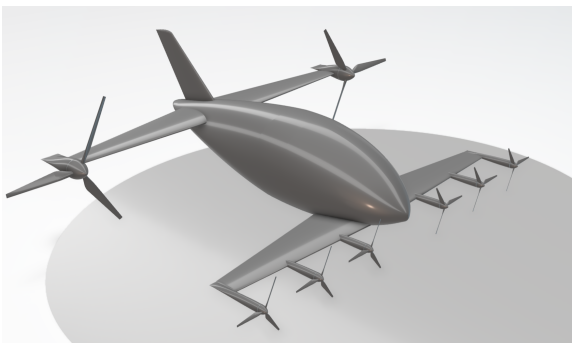


Figure 2: Preliminary aircraft design.



Figure 3: Final **HAROLD** design.

The preliminary design configuration for the aircraft, presented in Figure 2, was reached through an analytical evaluation, compromising between the Canard and Dragonfly concepts as identified in the concept generation phase of the project. The preliminary design consisted of two equally sized wings with the front wing supporting six smaller engines of 1.75 m diameter, three to either side of the aircraft centerline. On the tips of the trailing wing, however, two larger propellers of 4 m diameter were mounted. This design choice was found to contribute to the highest stability in VTOL flight as well as the highest amount of redundancy against single-point failures while maximising the efficiency of the propulsion system.

This design shows the most promising potential in the categories of energy efficiency and safety, which were deemed to be the two most important factors to fulfil for the aircraft to perform its mission successfully. Developing this further into the detailed design portrayed in Figure 3, various changes were made to the aircraft. These changes are provided in Table 1. The changes include the increase in the number of large propellers on the aft wing as well as the propeller size changes for both small as well as large propellers.

Wood is a viable material in multiple parts of the structure. Most significantly, both of the **HAROLD**'s wings are designed to be manufactured out of wood. In addition to that, the vertical tail of the aircraft is also constructed with a wooden structure. However, the fuselage was determined to be still made out of aerospace-grade aluminium in order to protect the passengers from the weather more effectively and cope with the higher stresses.

Material Analysis

A significant aspect of the project is the use of wood in the aircraft structure.

Higher-quality wood like Sitka spruce and Douglas fir can perform similarly to some aluminium alloys in terms of specific strength. However, this is dependent on the wood grain directions which must be handled carefully in the design process. One solution to solve this is to use custom-made wood laminates which have an alternating grain direction, increasing the stiffness and strength of wood to act more uniformly in multiple directions. Additionally, the mechanical performance of wood is influenced by the moisture content, temperature, fatigue and biological degradation meaning that the aircraft has to be properly maintained throughout its lifetime to ensure that the wood performs up to the required standard.

Substituting other aerospace materials such as metal alloys and CFRP with wood would result in reduced carbon footprints for the aircraft during its production part of the life cycle. Moreover, the end-of-life application options for wood roughly occupy the middle ground between composite materials and metals, with CFRP performing extremely badly in this aspect. The positive aspect of recycling and reusing wood is the small amount of energy required in the process when compared to metals, which need to be melted for recycling purposes.

The usage of wood possesses the opportunity to re-introduce a sustainable regenerative material to the eVTOL sector, helping the sector strive towards its sustainability goals. Thus, maximising the wood usage in the design is the driving philosophy of this project, as it sets it apart from other eVTOLs that are currently in development.

Weight Breakdown and Usage of Wood

The aircraft mass was evaluated to consist of 39.9% battery mass while the structure was found to take up 25.1% of the **HAROLD**'s mass. The mass fraction of wood utilised in the design amounts to 73.3% of the structural mass, equivalent to 18.4% of the total aircraft mass.

Energy Usage In Flight

Due to the current battery technology only allowing for a limited battery energy density of around 300Wh/kg, the amount of required energy becomes a driving factor in the design of an electric aircraft through battery mass. The vertical lift-off and landing capabilities along with the hovering phase of the flight are the most energy-intensive, constituting 35161 kWh of energy which is 18% of the total energy usage of the maximum flight distance. As the aircraft is fully powered by the battery, the source of this electrical energy becomes evermore important in the sustainability aspect of the design.

Ground Station Conceptual Design

In addition to the aircraft, the ground station design is a critical component of the WUAV system, ensuring efficient operations and sustainable energy supply. Green hydrogen was selected to power the ground station, and consequently the aircraft batteries, due to its top-of-the-class compactness and low environmental impact. Both of these were valuable qualities for this mission, aiming to promote sustainable air travel in urban areas. The final design of the ground station is provided in Figure 4

Table 1: Design changes between the preliminary and final designs.

Parameter	Preliminary Design	HAROLD
Number of aft propellers [-]	2	4
Number of front propellers [-]	6	6
Front propeller diameter [m]	1.75	1.63
Aft propeller diameter [m]	4.00	2.61
Wing span (w/o propellers) [m]	9.38	10.81
Fuselage length [m]	9.00	8.725



Figure 4: Ground station design.

Contents

Preface	i	8.3 Method	29
Executive Overview	ii	8.4 Results	33
Nomenclature	vi	8.5 Verification and Validation	34
1 Introduction	1	9 Wings & Empennage Sizing	35
2 Market Analysis	3	9.1 Wing Sizing and Requirements	35
2.1 State of the Market	3	9.2 Empennage	38
2.2 Main Competitors.	3	10 Aerodynamic Analysis	40
2.3 Possible Clients.	4	10.1 Wing Subsystem Requirements and Compliance Matrix	40
2.4 Marketing Strategies	4	10.2 Assumptions	40
2.5 Resulting recommendations	5	10.3 Aircraft aerodynamic performance.	41
3 Functional Analysis	6	10.4 Sensitivity Analysis	47
3.1 Functional Flow Diagram.	6	10.5 Verification of the Aerodynamic Model	49
3.2 Functional Breakdown Structure.	6	10.6 Validation of the Aerodynamic Model	50
4 Risk Analysis	7	10.7 Aerodynamics Recommendations	51
4.1 Risk Events	7	11 Propulsion System Design	52
4.2 Mitigation Strategies	7	11.1 Propulsion Subsystem Requirements & Assumptions	52
4.3 Subsystem Requirements	11	11.2 Propulsion System Design Method	53
5 Design Requirements & Constraints	13	11.3 Results	56
5.1 User Requirements.	13	11.4 Sensitivity Analysis	56
5.2 System Requirements	13	11.5 Verification and Validation	57
6 Concept Selection	17	11.6 Propulsion Recommendations	57
6.1 Concept Description	17	12 Power	58
6.2 Trade-Off	18	12.1 Subsystem Requirements and Compliance Matrix	58
6.3 Selected Concepts	21	12.2 Assumptions	59
7 Mission and Flight Profile	23	12.3 Method	59
7.1 Operational Requirements and Compliance Matrix.	23	12.4 Results	61
7.2 Assumptions	23	12.5 Sensitivity Analysis	63
7.3 Operational Modes	23	12.6 Verification and Validation	64
7.4 Flight Profile	24	12.7 Recommendations	65
7.5 eVTOL Dynamic Model.	25	13 Flight Performance Analysis	66
7.6 Transition Analysis	26	13.1 Assumptions	66
7.7 Assumption Validation	27	13.2 Payload-Range Performance	66
8 Fuselage Design	28	13.3 Rate of Climb Performance	66
8.1 Fuselage Subsystem Requirements and Compliance Matrix.	28	13.4 Headwind Performance	67
8.2 Assumptions	29	13.5 Verification and Validation	67
		13.6 Recommendations	68

14 Avionics & Software	69	18 Ground Station Design	107
14.1 Subsystem Requirements and Compliance Matrix	69	18.1 Ground Station Subsystem Requirements and Compliance Matrix	107
14.2 Assumptions	69	18.2 Method	108
14.3 Method	70	18.3 Results	108
14.4 Results	72	18.4 Overview & Recommendations	110
14.5 Conclusion	73	19 Sustainability Analysis	111
14.6 Recommendations	73	19.1 Sustainability Aspects	111
15 Material Analysis	74	19.2 Life Cycle Assessment	111
15.1 Materials Requirements and Compliance Matrix	74	19.3 End-of-Life	113
15.2 Assumptions	74	20 Operations & Logistics	114
15.3 Analysis of Wood as a Structural Material	74	20.1 Aircraft Operations & Logistics	114
15.4 Sustainability of Materials	77	20.2 In-flight Phase	114
15.5 Engineering Lumber	78	20.3 Post-flight Phase	115
15.6 Comparison of Wood With Other Aerospace Materials	78	20.4 Ground Station Operations & Logistics	115
15.7 Resulting Materials for Use in the HAR-OLD	79	21 Production Plan	116
15.8 Material Properties of the Selected Materials	79	21.1 Production Requirements and Compliance Matrix	116
16 Structural Analysis & Design	80	21.2 Supply Chain	116
16.1 Structures Subsystem Requirements and Compliance Matrix	80	21.3 Manufacturing of wooden wings	116
16.2 Preliminary Structure	80	21.4 Fuselage Production	120
16.3 Detailed Structure	86	21.5 Assembly Sequence	120
16.4 FEM Structure	91	21.6 AS9100	120
16.5 Structure Model Comparison	93	21.7 Volume	121
16.6 Landing Gear Design	94	21.8 Sustainable Manufacturing	121
16.7 Recommendations	98	22 Project Design and Development Logic	122
17 Design Integration & Results	99	22.1 Project Design and Development Logic Diagram	122
17.1 Integration Method	99	22.2 Gantt Chart	122
17.2 Weight and Centre of Gravity Estimation	100	23 Financial Analysis	123
17.3 Effects on Subsystem Design	102	23.1 R&D, Manufacturing and Sales Price	123
17.4 Design Results	103	24 Conclusion	126
		References	130
		A Large Diagrams	131

Nomenclature

Abbreviations

BOL	Beginning of Life
CAD	Computer-Aided Design
CG	Center of Gravity
CSV	Comma-Separated Values
DoD	Depth of Discharge
EOL	End of Life
eVTOL	Electric Vertical Take-Off and Landing
MISC	Miscellaneous
R&D	Research and Development
RPM	Rounds Per Minute
SOC	State of Charge
TMS	Thermal Management Sizing
TMS	Thermal Management System
VTOL	Vertical Take-Off and Landing

Symbols

α	Angle of Attack	[°]
α_r	Angle of Attack Derivative w.r.t. Radius [dg/m]	
α_s	Angle of Attack at Stall	[°]
α_{0L}	Angle of Attack at Zero Lift	[°]
$\alpha_{C_{L_{max}}}$	Compensation Term for Lift Reduction at Stall	[°]
$\bar{\xi}$	Normalised Stagger	[-]
ϵ	Down Wash	[°]
η	Airfoil Efficiency Factor	[-]
η_{tr}	Efficiency of the Transmission System	[-]
$\frac{d\epsilon}{d\alpha}$	Downwash gradient	[-]
κ	Allowed Degradation	
κ	Degradation	[-]
Λ	Sweep	[°]
λ	Taper Ratio	[-]
ω	Angular Velocity	[RAD/s]
ϕ	wing-tip strike angle	[deg]
ψ	Overturn angle	[deg]
ρ	Density	[kg/m]

σ_{sol}	Solidity of Rotor	[-]
θ	Pitch Angle	[°]
θ_f	Front Motors Angle with the Vertical	[°]
θ_r	Rear Motors Angle with the Vertical	[°]
φ	Propeller-tip strike angle	[deg]
A	Cross-Sectional Area	[m ²]
A_{pr}	Propulsion System Effective Area	[m ²]
AR	Aspect ratio	[-]
b	Wingspan	[m]
C_D	Drag Coefficient	[-]
C_L	Lift Coefficient of the Wing	[-]
C_l	Lift Coefficient of the Airfoil	[-]
C_T	Thrust Coefficient	[-]
C_{aed_m}	Additional Engineering and Design Cost	EUR
C_{aed_r}	Airframe Engineering and Design Cost	EUR
C_{apc_m}	Aircraft Production Cost	EUR
c_{clear}	Clearance Distance between Propeller Tips	[m]
C_{D_0}	Zero Lift Drag Coefficient	[-]
C_{D_i}	Induced Drag Coefficient	[-]
C_{dst_r}	Development Support and Testing Cost	EUR
C_{eam}	Cost for Propulsion, Battery and Avionics	EUR
C_{f_c}	Skin Friction Coefficient	[-]
C_{fin_m}	Cost of Financing the Manufacturing Program	EUR
C_{fin_r}	Cost to Finance the RDTE Phases	EUR
C_{ftar}	Flight Test Aircraft Cost	EUR
C_{ftom}	Flight test cost during manufacturing program	EUR 0
C_{ftor}	Flight Test Operation Cost	EUR
C_{int_m}	Interior Cost	EUR
C_{L_α}	Lift Slope of the Wing	[1/°]
C_{l_α}	Lift slope of the Airfoil	[1/°]
$C_{L_{des}}$	Design Lift Coefficient	[-]
C_{man_m}	Manufacturing Labour Cost	EUR
C_{man_u}	Manufacturing Cost per Unit	EUR
C_{man}	Cost of Manufacturing	EUR

C_{mat_m}	Material Cost	EUR	l_f	Front Propeller Longitudinal Distance from CG	[m]
C_{Pro_u}	Profit per Unit	EUR	l_m	Motor Axial Length	[m]
c_{pr}	Propeller Blade Chord	[m]	l_{main}	Location of the main landing gear from CG	[m]
C_{qc_m}	Quality Control Cost	EUR	l_{nose}	Location of the nose landing gear from CG	[m]
C_{RDTE_u}	RDTE Cost per Unit	EUR	M	Mach	[-]
C_{RDTE}	Total Cost for RDTE	EUR	m	Mass	[kg]
c_r	Propeller Blade Chord Derivative w.r.t. Radius	[m/m]	M_{len}	Length of manufacturing program	20 years
C_{tool_m}	Tooling Cost	EUR	$MTOW$	Maximum take-off weight	[kg]
C_{tsfr}	Test and Simulation Facilities Cost	EUR	n_{bat}	Number of Batteries	[-]
CG	Total center of gravity	[m]	N_{blades}	Number of Blades per Propeller	[-]
CG_i	CG of an individual component	[m]	N_{pr}	Number of Propellers per Wing Side	[-]
D	Drag	[N]	N_{r_r}	Test aircraft production rate during R&D	0.33/quarter
d	Diameter	[m]	P_m	Motor Power	[kW]
D^*	Contracted Slipstream Diameter	[m]	P_{req}	Power Required	[W]
d_f	Distance of Front Propellers to the CG	[m]	Q	Heat	[J]
d_f	Maximum Fuselage Diameter	[m]	R	Range	[m]
d_r	Distance of Rear Propellers to the CG	[m]	r	Radius	[m]
DoD	Depth of Discharge	-	S	Wing surface area	[m ²]
dt	Time Step	[s]	S_{wet}	Wetted Surface Area	[m ²]
e	Oswald Efficiency Factor	[-]	T	Thrust	[N]
e_{BOL}	Energy Density at BOL	[Wh/kg]	t	Thickness	[kg]
e_{EOL}	Energy Density at EOL	[Wh/kg]	T_r	Thrust Ratio	[-]
F_{cad}	Factor for CAD utilisation in design	0.8	T_{a_j}	Aft Propeller Thrust	[N]
F_{diff}	Difficulty factor in cost models [range: 1.5-2]		T_{f_i}	Front Propeller Thrust	[N]
F_{int}	Interior cost factor 3000 (USD, 1990 prices)		T_f	Front Wing Thrust	[N]
F_{pro}	Profit factor on R&D and production	10%	T_r	Rear Wing Thrust	[N]
FF	Form Factor	[-]	u	Fuselage Upsweep	[°]
h	Altitude	[-]	V	Velocity	[m/s]
h_s	Stagger Height	[m]	v_{cr}	Cruise velocity	m/s
h_t	Height of the Wing Tips	[-]	V_{dis}	Discharge Voltage	[V]
I_{yy}	Moment of Inertia around the y-axis	[kgm ²]	W	Weight	[N]
IF	Interference Factor	[-]	w	Wing velocity	m/s
K_{wf}	Fuselage-Wing Lift Slope Correction Factor	[-]	w_f	Fuselage Width	[m]
L	Lift	[N]	W_i	Weight of an individual component	[kg]
l_a	Aft Propeller Longitudinal Distance from CG	[m]	$w_{pr_{prop}}$	Propeller Total Mass	[kg]
			w_{pr}	Propulsion System Mass	[kg]

x/c	Chord-wise Position	[–]	z	CG height from ground when stationary	[m]
x_{ac}	Location of the aerodynamic centre	[m]	z_n	Propeller height from ground when stationary	[m]
y_e	Outboard location of engine	[m]	z_t	Tip height from ground when stationary	[m]
Y_{MLG}	Outboard location of main landing gear	[m]	AEP	Sales Price Per Unit	EUR

Chapter 1 | Introduction

The market for urban air mobility vehicles is posed to grow significantly over the next decades¹, with battery technology improving and cities looking to limit car usage [2, 3]. Current eVTOL concepts, mainly due to the use of batteries with limited lifetime [4], will not last as long as general aviation aircraft. This reduced lifetime makes it of essential importance to consider the end-of-life characteristics of the materials used; especially with energy intensive and end of life-complex carbon fibre reinforced composites becoming a popular material for aircraft lately².

The solution to this crossroads? Wood. A product of millions of years of evolution, wood is a material that not only does not require high energy input for its generation, but it also captures CO_2 during its growth, decreasing the carbon footprint of the aircraft. Contrary to composites, wood presents simple end-of-life possibilities, with worst case scenarios being as simple as returning the CO_2 to the ground burying the wooden elements in question and having them degrade completely in about 50 years. In the case of composites, the processing rapidly becomes expensive making dumping it a real possibility, with recycling processes still requiring significant efforts in research [5].

Wood is however not the panacea of eVTOL manufacturing. It presents performance losses when compared to typically used aerospace materials, and presents limitations when processing it. The objective of this design is thus to investigate the feasibility of designing, manufacturing and operating an eVTOL partially made of wood, with the aim of minimising emissions; this is covered by the Project Objective Statement and Project Objectives.

Project Objectives

The objective of the project is summarised in the Project objective Statement (POS), and refined with the primary and secondary project objectives:

Project Objective Statement (POS):

Design a urban air transport system that minimises lifetime carbon emissions using wood-based materials by 10 students within a 10-week time frame.

The primary objectives follow from the POS, and are defined as follows:

- **PO1:** Design an eVTOL capable of intra- and intercity flying utilising wood as a structural element.
- **PO2:** Design an eVTOL and ground station that operate safely and minimise carbon emissions from cradle to grave.

The secondary objectives are defined as the following separate objectives:

- **SO1:** Design an eVTOL that shall not introduce noise pollution in urban environments.
- **SO2:** Design an eVTOL that fits into the European eVTOL market demands.
- **SO3:** Design an eVTOL that maximises the usage of wood within its structure.

Scope and Design Philosophy

The proposed project objectives are ambitious, especially considering the personnel and time constraints imposed by the POS. As such, the scope for the design must be defined, together with a design philosophy that guides the design process. The scope of the project is to cover the main subsystems affected by the use of wood in the design, which for a system as interdependent as an aircraft implies looking at all the main subsystems. Effort is made in developing all subsystems to the same level of detail in order to avoid errors due to lack of resolution in a certain element affecting the entire design. For all subsystems, more detail can be added at the end of this project, and recommendations are provided to ease the continuation of this work. Overall, the definition of the scope predicts the design philosophy that follows.

The design process has followed a philosophy deeply rooted in the project objectives stated above, and a design was made in accordance to the following:

- **Wood Usage:** The design aims to maximise the usage of wood in the aircraft, this includes exploring unconventional designs and/or manufacturing techniques.

¹<https://www.mckinsey.com/industries/aerospace-and-defense/our-insights/advanced-air-mobility-in-2030/>

²<https://www.pentapatterns.co.uk/carbon-fibre-in-aerospace/> [cited 25-6-2023]

- **Safety:** Safety in the design is ensured by following the EASA regulation and not FAA because these are more constraining. Furthermore, safety factors were applied to critical calculations. In the structural design this factor is 1.5. For the battery sizing it is 1.25 because it is important to have power at all times.
- **Conservative Design:** To be able to come to a final design, it is important to have a conservative preliminary design. This is achieved by using a factor during the preliminary design phase. In most cases, this factor was 1.1.
- **Weights for criteria in Trade-Offs:** For each criterion in the trade-offs, the risk associated with the criterion is identified, and the weight of the criterion is chosen so as to reflect the severity of the risk.
- **Concept trade-off scores:** The scores of the concepts in the trade-off ranges from 0 to 1. The best performing score gets a score of 1, the score of 0 will be defined by the absolute worst case scenario possible for that criterion (this does not always correspond to the worst-performing concept). The remaining scores were linearly interpolated.
- **Functional Design:** To ensure a functional design, both tools and results are verified and validated.
- **Functional Model:** To ensure that the (mathematical) models are usable for the design, they must be conservative in the sensitivity and V&V analysis for them to be considered sufficient.

To verify and validate the models used for the design and the design itself several practices were followed during the design:

- **Industry Software:** In this project, industry software that has been used extensively by other companies or institutions will be considered as verified and can be used to V&V the models created in this project.
- **Proven Methods:** Numerical or Statistical methods that have been used extensively in the aerospace industry such as Roskam, they are deemed verified for use in this project.
- **V&V Tolerances:** The model or design is considered verified or validated when the percentage difference between the outcome of the model and the value with which it is compared is lower than a preset percentage. In this project, this percentage depends on the particular model or design.
- **Failed V&V:** If the difference between the model and comparison value is too large, the model should be revised and corrected until the difference is within bounds.
- **Impossible Validation:** Validation could not be possible for a reason, for example when no industry software or physical test model is available. When this happens, this should be reported and done when validation can be performed.

Report Structure

Firstly, a market analysis is presented in Chapter 2, analysing the state of the market, possible clients and current competitors in the eVTOL area; and generating recommendations for the design. Then, the function analysis of the WUAV is given in Chapter 3, where the functional flow and breakdown diagrams are given, these are also a source of functions the design should be able to complete. Afterwards, a risk analysis is presented in Chapter 4. The three previous chapters flow together with the needs presented by the user into Chapter 5, where the requirements to be met by the design are presented. As part of the design several concepts were preliminarily designed to then select one by means of a trade-off, presented in Chapter 6.

The rest of the report focuses on the design of the selected concept, the HAROLD (**H**oivering **A**erial **p**aRtially **w**ooden **L**ift-off **D**evice). Fuselage design is presented first in Chapter 8. Then, the wings and empennage sizing is given in Chapter 9 followed by the aerodynamic analysis in Chapter 10. The propulsion system design is given in Chapter 11 together with a sizing of the power supply system in Chapter 12. The flight performance of the resulting design is covered in Chapter 13, and in Chapter 14, the avionics and software of the aircraft is presented. The next two chapters, Chapter 15, and Chapter 16 cover the material analysis and structural design of the HAROLD, and look into the use of wood as a material. Since the sizing of an aircraft sees different subsystems having different priorities these have to be integrated in a closed sizing loop that arrives at an optimal design, this is presented in Chapter 17.

In parallel with the aircraft design given, the ground station is designed as shown in Chapter 18. Further, as sustainability is a major aspect the design process, the sustainability analysis of the design is given in Chapter 19. This is followed by a description of the operations and logistics, given in Chapter 20. The production plan for the aircraft is presented in Chapter 21. The next steps in the product's lifetime, extending beyond design, are given in Chapter 22. Finally, a financial analysis is performed in Chapter 23. The last chapter in the report, Chapter 24, concludes everything covered with the main results and recommendations for future work.

Chapter 2 | Market Analysis

Before launching a product, it is imperative to first have a good grasp on the market it is aiming to enter, especially if the technology is new and has not yet been established in the public conscience. In the case of HAROLD, a thorough investigation into the state of the market is required, as well as an analysis of the competition, the possible clients, and some of the marketing strategies that may be employed.

2.1. State of the Market

As of 2020, the global eVTOL market was estimated to be worth around 1.1 billion USD, and expected to reach 23.21 billion USD by 2028, as reported by Fortune¹. The anticipated growth for the North American region can be seen in Figure 2.1.

While this is the region expected to experience the largest growth, one must not forget that the European market is also going to experience drastic growth. As such, it is important to consider the regulatory bodies controlling both submarkets - the FAA and EASA. While the FAA has not yet published any specific regulations on commercial VTOLs, EASA has published "Means of Compliance with the Special Condition VTOL" - a document that can not be ignored when designing a vehicle for the European market.

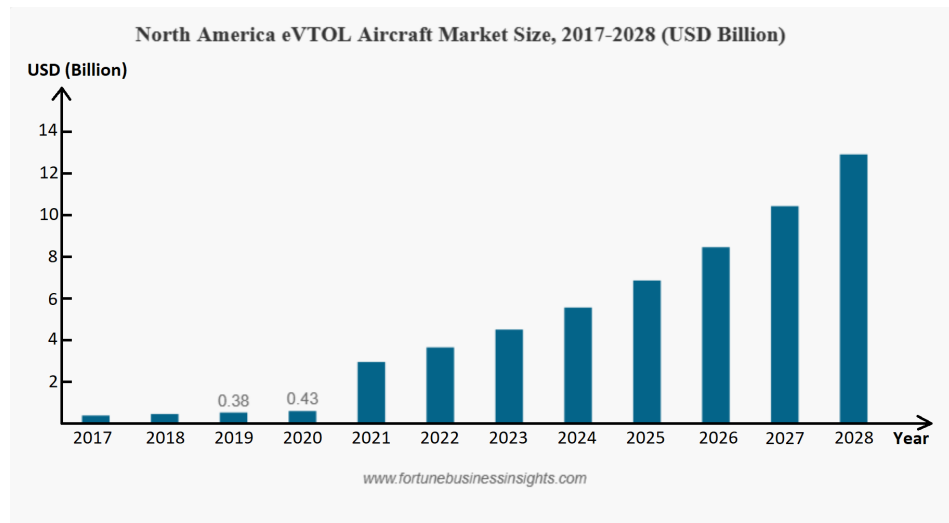


Figure 2.1: The expected size of the eVTOL market in according to Fortune.¹

There are multiple ways the market can be divided into subsections. Some of the categories include differentiating eVTOLs by their size, range, lift technology, use, maximum take-off weight, and geographical region. The HAROLD is a non-autonomous commercial urban aircraft with a MTOW of over 1500 kg, and a range of 200 km that is expected to function mainly in Europe. All of these data points correspond to different subcategories in the market, namely the 200-500 km range category, the semi-automated category, the battery-electric segment, and the commercial segment.

Some key companies in the current state of the market include Airbus S.A.S, Lilium, Joby Aviation, Volocopter GmbH, Ehang, and Eve Air Mobility. These companies either have a working prototype of their eVTOLs or have received a large quantity of orders already. The estimated TRL (Technological Readiness Level) for the eVTOLs is 8; prototypes exist and some have been certified to carry passengers [6]. Prices of these eVTOLs vary widely, with some starting from 300,000 EUR like the Volocopter (stated to be 250,000 EUR in 2013 in the Wall Street Journal, adjusted to inflation)² and Ehang's two seater at 334,000 USD³ to the Lilium jet's 10 million USD.

2.2. Main Competitors

This project would be entering an unpredictable and potentially rapidly rising market with an increasing market cap¹. Despite this sector's practical non-existence as of the third decade of the 21st century, there are many products and ideas on the cusp of making it into this untapped market. The most significant of such products is the CityAirbus NextGen, manufactured by Airbus. This aircraft is the successor of Airbus' CityAirbus, which had its full-scale flight tests in 2019. As of the time of writing this report, Airbus has yet to publish any reports

¹<https://www.fortunebusinessinsights.com/evtol-aircraft-market-106298>, [cited 14.06.2024]

²<https://www.wsj.com/articles/BL-TEB-5964> [cited 08.05.2024]

³<https://www.ainonline.com/news-article/2024-02-02/ehang-prices-its-two-seat-autonomous-evtol-aircraft-334000> [cited 08.05.2024]

on when and how flight tests of the CityAirbus NextGen would be carried out. The craft is supposed to carry up to three passengers and one pilot, making it slightly smaller than the HAROLD design.

Another aircraft that cannot be ignored is the Lilium jet. According to the Lilium website, the aircraft is supposed to have a range between 40 and 200 km at speeds up to 300 km/h, at a cruise altitude of around 3000 m, and with a passenger capacity of 7 passengers⁴. The Lilium jet, with an expected price of around 10 million USD⁵ per vehicle, has been in development since 2019 and is one of the most direct competitors to the product considered in this report. Additionally, Lilium reported a successful transition flight in 2022 that was done on their full-scale demonstrator vehicle⁶. It must be noted that in 2020 there was an anonymous report published claiming that Lilium could not meet their project goals⁷. This report was discredited by the company but supported by scientists from the Technical Universities of Berlin and Hamburg⁸.

A final aircraft to consider is Joby, an eVTOL in development at Joby Aviation⁹ (which is owned by Boeing). At this moment, Joby has completed three out of five stages of aircraft certification. The Joby aircraft has a range of 240 km and a maximum speed of 320 km/h as stated by the company. It can carry 5 people, including the pilot. Production has already begun, with the first eVTOL being produced in June 2023. Currently, Joby Aviation plans to increase their production to 500 aircraft per year thanks to a new production plant. They have also entered partnerships with NASA, Uber, Delta and they have a contract with the American Air Force worth 131 million USD. Of all the potential competitors, Joby Aviation has progressed the furthest and is the most important competitor in the field of urban eVTOL.

There are certain characteristics multiple of the HAROLD's direct competitors share. For example, all three of the mentioned aircraft have their silent propeller systems as one of their marketing points, with decibel levels being reported as 60-65 dB¹⁰. Therefore, it is easy to see that in order to not fall behind these products, the HAROLD must also make a considerable effort to keep its noise emissions below at least 95 dB. Another common selling point of the competition are their "intuitive displays", which is a concept that has permeated itself throughout all vehicle markets. While missing and "intuitive" display may be a welcome change for some, the current state of the market shows that such features are desired, and and such, the HAROLD should strive to have an easily readable, modern display to indicate vital information to the pilot. It must be noted that some of the main competitors in the market offer lower prices than the subject of this report. While it is true, it is also important to realise that the more budget-friendly options also have a smaller passenger capacity. The estimated price of the product is still competitive when it comes to high passenger capacity eVTOLs.

At the time of writing this report, none of the aforementioned vehicles have performed a commercial flight. However, all vehicles have had at least one full-scale prototype tested in a real life flight, with the exception of the Eve Air Mobility aircraft which, to the knowledge of the authors, has only had a simulation flight¹¹.

2.3. Possible Clients

Because of the price of the eVTOL and its accompanying infrastructure, the interested customers in the early stages of eVTOLS will most likely be wealthy individuals and private companies. In the case of the earlier mentioned competing companies, their customers mainly consist of wealthy individuals. After the market has grown, along with trust in the technology, the main customers is predicted to be taxi companies [7]. These companies will make travelling with the eVTOL cheaper and more accessible for the main public. Because taxi companies want more than one eVTOL for their operations, the sales of the eVTOLs will also increase significantly at this stage, creating more funds for further development of the vehicle. Another application for the eVTOL could be for Medevac (Medical Evacuation), as the ability of the aircraft to land in many different places and its fast cruise speed makes the eVTOL perfect for the evacuation of people, or the transportation of people between two hospitals.

2.4. Marketing Strategies

Behind every successful product, there stands a good marketing campaign. In the case of the product discussed in this report, there are no similar products currently in commercial circulation, making it very difficult to consider marketing specifications. Therefore, the promotions of this product would focus on increasing public trust in

⁴<https://lilium.com/newsroom-detail/technology-behind-the-lilium-jet> [cited 12.06.2024]

⁵<https://www.theverge.com/2023/10/18/23920803/lilium-evtol-air-taxi-sale-us-price-emc-jet> [cited 07.05.2024]

⁶<https://lilium.com/newsroom-detail/technology-demonstrator-main-wing-transition> [cited 12.06.2024]

⁷<https://www.aerokurier.de/elektroflug/lilium-jet-dossier/> [cited 13.06.2024]

⁸<https://www.aerokurier.de/elektroflug/lilium-weitere-experten-unterstuetzen-kritik/> [cited 13.06.2024]

⁹<https://www.jobyaviation.com/> [cited April 2024]

¹⁰<https://robbreport.com/motors/aviation/watch-this-whisper-quiet-evtol-hover-and-land-1234634956/> [cited 19 June 2024]

¹¹<https://www.eveairmobility.com/first-evtol-simulator-flight-by-embraerx/> [cited 07.05.2024]

what is currently a very radical idea. A brief SWOT analysis can be found in Table 2.1.

Table 2.1: SWOT analysis of the market.

	Helpful	Harmful
Internal	<ul style="list-style-type: none"> Novel technology Zero emission during operations Medium range Lower cost compared to competitors 	<ul style="list-style-type: none"> Little experience New material for the industry - limited maintainability
External	<ul style="list-style-type: none"> Few companies have >4 passenger vehicles Sustainability being sought after University support European subsidies for sustainability 	<ul style="list-style-type: none"> Distrust from the public (either because VTOL or wood) Market is new and unpredictable Inflation Few examples to look at Limited data Similar competitors further in development

The public relations strategy surrounding the product would initially focus on mitigating the general distrust and safety concerns clients would most likely have when confronted with such an unconventional idea. The eVTOL market has not yet established itself in the way the automobile or helicopter markets have, and as such public trust is an essential point. Demonstrations of the vehicle's emergency capabilities, such as landing after an engine failure, would serve as a great way to increase trust from the public. Additionally, one could utilise an accident rate statistic comparing the vehicle to cars. If it is not possible to produce such a statistic, a parallel could be made with helicopters instead of eVTOLs.

Building trust is the first step to launching a successful product, however, mitigation of negative attention is not enough to garner positive attention. Sustainability is one of the key aspects of this product, and it should be advertised as such. The use of wood as a structural material is the main feature that differentiates the HAROLD from competitors. Seeing as this is the product's distinguishing feature, it would be the biggest feature to draw customers in with. Possible ways to demonstrate the wooden structure could include a "blown out" model that shows the inside of the vehicle at eVTOL conferences. Additionally, one could make use of infographics which compare the net CO₂ emissions of this product and those of its competitors. Another advantage the product would have over its competitors would be its price. The total costs per vehicle are to be below 2,500,000 EUR, which is up to four times cheaper than competitors, greatly increasing the product's potential for success in the market.

Considering how new the eVTOL market is, it is important to realise that longevity of the product would play a large role in determining its staying power. This important both for marketing towards the public and towards investors - the public would not want to spend millions on a device that would function for less than a decade, and investors would be wary to invest in a product that could immediately be substituted with a new, more durable one. Having a short life cycle would also tarnish the HAROLD's sustainable image. Having a lifespan, similar to that of a car would legitimise the product in the eyes of investors and customers alike.

Another marketable quality would be compatibility with existing infrastructure. If HAROLD can land at already existing helipads and possibly charge at existing charging stations, that would greatly increase the reach of the product, as people highly value convenience. If the aircraft can only land on ground stations designed specifically for it, it would alienate potential clients who already own helipad infrastructure. As such, it is crucial that the HAROLD can utilise existing infrastructure. The HAROLD should also be able to provide the standard comforts of travel, such as protection from the elements, and ability to seat most of the population. Compatibility with existing skillsets should also not be underestimated - pilot training is expensive, and having a machine that behaves similarly to what many pilots were trained on would increase the reach of the product.

2.5. Resulting recommendations

From analysing the market, it was possible to derive certain recommendations to keep in mind when designing the eVTOL. These can be seen as:

- **MKT-01:** Minimise flight duration to appeal to a larger market.
- **MKT-02:** Keep noise emissions during cruise, take-off and landing low.
- **MKT-03:** Ensure a lifespan near-equivalent to that of a car
- **MKT-04:** Comply with the regulations of the target market
- **MKT-05:** Have an intuitive, well-defined display for the pilot to see vital parameters (velocity, altitude, etc.)
- **MKT-06:** Utilise existing infrastructure, such as helipads and possibly electric car chargers
- **MKT-07:** Have the standard comforts of travel in a car in terms of seating, accelerations, perceived inclination, and protection from the elements.
- **MKT-08:** Have controls be similar to other similar aircraft
- **MKT-09:** Make the aircraft safe to use

Chapter 3 | Functional Analysis

In this chapter, the functional diagram of the WUAV are given. These diagrams concern the operational phase of the WUAV aircraft and ground station, and also briefly cover the manufacturing and end-of-life procedure. The two diagrams used, the Functional Flow Diagram and the Functional Breakdown Structure, are presented in Section 3.1 and Section 3.2 respectively.

3.1. Functional Flow Diagram

The Functional Flow Diagram (FFD) encompasses every function and desired capability that the aircraft and the ground station should perform. This was then used to determine the functional requirements of the aircraft and ground station. For the aircraft, the FFD encompasses the manufacturing stage, the operational stage and the end-of-life process. The manufacturing stage mainly focuses on acquiring relevant materials, processing these into components and assembling them. The operational phase of the aircraft, instead, mainly consists of the flight mission and ground phase operations. It begins with a preparation phase before take-off in which the aircraft systems are checked and the payload is loaded. Once the aircraft is ready for taken off, it has two choices: it can either enter a climb phase, or enter the abort procedure. Should the aircraft abort its take-off (for example due to an electrical failure of one of the subsystems), either the passengers are evacuated if they are in immediate danger, or a decision must be made concerning whether to restart the takeoff phase or to cancel the flight should the aircraft be deemed unsafe.

During the cruise phase, a "check flight status" function was added, as the aircraft should continuously check its state up until it has reached its destination. Once at its destination, if the aircraft enters the descent phase it must also check its systems so as to ensure that the aircraft is capable of landing successfully. Should this be the case, the aircraft enters the approach phase. In case a failure has been found during the system check that results in a normal landing not being possible, an emergency landing can instead be performed. In the approach phase, it is possible for the aircraft to avert rather than land; this would occur when it is not possible to land successfully. This can be caused by many reasons, for example an obstruction of the landing pad. The aircraft must then go back to the check system phase. Please note the difference between the check system function and the approach function; the check system function evaluates the capability of landing, whilst the approach function evaluates the possibility of landing.

After a successful landing, the aircraft will be inspected. The remaining lifetime of the aircraft is evaluated after the inspection, and if the aircraft is deemed inoperable, it will then enter the end-of-life phase. If that is not the case, the battery system is recharged and any problems with the aircraft are repaired. At the end of the operational lifespan of the aircraft, a process dealing with the disposal and possible recycling of the system and subsystems of the aircraft is required.

For the ground station, instead, the FFD consists of an "aid landing" stage, a "provide power" stage and an "aid take-off" stage. In addition, the FFD includes functions that are undesirable but could still occur (for example, and emergency landing of the aircraft); these are found inside red blocks. In these cases, the functional flow represents what the product should follow in case something goes wrong during its operation. In order to further increase legibility of the diagram, aircraft sub-functions that are connected to the ground station are given a thick border. The full diagram can be seen in Chapter A.

3.2. Functional Breakdown Structure

The functional breakdown structure (FBS) offers more insight into each one of the functions described by the FFD, offering an overview of each function that the aircraft and ground station should be able to perform. In the FBS, some of the functions are derived directly from stakeholder requirements; in these cases, the requirement number is mentioned in the top right of the function's box. The FBS can be found in Chapter A.

Chapter 4 | Risk Analysis

This chapter discusses the technical risks which are relevant to the preliminary design phase. For each technical risk, a consequence, a mitigation strategy and a score is assigned to it. Finally, some subsystem requirements are derived from the technical risks.

4.1. Risk Events

In Table 4.1, top level system risks and subsystem-specific risks have been identified and reported. For each risk event, the consequence associated with it is also identified.

Table 4.1: Risk Events and their consequences

	ID	Risk Event	Consequence
System	R-TEC-01	Aircraft does not comply with EASA regulations	Aircraft can not be certified for customer use
	R-TEC-02	Product quality standards not met	High amount of rework recalls if undetected
	R-TEC-03	Critical subsystem failure	Passenger casualty
	R-TEC-04	Non-critical subsystem failure	Customer dissatisfaction
	R-TEC-05	Challenging maintainability	High maintenance cost, customer dissatisfaction
	R-TEC-06	Local noise regulations not met	Aircraft cannot operate in specific areas
Subsystem	R-TEC-07	Wood decay	Loss of structural integrity
	R-TEC-08	Undetected structural fatigue	Loss of structural integrity
	R-TEC-09	Lightning strike	Fire, damage to electrical systems
	R-TEC-10	Aerodynamic loads exceed capability	Damage to aircraft
	R-TEC-11	Damage to battery	Fire, loss of power
	R-TEC-12	Cabin fire	Immediate danger to passengers Damage to aircraft
	R-TEC-13	Loss of power during flight	No thrust No Vertical landing possible
	R-TEC-14	Loss of one engine	Loss of controllability
	R-TEC-15	Unable to find ground station for landing	Damage to structure
	R-TEC-16	Misses helipad during landing	Damage to ground station and structure
	R-TEC-17	Aircraft consumes more energy than expected	Decrease in Range and Failure of Subsystems
	R-TEC-18	The ground station is too expensive	Low Sales, insufficient ground station coverage
	R-TEC-19	The customer does not find the aircraft aesthetically pleasing	Low Sales, Break-even cant be reached
	R-TEC-20	Aircraft is too large to land within cities	Limits operations , Low Sales,
	R-TEC-21	Aircraft is difficult to manoeuvre during VTOL operations	Overall operation becomes more fuel consuming and slow
	R-TEC-22	Ground station is too large and thus cannot fit in most cities	Low Sales, insufficient ground station coverage
	R-TEC-23	Ground station produces lots of emissions during operation	Sustainability Project objective (PO2) is not reached

4.2. Mitigation Strategies

After having identified the risk events that could potentially affect the aircraft and/or ground station, it is important to find mitigation strategies that reduce the likelihood of the risk occurring and the effect of the risk. For each risk event, a mitigation strategy is presented. In addition, the likelihood of it occurs is assessed before (LB) and after (LA) the implementation of the mitigation strategy is defined, and the effect of the risk should it occur before the mitigation (EB) and after the mitigation (EA) is also assessed. Finally, a contingency strategy (CS) was determined to decide how to handle the risk event should it occur. These six points are detailed below for all sixteen risk events.

R-TEC-01 Aircraft does not comply with EASA regulations.

- LB: Regulations are used for the design requirements.
- EB: Non-compliance can prevent certification, blocking the aircraft from entering the market.
- MS: Implement continuous compliance checks into the design processes.
- RA: Regular checks and updates ensure ongoing compliance with regulations.
- EA: Non-compliance would still block certification but because of regular checks these can be detected earlier and have a less impact.
- CS: Redesign affected components or systems to meet regulatory requirements.

R-TEC-02 Product quality standards not met.

- LB: When producing in large quantities, it's almost certain that deficiencies will occur due to imperfect processes and errors. This makes deviations from quality standards highly probable.
- EB: If quality deficiencies are detected before shipment, rework of the affected units will be required, impacting costs and timelines. If defects are discovered post-shipment, a recall would be necessary, resulting in substantial financial losses and potential damage to the brand's reputation.
- MS: Implement quality control and design to minimise the possibility of errors in the manufacturing process.

Integrate continuous improvement of assembly process and use state-of-the-art inspection technologies to guarantee no aircraft with deficiencies is shipped out.

- LA: Improved design and processes help minimising the likelihood of their occurrence, however mistakes in the production due to human error are still possible.
- EA: Quality control and advanced inspection methods allow to detect quality issues early on where they can be fixed more easily.
- CS: Rework aircraft if a deficiency is found before shipment. If found by the customer, conduct product recalls and initiate a thorough investigation to identify and rectify production issues.

R-TEC-03 Critical Subsystem failure.

- LB: Critical systems are designed to meet rigorous safety standards, but the complexity of critical systems means failures can still occur unexpectedly.
- EB: Failures in critical subsystems can lead to catastrophic outcomes such as passenger casualties and grounding of the fleet, all of which have severe legal and financial consequences.
- MS: Enhance redundancy in critical subsystems, conduct rigorous and frequent validation, and implement real-time monitoring to detect and address potential failures before they escalate.
- LA: Increased redundancy and enhanced monitoring significantly reduce the probability of unexpected critical failures.
- EA: Although the mitigated effect remains high due to the potentially severe consequences of failure, the improved monitoring helps to manage and contain failures more effectively.
- CS: Implement immediate corrective actions, communicate transparently with stakeholders, and conduct a root cause analysis to prevent future occurrences.

R-TEC-04 Non-critical Subsystem failure.

- LB: Non-critical subsystems are designed with lower safety standards than critical subsystems; failures due to defects or wear are possible.
- EB: Such failures typically result in customer dissatisfaction and potential reputational damage, but do not generally lead to severe safety risks.
- MS: Establish a routine maintenance schedule to detect and fix issues early.
- LA: Regular maintenance reduces the frequency of failures.
- EA: Early issue resolution minimises customer dissatisfaction and reputational damage.
- CS: Schedule immediate repairs or replacements and analyse failure modes to improve system designs in future iterations.

R-TEC-05 Challenging maintainability.

- LB: Complex designs and new technologies can complicate maintenance procedures.
- EB: Difficult maintenance leads to higher operational costs and customer dissatisfaction, potentially diminishing client retention and increasing total ownership costs.
- MS: Design systems for easy part replacement and long durability.
- LA: High durability minimises maintenance frequency.
- EA: Simplified part replacement reduces maintenance costs.
- CS: Revise the design for easier maintenance and provide support and training for maintenance teams to ensure efficient servicing and repairs.

R-TEC-06 Local noise regulations not met.

- LB: Current regulations are used as Design Requirements but these could change
- EB: Limited usability in areas where noise regulation are not met
- MS: Work closely together with regulatory bodies to anticipate changes in requirements
- LA: Planned changes can already be implemented decreasing the likelihood of not meeting them
- ERA: Effect does not change after mitigation
- CS: Revise the design to lower noise levels

R-TEC-07 Wood decay caused by fungi

- LB: Wood can experience decay from various fungi species, especially when exposed to humid environments.
- EB: Decay will significantly affect structural integrity, requiring costly repair or, if not detected, could cause failure.
- MS: Apply decay treatment to wooden components.
- LA: The treatment will significantly decrease the likelihood of decay occurring.

- EA: If decay occurs it will be less severe because of the treatment.
- CS: Ground aircraft until affected parts are replaced.

R-TEC-08 Undetected structure fatigue

- LB: Regular maintenance should make undetected fatigue unlikely.
- EB: Undetected fatigue leads to structural failure and possibly a fatal crash.
- MS: Structure must have detectable crack propagation (damage tolerant design).
- LA: Damage tolerant design makes fatigue detectable before structural failure occurs.
- EA: Should undetectable fatigue still occur, the effect will be the same.
- CS: Initiate emergency landing procedure.

R-TEC-09 Lightning strike

- LB: A Small aircraft constructed mostly of wood has a low probability of being hit by lightning.
- EB: A Lightning the aircraft could easily damage electronics or set the wooden components on fire.
- MS: Add a conductive top layer to outward-facing surfaces.
- LA: A conductive top layer increases the likelihood of being hit by lightning.
- EA: The conductive top layer creates a Faraday cage protecting interior components, the top layer might still be damaged.
- CS: Conduct a thorough inspection for damage before the next flight.

R-TEC-10 Aerodynamic loads exceed capability

- LB: Unlikely if the aircraft is correctly operated as a safe load factor requirements are set and tested by regulatory bodies.
- EB: Because of the semi-brittle nature of wood, damage to the structure would be especially fatal.
- MS: Include a warning system that warns the pilots before aerodynamic loads exceed capability.
- LA: Allows the pilot to react before damage occurs.
- EB: The mitigation strategy will not affect the design.
- CS: Initiate emergency landing procedure, and replace damaged parts.

R-TEC-11 Damage to battery

- LB: Unlikely as the design must use batteries approved by regulatory bodies.
- EB: Can cause fire and loss of power.
- MS: Enclose the battery in a metal container.
- LA: Protects the battery from damage.
- EA: Limits spills and fire spreading in case of damage.
- CS: Initiate emergency landing, exit vehicle and call the fire department.

R-TEC-12 Cabin fire

- LB: The aircraft's reliance on wooden structure makes cabin fires more likely.
- EA: The aircraft's reliance on wooden structure makes cabin fires more severe.
- MS: Use fire retardant treated wood, use inflammable materials in areas where fires are most likely (eg. Battery, Engines,...), have fire extinguishing systems in high-risk areas.
- LA: Fires are less likely to start as materials require more energy to start burning.
- EA: If fires occur they do not spread as fast and are more contained.
- CS: Initiate emergency landing, exit vehicle and call the fire department.

R-TEC-13 Loss of power during flight

- LB: Many events can lead to a loss of power (Eg. damage to the battery, excessive flight time, damage to the power lines, ...).
- EB: Can cause a fatal crash.
- MS: Apply safety factor on Battery capacity
- LA: The mitigation strategy prevents some events but many reasons that could lead to power loss remain.
- EA: Emergency landing might injure passengers and damage the aircraft, horizontal landing might not be possible during loss of power at low altitudes/speeds.
- CS: Initiate emergency landing procedure.

R-TEC-14 Loss of one Engine

- LB: Loss of one engine is likely and can occur through various events (eg. bird Strike, failure of Motor,

failure of power supply, engine fire, ...).

- EB: Loss of one engine will cause the engine torques not to cancel anymore and create a net torque. If this happens during vertical flight, the aircraft can start spinning uncontrollably and fatally crash.
- MS: Design a control system with enough engines so that the net zero engine torque can be reached.
- LA: Does not affect likelihood.
- EA: No effect on flight operation but the damaged engine needs to be replaced.
- CS: Land aircraft at the closest ground station.

R-TEC-15 Unable to find a free ground station

- LB: It is possible to occur if flying in areas with less developed infrastructure, and when having to perform an unexpected landing.
- EB: Damage to aircraft and terrain during landing outside of the ground station.
- MS: Design aircraft to be able to land on various terrains without damage to itself or the terrain.
- LA: Does not affect likelihood.
- EA: Can still get damaged when no suitable landing spot is available and landing in rough terrain.
- CS: Land aircraft in a different location.

R-TEC-16 Misses Helipad during landing

- LB: It is possible for a landing aircraft to get out of bound of the helipad
- EB: When missing the helipad during landing surrounding buildings as well as the aircraft can be damaged
- MS: Design aircraft to be smaller
- LA: as smaller aircraft makes it less likely to get out of bond of the helipad
- EA: Can still get damaged when landing pad is missed
- CS: Land aircraft in a different location.

R-TEC-17 Aircraft consumes more energy than expected

- LB: due to potential deviations in energy consumption from initial estimates caused by system integration and sub optimal operational conditions.
- EB: Compromises the aircraft's operational range and efficiency and also impacts multiple subsystems
- MS: Consider energy consumption in trade off
- LA: Reduced by consideration during trade off
- EA: Does not affect effect score
- CS: Decrease operational range or redesign

R-TEC-18 The ground station is too expensive

- LB: Snowballing cost are common in especially when designing new concepts
- EB: High ground station cost reduces
- MS: Consider ground station Price during trade off
- LA: Reduced by consideration during trade off
- EA: Does not affect effect score
- CS: Lobby the government to invest into eVTOL infrastructure

R-TEC-19 The customer does not find the aircraft aesthetically pleasing

- LB: A utilitarian design can sometimes not be aesthetically pleasing
- EB: Low sale Numbers might lead to decrease in profit
- MS: Consider aesthetics during trade off
- LA: Reduced by consideration during trade off
- EA: Does not affect effect score
- CS: Redesign exterior as far as possible and Focus on aesthetically pleasing interior

R-TEC-20 Aircraft is too large to land within cities

- LB: If not considered a aerodynamically optimal design might have a high wingspan
- EB: Not be able to land in most city's landing
- MS: Consider aircraft size during trade off
- LA: Reduced by consideration during trade off
- EA: Does not affect effect score
- CS: Redesign to allow operations inside cities

R-TEC-21 Aircraft is difficult to manoeuvre during VTOL operations

- LB: VTOL design usually allow for high manoeuvrability
- EB: fuel consuming and slow operations increase operational cost
- MS: Consider manoeuvrability during trade off
- LA: Reduced by consideration during trade off
- EA: Does not affect effect score
- CS: Redesign to allow better manoeuvrability

R-TEC-22 Ground station is too large and thus cannot fit in most cities

- LB: If not considered, a high footprint design is possibly best performing
- EB: Not be able to operate in most city's
- MS: Consider Ground station size during trade off
- LA: Reduced by consideration during trade off
- EA: Does not affect effect score
- CS: Redesign to allow for small size

R-TEC-23 Ground station produces lots of emissions during operation

- LB: most common design have high emissions
- EB: Failure of a Project objective means that the project at least partially failed
- MS: Consider emission during trade off
- LA: Reduced by consideration during trade off
- EA: Does not affect effect score
- CS: Redesign for lower emissions

In order to quantify the data described above, a table is generated in which the LB, EB, RB, LA, EA and RA are scored for each risk, and a designated responsible team member is defined. The likelihoods are ranked on a scale from 1 to 5, with each value representing different probabilities: 1—remote ($PR < 1\%$), 2—rare ($1\% \leq PR < 30\%$), 3—unlikely ($30\% \leq PR < 50\%$), 4—possible ($50\% \leq PR < 70\%$), 5—likely ($PR \geq 70\%$). Moreover, the effect of each risk event is also assessed based on the risk event's level of impact on mission success. Once again, this is done using a scale from 1 to 5: 1—negligible, 2—low, 3—medium, 4—high, 5—very high. The risk levels before (RB) and after (RA) mitigation were calculated for each event by multiplying the effect score by the likelihood score. All of these scores are presented in Table 4.2.

Table 4.2: Risk scores and responsible members.

ID	LB	EB	RB	LA	EA	RA	Responsible Member
R-TEC-01	3	5	15	2	3	6	Systems Engineer
R-TEC-02	5	5	25	4	3	12	Chief Manufacturing
R-TEC-03	3	5	15	2	4	8	Risk Manager
R-TEC-04	4	3	12	3	2	6	Risk Manager
R-TEC-05	4	4	16	3	3	9	Chief Manufacturing
R-TEC-06	3	3	9	2	3	6	Chief Aerodynamics
R-TEC-07	4	4	16	2	3	6	Chief Materials
R-TEC-08	3	5	15	2	5	10	Chief Structures
R-TEC-09	2	5	10	3	2	6	Chief Materials
R-TEC-10	3	5	15	2	5	10	Chief Performance
R-TEC-11	3	5	15	2	4	8	Chief Propulsion
R-TEC-12	4	5	20	2	4	8	Safety & Reliability Officer
R-TEC-13	3	5	15	2	4	8	Chief Aerodynamics
R-TEC-14	5	5	25	5	2	10	Chief Control & Stability
R-TEC-15	4	4	16	4	2	8	Chief Structures
R-TEC-16	4	4	16	2	4	8	Chief Structures
R-TEC-17	4	4	16	2	4	8	Chief Sustainability
R-TEC-18	3	5	15	2	5	10	Chief Sustainability
R-TEC-19	2	3	6	1	3	3	Visual Designer
R-TEC-20	3	4	12	2	4	8	Systems Engineer
R-TEC-21	3	3	9	2	3	6	Chief Control & Stability
R-TEC-22	3	4	12	2	4	8	Chief Ground Operations
R-TEC-23	4	5	20	2	5	10	Chief Ground Operations

Table 4.3: Riskmap prior to mitigation.

Very High	-	9	1,3,8,10,11,13,18,22	12,23	2,14	
High	-	-	20	5,7,15,17	-	
Medium	-	19	6,21	4	-	
Low	-	-	-	-	-	
Negligible	-	-	-	-	-	
		Remote	Rare	Unlikely	Possible	Likely

Table 4.4: Riskmap after mitigation.

Very High	-	8,10,18,23	-	-	-	
High	-	3,11,12,17,20,22	-	-	-	
Medium	19	1,6,7,21	5,13	2	-	
Low	-	-	4,9	15	14	
Negligible	-	-	-	-	-	
		Remote	Rare	Unlikely	Possible	Likely

Finally, Table 4.3 and Table 4.4 give an overview of the effect of the mitigation strategy of each risk, with the columns indicating the likelihood of each risk event occurring and the rows indicating the impact that the risk event has on the project.

4.3. Subsystem Requirements

In order to help ensure that the previously-identified risk events do not occur, subsystem requirements that try to mitigate the risks can be defined. These can be found in Table 4.5, with the risk associated with the requirement also mentioned in the table. Each risk has at least one requirement associated with it. The compliance of each

of these requirements is done in the respective subsystem's section.

Table 4.5: Subsystem requirements derived from the technical risks.

Requirement Identifier	Requirement	Risk Identifier
REQ-OPE-04	The aircraft shall be able to glide with a 9:1 glide ratio.	R-TEC-13
REQ-AVI-16	The avionics subsystem shall include a sensor capable of measuring flight loads with an accuracy of +0.1 G.	R-TEC-10
REQ-AVI-17	The cockpit shall indicate the measured flight load.	R-TEC-10
REQ-PRP-14	The propulsion subsystem of the aircraft shall provide access for a pre-flight inspection.	R-TEC-03, R-TEC-04
REQ-PRP-17	The propulsion subsystem noise level in effective perceived noise in decibels (EPNdB) shall be lower than 92 EPNdB during takeoff.	R-TEC-06
REQ-PRP-18	The propulsion subsystem overflight noise level shall be lower than 90 EPNdB.	R-TEC-06
REQ-PRP-19	The propulsion subsystem approach noise level shall be lower than 95 EPNdB.	R-TEC-06
REQ-PRP-21	The propulsion subsystem shall be capable of providing sufficient thrust for hovering after the loss of 1 motor.	R-TEC-14, R-TEC-03, R-TEC-04, R-TEC-14
REQ-PRP-22	The propulsion subsystem shall be capable of providing sufficient thrust for hovering after the loss of 1 propeller.	R-TEC-14, R-TEC-03, R-TEC-04
REQ-PRP-23	The propulsion subsystem motors shall have a fire retarding subsystem	R-TEC-03, R-TEC-04
REQ-PRP-24	The propulsion subsystem motors shall self-contain a fire for a minimum of 5 minutes.	R-TEC-03, R-TEC-04
REQ-EMP-01	The empennage shall ensure the aircraft remains controllable in every motor failure mode.	R-TEC-14
REQ-FUS-14	The fuselage cabin shall include a fire extinguisher.	R-TEC-12
REQ-LDG-06	The landing gear shall be able to land on asphalt without impairing its functioning for subsequent flights.	R-TEC-15
REQ-STR-01	As per the CS 25.303 regulations, a safety factor of 1.5 shall be applied to the prescribed limit loads which are considered external loads on the structure.	R-TEC-10
REQ-STR-02	All structural parts need be inspectable using non-destructive methods.	R-TEC-05
REQ-STR-03	All structural parts need be maintainable using non-destructive methods.	R-TEC-05
REQ-STR-04	All wooden components outside the interior cabin shall reach EN 335 Use Class 3 specifications.	R-TEC-07
REQ-STR-05	All wooden components shall be treated to Euro Class B.	R-TEC-12
REQ-STR-06	Outward facing surfaces have to have an electrical resistance of max $2.5m\Omega$.	R-TEC-09
REQ-STR-09	The structure shall not buckle when the aircraft is loaded at maximum take off weight.	R-TEC-03, R-TEC-04
REQ-STR-10	The structure shall not yield when the aircraft is loaded at maximum take off weight.	R-TEC-03, R-TEC-04
REQ-STR-11	The structure shall not fracture when the aircraft is loaded at maximum take off weight.	R-TEC-03, R-TEC-04
REQ-STR-12	The structure shall not experience vibrations at its natural frequency.	R-TEC-03, R-TEC-04
REQ-STR-16	The production process of the structure shall comply with ISO 9002.	R-TEC-2
REQ-BAT-01	The battery shall fully power the aircraft's operations until end-of-life.	R-TEC-13
REQ-BAT-07	The battery shall be protected from the environment as per IP67 standards.	R-TEC-11
REQ-BAT-08	The battery shall be able to self-contain a fire for a minimum of 5 minutes.	R-TEC-11
REQ-BAT-13	The battery system shall not have a single point of failure.	R-TEC-03, R-TEC-13
REQ-LAN-01	The landing pad shall have a safety area* with a diameter of at least 2 times the HAROLD maximum dimension.	R-TEC-16
REQ-CHA-07	A standard maintenance routine of the charging unit shall not take longer than 4 hours per unit by one mechanic.	R-TEC-05
REQ-SYSAC-86	The aircraft shall comply with the EASA "Means of Compliance with the Special Condition VTOL".	R-TEC-1

Chapter 5 | Design Requirements & Constraints

This chapter presents the requirements and constraints guiding the design of the HAROLD and its ground station. On a first level, the user requirements presented in Section 5.1 point to the main characteristics the design shall have. These user requirements were derived from the user needs, and provided as a starting point for the design. The user requirements, however, do not constrain the design sufficiently, which is why a level of detail is added with the system requirements, presented in Section 5.2. These requirements flow down not just from the aforementioned user requirements, but also from the market, risk, and functional considerations presented in Chapter 2, Chapter 3, and Chapter 4, respectively.

5.1. User Requirements

The user requirements guiding the design are presented in Table 5.1, and were provided at the start of the design as conditions to be met by the design. The identifier corresponding to each requirement is presented, together with the requirement itself, and whether it is verified or not.

The requirements that have both a checkmark, as well as a cross, are partially compliant, meaning that there are subsystem requirements that comply with this requirement and subsystem requirements that do not at this stage of the design. In some cases, the non-compliance only originates from the fact that an objectively comprehensive verification test cannot be completed for this requirement.

Table 5.1: User Requirements Compliance Matrix.

Identifier	Requirement	Compliance/ Reason for removal
REQ-USR-01	The aircraft shall be able to transport 6 passengers, including the pilot, with an average weight of 80 kg per passenger.	✓
REQ-USR-02	The aircraft shall have a flight range of 200 km.	✓
REQ-USR-03	The aircraft shall have the ability to fly autonomously	✓
REQ-USR-04	The aircraft weight without passengers and pilot shall be less than 3000 kg.	✓
REQ-USR-05	The aircraft shall be able to take off vertically.	✓
REQ-USR-06	The aircraft shall be able to land vertically.	✓
REQ-USR-07	The aircraft shall have a maximum cruise speed of 250 km/h	✓
REQ-USR-08	The aircraft shall have a maximum turnaround time of 2 hours.	✓
REQ-USR-09	The aircraft shall have a maximum flight altitude of 1 km	✓
REQ-USR-10	The aircraft shall be able to fly in wind speeds up to 60 km/h in all directions	✓
REQ-USR-11	The aircraft shall have an operational temperature range of -20°C to 47°C.	✓
REQ-USR-12	The aircraft shall be powered by a battery.	✓
REQ-USR-13	The aircraft shall use safe battery options.	✗
REQ-USR-14	The aircraft shall be able to perform an emergency landing in case of power failure.	✗
REQ-USR-15	The design shall use CO ₂ capturing wood as a renewable structural material.	✓/✗
REQ-USR-16	The design shall suggest end-of-life options for battery and structures.	✗
REQ-USR-17	The design shall include emission-free charging stations powered by renewable energy.	✗
REQ-USR-18	The cost per vehicle shall be lower than 1,000,000 EUR.	Changed to REQ-USR-21
REQ-USR-19	The structural manufacturing costs per vehicle shall be lower than 150,000 EUR	Changed to REQ-USR-22
REQ-USR-20	The construction costs per ground station shall be lower than 1,000,000 EUR	✗
REQ-USR-21	The cost per vehicle shall be lower than 2,500,000 EUR.	✓
REQ-USR-22	The structural manufacturing costs per vehicle shall be lower than 300,000 EUR	✗

5.2. System Requirements

The aforementioned user requirements lead, together with the contents of Chapter 2, Chapter 3, and Chapter 4, to the system requirements presented in Table 5.2. The requirements and identifiers are presented below in the shape of a compliance matrix, with a reference to the source of each requirement, where it is covered in the report, and whether it is verified at this stage in the design.

Table 5.2: System Requirements Compliance Matrix.

Identifier	Requirement	Source(s)/Reason for removal	Compliance
REQ-SYS-AC-01	The aircraft shall be able to transport 6 passengers, including the pilot	REQ-USR-01	✓
REQ-SYS-AC-02-A	The aircraft shall be able to carry a design payload of 480 kg.	REQ-USR-01	✓
REQ-SYS-AC-02-B	The aircraft shall be able to carry a maximum payload of 600 kg.	REQ-USR-01	✓
REQ-SYS-AC-03	The aircraft's weight without passengers and pilot shall be under 3,000 kg.	REQ-USR-04	✓
REQ-SYS-AC-04	The aircraft shall have an entrance for passengers and pilot.	MKT-07	✓
REQ-SYS-AC-05	The aircraft shall allow for the storage of 10 kg of luggage per passenger.	MKT-07	✓
REQ-SYS-AC-06	The aircraft shall have a flight range of at least 200 km throughout its lifetime, carrying its design payload and with neutral wind conditions.	REQ-USR-02	✓
REQ-SYS-AC-07	The aircraft shall be able to reach a cruise speed of 250 km/h	REQ-USR-07	✓
REQ-SYS-AC-08	The aircraft shall have a maximum flight altitude of 1 km above sea level.	REQ-USR-09	✓
REQ-SYS-AC-09	The aircraft shall be able to take off vertically.	REQ-USR-05	✓
REQ-SYS-AC-10	The aircraft shall be able to provide more lift than its maximum take off weight.	F-AC-2.2, F-AC-2.3	✓
REQ-SYS-AC-11	The aircraft shall be able to provide variable levels of lift.	F-AC-2.3.1	✓
REQ-SYS-AC-12	The aircraft shall be able to switch from vertical flight into climbing flight.	F-AC-2.3.2	✓/X
REQ-SYS-AC-13	The aircraft shall be able to provide variable levels of thrust.	F-AC-2.3.2	✓/X
REQ-SYS-AC-14	The aircraft shall be able to control its flight path angle.	F-AC-2.3.2	✓
REQ-SYS-AC-15	The aircraft shall be able to switch from climbing flight into horizontal flight.	Included in REQ-SYS-AC-14	N/A
REQ-SYS-AC-16	The aircraft shall be able to provide the thrust required to sustain flight in all flight profile conditions.	F-AC-2.2, F-AC-2.3, F-AC-2.4, F-AC-2.7	✓
REQ-SYS-AC-17	The aircraft shall be able to maintain its attitude in horizontal flight.	F-AC-2.4.2	✓
REQ-SYS-AC-18	The aircraft shall be able to be trimmed in cruise condition.	F-AC-2.4.2	✓
REQ-SYS-AC-19	The aircraft shall be able to switch from horizontal flight into descending flight.	Included in REQ-SYS-AC-14	✓
REQ-SYS-AC-20	The aircraft shall be able to switch from descending flight into vertical flight.	F-AC-2.5.3	X
REQ-SYS-AC-21	The aircraft shall be able to land vertically.	REQ-USR-06, F-AC-2.8	✓
REQ-SYS-AC-22	The aircraft shall be able to rotate around the yaw axis in vertical flight.	F-AC-2.11.3	✓
REQ-SYS-AC-23	The aircraft shall be able to control its movement along all three body axes in vertical flight.	F-AC-2.11.3	✓/X
REQ-SYS-AC-24	The aircraft shall be able to takeoff in wind speeds up to 60 km/h from all directions.	REQ-USR-10	✓/X
REQ-SYS-AC-25	The aircraft shall be able to land in wind speeds up to 60 km/h from all directions.	REQ-USR-10	✓
REQ-SYS-AC-26	The aircraft shall be able to take off from an H2 type helipad.	MKT-06	✓
REQ-SYS-AC-27	The aircraft shall be able to land on an H2 type helipad.	MKT-06	✓
REQ-SYS-AC-28	The aircraft shall have the required sensors for autonomous flight.	REQ-USR-03	✓
REQ-SYS-AC-29	The aircraft shall be able to switch from manual to autonomous flight.	REQ-USR-03	X
REQ-SYS-AC-30	Aircraft shall be able to switch from autonomous flight to manual flight.	REQ-USR-03	X
REQ-SYS-AC-31	The aircraft shall have an operational ambient air temperature range of -20 °C to 47 °C.	REQ-USR-11	X/✓
REQ-SYS-AC-32	The aircraft shall be powered by a battery.	REQ-USR-12	✓
REQ-SYS-AC-33	The aircraft shall have a rechargeable battery.	REQ-USR-12	✓/X
REQ-SYS-AC-34	The aircraft shall prevent a potential battery fire from spreading to surrounding subsystems for a minimum of 5 minutes.	R-TEC-11	✓/X
REQ-SYS-AC-35	The aircraft shall protect passengers and pilot from ambient precipitation.	MKT-07	✓
REQ-SYS-AC-36	The aircraft shall protect the passengers and pilot from winds.	MKT-07	✓

Continued on next page

Identifier	Requirement	Source(s)/Reason for removal	Compliance
REQ-SYS-AC-37	The aircraft shall allow the seating of 95% of the European population as of 2024 without touching objects other than the seat and floor.	MKT-07	✓
REQ-SYS-AC-38	The entrance of the aircraft shall have a minimum clearance of 1.5 m to the nearest element of the propulsion system.	MKT-09	✓/X
REQ-SYS-AC-39	The acceleration of the aircraft shall remain within a range of 0.5-1.5 G in a nominal flight profile.	MKT-07	✓
REQ-SYS-AC-40	The aircraft shall accommodate the communication between the pilot and passengers.	MKT-07	✓
REQ-SYS-AC-41	The aircraft shall allow the seating of 95% of European pilots without touching objects unrelated to piloting the aircraft.	Not a constant requirement	-
REQ-SYS-AC-42	The aircraft shall allow the pilot to reach all the controls in the cockpit from a single position.	MKT-05	X
REQ-SYS-AC-43	The aircraft shall provide a longitudinal visibility range of at least -15 ° to 15 °.	R-TEC-16	✓
REQ-SYS-AC-44	The aircraft shall provide a directional visibility range of at least -90 ° to 90 °.	R-TEC-16	✓
REQ-SYS-AC-45	The aircraft shall have conventional responses to pilot input (e.g. moving controls forward pitches the nose down).	MKT-08	✓
REQ-SYS-AC-46	The aircraft shall be longitudinally statically stable.	R-TEC-01	✓
REQ-SYS-AC-47	The aircraft shall be directionally statically stable.	R-TEC-01	✓
REQ-SYS-AC-48	The aircraft shall be able to attain the full range of angles of attack of the required mission profile.	R-TEC-01	✓
REQ-SYS-AC-49	The aircraft shall be able to attain the full range of sideslip angles of the required mission profile.	R-TEC-01	✓
REQ-SYS-AC-50	The aircraft shall be able to attain the full range of required roll angles of the required mission profile.	R-TEC-01	✓
REQ-SYS-AC-51	The aircraft shall provide the pilot with conventional flight information.	Changed to REQ-SYS-AC-91,92,93	-
REQ-SYS-AC-52	The aircraft shall indicate the state of charge of the battery.	REQ-USR-12	✓
REQ-SYS-AC-53	The aircraft shall have an Automatic Dependent Surveillance-Broadcast system.	MTK-04	✓
REQ-SYS-AC-54	The aircraft shall have an EASA-certified ¹ radio system onboard for communication with parties outside the aircraft.	MKT-04	✓
REQ-SYS-AC-55	The aircraft shall be able to land autonomously at the nearest ground station in case of a non-system-related emergency.	MKT-09	X
REQ-SYS-AC-56	The aircraft shall be able to land without pilot and passenger fatalities in case of a power failure.	Depending on the flight phase requirement is not feasible.	-
REQ-SYS-AC-57	The aircraft flight profile shall comply with the section "MOC – SUBPART B – FLIGHT" of the EASA "Second Publication of Means of Compliance with the Special Condition VTOL".	Changed to REQ-SYS-AC-86	-
REQ-SYS-AC-58	The aircraft structure subsystem shall comply with the section "MOC – SUBPART C – STRUCTURES" of the EASA "Second Publication of Means of Compliance with the Special Condition VTOL".	Changed to REQ-SYS-AC-86	-
REQ-SYS-AC-59	All aircraft subsystems shall comply with the section "MOC – SUBPART D – DESIGN AND CONSTRUCTION" of the EASA "Second Publication of Means of Compliance with the Special Condition VTOL".	Changed to REQ-SYS-AC-86	-
REQ-SYS-AC-60	The aircraft propulsion subsystem shall comply with the section "MOC – SUBPART E – LIFT/THRUST SYSTEM INSTALLATION" of the EASA "Second Publication of Means of Compliance with the Special Condition VTOL".	Changed to REQ-SYS-AC-86	-
REQ-SYS-AC-61	The aircraft cockpit subsystem shall comply with the section "MOC – SUBPART G – FLIGHT CREW INTERFACE AND OTHER INFORMATION" of the EASA "Second Publication of Means of Compliance with the Special Condition VTOL".	Changed to REQ-SYS-AC-86	-
REQ-SYS-AC-62	The aircraft shall have a maximum turnaround time of 2 hours.	REQ-USR-08	✓
REQ-SYS-AC-63	A standard pre-flight inspection routine of the aircraft shall not take longer than 10 minutes.	MKT-07	✓
REQ-SYS-AC-64	The propulsion system of the aircraft shall provide access for a pre-flight inspection.	Changed to REQ-SYS-AC-85	-
REQ-SYS-AC-65	The battery system of the aircraft shall provide access for a pre-flight inspection.	Changed to REQ-SYS-AC-85	-
REQ-SYS-AC-66	The control surface system of the aircraft shall provide access for a pre-flight inspection.	Changed to REQ-SYS-AC-85	-
REQ-SYS-AC-67	The propulsion system of the aircraft shall provide access for maintenance.	Changed to REC-SYS-AC-84	-
REQ-SYS-AC-68	The battery system of the aircraft shall provide access for maintenance.	Changed to REC-SYS-AC-84	-
REQ-SYS-AC-69	The control surface system of the aircraft shall provide access for maintenance.	Changed to REC-SYS-AC-84	-
REQ-SYS-AC-70	The annual inspection of the aircraft shall be able to be performed in 32 working hours for one qualified mechanic, not including repairing or replacing parts.	MKT-07	X

Continued on next page

¹<https://www.easa.europa.eu/en/regulations> [cited 15.06.2024]

Identifier	Requirement	Source(s)/Reason for removal	Compliance
REQ-SYS-AC-71	The aircraft take-off noise level in effective perceived noise in decibels (EPNdB) shall be lower than 92 EPNdB.	MKT-02	✗
REQ-SYS-AC-72	The aircraft overflight noise level shall be lower than 90 EPNdB.	MKT-02	✗
REQ-SYS-AC-73	The aircraft approach noise level shall be lower than 95 EPNdB.	MKT-02	✗
REQ-SYS-AC-74	At least 25% of the aircraft's airframe weight shall consist of wood.	REQ-USR-15	✓/✗
REQ-SYS-AC-75	The aircraft shall be able to be manufactured compliant to EASA Part 21.	Changed to REQ-SYS-AC-90	-
REQ-SYS-AC-76	At the end-of-life, at least 20% of the airframe shall be repurposed.	REQ-USR-16	✓
REQ-SYS-AC-77	At end of life, the aircraft's battery shall be able to be repurposed.	REQ-USR-16	✗
REQ-SYS-AC-78	The aircraft shall have a lifespan of at least 8 years.	MKT-03	✓/✗
REQ-SYS-AC-79	The manufacturing cost per vehicle shall be less than 1,000,000 euros.	Changed to REQ-SYS-AC-94	-
REQ-SYS-AC-80	The manufacturing cost for structural parts shall be less than 150,000 euros per vehicle.	Changed to REQ-SYS-AC-95	-
REQ-SYS-AC-81	The aircraft detailed conceptual design shall be completed by 10 students.	Not a system requirement.	-
REQ-SYS-AC-82	The aircraft detailed conceptual design shall be completed in 10 weeks.	Not a system requirement.	-
REQ-SYS-AC-83	The aircraft detailed conceptual design shall be completed using TU Delft facilities.	Not a system requirement.	-
REQ-SYS-AC-84	The aircraft shall provide access for maintenance.	F-AC-2.14	✓/✗
REQ-SYS-AC-85	The aircraft shall provide access for pre-flight inspection.	F-AC-2.13	✓
REQ-SYS-AC-86	The aircraft shall comply with the EASA "Means of Compliance with the Special Condition VTOL" [8].	MKT-04	✗/✓
REQ-SYS-AC-87	The aircraft shall protect the passengers, pilot and all subsystems from lightning strikes.	R-TEC-09	✓
REQ-SYS-AC-88	The aircraft shall be able to perform an emergency horizontal landing (as discussed in 7) in less than 8 minutes.	R-TEC-12	✓
REQ-SYS-AC-89	The manufacturing of the aircraft shall comply with ISO 9002 guidelines ² .	MKT-04	✓
REQ-SYS-AC-90	The aircraft shall be able to operate in rain conditions with an intensity of at least 4 mm/hour.	MKT-07	✓/✗
REQ-SYS-AC-91	The aircraft shall provide the pilot with the indicated airspeed measurements.	MKT-05	✓
REQ-SYS-AC-92	The aircraft shall provide the pilot with live pressure altitude measurements.	MKT-05	✓
REQ-SYS-AC-93	The aircraft shall provide the pilot with live heading information.	MKT-05	✓
REQ-SYS-AC-94	The manufacturing cost per vehicle shall be less than 2,000,000 euros.	REQ-USR-21	✓
REQ-SYS-AC-95	The manufacturing cost for structural parts shall be less than 300,000 euros per vehicle.	REQ-USR-21	✗
REQ-SYS-AC-96	The aircraft shall have an absolute cruise angle that is below 5 degrees.	MKT-07	✗
REQ-SYS-AC-97	The aircraft shall withstand all loads within the flight envelope	R-TEC-10	✓

²<https://www.iso.org/obp/ui/en/#iso:std:iso:ts:9002:ed-1:v1:en> [cited 25.06.2024]

Chapter 6 | Concept Selection

In this chapter, four potential aircraft concepts and three potential ground station concepts are presented in Section 6.1. In order to select the best concept, criteria and their weights are selected for a trade-off in Section 6.2. This trade-off was then performed for both the aircraft and ground station.

6.1. Concept Description

In order to find the most suitable concept for the HAROLD aircraft and its corresponding ground station, it was important to first explore as many concepts as possible; this was done by building a design option tree (DOT) for both the aircraft and the ground station energy supply. From the aircraft DOT, four concepts were selected, and from the ground station DOT, three concepts were selected. The full concept generation and selection procedure can be found in the midterm report [1]. Each one of the chosen concepts is explored in more detail in Section 6.1.1 and Section 6.1.2.

6.1.1. Aircraft Concepts

The four concepts selected from the aircraft DOT are presented in this subsection: the Swift, the Canard, the Dragonfly and the Hummingbird.

Swift: The first concept, the Swift (shown in Figure 6.1), is a design that focuses on simplicity. As such, it is the aircraft that most resembles the aircraft used for civil aviation. As can be seen in Figure 6.1, the Swift has a main wing and a conventional tail. In addition, this concept only uses fixed propellers. For horizontal flight, the aircraft uses a vertical rotor placed on its nose. For vertical flight, the aircraft has two horizontal rotors placed inside the wing (these have deployable hatches that are used to make the wing shape more aerodynamic during horizontal flight) and two additional horizontal rotors at the wing tips.

Canard: As indicated by the name, this aircraft concept uses a canard for its horizontal stabiliser. As can be seen in Figure 6.2, the canard is placed in front of the main wing. A vertical stabiliser is also placed at the back of the aircraft so as to ensure controllability and stability in yaw. In order to propel itself during both horizontal and vertical flight, the Canard has two tilting propellers on the edges of the main wing, and six additional rotors on the canard. In this case, it is not the rotors that are tilting, but rather the full canard surface.

Dragonfly: The unique feature of the Dragonfly concept is its tandem wing; one wing is placed at the front of the aircraft, while the other is placed at the back of the aircraft. This can be seen in Figure 6.3. Only a vertical tail is needed for this aircraft since one of the two wings can be used as a horizontal stabiliser. In terms of propulsion, this concept uses only tilting rotors. It has two rotors per wing, with the rotors of the front wing being placed slightly more inward so as to reduce the induced wake effects. This inward placement of the front rotors allows the front wing tips to rotate with the rotor; this is done so as to reduce drag during vertical flight. Due to the small size of the wing tips, the mass of the additional rotation mechanism required for this rotation should be relatively small and thus not affect the performance of the aircraft. For redundancy, an additional pusher tilt-rotor is positioned at the rear of the aircraft.

Hummingbird: The final concept, the Hummingbird, can be distinguished by its V-tail, depicted in Figure 6.4. The aircraft has a main wing with two tilting rotors placed at tips of the wing, however these need to be complemented during vertical flight. As such, two additional horizontal rotors must be added to the aircraft. Having a V-tail is the best way to do this as it allows for the engines to be placed on the tips of the tail, where they are outboard of the fuselage and thus not in its wake, while still being lighter than alternative tails such as the T-tail.

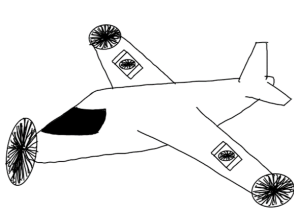


Figure 6.1: Swift concept aircraft

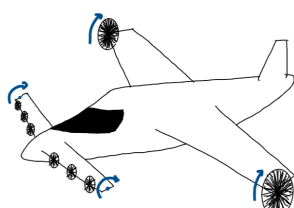


Figure 6.2: Canard concept aircraft

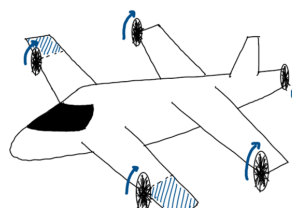


Figure 6.3: Dragonfly concept aircraft

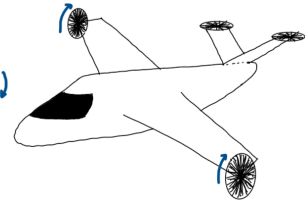


Figure 6.4: Hummingbird concept aircraft

6.1.2. Ground Station Concepts

The three concepts selected from the ground station energy supply DOT are presented in this subsection: using a solar panel/ grid hybrid, using hydrogen, and using a grid connection.

Solar panel / grid hybrid: For this first concept, the ground station energy supply comes from two sources. 50 % of the power comes from solar panels, and the remaining 50 % from the local electrical grid. This grid connection is necessary as it is not always possible to ensure that the solar panels will provide the required energy due to weather and location concerns.

Hydrogen: In order to power the ground station using hydrogen, it is necessary for the ground station to have 1608 kg of hydrogen storage on-site. This amount is sufficient to supply energy for a week in which the charging station is constantly being using. The hydrogen shall be outsourced, with deliveries to the ground station occurring once a week. In addition, this ground station concept has a fuel cell electric generator so as to generate electricity from the hydrogen.

Grid connection: The final ground station concept is entirely powered by the local electrical grid. As such, it only requires a connection to the grid.

6.2. Trade-Off

In order to perform a trade-off, it is first important to determine which relevant criteria to use. The project objectives, presented in Chapter 1, were used to guide the selection of criteria. After the criteria were selected, weights were given to each criterion. The weight of each criterion has a maximum value of 5 and is based on the relevance of the criterion to the project objectives, risks and stakeholder requirements. Any criteria in which all concepts scored similarly were then discarded since they do not add value to the trade-off. Each concept was then evaluated for each criterion, and the best-performing concept was selected for the subsequent phases of the design. The full calculations and method used to evaluate the criteria can be found in the midterm report [1].

6.2.1. Aircraft Criteria Selection

For the aircraft trade-off, five criteria were defined to encompass the primary and secondary project objectives: energy consumption, size, redundancy, VTOL controllability and aesthetics. In each case, the risk associated to the criterion is determined and, based on the severity of the risk determined in Chapter 4, a weight reflecting this severity is assigned to the criterion; this stems from the design philosophy introduced in Chapter 1.

Energy Consumption: This criterion refers to the amount of energy needed by the aircraft concept to fly the required range of 200 km (from REQ-STK-02) plus a 20 km diversion range. When looking at the risk events described in Table 4.1, the risk event associated with this criterion is R-TEC-17. As explained throughout Chapter 4, this risk has a high severity and is the most severe one from all of the trade-off criteria. Having a high energy consumption would result in a larger battery being required; this would affect almost every subsystem of the aircraft, however the most critical risk is the snowball effect it would induce: an increase in battery size results in an increase in aircraft mass which in turn results in an increase of the battery size. If the aircraft is to meet the mass specified in REQ-STK-04, it is important to minimise the energy consumption. As such, the energy consumption criterion is assigned a weight of 5.

Size: This criterion refers to the wing span of the aircraft. The wingspan of the aircraft influences its intra-city flight capabilities, a feature of the aircraft that is specified by PO1 and REQ-STK-24; a large wingspan would result in the aircraft being difficult to use in cities as, beyond being more difficult to manoeuvre in such tight spaces, it is unlikely that the aircraft will have a place to land. This is because it will require a large landing pad, and with the limited space in cities it is unlikely that enough landing pads can be constructed to make the aircraft a practical transportation option. This consequence is associated with the risk event R-TEC-20 found in Chapter 4. Since R-TEC-20 has a medium severity, this criterion is assigned a weight of 3.

Redundancy: This criterion refers to the level of redundancy each concept has incorporated in its design. This is essential for safety which, as specified by PO2, is vital to the design. The aircraft redundancy was measured by analysing the probability and consequences of potential non-fatal engine failures. As such, this criterion is also related to REQ-STK-14 because it evaluates the possibilities for emergency landings. This criterion is associated with the risk event R-TEC-14 defined in Chapter 4 which looks at non-fatal engine failures; the risk event has a medium severity, and as such the criterion is associated a weight of 3.

VTOL Controllability: This criterion analyses the manoeuvrability of the aircraft during the vertical take-off and landing flight phases. This influences both REQ-STK-05 and REQ-STK-06. The controllability of the aircraft is

found by looking at the moment generated by different thrust forces about each axis; the larger the moment, the easier and less fuel-intensive it is to control the aircraft. This criterion corresponds to the risk event R-TEC-21 in Chapter 4. This risk event has a fairly low severity, and as such the criterion is assigned a weight of 2.

Aesthetics: The final criterion evaluates how appealing the aircraft design is to the wider public. This criterion is associated with the risk event R-TEC-19 in Chapter 4 which has a very low severity, as a design that is not aesthetically pleasing does not affect aircraft performance but could affect how easy it is to sell the aircraft. As such, this criterion is assigned a weight of 1.

6.2.2. Aircraft Criteria Evaluation

The method used to evaluate each of the aircraft criteria is explained here, and the score of each concept is given. For the scoring, the method explained in the design philosophy (described in Chapter 1) was used; for each criterion, the best performing concept gets a score of 1, and a hard limit was chosen per criterion to determine what a score of zero would be. The remaining scores were linearly extrapolated.

Energy Consumption Evaluation: In order to evaluate this criterion, the energy consumption of each aircraft concept while flying a preliminary flight profile was calculated. This profile is found in Figure 6.5. In order to calculate the energy consumption, first the power required to fly each phase of the flight profile was calculated, and then the power required per phase was integrated over the duration of the phase, resulting in the energy consumption. The total energy consumed by each aircraft concept can be found in Table 6.1. For the scoring, the concept with the lowest energy consumption was automatically assigned a score of 1. A score of 0 corresponds to an energy consumption that leads to a battery weight to maximum takeoff weight ratio, $\frac{W_{bat}}{W_{TO}}$, of 0.4. This value was chosen as, according to Wolleswinkel [9], it is a limit value for electric aircraft. The remaining concepts are linearly extrapolated from this range, and as such the higher the score, the lower the energy consumption.

Size Evaluation: The span of each concept can be calculated using the aircraft mass calculated when evaluating the energy consumption criterion, an assumed wing loading value and an assumed aspect ratio value. The expression used is shown in Equation 6.1, where the value of k used accounts for how much lift is being produced by the main wing. For example, with the dragonfly, $k = 0.5$ since the concept has two wings, with each wing producing 50% of the total lift. The score was calculated by setting the minimum score of 0 to be the size of the H2 helipad (derived from REQ-SYS-AC-26 and REQ-SYS-AC-27). Subsequently, the maximum score of 1 was defined as the smallest span between all concepts, and the remaining concepts are scored in the same way as for the Energy Consumption criterion. The sizes of each concept can be found in Table 6.1.

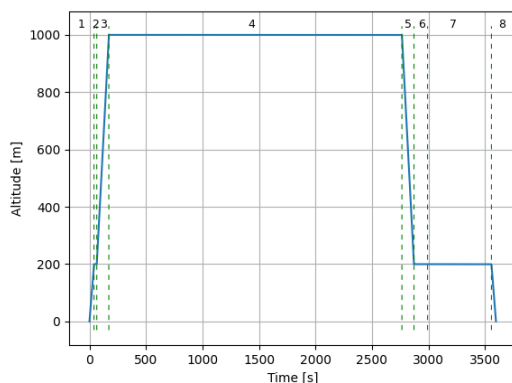


Figure 6.5: Preliminary flight profile.

$$b = \sqrt{AR \cdot \frac{W}{W/S}} \cdot k \quad (6.1)$$

Redundancy Evaluation: The redundancy criterion was evaluated by examining different failure cases. For every concept, the limiting cases of engine and propeller failures are considered. In order to determine which failure cases were the worst ones, two factors were considered: the severity of the failure (in terms of the failure's consequences) and the probability of the failure occurring. Both of these were scored on a scale from 0 to 1, with 1 being the most severe or probable. Then, the probability and severity scores were multiplied so as to find a final score for each failure case. Finally, the average severity-probability value for all of the failure cases was found for each concept; these values can be found in Table 6.1 under the "severity-probability" column. In order to score the concepts, the method described in the design philosophy was employed, with the concept having the lowest severity-probability score being assigned a 1.

VTOL Controllability Evaluation: In order to ensure the safety and comfort of the passengers, one must consider controllability. For the preliminary trade-off, only the roll stability of each concept was considered, as determining yaw and pitch sensitivity would require a more detailed aircraft design. To judge the controllability of each concept, the maximum moment that can be provided by the engines during vertical flight was calculated; this was calculated by using preliminary measurements of the total thrust to be provided by the propulsion system per engine and the initial estimation of the wingspan for a moment arm. This value was then divided by the moment of area (calculated by assuming a cylindrical fuselage and a hollow wing) to find the maximum $\frac{M}{I}$ ratio. It was determined that the highest moment-to-moment-of-area ratio would be the most controllable, with the concept with the highest ratio being assigned a score of 1 and a ratio equal to zero being assigned a score of 0. The results of the different concepts can be found in Table 6.1.

Aesthetics Evaluation: To analyse the aesthetics of each aircraft concept, external input was required. As such, an anonymous poll was conducted with participants that have both technical and non-technical backgrounds. A concept would get a score of 0 in case it received no votes at all, and the concept with the most votes was assigned a score of 1. Linear interpolation was used to determine the scores of the remaining concepts. The results of the poll are summarised in Table 6.1.

Table 6.1: Values of the aircraft concepts for each of the trade-off criteria.

Concept	Energy Consumption [kWh]	Span [m]	Severity-probability	Maximum value $\frac{M}{I}$	Number of votes
Swift	232	15.2	0.2533	1683	11
Canard	198	13.6	0.2171	1556	13
Dragonfly	196	10.8	0.2475	1049	23
Hummingbird	328	11.8	0.2767	1131	22

6.2.3. Ground Station Criteria Selection

For the ground station trade-off, three criteria were defined to encompass the project objectives: the surface area required, the power system carbon emissions and the energy cost.

Surface Area: This criterion considers the total surface area that the ground station concept is projected to need. A large surface area will not make the project infeasible, however it will make it difficult to build ground stations in urban areas, thus not complying with PO1. This criterion is linked to the risk event R-TEC-22 from Chapter 4, which has a medium severity. As such, the criterion is assigned a weight of 3.

Carbon Emissions: This criterion evaluates the CO₂ emissions of the ground station concept during the operational time of the station; the emissions are measured in kg/day. As indicated by PO2, sustainability is the main driver of the design, and the energy used to charge the aircraft and run the ground station is translated into operational carbon emissions which in turn affect the lifetime carbon emissions. This criterion is assigned to the risk event R-TEC-23 which has a very high severity, as high emissions would defeat the point of the project, which strives for sustainable aviation. To reflect this, the criterion was assigned a weight of 5.

Energy Cost: This criterion covers the estimates the initial installation and construction costs of the station per kWh of energy. As per the market analysis in Chapter 2, in order to make the ground station accessible to a larger client base, it is important to minimise the cost. However, the energy cost is of lower importance than the functioning of the ground station itself. This corresponds to the risk event R-TEC-18 given in Chapter 4, which has a fairly low severity. As such, this criterion is assigned a weight of 2.

6.2.4. Ground Station Criteria Evaluation

The method used to evaluate each of the ground station criteria is explained here, and the score for each concept is also given. The scoring follows the same method as in Section 6.2.2, which is based off of the design philosophy from Chapter 1.

Surface Area: In order to analyse this criterion, the surface area required by each ground station concept must be calculated. The area takes into account everything required for the energy generation process; for example, for the hydrogen concepts this area comprises the space required for hydrogen storage and a fuel cell electric generator. The total area and corresponding score for each concept is given in Table 6.2.

Carbon Emissions: The scoring of each concept for this criterion depends on the amount of emissions produced by the energy source. For the solar panel / grid hybrid, solar power emits no CO₂, thus only the power

sourced from the grid is considered. For the hydrogen concept, the emissions from the hydrogen deliveries are considered. The total carbon emissions per concept can be found in Table 6.2.

Energy Cost: In order to analyse this criterion, the initial installation and construction costs must be analysed for each concept. For example, energy cost of the solar power / grid hybrid consists of the cost of the solar panels, batteries and connection to the grid. The total energy cost for each concept can be found in Table 6.2.

Table 6.2: Values of the ground station concepts for each of the trade-off criteria.

Concept	Surface area [m ²]	Carbon emissions [kg/day]	Energy cost [€/kWh]
Solar panel / grid hybrid	2698.29	460	196.83
Hydrogen	69.63	5.65	158.11
Grid connection	0.58	920	40.98

6.3. Selected Concepts

After having defined all of the criteria and evaluated how each concept performs for them, it is time to pick which aircraft and ground station concept will be used. This is discussed in the subsequent subsections.

6.3.1. Aircraft Selected Concept

Looking at the performance of each aircraft concept for the five criteria in Table 6.1 and the scoring explanations given throughout Section 6.2.2, a trade-off table can be generated. This can be found in Table 6.3.

Table 6.3: Aircraft concept trade-off table.

	Energy consumption	Size	Aesthetics	Redundancy	VTOL Controllability	Total
<i>Weights</i>	5	3	1	3	2	<i>out of 14</i>
Swift	0.759	0.663	0.478	0.862	1	10.847
Dragonfly	1	1	1	0.885	0.623	12.9
Canard	0.989	0.784	0.565	1	0.925	12.715
Hummingbird	0.145	0.922	0.957	0.774	0.672	8.114

From Table 6.3, it becomes apparent that the the Dragonfly and the Canard are the main contenders for the final design, whilst the Hummingbird and the Swift have an unsatisfactory performance. The Dragonfly performs particularly well in terms of energy consumption, size and aesthetics; this is mainly due to the concept having two shorter wings rather than one longer wing. The Canard, instead, has very good scoring for the redundancy and VTOL controllability criteria due to its high number of engines, and it also scores well in terms of energy consumption. The score of these two concepts is too close for one to be selected as a winner, as such a sensitivity analysis must be performed so as to reduce the uncertainty of the scoring. Since the energy consumption criterion is the criterion with the highest weight, this is the one for which the analysis shall be performed using a Monte Carlo analysis.

For each concept, 10000 C_{D_0} values were randomly generated from a normal distribution with a mean of 0.03 and a standard deviation of 0.05; the C_{D_0} was varied because the initial value (0.03) was not a design choice but rather was obtained as an estimation from Roskam [10], and thus risked being the most incorrect value in the calculation. The resulting mean of the distribution of energy consumption values reflected the score that each concept had been assigned in the trade-off, with the Dragonfly and the Canard configuration having almost the exact same mean value and energy consumption value. This is coherent with their almost identical scores, with the dragonfly having a slightly better score than the canard. Another Monte Carlos analysis was carried out, but this time with a variation of the criteria weights. It was found that even when the criteria weights had varied by 70 %, only the Dragonfly and the Canard ever won the trade-off.

Due to the Canard and Dragonfly concepts having such a close scoring, it is difficult to pick one of the concepts as the winner. As such, a better course of action would be to create a better-performing concept that combines the best aspects of both concepts, resulting in the HAROLD; a drawing of the concept can be seen in Figure 6.6. This aircraft maintained the tandem wing of the Dragonfly concept, but incorporated the propulsion system of the Canard. In order to ensure that the HAROLD is indeed the best concept out of the three, the trade-off was performed again between the three concepts (with the exception of the aesthetics criterion since it was not possible to redo the poll). The trade-off results are found in Table 6.4. A Monte-Carlo analysis was also

performed for this trade-off, and it was found that the HAROLD outperformed the Canard and Hummingbird concepts even when varying the weights by $\pm 70\%$. Thus, the HAROLD is the final selected aircraft concept.

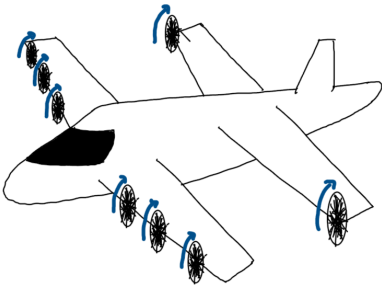


Figure 6.6: The HAROLD aircraft configuration.

Table 6.4: Aircraft second trade-off table including the hybrid option.

	Energy	Size	Redund.	Controllab	Total
<i>Weights</i>	5	3	3	2	<i>out of 13</i>
Dragonfly	1	1	0.885	0.623	11.9
Canard	0.989	0.784	1	0.925	12.149
HAROLD	0.989	1	1	0.61	12.168

6.3.2. Ground Station Selected Concept

Looking at the performance of each ground station concept for the three criteria in Table 6.2 and the scoring explanations given throughout Section 6.2.4, a trade-off table can be generated. This can be found in Table 6.5.

Table 6.5: Ground station trade-off table.

	CO ₂ Emissions	Surface area	Energy cost	Total
<i>Weights</i>	5	3	2	<i>out of 10</i>
Hydrogen	1	0.977	0.496	8.923
Solar Panels	0.543	0.084	0.322	3.610
Grid	0.080	1	1	5.402

As can be seen in Table 6.5, the hydrogen powered concept was determined to be the best option out of the proposed ones. Compared to the other two concepts, it has the smallest environmental impact and a very small area. Even though it doesn't perform very well in terms of energy cost, the very high performance in the previous two criteria compensate for this.

Before selecting a concept, it is important to perform a sensitivity analysis to ensure that uncertainty in the scoring is low. Once again, a Monte Carlo analysis was performed in which the weights of the criteria were varied. It was found that, even at a variation limit of $\pm 70\%$, the hydrogen concept always won over the other two. Thus, the hydrogen ground station concept is selected.

Chapter 7 | Mission and Flight Profile

This chapter defines the mission to be conducted by the HAROLD, a main element from the design that affects the sizing of several subsystems, including the power and propulsion elements of the aircraft. First the operational requirements are presented in Section 7.1, followed by the assumptions related with the mission analysis in Section 7.2. This is followed by a brief description of the operational modes of the aircraft in Section 7.3, and a description of the flight profile in Section 7.4. Lastly, the analysis of the VTOL and transition phases of the aircraft is presented in Section 7.5 and Section 7.6.

7.1. Operational Requirements and Compliance Matrix

This section presents the operational requirements that have to be met by the design, and thus constrain the mission definition. These requirements stem from the user requirements, together with some system requirements and regulations. Table 7.1 presents the operational requirements the design has to meet; together with a check of compliance and a reference to where in the text is each requirement covered.

Table 7.1: Operational requirements compliance matrix.

Identifier	Requirement	Source(s)	Compliance	Method of verification
REQ-OPE-01	The aircraft shall be able to take off vertically under 60 km/h gust winds without exiting a vertical cylinder of 30 m diameter.	RAMS-09,REQ-SYS-AC-24	✓	Analysis in Section 7.5, testing during flight tests
REQ-OPE-02	The aircraft shall be able to land vertically under 60 km/h gust winds without exiting a vertical cylinder of 30 m diameter.	RAMS-09,REQ-SYS-AC-25	✓	Analysis in Section 7.5, testing during flight tests
REQ-OPE-03	The aircraft shall transition from vertical to horizontal flight.	REQ-SYS-AC-88, R-TEC-13	✓	Analysis in Section 7.6, testing during flight tests
REQ-OPE-04	The aircraft shall transition from horizontal to vertical flight.		✓	Analysis in Section 7.6, testing during flight tests
REQ-OPE-05	The acceleration of the aircraft shall remain within a range of -0.5 G to 1.5 G in a nominal flight profile.	REQ-SYS-AC-39	✓	Analysis in Section 7.4, testing during test flights
REQ-OPE-06	The aircraft shall be able to conduct a bailed landing before transitioning to vertical flight to land	EASA MOC-2-SC-eVTOL	✓	Analysis in Section 7.4, testing during flight tests
REQ-OPE-07	The aircraft shall cruise at an altitude no lower than 900 m above sea level.	EASA MOC-2-SC-eVTOL	✓	Inspection of the flight profile in Section 7.4
REQ-OPE-08	The aircraft shall cruise at an altitude no higher than 1050 m above sea level.		✓	Inspection of the flight profile in Section 7.4.
REQ-OPE-09	A nominal flight shall have a duration of less than 60 minutes	MKT-01	✓	Inspection of the flight profile in Section 7.4
REQ-OPE-10	The aircraft shall achieve a ROC of at least 5 m/s	MKT-01	✓	Analysis of the climb performance in Chapter 13
REQ-OPE-11	The aircraft shall have a nominal range of 200 km		✓	Analysis of the flight profile in Section 7.4, testing during test flights
REQ-OPE-12	The aircraft shall have a cruise velocity of 250 km/h		✓	Analysis in Section 13.3 testing during test flights.

7.2. Assumptions

The main assumptions made in the definition and analysis of the flight profile are presented below in Table 7.2 together with their expected effect.

Table 7.2: Assumptions used for the flight profile analysis.

Identifier	Assumption	Expected Effect
A-FP-01	The earth is assumed to be flat for the region covered during the mission.	Deviation in real flight path
A-FP-02	Gravity is assumed to be constant and equal to 9.81 m/s ²	Deviation in lift and drag calculations.
A-FP-03	Earth is assumed to be non-rotating.	Deviation in real flight path.
A-FP-04	Deceleration is assumed to not use energy compared with constant velocity flight.	Overestimation of energy consumption
A-FP-05	The aircraft is assumed to not use energy in countering aerodynamic moments during horizontal flight.	Underestimation of energy requirements during cruise

7.3. Operational Modes

Due to the nature of its design the HAROLD has three main operational modes. First there is the vertical mode, then transition mode, and then horizontal mode. In vertical mode the aircraft has its propellers pointing directly upwards, while in transition mode the propellers go from fully upwards to pointing forward or vice versa.

In horizontal flight, like any conventional aircraft, the HAROLD has its propellers pointing forward, providing thrust in the direction of flight. In Figure 7.1, Figure 7.2 and Figure 7.3 below a render of the aircraft in the three different operational modes is provided. These modes follow from the functional analysis presented in Chapter 3.



Figure 7.1: Aircraft in vertical mode.



Figure 7.2: Aircraft in transition mode.



Figure 7.3: Aircraft in horizontal mode.

7.4. Flight Profile

In order to size the HAROLD it is necessary to analyse the mission it is to complete. Due to the aircraft being an eVTOL, this mission presents differences from typical flight profiles. The mission profile for a typical flight with the HAROLD, or any eVTOL for that matter, starts with the vertical take-off. In the case of this aircraft after ascending vertically until height h_2 , the aircraft tilts slightly forward, climbing vertically while gaining some horizontal velocity. This horizontal velocity aids the aircraft in achieving transition, in which the aircraft is configured for conventional horizontal flight. After transition the aircraft accelerates to its climb speed, set to minimise power requirements, to then cruise. Cruise is followed by descent to transition altitude, after which transition to vertical mode and landing take place in a regular mission. Since the aircraft must be designed to performed a bailed landing according to regulations (REQ-OPE-05), the mission analysis continues with a diversion phase, which starts after descent and before transition to vertical configuration. The diversion phase takes place at the velocity for minimum power and once that is done vertical transition and landing take place. Figure 7.4 below provides a labelled flight profile sketch, with each phase and defining parameters numbered underneath. The region shaded in red refers to the flight phases only to be conducted in case of an emergency.

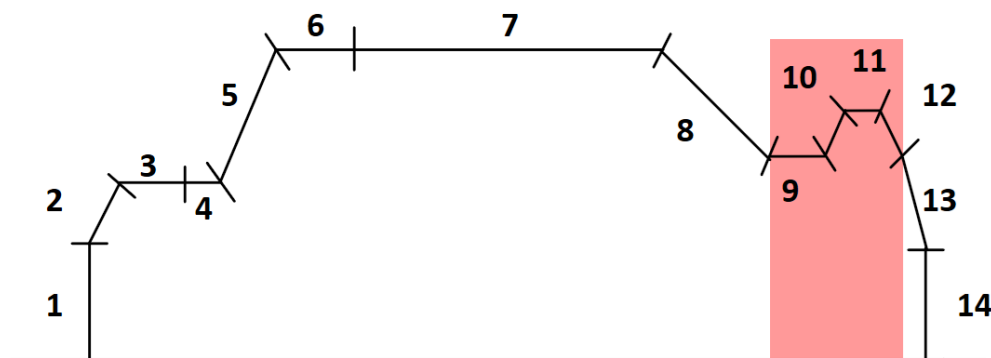


Figure 7.4: Flight profile for the HAROLD detailed mission analysis.

1. **Take-off (Vertical Mode):** In this phase the aircraft takes-off from an altitude of 0 m, accelerates to its take-off velocity v_{to} before reaching altitude h_1 and then climbs until its end of take-off altitude h_2 .
2. **Vertical climb (Transition Mode):** The HAROLD applies a slight thrust differential between front and rear motors, tilting forward to gain horizontal velocity, it climbs from h_2 to transition altitude one, h_{tr1} (this phase is covered in Section 7.5).
3. **Transition to horizontal flight (Transition Mode):** The aircraft rotates its motors from vertical configuration (pointing vertically) to horizontal configuration (pointing forward), in this process sufficient thrust is provided to accelerate to a safe velocity (this phase is detailed below in Section 7.6)
4. **Acceleration to climb velocity (Horizontal Mode):** Once in horizontal mode the aircraft accelerates to reach the velocity for minimum power at which it will climb $v_{min,P}$.
5. **Climb (Horizontal Mode):** The aircraft sets a positive rate of climb ROC and climbs from h_{tr1} to the cruise altitude h_{cr} .

6. **Acceleration to cruise (Horizontal Mode):** The aircraft accelerates in a distance $d_{acc,cr}$ to cruise velocity.
7. **Cruise (Horizontal Mode):** The aircraft covers most of the mission in this phase.
8. **Descent (Horizontal Mode):** The aircraft descends to the second transition altitude h_{tr2} , again at velocity $v_{min,P}$, and with rate of descent ROD .
9. **Balked landing (emergency) (Horizontal Mode):** In case the aircraft cannot land for any reason, it aborts landing before transitioning, covering a distance d_{balk} at $v_{min,P}$ before climbing again.
10. **Diversion climb (emergency) (Horizontal Mode):** The aircraft climbs, still at $v_{min,P}$, to diversion altitude h_{div} .
11. **Diversion (emergency) (Horizontal Mode):** The aircraft covers a distance $f_{div} \cdot R$ during its diversion, where R is the mission range.
12. **Diversion descent (emergency) (Horizontal Mode):** The aircraft descends with rate of descent ROD to the second transition altitude h_{tr2} .
13. **Transition to vertical flight (Transition Mode):** While it descends further from h_{tr2} to h_2 the aircraft rotates its propellers back, preparing for landing (this phase is covered in Section 7.6)
14. **Hover and Landing (Vertical Mode):** The aircraft first hovers during a time t_{hov} at altitude h_2 before descending at constant velocity until h_1 , and decelerating until touching down at the ground station.

The values used for the flight profile parameters are presented below, in Table 7.3.

Table 7.3: Flight profile parameters.

Parameter	Value	Unit	Rationale
h_1	20	m	Selected to limit the accelerations in take-off
h_2	30	m	Derived from EASA MOC-2-SC-eVTOL
h_{tr1}	70	m	Derived from EASA MOC-2-SC-eVTOL
h_{cr}	1000	m	Derived from REQ-USR-09
h_{tr2}	100	m	Increased from h_{tr1} to allow for a less power hungry transition
f_{div}	0.1	-	Selected to allow for diversion outside of any major European city
$d_{acc,cl}$	200	m	Set to limit required acceleration without covering excessive distance.
d_{balk}	50	m	Minimised to avoid nearby buildings while accounting for pilot reaction times.
t_{hov}	60	s	Set to allow for the take-off or removal of a vehicle in the launch pad.

7.5. eVTOL Dynamic Model

In order to understand the movement of the eVTOL when in vertical configuration, a dynamic model is created, using the system of differential equations presented below in Equation 7.1, Equation 7.2, Equation 7.3 and Equation 7.4.

$$\frac{dv_x}{dt} = \frac{1}{m} \cdot \left(T_f \cdot \sin(\alpha_t + \theta_f) + T_r \cdot \sin(\alpha_t + \theta_r) - D \cdot \frac{v_x^2}{v_x^2 + v_y^2} \right) \quad (7.1)$$

$$\frac{dv_y}{dt} = \frac{1}{m} \cdot \left(T_f \cdot \cos(\alpha_t + \theta_f) + T_r \cdot \cos(\alpha_t + \theta_r) - D \cdot \frac{v_y^2}{v_x^2 + v_y^2} - mg \right) \quad (7.2)$$

$$\frac{d\alpha_t}{dt} = \omega \quad (7.3)$$

$$\frac{d\omega}{dt} = \frac{T_r \cdot \cos(\theta_r) \cdot d_r - T_f \cdot \cos(\theta_f) \cdot d_f}{I_{yy}} \quad (7.4)$$

In these equations α_t represents the pitch angle of the aircraft with the vertical, θ_r and θ_f represent the motor angle with the vehicles vertical, and T_f and T_r represent the thrust provided by the front and rear propellers respectively. The model is 2D to facilitate the analysis, although a more detailed control analysis, outside the scope of this design stage, should cover lateral motion in this phase.

The aforementioned differential equations are used to model the dynamics of the eVTOL using a Runge-Kutta solver, to which a PID controller is applied. The purpose of applying a controller to the system is not arriving at an optimal control solution, since such a non-linear system requires of something more complex than PID control; but rather to determine what thrust to weight ratio is sufficient for the eVTOL to successfully control its motion in this phase. Regarding the drag model for this motion, the extended aerodynamic model presented in Chapter 10 is used to predict drag forces with angles of attack close to perpendicular to the aircraft.

The results from the analysis are summarised below, presenting the achieved trajectories of the aircraft when setting the maximum T/W to 1.3. The desired attitude values were selected to ensure passenger comfort, minimising pitch angle variations and large velocity changes. The satisfactory behaviour with the selected T/W resulted in this value being set as the requirement for the propulsion system. In order to comply with the operational requirements involving wind gusts, a sinusoidal wind with a maximum of 60 km/h and average of 30 km/h was induced on the model, which successfully controlled its attitude establishing the thrust to weight ratio of 1.3 as sufficient. Once a design was converged to the analysis was repeated to confirm the validity of the ratio. Next section covers the analysis of the transition to and from horizontal flight.

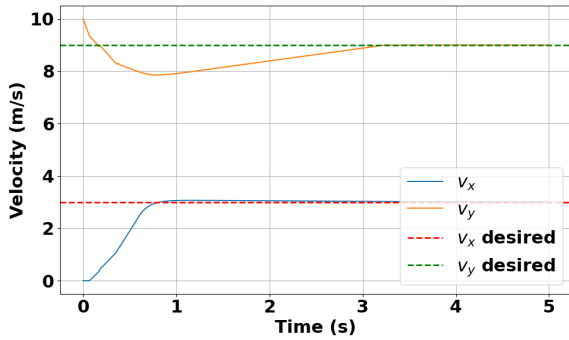


Figure 7.5: Velocity components of aircraft when starting vertical climb.

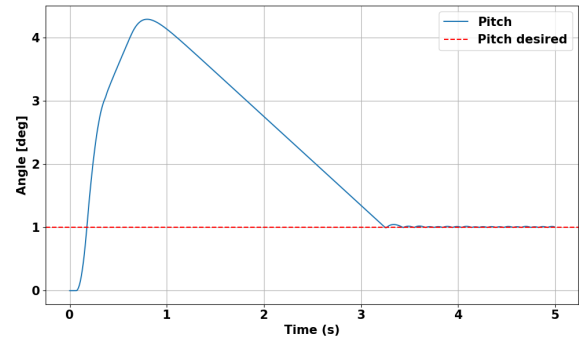


Figure 7.6: Pitch angle of aircraft with vertical during start of vertical climb.

7.6. Transition Analysis

In stages 3 and 13, the aircraft rotates its propellers from a VTOL configuration to the horizontal configuration or vice versa. Firstly, the transition between VTOL and horizontal flight is discussed.

As the aircraft leaves stage 2, it will rotate its engines from the vertical position to the horizontal position. For clarity, an propeller rotation angle of 0° represents a vertical configuration, whilst an angle of 90° represents a horizontal configuration. Once the rotors start rotating, a thrust will be generated in the horizontal direction. This thrust will accelerate the aircraft. As the aircraft increases its horizontal velocity, the wings start producing lift. Once the lift has offset the decrease in total vertical force due to the engines rotating, the engines will rotate further. This sequential approach continues until the rotors have rotated 90° . The velocity of the aircraft is dependent on the drag, which in turn is dependant on the velocity as well. Due to this interdependence, Euler's method was applied to calculate the velocity in a step wise approach and is detailed in Equation 7.5. The drag is calculated following Bernoulli and uses the velocity corresponding to time step n . T_{\perp} is the horizontal component of the thrust.

$$V_{n+1} = V_n + dt \cdot \frac{T_{\perp n} - D_n}{m} \quad (7.5)$$

The aircraft then enters the next stage with a given horizontal velocity. During this stage, the total vertical force has been kept equal to the weight such that the aircraft does not climbs or descents. Plots of the velocity, angle of propellers and forces acting on the aircraft are given in Figure 7.7 and Figure 7.8.

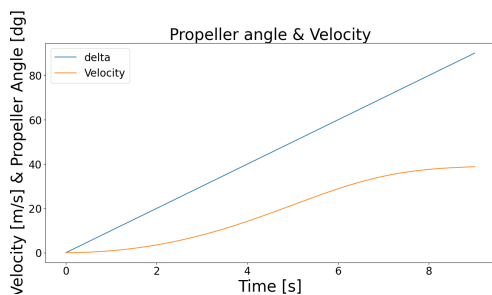


Figure 7.7: Velocity and propeller angle during climb transition.

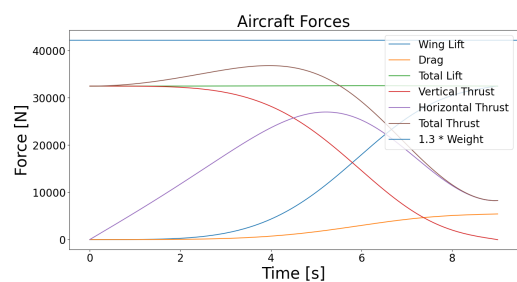


Figure 7.8: Forces acting on the aircraft during climb transition.

For the descent transition, the same approach was taken. However, in this stage, the vertical position is not

kept constant as descending during this stage will cause for a more energy efficient flight profile. The descent transition will start with a vertical and horizontal velocity. This phase ends once the aircraft reaches the desired altitude. Again, the plots of the velocity, angle of propellers and forces acting on the aircraft are given in Figure 7.9 and Figure 7.10. In the forces plot, it can be seen that the thrust only acts after a couple of seconds. During this period, the lift force is sufficient for flying horizontally. Once the lift force reduces, the thrust will be turned on. In reality, this kink could be negated by leaving the propulsion system active.

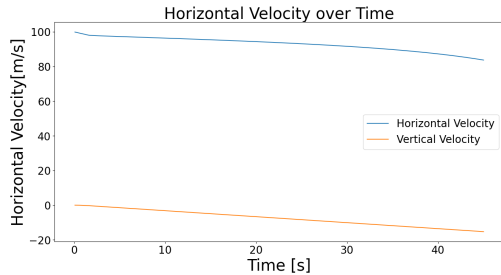


Figure 7.9: Velocity and propeller angle during descent transition.

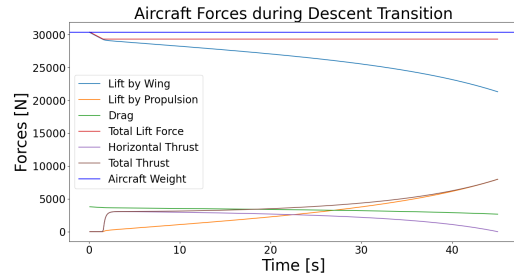


Figure 7.10: Forces acting on the aircraft during descent transition.

7.7. Assumption Validation

In Table 7.4 below the validation for the assumptions used in the flight profile analysis is presented.

Table 7.4: Validation of the assumptions used for the flight profile analysis.

Identifier	Validation
A-FP-01	For a range of 200 km the difference in altitude is 0.01% of the Earth's radius, which can be found using trigonometry; the effect is thus negligible for the accuracy required at this stage of the performance analysis.
A-FP-02	Gravity varies from 9.81 on Earth's surface to about 9.5 m/s at 100 km altitude, the error at 1km altitude is thus smaller than 1%, and can be neglected [11]
A-FP-03	The effect of Coriolis acceleration on the flight path has an effect on detail profile design, for which less uncertainties in design are necessary, the effect of this assumption must be analysed when advancing with the design.
A-FP-04	When decelerating the aircraft's inertia will lower the power requirements, the length of the stage mean the battery is not significantly oversized, but the assumption is still conservative.
A-FP-05	The presence of a rudder and wings in the design stabilises the aircraft, minimising the necessary stabilisation with thrust and thus power.

Some of the assumptions used in this chapter are also used in Chapter 13, where the performance of the aircraft is analysed.

Chapter 8 | Fuselage Design

The fuselage is an important subsystem, as it functions as a central connection between the other subsystems and houses the batteries and payload. Its design is not only related to the technical performance of the aircraft, but it also directly influences passenger and pilot comfort during operation. In this chapter, the method and results of the fuselage design is discussed. In Section 8.1, the subsystem requirements are presented and compliance is checked. In Section 8.2, the assumptions made for the fuselage design process are listed. The design method itself is covered by Section 8.3. The results of the design process are presented in Section 8.4. Finally, the verification and validation of the fuselage design is discussed in Section 8.5.

8.1. Fuselage Subsystem Requirements and Compliance Matrix

In Table 8.1 below, the fuselage subsystem requirements are listed, as well as the system requirements and technical risks they stem from. Additionally, compliance with the requirements and the method of verification are given as well.

Table 8.1: Fuselage subsystem requirements compliance matrix.

Identifier	Requirement	Source(s)	Compliance	Method of Verification / Reason for Removal
REQ-FUS-01	The fuselage shall be able to accommodate 6 passengers, including the pilot(s).	REQ-SYS-AC-01	✓	Visual inspection of the cabin volume in the CAD model (see Figure 8.4)
REQ-FUS-02	The fuselage shall have a door for the passengers and pilot(s) to enter.	REQ-SYS-AC-04, REQ-SYS-AC-84	✓	Visual inspection of the CAD model in (see figures in Section 17.4)
REQ-FUS-03	The fuselage shall have a door for the entrance of the luggage.	REQ-SYS-AC-05, REQ-SYS-AC-84	✓	Visual inspection of the CAD model in (see figures in Section 17.4)
REQ-FUS-04	The fuselage shall allow the seating of at least 95% of the passengers without touching objects other than the seat and floor.	REQ-SYS-AC-37	✓	Visual inspection of the cabin volume of the CAD model in (see Figure 8.4)
REQ-FUS-05	The passenger door shall have a minimum clearance of 1.5 m to the propulsion system.	REQ-SYS-AC-38	✓	Visual inspection of the CAD model
REQ-FUS-06	The luggage hatch shall have a minimum clearance of 1.5 m to the propulsion system.	REQ-SYS-AC-38	✗	Visual inspection of the CAD model
REQ-FUS-07	The fuselage shall allow for the communication between the pilot(s) and passengers.	REQ-SYS-AC-40, REQ-SYS-AC-86	✓	Visual inspection of the CAD model in (see Figure 8.5), testing in prototype stage
REQ-FUS-08	The fuselage shall allow the seating of at least 95% of the pilots without touching objects unrelated to piloting the aircraft.	REQ-SYS-AC-41	✓	Visual inspection of cabin volume of the CAD model (see Figure 8.4)
REQ-FUS-09	The fuselage shall allow the pilot(s) to reach all the controls in the cockpit from a single position.	REQ-SYS-AC-42	✗	Visual inspection of the CAD model, testing in the prototype stage
REQ-FUS-10	The fuselage shall provide a longitudinal pilot visibility range of at least -15 ° to 15 °.	REQ-SYS-AC-43	✓	Visual inspection of the CAD model
REQ-FUS-11	The fuselage shall provide a directional pilot visibility range of at least -90 ° to 90 °.	REQ-SYS-AC-44	✓	Visual inspection of the CAD model
REQ-FUS-12	The manufacturing cost of the fuselage subsystem shall be less than 100000 euros.	REQ-SYS-AC-94		<i>It was found to be unnecessary to constraint the fuselage design by imposing a subsystem cost constraint.</i>
REQ-FUS-13	The fuselage shall be able to maintain a cabin temperature between 19 ° C and 23 ° C with an ambient air temperature range of -20 ° C to 47 ° C.	REQ-SYS-AC-31	✗	Testing the aircraft in the specified conditions
REQ-FUS-14	The fuselage cabin shall include a fire extinguisher.	REQ-SYS-AC-34, REQ-SYS-AC-86, R-TEC-12	✓	Visual inspection of the CAD model in (see Figure 8.5)
REQ-FUS-15	The fuselage shall prevent the exposure of the passengers and pilot(s) to ambient precipitation.	REQ-SYS-AC-35	✓	Visual inspection of the CAD model, testing for watertight seals in the prototype stage
REQ-FUS-16	The fuselage shall prevent the exposure of the passengers and pilot(s) to winds.	REQ-SYS-AC-36	✓	Visual inspection of the CAD model, testing in the prototype stage
REQ-FUS-17	The luggage hold shall be able to self-contain a fire for a minimum of 5 minutes.	REQ-SYS-AC-86	✗	Testing in the prototype stage
REQ-FUS-18	The fuselage shall have at least one emergency exit on both sides.	REQ-SYS-AC-86	✓	Visual inspection of the CAD model in (see figures in Section 17.4)
REQ-FUS-19	Snow shall be able to be removed from the windshields during the complete flight profile.	REQ-SYS-AC-90		<i>This requirement is not quantifiable and it does not effect the design of the fuselage itself.</i>

As can be observed in Table 8.1, not all fuselage subsystem requirements have (yet) been complied with. Below, for each of these, an explanation is given either for why compliance is not possible or for how this can be shown

in a further design stage.

- **REQ-FUS-06:** In order to prevent the centre of gravity from moving more aft, the choice was made to place the luggage hold directly after the passenger cabin, as discussed in Section 8.3.4. As a result, both the horizontal and vertical distance of the luggage hatches to the propulsion system in VTOL mode is approximately 0.5 m. However, the requirement was set up in order to maximise passenger safety. A procedure can be put in place in which the pilot places the luggage in the holds before anyone is allowed to enter the aircraft. This way, the propulsion system cannot be accidentally activated by anyone during the placement of the luggage.
- **REQ-FUS-09:** At this stage of the design, a detailed cockpit layout including the flight control systems has not yet been designed. Therefore, compliance to this requirement can not yet be checked. In a future design stage, compliance can be checked via visual inspection of a CAD model and by testing in the prototype stage.
- **REQ-FUS-13:** As the fuselage design method in this stage of the design process, explained in Section 8.3, entails mainly the shape and configuration, compliance with this requirement cannot yet be confirmed. However, it is taken into account in assumption A-FUS-01 (Table 8.2), which is made partly to account for an insulation layer. Furthermore, the possibility of heating the cabin is discussed in Section 12.3.2 and a climate control system is taken into account in the avionics. In a future design stage, compliance with this requirement could be checked during test flights without passengers.
- **REQ-FUS-17:** For similar reasons as for REQ-FUS-13, compliance with this requirement cannot yet be checked. However, the requirement is taken into account by fully closing off the luggage compartment. Additionally, assumption A-FUS-03 is made partly to account for the material thickness required to contain a fire (see Table 8.5). Compliance with this requirement could be checked by performing tests in a future design stage.

8.2. Assumptions

In Table 8.2 below, the assumptions made for the fuselage design process are listed and their expected effect on the design results are given. The three assumptions made all regard structural thicknesses. In this stage of the design, estimations for these are not yet available. Therefore, assumptions partially based on values from literature need to be made now, such that the outer fuselage shape can be constrained.

Table 8.2: Assumptions used for the fuselage design.

Identifier	Assumption	Expected Effect
A-FUS-01	The structural thickness of the fuselage outer wall is equal to 50 mm.	This assumption influences the eventual fuselage length, maximum cross-sectional area and wetted area, as it influences the fuselage shape design method explained in Section 8.3.3. However, the expected influence is minor, as the maximum deviation from the assumed value is in the order of tens of millimetres, and fuselage dimensions are in the order of thousands of millimetres.
A-FUS-02	The structural thickness of the cabin floor is equal to 50 mm.	This assumption influences the available volume underneath the cabin floor. However, the expected influence is minor, as the maximum deviation from the assumed value is in the order of tens of millimetres, and the dimensions under the floor are in the order of hundreds of millimetres.
A-FUS-03	The structural thickness of interior walls is equal to 50 mm.	This assumption influences the length of the cabin, as a wall is present between the cockpit and the cabin. It also influences the available volume for the main battery, as it is encapsulated by a wall of the same thickness. However, the expected influence is minor, as the maximum deviation from the assumed value is in the order of tens of millimetres, and the dimensions of the main battery pack are in the order of hundreds of millimetres. The available volume for the luggage compartment is not influenced, as this is constrained already made smaller than required, as further explained in Section 8.3.4.

8.3. Method

This section entails the method used for the design of the fuselage. First, an interior configuration was determined, as discussed in Section 8.3.1. Then, a cabin sizing was performed, as explained in Section 8.3.2. The subsequent design of the shape of the fuselage is covered by Section 8.3.3. Finally, in Section 8.3.4, the design of the fuselage interior, windows and doors is discussed.

8.3.1. Interior Configuration

The foundation of the fuselage design process is the selection of an interior configuration. Several configurations with different seat arrangements have been considered, out of which the configuration shown in Figure 8.1 was deemed to be the optimal one.

It was chosen to have only one pilot, as having two pilots is not necessary for an aircraft of this size and in order to maximise the amount of passengers carried. Given that the fuselage gets smaller around the cockpit, only the pilot is seated in the cockpit to maximise their comfort and the ability to operate of the aircraft. Behind the cockpit, the passengers are seated in two rows. Instead of placing a door at each seat, as is the case for some small aircraft, it was chosen to have a single passenger entrance door. This was done in order to comply with requirement REQ-FUS-05 and because of the fact that one of the rows only consists of a single seat, allowing for a general entrance door at the vacant spot. To allow the passengers to reach their seats, an aisle is placed between the two rows of seats. In order to comply with REQ-FUS-18, a smaller emergency door is present on the other side of the aircraft, encapsulating the window of the passenger seat opposite to the entrance door. Behind the most aft passengers, where the fuselage gets smaller, a luggage hold is present that can be accessed by hatches on both sides of the aircraft to allow for proper placement and securing of the luggage. The cockpit is separated from the passenger cabin by a thin wall to respect the pilots privacy and their ability to stay focused on piloting the aircraft. The thin wall has an opening at the door side of the aircraft to allow the pilot to enter the cockpit. It was chosen to not place a door in this opening in order to allow communication between the pilot and passengers, and thus to comply with REQ-FUS-07. Although an intercom system is also present in order to make communication easier, as mentioned in Section 14.4, a direct opening between the cockpit and passenger cabin ensures the possibility for communication at all times. Furthermore, extra structural complexity is prevented.

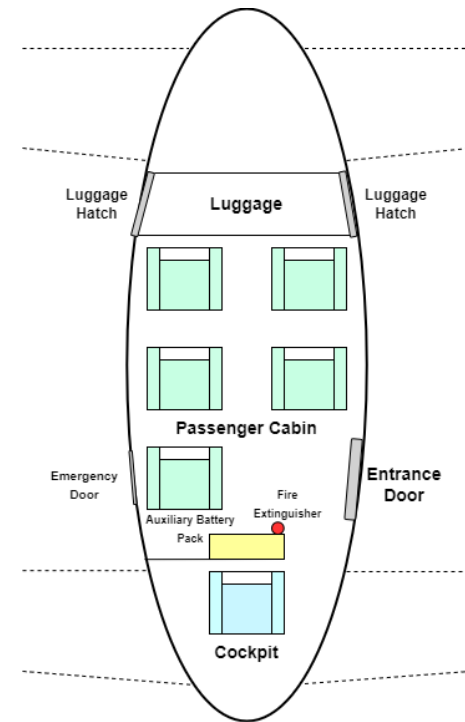


Figure 8.1: Cabin layout top view.

During the design integration it was found that the centre of gravity had to be shifted more forward in order to achieve longitudinal stability of the aircraft. To accomplish this, it was decided to place the main battery pack vertically at the centre of the passenger side of the wall separating the cockpit from the passenger cabin, as explained in Section 17.3. As explained in Section 8.3.2, the passenger seats were able to be moved more aft to ensure that the seat opposite to the entrance door could still be accessed by passengers. The main battery pack is well insulated in order to prevent a potential fire spreading to the cabin, as explained in Section 12.3.1. Additionally, the pack is closed off by a thin wall for esthetical purposes. A fire extinguisher is placed at the door side of the main battery pack to allow for quick access by both passengers and pilot and to comply with requirement REQ-FUS-14. The auxiliary battery pack and the thermal management system are located underneath the passenger cabin floor, as well as some additional volume to allow for electrical components and wiring, such as the pump required for the thermal management system and the wires connecting the cockpit to the avionics in the aft wing and empennage.

8.3.2. Cabin Sizing

Based on the interior configuration, the cabin, referring to both the passenger cabin and cockpit, can be sized. To determine the minimum required cross-sectional dimensions of the fuselage, the minimum dimensions of seat and passenger elements are established. The definitions of these dimensions are given in Figure 8.2. In the figure, the most constraining corners are connected to make an outline of the minimum required cross-sectional shape of the cabin. This outline was then extruded to obtain the minimum required volumetric shape of the cabin. At the point where the passenger cabin transitions into the cockpit, the corners of the cabin cross-sectional profile were connected to minimum dimensions at the front of the cockpit. These minimum dimensions were found by setting a minimum width at the feet of the pilot, a minimum height equal to the maximum eye height and a minimum width at this eye height equal to the maximum head width (see Table 8.3). In order to allow for a more aerodynamic fuselage shape, the pilot is seated lower than the passengers. The aisle lowering depicted in Figure 8.2 is set to the same floor level as the cockpit. It has to be noted that this aisle lowering was set to be optional, as the exact required volume of the auxiliary battery pack and thermal management system are not yet known at this stage of the design. This is also the reason why these components are not included in the cross-sectional profile. Due to the way the fuselage is shaped, as discussed in Section 8.3.3, additional volume is present underneath the passenger cabin. During the battery sizing and design integration, it was checked whether this volume was sufficient or whether the aisle lowering had to be adjusted.

A side view of the resulting volumetric shape and the corresponding dimension definitions are given by Figure 8.3. The cut-offs were made in order to reduce the required volume were possible, and in order to prevent a cramped cockpit feeling, it was chosen to maintain a minimum distance between the cockpit glass and the

eyes of the pilot. The values of the dimensions in Figure 8.2 and Figure 8.3, as well as explanations for how these values were obtained, are provided in Table 8.3.

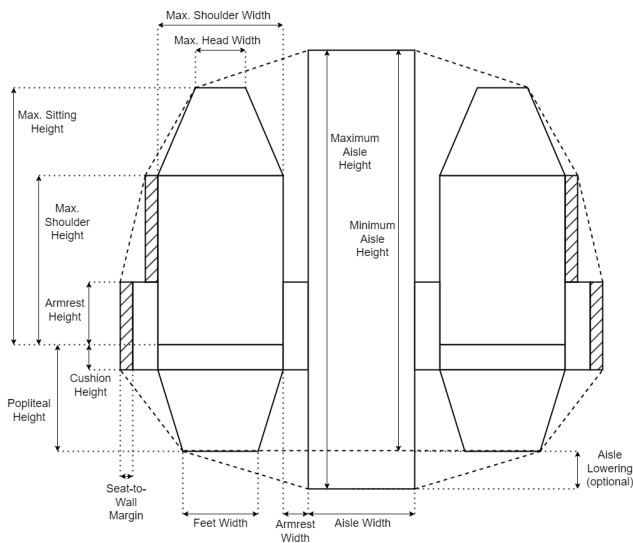


Figure 8.2: Minimum required cabin cross-sectional profile.

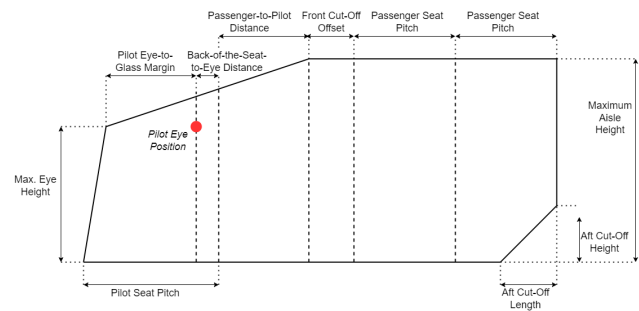


Figure 8.3: Minimum required cabin volume side view.

8.3.3. Fuselage Shape Design

The design of the fuselage shape of the eVTOL is relatively free, as it does not need to be pressurized due to the low cruise altitude of 1 km. In order to optimise aircraft aerodynamics, it is decided to design the fuselage shape in such a way that sudden deflections in the airflow streamlines are prevented. In practice, this is achieved by utilising CAD software in which the fuselage shape is defined by single splines over the majority of the length of the fuselage. The splines are only interrupted near the beginning and end of the fuselage, in order to properly close off the fuselage. Still, tangencies between the splines are present at these interruptions to prevent sharp corners.

The dimensions of the fuselage shape are minimised, with the cabin volume from Section 8.3.2 as the constraint, taking into account the fuselage wall thickness from assumption A-FUS-01. The resulting shape of the outer fuselage surface, together with the minimum cabin volume, are shown in Figure 8.4. The fuselage shape is cut in half in the figure in order to show the minimum cabin volume.

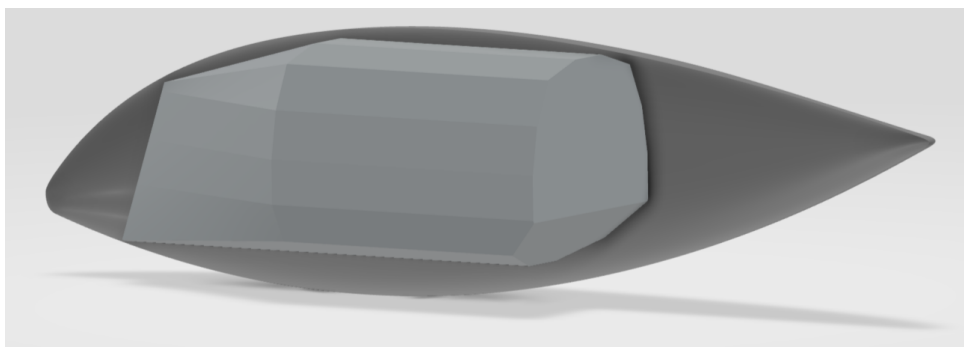


Figure 8.4: Right half of the outer fuselage surface with the minimum required cabin volume.

As discussed in Section 17.3, more volume for the auxiliary battery pack was eventually required than was available under the cabin floor at the front of the passenger cabin in case of an aisle lowering. Therefore, it was chosen to remove the lowering of the aisle. The aisle lowering was found not to be the part of the cabin cross section that is constraining for the fuselage shape. As a result, this design decision did not lead to the need of adjusting the fuselage shape. As discussed previously in Section 8.3.1, it was found during a later design stage that the main battery pack had to be placed at the wall separating the passenger cabin from the cockpit. In order to prevent the CG from shifting significantly away from the aircraft centerline, the battery pack was made symmetrical, meaning the passenger sitting opposite to the entrance door still has the sufficient legroom.

Still, the seat must be properly accessible. After a preliminary design for the seats was made, discussed in Section 8.3.4, it was found that the passenger seats could be shifted 300 mm aft without requiring an extension of the fuselage, resulting in proper accessibility of the seat. This shift also proved to allow for a sufficient volume for the main battery. The final fuselage shape, including doors and windows, is shown in the figures in Section 17.4.

8.3.4. Interior, Windows and Doors Design

The fuselage interior can be split up into three sections: the cockpit, the passenger cabin and the luggage hold. In this stage of the design, the cockpit dashboard and flight control layout has not been designed. The floor and a simple design for the pilot seat however have been added to the CAD model. In the passenger cabin, a simple design for the seats has been made. The seats have been modelled with a certain ground length, ground width, height, recline, structural thickness and back-of-the-seat thickness, as specified in Table 8.3. The other seat parameters have already been defined in the cabin sizing, discussed in Section 8.3.2. The pilot seat has been modelled in the same way as the passenger seats, but the armrests are not included. The compartment for the main battery pack has also been added to model, for which the dimensions are specified in Table 8.3. Additionally, a simple representation of the fire extinguisher, modelled after the C354TS-3.0 lb. Halon Fire Extinguisher from H3R Aviation ¹, was added to the CAD model.

The size of the luggage compartment was minimised in order to prevent the luggage hatches from being larger than they need to be and thus to save structural weight and complexity. The minimum size of the luggage compartment was based on a maximum amount of 6 luggage items (1 per passenger/pilot), each with set maximum dimensions as specified in Table 8.3. The luggage items can be placed in two rows of three, where a margin is taken between the two rows to allow the pilot to properly secure the items with bands. The same margin has been applied on top of the luggage items to allow for some deviation in dimensions. As previously mentioned in Section 8.3.1, the luggage hold has a hatch on both sides of the aircraft in order to allow for proper placement and securing of the luggage. In order to allow for the best possible access by the pilot, the vertical position of the luggage hold was set as low as possible, up until the point where there is a margin of 100 mm between the outer luggage item and the outer hatch surface to account for the structural thickness of the hatch and small deviations in luggage dimensions.

The cockpit windows have been sized such that REQ-FUS-10 and REQ-FUS-11 can be made. Lines with angles corresponding to the requirements have been drawn in the CAD model from the position of the eyes of the pilot. Here, the maximum eye height from Table 8.3 was taken. Although the length of pilots can vary, it is assumed the pilot seat can be raised and shifted forward to account for this. Although not yet implemented, windows in the floor of the cockpit have also been regarded as crucial, as these allow the pilot to have the required field of view during vertical landing. In a future design stage, these windows will be sized and added to the CAD model. In the passenger cabin, large windows have been added on each side of the aircraft spanning the aft two rows of seats. The windows are relatively large, but this still leads to relatively low structural concerns as the fuselage is not pressurised. For the front row seat on the right side of the aircraft, a single window has been added such that the emergency door can be formed around this window. On the other side of the aircraft, the same has been done for the entrance door. The entrance door is split in the middle such that when it is opened, the top half containing the window rotates upwards and the lower half rotates downwards as to form a stair for entering the aircraft. Other rationales for important window and door design parameters can be found in Table 8.3.

Figure 8.5 shows the right half of the fuselage with windows and the emergency door, together with the fuselage interior. The battery packs have also been added for visualisation of their location. Mannequins of various sizes have been placed in the cockpit passenger cabin for reference. The fully closed off fuselage including the entrance door and luggage hatch can be seen in the figures in Section 17.4.

¹<https://www.h3raviation.com/products/c354ts-3-0-lb-halon-fire-extinguisher> [cited 18.06.2024]



Figure 8.5: Right half of the outer fuselage surface including the windows, the emergency door and the interior, including the floor, walls, seats, luggage (red), fire extinguisher, battery packs (yellow) and mannequins for reference.

8.4. Results

In Table 8.3 below, the results of the fuselage design are presented. Rationales are provided for parameters that were either chosen or estimated. For most of the seating dimensions, datasets from the Dined Anthropometric Database from the TU Delft² have been used. Since it is not yet known in what exact European countries the aircraft will be operated, the 95th percentiles of the most constraining European datasets have been selected for constraining seat dimensions in order to comply with REQ-FUS-04. In most cases, the most constraining European dataset was Dutch males ranging between 20 and 30 years of age. In case this dataset was used, the most up to date version available was used. For non-constraining dimensions, averages of European datasets have been taken or values were selected based on tests performed by the design team.

Table 8.3: Design parameters of the fuselage design.

Parameter	Value	Unit	Rationale
Popliteal Height	424	[mm]	Dined Anthropometric Database, average of the means of the European datasets
Maximum Shoulder Height	680	[mm]	Dined Anthropometric Database, Dutch males of ages 20-30, 95th percentile
Maximum Sitting Height	1048	[mm]	Dined Anthropometric Database, Dutch males of ages 20-30, 99th percentile. It was deemed extra important to allow as large a fraction of the population as possible to be seated without hitting the ceiling, so the 99th percentile of the most constraining dataset was chosen instead of the 95th.
Maximum Shoulder Width	511	[mm]	Dined Anthropometric Database, Dutch males of ages 20-30, 95th percentile
Maximum Head Width	194	[mm]	Dined Anthropometric Database, Northern European males, 99th percentile. It was deemed extra important to allow as large a fraction of the population as possible to be seated without hitting the ceiling, so the 99th percentile of the most constraining dataset was chosen instead of the 95th.
Feet Width	350	[mm]	Deemed to be sufficient by the design team
Cushion Height	100	[mm]	Deemed to be sufficient by the design team
Armrest Height	250	[mm]	Deemed to be a comfortable value by the design team
Armrest Width	75	[mm]	Deemed to be a comfortable value by the design team
Aisle Width	400	[mm]	Deemed to be sufficient by the design team
Maximum Aisle Height	1750	[mm]	Deemed to be sufficient by the design team
Minimum Aisle Height	1600	[mm]	Follows from subtracting the optional aisle lowering from the maximum aisle height
Optional Aisle Lowering / Cockpit Floor Lowering	150	[mm]	This value was observed to be optimum for ensuring an aerodynamic fuselage shape.
Eventual Aisle Lowering	0	[mm]	The aisle lowering had to be removed due to the integration of the battery pack (Section 8.3.3).
Eventual Maximum Aisle Height	1707	[mm]	Higher than the minimum aisle height in the centre of the passenger cabin due to the shape of the fuselage
Seat-to-Wall Margin	20	[mm]	Deemed to be sufficient by the design team
Passenger Seat Pitch	965	[mm]	Comparable to premium economy class seat pitch values from multiple airlines. It was deemed crucial to provide a comfortable travel experience, but a seat pitch comparable to business class values was not considered necessary due to the relatively short flight time.
Passenger-to-Pilot Distance	1209	[mm]	Determined such that the distance of the most forward passenger to the cockpit wall on knee height is the same as for the other seats.
Pilot Seat Pitch	1331	[mm]	Determined based on the pilot seat dimensions and the 95th percentile lower and upper leg length values from the Dined Anthropometric Database dataset for Dutch males of ages 20-30. An additional 150 mm of margin was taken to account for shoes and the mounting of rudder paddles on the floor.
Pilot Feet Width	500	[mm]	Deemed sufficient by the design team

Continued on next page

²<https://dined.io.tudelft.nl/en/database/tool> [cited 18.06.2024]

Parameter	Value	Unit	Rationale
Pilot Eye-to-Glass Margin	639	[mm]	It was chosen to maintain a distance between the eyes of the pilot (at maximum eye height) and the outer surface of the cockpit glass of at least one upper arm length. The value used is from the Dined Anthropometric Database, Dutch males 18-30, 95th percentile.
Back-of-the-Seat-to-Eye Distance	350	[mm]	Estimate by the design team
Back-of-the-Seat-Thickness	100	[mm]	Deemed to be sufficient by the design team. It was considered important for the seats to be comfortable, but an excessive cushion thickness in the back of the seat was not deemed necessary considering the relatively short flight time.
Seat Recline	10	[deg]	Deemed to be sufficient by the design team. It was considered important for the seats to be comfortable, but excessive seat recline was not deemed necessary considering the relatively short flight time.
Seat Ground Length	354	[mm]	Based on extrapolating the seat recline downwards from the popliteal height and a chosen cushion length with a value taken from the dataset of the Dined Anthropometric Database, Dutch females 60+, 1st percentile as this was the most constraining available dataset. The cushion length was minimised as to allow as many passengers as possible to sit comfortably.
Seat Ground Width	350	[mm]	Set equal to the feet width
Seat Height	1350	[mm]	Chosen by the design team. This value is relatively high, but it allows for 95% of the most constraining population (Dutch males of ages 20-30) to rest their head on the seat, which was considered to be crucial. Additionally, a high seat height leads to an increased sense of privacy in the passenger cabin, which is deemed important by the design team.
Seat structural thickness	50	[mm]	Deemed sufficient by the design team
Maximum Eye Height	1330	[mm]	Dined Anthropometric Database, Dutch males of ages 20-30, 95th percentile
Mean Eye Height	1194	[mm]	Dined Anthropometric Database, average of the means of the European datasets
Luggage Item Height	550	[mm]	Based on the maximum hand luggage dimensions from various airlines
Luggage Item Width	400	[mm]	Based on the maximum hand luggage dimensions from various airlines
Luggage Item Length	250	[mm]	Based on the maximum hand luggage dimensions from various airlines
Luggage Margin	150	[mm]	Deemed to be sufficient by the design team
Luggage Compartment Floor Height from the Ground	1119	[mm]	N/A
Fuselage Outer Wall Thickness	50	[mm]	Assumption made by the design team
Cabin Floor Thickness	50	[mm]	Assumption made by the design team
Interior Walls Thickness	50	[mm]	Assumption made by the design team
Passenger Cabin Window Height	600	[mm]	Maximised until the window in the entrance door became too large for the split of the door
Entrance Door Height (in the middle)	1500	[mm]	Deemed sufficient by the design team
Entrance Door Width / Emergency Door Width	750	[mm]	Set such that it is able to encapsulate the window in the door. This width is more than sufficient for a fast exit of the passengers in case of an emergency (in comparison with the maximum shoulder width).
Emergency Door Height	900	[mm]	Chosen such that a sufficiently large opening is present for a fast exit, while minimising the door size for structural reasons
Fuselage Length	8725	[mm]	Result from the fuselage shape design (Section 8.3.3)
Fuselage Maximum Cross-Sectional Area	4.021	[m ²]	Result from the fuselage shape design (Section 8.3.3)
Fuselage Wetted Area	46.214	[m ²]	Result from the fuselage shape design (Section 8.3.3)
Main Battery Pack Compartment Length	350	[mm]	Maximum length for which the seat opposite to the entrance door is still properly accessible
Main Battery Pack Compartment Width	750	[mm]	Maximum width for which the opening to the cockpit is still sufficiently wide for the pilot to enter the cockpit without excessive effort
Main Battery Pack Compartment Height	1500	[mm]	Maximum height for which the battery pack has a margin to the fuselage outer surface equal to the outer wall thickness from A-FUS-01
Available Main Battery Pack Volume	0.293	[m ³]	Result from the Compartment Length, Width and Height given above, taking into account the interior wall thickness from A-FUS-03 once for the length and twice for the width

8.5. Verification and Validation

As the fuselage design method was mainly based upon published statistics, CAD software used by industry (3DEXPERIENCE CATIA) and design choices made by the design team, no verification and validation of the tools is required. The validity of the assumptions listed in Table 8.2 is discussed in Table 8.5 below.

Table 8.5: Validation of the assumptions used for the fuselage design.

Identifier	Validation
A-FUS-01	The total fuselage outer wall thickness, including insulation, of modern airliners is around 80 mm [12]. As the HAROLD will have a smaller structure than a conventional airliner and less required insulation due to its relatively low cruising altitude, a lower but conservative value of 50 mm is taken.
A-FUS-02	Just like the fuselage outer wall thickness, the floor requires a structure and insulation, and therefore the same value of 50 mm is taken. In this case, the insulation regards the prevention of a potential fire spreading from the auxiliary battery pack to the passenger cabin. Although insulation has already been taken into account in the battery pack specific energy density and volumetric energy density (see Section 12.3.1), it is taken into account here as well in order to be conservative.
A-FUS-03	Although the interior walls do not need significant structural thickness, the walls around the main battery pack and luggage hold require insulation to prevent a potential fire from spreading, and in a later design stage it might be chosen to run electrical wiring to some of these walls. Therefore, a value of 50 mm is taken as a conservative estimate.

Chapter 9 | Wings & Empennage Sizing

This chapter explains how the wing and empennage were sized as well as the requirements that the wings and empennage need to meet. The wings and the wing requirements are explained in Section 9.1 while the empennage and the empennage requirements are explained in Section 9.2.1.

9.1. Wing Sizing and Requirements

Firstly, this section presents the requirements for the wings in Section 9.1.1. Afterwards, the wing is sized in a Section 9.1.2 while the airfoil for the wing is picked in Section 9.1.3.

9.1.1. Subsystem Requirements and Compliance Matrix

The requirements for the wings which are flown down from the system requirements can be found in Table 9.1.

Table 9.1: Wing Subsystem Requirements Compliance Matrix.

Identifier	Requirement	Source(s)	Compliance	Method of Verification
REQ-WNG-01	The wingspan shall be lower than 24m.	REQ-SYS-AC-26, REQ-SYS-AC-27	✓	Inspection of the CAD model, done in Section 9.1.2
REQ-WNG-02	The wings shall provide a lift coefficient higher than 1.5.	REQ-SYS-AC-12	✓	Analysis of the wing using the aerodynamic model created in Section 10.3
REQ-WNG-03	The wings shall be able to ensure a controllable angle of attack in the range of -12 to 12 degrees.	REQ-SYS-AC-11, REQ-SYS-AC-14, REQ-SYS-AC-15, REQ-SYS-AC-19, REQ-SYS-AC-48	✓	Analysis by aerodynamic analysis in Chapter 10, stability analysis (not included in report)
REQ-WNG-04	The wings shall ensure a negative aircraft pitching moment derivative with respect to the angle of attack.	REQ-SYS-AC-46	✓	Analysis of the aerodynamics, done in Chapter 10, as well as stability analysis (not included in this report)
REQ-WNG-05	The wings shall ensure that the aircraft is longitudinally trimmable in cruise, climb and descent conditions.	REQ-SYS-AC-17, REQ-SYS-AC-18	✓	Analysis by aerodynamic analysis, in Section 10.3
REQ-WNG-06	The wings shall be able to ensure a roll angle range of -30 to 30 degrees.	REQ-SYS-AC-50	✓	Analysis by aerodynamic analysis in Chapter 10, stability analysis (not included in report)
REQ-WNG-07	The wings shall function in an ambient temperature range of -20 °C to 47 °C.	REQ-SYS-AC-31	X/✓	This requirement should be verified using a test and analysing the performance of the aircraft in different temperatures. The reason for the checkmark is due to the performance of the wings shortly being covered in Section 10.3. An analysis was shortly performed where the difference in aerodynamic performance was analysed at different temperatures.
REQ-WNG-08	The pilot shall be able to tell when the aircraft is stalling without having to perform sudden manoeuvres.	REQ-SYS-AC-86	X/✓	This requirement should be verified using a test to see the stalling characteristic of the aircraft. The reason for the checkmark is due to the way the wings were designed. An active effort was made to chose an airfoil that promotes a safe, non-abrupt stall. The checkmark design is a result of actively choosing a specific airfoil aimed at promoting a safe, non-abrupt stall as explained in Section 9.1.3
REQ-WNG-09	The wings shall not induce stable stability derivatives.	REQ-SYS-AC-86	✓	Analysis by aerodynamic analysis in Chapter 10, stability analysis (not included in report)
REQ-WNG-10	The aircraft shall have an absolute cruise angle of attack below 5 degrees.	REQ-SYS-AC-96	✓	The verification can be found in Section 10.3.1.

9.1.2. Wing Sizing

During the preliminary design, the concept for the aircraft was chosen to be the dragon fly. In other words, an aircraft that utilises two lifting surfaces of similar size. The sizing process of the wings starts with the wing loading obtained from the flight performance. The wing loading determines the needed lifting surface area of the aircraft which was split equally across both of the lifting surfaces to minimise the induced drag penalty [13]. To further decrease the drag, the wings will be placed as far apart longitudinally as possible, while taking into account the stability and controllability of the aircraft as well as the fuselage design limitations. Additionally, the front wing will be placed low while the rear wing will be placed high, again taking into account the stability and controllability as well as the fuselage design limitations. In turn, this should reduce the effect of down wash on the wings, decreasing the induced drag.

To ensure sufficient ground clearance and improve the lateral stability of the aircraft, a dihedral of 2.5 degrees was chosen for the front wing. This was applied only for the front low wing due to the rear high wing already providing better lateral stability and having sufficient ground clearance due to its vertical positioning. To continue the sizing, the aspect ratio and the taper ratio were selected as design points. The aspect ratio was selected at 8 from literature [14], while the taper ratio λ is selected as 0.4 to obtain an almost elliptical lift distribution which gives an increase in lift induced drag less than 1% higher than the value associated with the optimal elliptical distribution, but the manufacturing of such trapezoidal wing is far easier [15]. Lastly, the sweep at quarter chord was selected to be 0 degrees due to the low operating speed. With these parameters in mind, numerous wing parameters of interest can be calculated which can be seen in Table 9.2. The formulas used were conventional formulas for a trapezoidal wing.

Table 9.2: Parameters describing the final geometry of a single wing

Parameter	Value	Unit
S	10.149	[m ²]
b	9.011	[m]
AR	8	[-]
λ	0.4	[-]
c _r	1.609	[m]
c _t	0.644	[m]
c _{mac}	1.195	[m]
Λ _{LE}	3.066	[°]

It is important to note that these parameters describe only one wing, but they are identical for both wings. These parameters, excluding the previously mentioned design points, were utilised in the design iteration loop, defining the drag and lift performance. This, in turn, creates a snowball effect influencing various other departments such as flight performance, structures, etc. Additionally, it should be mentioned that the wingspan presented in Table 9.2 represents the span of the wing outside of the fuselage, thus excluding the wing portion within the fuselage. The maximum width of the fuselage is 2 meters, ensuring the total wing span is below 11.011 meters. With this consideration, the final wing span design complies with the REQ-WNG-01 requirement, ensuring that the aircraft can take off and land on an H2 helipad. Additionally, the wingspan fits within an H1 helipad with a diameter of 15 meters. This result enhances the aircraft's flexibility and increases its marketability.

9.1.3. Airfoil Trade-off

To pick an airfoil, the lift coefficient in cruise first needed to be computed. This was done using Equation 9.1.

$$C_{L_{des}} = \frac{2W/S}{\rho_{cruise} V_{cruise}^2} \quad (9.1)$$

where W/S is the wing loading, ρ is the density at cruise altitude, and the V_{cruise} is the cruise speed set at 250 km/h. This leads to a design lift coefficient of 0.637. However, the obtained lift coefficient needs to be converted to the lift coefficient of the airfoil. To compute the lift coefficient of the airfoil, Equation 9.2 is used. It was found that the lift coefficient of the airfoil is 0.64 due to the low sweep.

$$C_{l_{des}} = \frac{C_{L_{des}}}{\cos^2(\Lambda_{LE})} \quad (9.2)$$

During the preliminary sizing, the TU Delft airfoil database¹ was used to obtain potential candidates. To avoid having to simulate every airfoil in the database, a few conditions were set.

- The chord to thickness ratio should not be lower than 11% to provide an adequate structural strength to the wing [13].
- The chord to thickness ratio should not be higher than 18% due to increased skin friction drag.
- The airfoil should have a conventional shape which includes no holes or bumps. This was done due to the use of normal wings for the aircraft and the XFLR5 having difficulties to accurately simulate such airfoils.
- The $C_{l_{max}}$ should be higher than 1.65 to ensure safe transition. One can use Equation 9.2 to obtain $C_{l_{max}}$ or use a more conservative 10% safety factor method where $C_{L_{max}} \cdot 1.1 = C_{l_{max}}$. The authors of this report decided on a more conservative option because it is believed that the airfoils that barely meet the condition won't win the upcoming trade off due to the $C_{l_{max}}$ having a high weight.

The first three conditions were used to visually eliminate the airfoils without any simulation. Subsequently, the remaining 108 airfoils were simulated in XFLR5, using default conditions provided by XFLR5, except the Reynolds number Re which was computed using Equation 9.3:

$$Re = \frac{\rho V C_{MAC}}{\mu} \quad (9.3)$$

where ρ is adjusted for the flight altitude, V is the cruise speed of 250 km/h, C_{MAC} is the mean aerodynamic chord and μ is the dynamic viscosity of air. With the Reynolds number of 5.218e6 [-] obtained, the simulations were run and the airfoils that didn't comply with the fourth condition were discarded, leaving 45 airfoils. Additionally, it should be noted that XFLR5 comes with its own set of limitations such as potential flow in the free stream, laminar flow, laminar boundary layers, no 3D effects inside the boundary layer, etc.

Before proceeding further, the selection criteria and their weights, which will aid in the picking of an airfoil, were defined:

¹<https://aerodynamics.lr.tudelft.nl/cgi-bin/afCDB> [cited 22.05.2024]

- $C_{l_{max}}$: A higher lift coefficient of the airfoil $C_{l_{max}}$ translates into a higher wing loading. Thus, by reducing the wing size decreases the stall speed, one can ensure that the stall speed is significantly below the lowest transition speed expected, enabling a safe transition phase. A smaller wing size would subsequently reduce drag, thereby enhancing the aircraft's energy efficiency. This improvement in efficiency contributes to a more sustainable design. A weight of 1 is given for this criteria.
- α_{stall} : The angle of attack at which the airfoil stalls should be higher to allow more wiggle room when operating the aircraft, making it safer to operate. A weight of 3/8 is given for this criteria.
- C_d at $C_{l_{des}}$: The lower the drag coefficient of the airfoil at the designed lift coefficient, the better due to it requiring less battery energy usage during cruise, thus decreasing the battery weight and triggering a snowball effect which leads to a more energy efficient and sustainable design. A weight of 1 is given for this criteria.
- C_m at $C_{l_{des}}$: The higher the moment coefficient of the airfoil at the designed lift coefficient, the more the controllability curve shifts to the left, thus improving controllability. A weight of 2/8 is given for this criteria.
- Drag bucket: A larger drag bucket allows the aircraft to be used for a wider range of angle of attack. A weight of 0.125 is given for this criteria.
- Stall characteristics: A smoother drop-off in the lift coefficient, after the maximum lift coefficient is reached, is considered safer, thus beneficial. This criteria was judged by visually inspecting the curves and assigning scores of 1 to 5. A weight of 0.5 is given for this criteria.

All the airfoils are scored based on relative performance, where the top performer got a score of 5 and the lowest performer had a score of 1 assigned to it. The airfoils in between have a defined interval based on the difference between the top and lowest performer values, which was then divided by 5. If the performance of the airfoil was within one interval of the lowest or top performer, it would still be assigned a score of 1 or 5 respectively. After performing the initial analysis of 45 different airfoils, the 6 top performing airfoils were selected for another trade off iteration as seen in Table 9.3. Thus, allowing for a more relative comparison between the 6 best-performing airfoils. Additionally, the intervals were recalculated based on the top 6 performers, and scores were assigned again. It should be noted, that sometimes the points of interest, such as the design lift coefficient, were between two simulated points, which led to the use of linear approximation for the point of interest. Lastly, the stall characteristics are the only criteria that were visually evaluated. Thus, the scores from the first trade-off analysis were carried over to the new analysis. A future recommendation is to research a stall gradient to have a more quantifiable way of scoring the stall characteristic.

Table 9.3: Relative trade-off table between the 6 best-performing airfoils

Airfoil/Criteria	$C_{l_{max}}$	α_{stall}	C_d at $C_{l_{des}}$	C_m at $C_{l_{des}}$	Drag bucket	Stall characteristics	Result (max: 16.25)
B737c	2	1	3	5	3	2	7.375
C141A	1	2	3	4	1	5	7.875
K3	4	1	1	1	4	3	7.5
LA203a	5	5	5	1	2	4	14.25
MS317	5	2	3	3	5	4	11.75
NLR7301	5	3	1	3	4	3	9.5

After performing the trade-off analysis for the detailed design, it can be seen that the Douglas LA203a airfoil came on top. It can be seen that the LA203a airfoil performs above average in most criteria except the C_m at $C_{l_{des}}$. However, this is due to the analysis being a relative trade-off analysis between the top 6 performers. Against a bigger sample size such as the first trade-off analysis, the LA203a airfoil still performs rather well in the C_m at $C_{l_{des}}$ criteria as well. The aerodynamic characteristics and the quantified performance of all the airfoils can be seen in Table 9.4.

Table 9.4: Performance data for the 6 best-performing airfoils, $Re = 5.218e6$ [-]

Airfoil	$C_{L_{max}}$	α_{stall}	C_d at $C_{l_{des}}$	C_m at $C_{l_{des}}$	Drag bucket
B737c	1.893	19.5	0.007	-0.01	19.5
C141A	1.769	20.8	0.007	-0.031	18.5
K3	2.09	19.8	0.008	-0.153	14.5
LA203a	2.046	23.4	0.006	-0.179	16.5
MS317	2.099	20.6	0.007	-0.092	15
NLR7301	2.092	21.8	0.008	-0.078	14

It can be seen that the lift coefficient is sufficiently high to ensure safe transition as mentioned in the conditions for airfoil trade-off, while the expected drag coefficient is minimised to ensure a more efficient flight. The lift coefficient for transition was computed by the performance department when simulating the transition phase.

It should be noted, in case the design is changed in the future, this trade-off should be iterated with the new parameters ensuring that the most optimal airfoil is chosen. Additionally, the chosen airfoil promotes an above average stall characteristic, giving a non-abrupt stall as required by REQ-WNG-08.

9.2. Empennage

This section describes the design of the empennage. Firstly, the requirements are explained in Section 9.2.1 which is followed by the assumptions used in Section 9.2.2. Lastly, the empennage was designed in Section 9.2.4

9.2.1. Subsystem Requirements and Compliance Matrix

Table 9.5: Empennage subsystem requirements.

Identifier	Requirement	Source(s)	Compliance	Location
REQ-EMP-01	The empennage shall ensure the aircraft remains controllable in every motor failure mode.	REQ-SYS-AC-88, REQ-SYS-AC-56, R-TEC-14	✓	Analysis by stability analysis (not included in report), testing during flight testing
REQ-EMP-02	The empennage shall ensure the aircraft can maintain its direction in every motor failure mode.	REQ-SYS-AC-56	✓	Analysis by stability analysis (not included in report), testing during flight testing
REQ-EMP-03	The empennage shall ensure that the aircraft is directionally trimmable in cruise, climb and descent conditions.	REQ-SYS-AC-18	✓	Analysis by stability analysis (not included in report), testing during flight testing
REQ-EMP-04	The empennage shall be able to ensure a constant yaw angle degrees.	REQ-SYS-AC-22, REQ-SYS-AC-23, REQ-SYS-AC-49	✓	Analysis by stability analysis (not included in report), testing during flight testing
REQ-EMP-05	The manufacturing cost of the empennage subsystem shall be less than 25000 euros.	REQ-SYS-AC-94	✓	Analysis by financial analysis in Chapter 23
REQ-EMP-06	The empennage shall ensure a positive aircraft yawing moment derivative with respect to the yawing angle.	REQ-SYS-AC-47	✓	Analysis by stability analysis (not included in report)
REQ-EMP-07	The empennage shall function in an ambient temperature range of -20 °C to 47 °C.	REQ-SYS-AC-31	✗	Testing in the prototyping phase

9.2.2. Assumptions

Table 9.6: Assumptions used for the empennage design.

Identifier	Assumption	Expected Effect
A-EMP-01	Subsonic flow around the vertical tail	The rudder can function
A-EMP-02	Maximum rudder deflection angle does not stall	Can calculate the rudder control derivative

9.2.3. Method

The empennage, unlike other subsystems, requires what may seem like a backwards approach to its design. Instead of basing the design on an analytical model, the way to compute the tail parameters is by selecting certain values for said parameters, computing the rest of the tail dimensions, then checking if that tail can provide a sufficient counter-moment, and optimising it. In the case of the HAROLD, the parameters that were initially picked were the aspect ratio, taper ratio, sweep, volume coefficient, and tail arm. The volume coefficient is based on statistics provided by Scholz [16]. Afterwards, the aspect ratio, taper, and sweep are selected based on the data presented in the course AE1222-II ADSEE lecture 7: "Empennage and Undercarriage Design" [17]. After this, the tail arm is manually determined by examining the already existing CATIA model. Following that, the tail surface area is computed by utilising the formula for the specific volume coefficient. From there and the aspect ratio, the mean aerodynamic chord and the span are found. Using the span, area, and taper ratio, one can find the root chord and the tip chord of the tail. The mean aerodynamic chord is also obtained from the area and the span of the tail. With this, the first iteration of the tail sizing is finished.

Once the preliminary dimensions of the tail are known, the rudder is sized. The first step is to obtain the maximum moment to be counteracted during one of the aircraft's limiting cases. The procedure followed for the design of the rudder closely resembles the procedure detailed by Mohammad H. Sadraey in the book "Aircraft Design: A Systems Engineering Approach", chapter 12 [18]. Based on the maximum moment and the tail moment arm, the force required to be produced by the tail is obtained. Additionally, the sweep at the halfway chord point is calculated to be used as a variable in the formula to calculate the lift coefficient gradient of the tail by using the formula provided by ESDU 70011 [19]. Following that, the dynamic pressure is obtained, and by using the formula for the vertical tail stability derivative the derived by Fabrizio Nicolosi et. al. in "A Comprehensive Review of Vertical Tail Design" [20]. Based on the stability derivative, the rudder control derivative is computed when assuming the maximum deflection angle. From there, one can obtain the angle of attack effectiveness of the tail, and from there it is possible to find the chord ratio between the rudder chord and the root chord of the tail.

Once the rudder chord is found, it is time to check whether enough of the rudder would be outside of the wake

of the back wing in case the aircraft needs to recover from spinning, which is defined as the area between the line drawn at a 60 degree angle with the chord from the leading edge and the line that can be drawn at 30 degree from the chord at the trailing edge. If less than one third of the total rudder area is outside of the wake of the back wing, the tail is either moved or its sweep increased.

9.2.4. Results

After the final iteration of the aircraft structure and subsystems, the tail parameters were finalised, and can be seen in Table 9.7.

Table 9.7: Values of empennage sizing parameters and corresponding rationales.

Parameter	Value	Unit	Rationale
Airfoil	NACA 0012	-	Airfoil used for the tail
S_{tail}	2.141	m ²	Surface area of the tail
λ_{tail}	0.5	-	Taper ratio of the vertical tail
Λ_{tail}	50.0	deg	Sweep of the vertical tail
AR_{tail}	1.0	-	Aspect ratio of the vertical tail
l_{tail}	4.704	-	Moment arm of the tail
V_{tail}	0.06	-	Volume coefficient of the tail
$c_{roottail}$	1.951	m	Root chord of the tail
$c_{mactail}$	1.463	m	Mean aerodynamic chord of the vertical tail
b_{tail}	1.463	m	Span of the vertical tail
$L_{cruise\ empennage}$	1116.18	N	Lift produced by the empennage in cruise conditions at maximum deflection of rudder
c_{rudder}	0.887	m	Chord length of the rudder
b_{rudder}	1.463	m	Span length of the rudder
S_{rudder}	1.298	m ²	Area of the rudder

For the tail, the NACA 0012 was selected as an airfoil based on the fact that it is symmetric, its relatively high lift-to-drag ratio and low drag coefficient [21]. The aspect ratio of the tail was kept as low as possible in order to maximise the root chord length in order to provide a stable and secure connection with the fuselage, as the attachment point of the tail is quite aft. Furthermore, during iteration it was concluded that a lower aspect ratio led to a lower structural weight. The taper is minimised in order to minimise the structural weight, however it is kept at 0.5 to account for the rectangular rudder. Sweep is maximised once again to ensure a long tail arm, as well as to "push" the rudder as much as possible outside of the spiral wake of the back wing. It must be noted that regardless of the high sweep, the initial tail placement could not fulfil the spiral stability requirement. As such, the rudder was extended below the fuselage.

9.2.5. Verification and Validation

The code used for the tail sizing was verified by hand calculations of the functions defined in the scripts, as well as by cross-checking certain functions between possible sources to obtain them. At this stage of the project, validation of the stability derivatives was not performed, as eVTOLs are an emerging product, and as such, there is not as much data on their functioning. The best way to validate the method and values obtained in this report would be by experimentation with this particular product, which impossible on the scale that the project is currently being conducted. As for the assumptions mentioned in Table 9.6, AS-EMP-01 was checked examining whether the conditions allowed for trans-sonic airflow, and AS-EMP-02 was verified by calculating the effective angle of attack and checking whether the tailplane would stall at it.

Chapter 10 | Aerodynamic Analysis

This chapter focuses on evaluating the aerodynamic characteristics of the aircraft. Firstly, the requirements related to the wings are referred to in Section 10.1. This is followed by an explanation of all the assumptions used in this chapter which is found in Section 10.2. Afterwards, Section 10.3 explains how the aerodynamic performance was modelled. This is followed by a sensitivity analysis of the aerodynamic model performed in Section 10.4. Lastly, verification and validation were carried out in Section 10.5 and Section 10.6 respectively.

10.1. Wing Subsystem Requirements and Compliance Matrix

All subsystem requirements of the wing subsystem carry over from Chapter 9 where the wing and empennage were sized. More specifically, these subsystem requirements were given in Table 9.1.

10.2. Assumptions

This section shortly summarises the assumptions made in this chapter in Table 10.1. However, when presenting the methods used in the following sections, these assumptions are iterated upon.

Table 10.1: Assumptions used for the aerodynamic methods.

Identifier	Assumption	Expected Effect
A-WNG-01	Performance of the wing is the same across varying temperatures.	This should introduce an error in the slope of the wings. However, this error was evaluated to be 2.59% for the worst expected scenario as found in Section 10.3.1.
A-WNG-02	Fuselage lift slope interference factor formula is applicable for low sweep wings.	This formula assumes no sweep of the wing. However, in this project the wing has a slight sweep at the leading edge. This will introduce an error in the calculation. However, it is expected to be negligible.
A-WNG-03	The front wing doesn't experience down wash induced by the rear wing.	This assumption gives a higher lift coefficient than in reality. Although this is a non-conservative assumption, the effect is expected to be small. This is due to the wings being separated approximately 5 times of their average chord.
A-WNG-04	Boundary layer transition points.	The boundary layer transitions were estimated using literature [15]. However, a very conservative approach was taken due to limited data for wooden structures.
A-WNG-05	Interference factors for the zero lift drag of each component is assumed based on literature.	The interference factors between the wings, tail, nacelle and fuselage are assumed based on literature [15]. An effort was made to take conservative interference factors through the design to make the calculations conservative. Additionally, the nacelles were given a safety factor of 1.1 although literature suggest to only take 1.
A-WNG-06	The stall angle of the wings is assumed to be the same with and without propeller interaction.	It is expected that the stall angle is going to change due to the propellers. However, it is difficult to estimate if the swirl produced from the propellers will energise the boundary layer and increase the stall angle, or will the increased velocity give an earlier stall. Nonetheless, it is recommended that this effect it analysed during the prototype testing.
A-WNG-07	The fuselage is assumed to be a cylinder in vertical take-off and landing when performing the aerodynamic evaluation.	This assumption is a conservative assumption due to the fuselage having a more streamlined shape instead of a circle. Thus, creating less drag.
A-WNG-08	The fuselage is assumed to induce no lift.	This was assessed during the CFD analysis where the fuselage reached a maximum of 1.6% of the total lift in conventional flight. This was done in the Section 10.6.
A-WNG-09	The additional angle near the stall regions is estimated using the DATCOM method by applying a $\Delta\alpha_{C_{Lmax}}$ correction.	This was approximated using graphical figures presented by the DATCOM method as well as using the shape of the airfoil and it's sharpness factor as can be found in [15].
A-WNG-10	The skin friction drag coefficient of the aircraft is assumed to be equal to the skin friction drag coefficient of a flat plate.	This underestimates the skin friction coefficient of the aircraft as it is not a flat plate, thus having a different boundary layer development. However, the method presented takes this into account by applying a safety margin at the end of the full calculations.
A-WNG-11	The drag in post stall is assumed to be induced by the fuselage and wing only.	This simplifies the analysis and as such introduces an error by not including the nacelles, landing gear, propellers and the tail. The effect of this assumption should be estimated when validating the model by the use of CFD.
A-WNG-12	The fuselage is assumed to be a cylinder in vertical flight.	This will introduce a conservative error due to the fuselage being more streamlined than a cylinder.
A-WNG-13	The profile drag is taken into account by the form factors FF.	This is an assumption of the method that quantifies the form drag coefficients using an empirical formula presented in Section 10.3.4

10.3. Aircraft aerodynamic performance

This section starts off with an analysis of the lifting performance of the aircraft in Section 10.3.1. This is heavily affected by the down wash of the wings which is assessed in Section 10.3.2. Afterwards, to reduce the effect of the tip vortexes, the wing tips were modelled in Section 10.3.3. With the wing tips modelled, the drag estimation can finally be modelled in Section 10.3.4. Furthermore, the effect of the wing-propeller interaction was assessed in Section 10.3.5. Lastly, the lift and drag curve were extended beyond stall in Section 10.3.6 to give aerodynamic predictions for vertical take-off and transition.

10.3.1. Lift Estimation

Unfortunately, the airfoil performance does not translate to the performance of the wing due to its finite length. In turn, a model was created to transform the airfoil performance into the performance of the wing. For this, the DATCOM method found in literature was employed [15]. The wing slope was found using Equation 10.1

$$C_{L\alpha} = \frac{C_{l\alpha} \cdot AR}{2 + \sqrt{4 + \frac{AR^2 \cdot (1 - M_{cruise}^2)}{\eta^2} \left(1 + \frac{\tan^2 \Lambda_{0.5c}}{1 - M_{cruise}}\right)}} \quad (10.1)$$

where η is the airfoil efficiency factor which is approximately 0.95 [15], $\Lambda_{0.5c}$ is the sweep at half chord, and the M_{cruise} is the Mach speed at cruise which can be computed by dividing the cruise velocity with the speed of sound at cruise altitude. The Mach was found to be 0.2. However, the aircraft will not always be flying in cruise conditions. Due to this, a quick evaluation of the wing performance was done by varying the temperature from -20 °C to 47 °C due to the REQ-WNG-07 requirement, and the velocity from 36 m/s to 69.444 m/s. This was also combined for the worst case scenario of 47 °C and 36 m/s, resulting in a maximum error of 1.26%. To account for boundary layer friction and separation temperature effects, a the maximum expected temperature was multiplied by 1.5 to quantify the difference in the lift slope. It was found that this resulted in an error of 2.59%.

The slope of the wing still needs to be adjusted due to the fuselage interference. This can be done using a correction factor which can be calculated using Equation 10.2 [22]:

$$K_{wf} = 1 + 0.025 \left(\frac{d_f}{b}\right) - 0.25 \left(\frac{d_f}{b}\right)^2 \quad (10.2)$$

where d_f is the maximum fuselage diameter. It should be noted that Equation 10.2 is not part of the method presented before. However, the used method does not take into account the lift slope reduction of the fuselage. Thus, when estimating the lift slope, using this formula makes the estimation more conservative then continuing with the traditional DATCOM method as seen in [15].

The maximum lift coefficient of the wing can be approximated using Equation 10.3:

$$C_{L_{max}} = \left[\frac{C_{L_{max}}}{C_{l_{max}}} \right] C_{l_{max}} + \Delta C_{L_{max}} \quad (10.3)$$

where $\frac{C_{L_{max}}}{C_{l_{max}}}$ can be estimated to be around 0.9 due to the wing's very low sweep nature as long as the aforementioned Mach number and airfoil apply [15], and $\Delta C_{L_{max}}$ is a term accounting for compressibility effects above Mach 0.2 thus negligible in this analysis [14]. This is different compared to Equation 9.2, however this method introduces a level of safety when designing a wing, thus giving a further level of safety during the design phase. Furthermore, the stall angle of the wing can be approximated using Equation 10.4 [15]:

$$\alpha_{stall} = \frac{C_{L_{max}}}{C_{L\alpha}} + \alpha_{0L} + \Delta\alpha_{C_{L_{max}}} \quad (10.4)$$

where $C_{L_{max}}$ and $C_{L\alpha}$ were obtained as shown previously, α_{0L} is the zero lift angle of attack which is a known characteristic from the airfoil simulation, and $\Delta\alpha_{C_{L_{max}}}$ is a compensation term for the reduced slope near the stall angle due to the formation of leading-edge vortexes. Using the leading edge sharpness parameter which can be obtained from the airfoil's coordinates, the $\Delta\alpha_{C_{L_{max}}}$ can be approximated to be 3 degrees and 1 degree for the positive and negative stall angle respectively using literature [15].

Furthermore, the lift coefficient of the whole aircraft was calculated using Equation 10.5:

$$C_{L_{aircraft}} = 0.5 \cdot C_{L\alpha} (\alpha - \alpha_{0L}) + 0.5 \cdot C_{L\alpha} \left(1 - \frac{d\epsilon}{d\alpha}\right) (\alpha - \alpha_{0L}) \quad (10.5)$$

where $C_{L\alpha}$ is the previously calculated wing slope including the correction factor K_{wf} , and $\frac{de}{d\alpha}$ is the down wash gradient affecting the rear wing created by the front wing which is further discussed in Section 10.3.2. Equation 10.5 assumes that the down wash created by the rear wing does not affect the front wing. This introduces an error that reduces the lift slope of the front wing. However, the forward propagation of the down wash effect is difficult to predict. Therefore, to simplify the calculations, this down wash effect was neglected, but it should be kept in mind as this overestimates the lift coefficient created. Additionally, Equation 10.5 is only valid until the non-linear lift curve starts. In mathematical terms, this non-linearity begins from an angle of attack that can be computed by subtracting the $\Delta\alpha_{C_{L_{max}}}$ from the stall angle of the wing. Afterwards, the lift coefficient is computed by manually adding up the lift coefficient curves of both the front and rear wing.

Lastly, the angle of attack at which the wing has to fly in order to deliver the design lift coefficient $C_{L_{des}}$ can be approximated using Equation 10.6:

$$\alpha_{trim} = \frac{C_{L_{des}}}{C_{L\alpha_{aircraft}}} + \alpha_{0L} \quad (10.6)$$

where $C_{L\alpha_{aircraft}}$ is the slope of the aircraft after combining both lift curves of the wings. If this angle was substantially high in an absolute sense, the aircraft would create passenger discomfort in cruise. Thus, if this was the case, the incidence angle of the wings would be changed to ensure comfort during cruise.

The results of these calculations can be found in Table 10.2.

Table 10.2: Performance of the aircraft

Parameter	Value	Unit
$C_{L_{max}}$	1,6796	[-]
$C_{L\alpha}$	0.0776	[1/°]
α_{trim}	1,7	[°]
α_{0L}	-6,5	[°]

It can be seen that the aircraft generates sufficiently high lift, thus complying with requirement REQ-WNG-02. Additionally, it can be observed that the trim angle is relatively low at 1.7 degrees. This ensures that requirement REQ-WNG-05 and REQ-WNG-10 is met to ensure passenger comfort and allowing the wings to operate without incidence. Although not seen here, it was ensured that aircraft should perform missions within angles of attack where the rear wing is not in the wake of the front wing. This angle was calculated by taking the arctan of the stagger divided by the gap which was found to be approximately 14 degrees, while the maximum angle expected during flight equated to 12 degrees. This result comes from an emergency landing in case the aircraft is landing as a conventional aircraft.

10.3.2. Down Wash Gradient

To estimate the down wash gradient of the front wing affecting the rear wing, a method suggested by Mondher was used [23]. Mondher used the vortex lattice method VLM to obtain data points for a given taper, aspect ratio and the gap, while the stagger was varied. This would give several points which were interpolated to give Equation 10.7. Additionally, Mondher compared the model with experimental data, finding a maximum error of 10%. However, this was for two wings with a taper of 1, low aspect ratio and no gap. The maximum error reduced to 6% for wings with lower taper ratios and a normalised gap of 0.1. Mondher showed that a higher gap tends to reduce the error of the method. Thus, a gap of 0.271 is expected to reduce the maximum error even further.

$$\frac{de}{d\alpha} = \frac{1 + c_1\bar{\xi}}{c_2 + c_3\bar{\xi}} \quad (10.7)$$

where $\bar{\xi}$ is the normalised stagger which is obtained by dividing the stagger with half the wing span of the wing, while c_1 , c_2 and c_3 are constants that are defined based on the aspect ratio, wing span, normalised gap, taper ratio and sweep of the front wing. It should be noted that the maximum normalised gap available in literature was 0.2 [23]. However, the final design uses a normalised gap of 0.271. Thus, to have a conservative estimate, the constants belonging to the normalised gap of 0.2 were used. For this project, these constants c_1 , c_2 and c_3 were equal to 0.9, 1.03 and 5.28 respectively, giving a down wash gradient of 0.28. It is expected that his value will be lower in reality due to the conservative approach of using constant related to a lower normalised gap than used in this design.

10.3.3. Wing Tip Modelling

To improve the aerodynamic efficiency of aircraft wings, wing tip devices such as winglets or raked wing tips are employed to mitigate drag induced by wing tip vortices. These devices are designed to alter airflow patterns at the wingtips, preventing high pressure air from spilling over into low pressure regions, thereby reducing drag and enhancing energy efficiency. Additionally, wingtip designs contribute to greater stability and control of the aircraft, optimising overall aerodynamic performance and operational effectiveness. In physical terms, the way this reduction in induced drag is modelled is by introducing an addition to the aspect ratio of the wing. Using Equation 10.8, this addition can be calculated for wing tips [15].

$$\Delta AR = 1.9 \frac{h_t}{b} AR \quad (10.8)$$

where h is the height of the wing tips. The results of Equation 10.8 are added to the current wing aspect ratio for the induced drag calculation and a reduced drag can be computed. However, the incorporation of wing tips introduces drawbacks, such as increased cost and additional weight, which can negatively impact energy usage. This was assessed by varying the wingtip size from 0 m to 0.5 m and considering the added weight of the wings, with the 0.5 m limit ensuring sufficient clearance between the wingtips and propellers in landing configuration. It was found that wing tips reduce energy usage by 4% compared to no wingtips, leading to the selection of 0.5 m as the best feasible wing tip height for each wing, improving the sustainability of the aircraft.

As a final note on the wing tips, Equation 10.8 depends only on the wing tip's height. This will give a sufficiently accurate answer on the effect the wing tips have on the induced drag. However, a more detailed design, and its performance should be evaluated using a more accurate way such as using CFD or performing a wind tunnel test. This will not only give a more accurate estimation of their effect on the induced drag, but also give an evaluation of the stability and controllability improvements, leading to a potential tail size reduction.

10.3.4. Drag Estimation

The drag of the aircraft can be split in two components. The lift induced drag and the zero lift drag. The zero lift drag coefficient C_{D_0} can be calculated using the component drag build-up method found in literature [15]. This method is described by Equation 10.9:

$$C_{D_0} = \frac{1}{S_{ref}} \sum_c C_{f_c} FF_c IF_c S_{wet_c} + C_{D_{misc}} \quad (10.9)$$

where C_{f_e} is the flat plate skin friction coefficient, FF is the form factor, IF is the interference factor, S_{wet_c} is the wetted surface area of each component, and $C_{D_{misc}}$ is other miscellaneous. To calculate the flat plate skin friction coefficient, the transition of the boundary layer from laminar flow to turbulent flow has to be estimated. This was done per component based on statistical data found in literature [15]. For the wings and vertical tail, the transition point was chosen at 10% of the chord, while the nacelles and the fuselage have a fully turbulent boundary layer. The chosen transition points are conservative estimates because they assume poor surface finish inducing early transitions making this estimate a conservative one when it comes to skin friction drag. The skin friction coefficient can be calculated for each component using the skin friction coefficients of a flat plate as seen in Equation 10.10 and Equation 10.11. This assumption was explained in Table 10.1.

$$C_{f_{laminar}} = \frac{1.328}{\sqrt{Re}} \quad (10.10) \quad C_{f_{turbulent}} = \frac{0.455}{(\log_{10} Re)^{2.58} (1 + 0.144 M^2)^{0.65}} \quad (10.11)$$

where Re is the Reynolds number depending on the characteristic length, density, dynamic viscosity, and the velocity. These skin friction coefficients are averaged based on the transition point.

The form factor for the wings and tail, fuselage, and nacelle can be calculated using Equation 10.12, Equation 10.13 and Equation 10.14 respectively. Parameter f , seen in the fuselage and nacelle calculations, can be calculated using Equation 10.15 where l is the body length and A_{max} is the maximum cross-sectional area. Additionally, t/c is the maximum thickness over chord, $(x/c)_m$ is the position along the chord where the maximum thickness is located, M is the Mach number, and Λ_m is the sweep at $(x/c)_m$.

$$FF = \left[1 + \frac{0.6}{(x/c)_m} \frac{t}{c} + 100 \left(\frac{t}{c} \right)^4 \right] [1.34 M^{0.18} \cos(\Lambda_m)^{0.28}] \quad (10.12) \quad FF = 1 + \frac{60}{f^3} + \frac{f}{400} \quad (10.13)$$

$$FF = 1 + \frac{0.35}{f} \quad (10.14) \quad f = \frac{l}{\sqrt{(4/\pi) A_{max}}} \quad (10.15)$$

It should be noted that the formulas used for the form factors were compared to different methods that estimate these form factors. It was found that the form factors of the fuselage and nacelle used in this report are more conservative estimates when comparing all of the different methods ¹. On the other hand, the form factor formulas for the wings and tail show a more average prediction compared to other methods. Nonetheless, the form factor formulas for the wing and tail were kept due to their incorporation of the Mach number, sweep and position of the maximum thickness of the airfoil unlike the other methods.

The interference factor was obtained using literature [15]. The interference factor for the front wing was assumed to be $1.25 \cdot 1.4$ due to having objects mounted to the wings such as the nacelles, and due to its low position. The rear wing has a 1.25 interference factor due to having objects mounted to it. For the tail, an interference factor of 1.05 was chosen due to the use of a conventional tail. When it came to the fuselage, a factor of $1.1 \cdot 1.1$ was used because of the two wings. In case the fairing is well designed, this interference factor could drop to 1. However, to keep the estimate conservative, a well designed fairing assumption was avoided. Lastly, the nacelles normally don't have an interference factor. However, a factor of 1.1 was still given to ensure the drag is not underestimated.

Lastly, as part of the $C_{D_{misc}}$, the fuselage upsweep drag, which present the drag due to flow separation, needs to be estimated. This can be done as illustrated in Equation 10.16 [15].

$$C_{D_u} = \frac{3.83u^{2.5}A_{max}}{S_{ref}} \quad (10.16)$$

where the u is the upsweep of the fuselage in radians, and S_{ref} is the surface area of the wings. As can be seen in Equation 10.16, the upsweep angle has an exponent of 2.5. Thus, during the fuselage design, it was important to reduce the upsweep as much as possible to reduce the drag created. However, it was still important to ensure the down wash gradient presented in Section 10.3.2 and the packaging were taken into account. The former being important to ensure a sufficient maximum lift coefficient is created and the cruise angle is not in a zone where the passengers feel uncomfortable. Furthermore, the landing gear was not taken into account due to it folding into the aircraft during flight operations. However, to account for any miscellanea not included in this drag estimation method, a further 10% of the total zero lift drag was added as suggested in literature [15].

Lastly, the lift induced drag needs to be calculated. To do this, the Oswald efficiency factor needs to be estimated using the method presented by Nita and Scholz [24]. This method predicts the Oswald efficiency factor both the wings combined using Equation 10.17.

$$\frac{e_{tan}}{e_{ref}} = 0.5 + \frac{1 - 0.66h_s/b}{2.1 + 7.4h_s/b} \quad (10.17)$$

where h_s/b is the gap of the wings divided by the wing span, and e_{ref} is the Oswald efficiency factor of the reference wing. In this case, the reference wing is the equivalent wing if the front and rear wing were combined, making the reference wing have their combined surface area while the span is the same. This halves the aspect ratio of the reference wing. To estimate the Oswald efficiency factor of the reference wing, Nita and Scholz present the formula as seen in Equation 10.18.

$$e_{ref} = 1.78(1 - 0.045AR^{0.68}) - 0.64 \quad (10.18)$$

With the Oswald efficiency factor estimated, the induced drag can be calculated as illustrated in Equation 10.19.

$$C_{D_i} = \frac{C_L^2}{\pi AR_{tan}e_{tan}} \quad (10.19)$$

where C_L is the lift coefficient of the whole aircraft which was explained in Section 10.3.1, and the AR_{tan} is the aspect ratio of the combined reference wing.

With these results obtained, the drag polar can be plotted as seen in Figure 10.1. The breakdown of the drag coefficient can be seen in Figure 10.2, while the values itself can be seen in Table 10.3.

¹<https://openvsp.org/wiki/doku.php?id=parasitedrag>

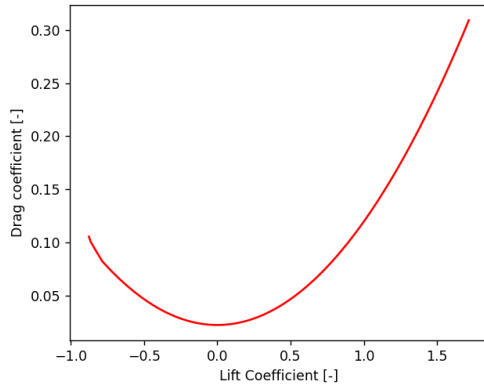


Figure 10.1: Drag polar of the aircraft

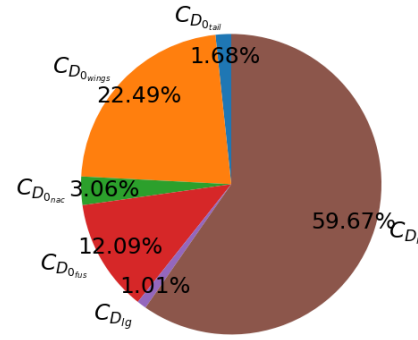


Figure 10.2: Drag breakdown in cruise conditions

Based on this, the induced drag is taking up more than 59.67% of the total drag at cruise. It should be noted that this also takes into account the drag caused by the fuselage due to separation. However, it is also the parameter which the authors have the least confidence in. This is due to the induced drag depending on multiple empirically obtained parameters such as the lift coefficient and the Oswald efficiency factor. Thus, if a large error between the model's prediction and the aircraft is created, this would be the first parameter that should be further analysed along with the lift coefficient.

Table 10.3: Drag Coefficient Breakdown in Cruise

Parameter	Value	Unit
$C_{D_{0tail}}$	0.0011	[-]
$C_{D_{0wings}}$	0.0147	[-]
$C_{D_{0fus}}$	0.0079	[-]
$C_{D_{0nac}}$	0.002	[-]
$C_{D_{ig}}$	0.00066	[-]
C_{D_i}	0.039	[-]

10.3.5. Wing-Propeller Interaction

The final design contains 6 engines on the front and 4 engines on the rear. Thus, it is expected that the propellers will have a noticeable effect on the wings and their aerodynamic performance. To better understand this effect, an analysis was performed using the method suggested by Vos [25]. Firstly, the velocity increase over the wing needs to be computed using Equation 10.20.

$$\Delta V = v_{cruise} \left(\sqrt{1 + C_T \frac{S_{wing}}{n_e \frac{\pi}{4} D^2}} - 1 \right) \quad (10.20)$$

where C_T is the thrust coefficient, D is the diameter of the propellers, and S_{wing} is the surface area of the wing. It is important to notice that this should be applied per wing. Thus, the thrust should be split into the forward and rear thrust coefficient. Equation 10.20 has the limitation of only using propellers of equal size. Fortunately, the final design has propellers of equal size per wing ensuring this limitation is not an issue. Another assumption that Equation 10.20 assumes is that the increase in velocity is uniform across the whole wing, while the swirl which could help delay stall by re-energising the boundary layer, and directional translation are neglected, thus the stall angle is assumed to be the same. Of course, this will never be the case, and should be further investigated once the propellers are built by performing tests which evaluate the propellers performance and slipstream effect. With that in mind, the contracted slipstream diameter can be calculated as illustrated in Equation 10.21.

$$D^* = D \sqrt{\frac{v_{cruise} + \Delta V/2}{v_{cruise} + \Delta V}} \quad (10.21)$$

Finally, the lift coefficient effect can be calculated by employing Equation 10.22.

$$\Delta C_L = \frac{2}{S_w} n_e \frac{\pi}{4} D^{*2} \left(\frac{(v_{cruise} + \Delta V)^2}{v_{cruise}^2} \frac{2C_{L\alpha}}{\pi A_{s,eff}} \sin(\alpha_s) - \frac{2C_{L_w}}{\pi A R_w} \right) \quad (10.22)$$

where S_w and A_w are the area and aspect ratio of one wing, $C_{L\alpha}$ is the lift slope of the wing, α_s is the angle of attack of the wing part immersed in the slipstream, and $A_{s,eff}$ is the effective aspect ratio of the wing part immersed in the slipstream. The effective aspect ratio can be calculated using Equation 10.23, while Equation 10.24 can be used to compute α_s .

$$A_{s,eff} = A_S + (A_W - A_S) \left(\frac{v_{cruise}}{v_{cruise} + \Delta V} \right)^{A_w - A_s} \quad \alpha_s = \alpha^* - \alpha_{0L} \quad (10.24)$$

where α_{0L} is the zero lift angle of attack, while α^* and A_s are calculated using Equation 10.25 and Equation 10.26 respectively.

$$\alpha^* = \arctan \left(\frac{v_{cruise} \sin(\alpha)}{v_{cruise} \cos(\alpha) + \Delta V / 2} \right) \quad A_s = n_e \frac{\pi}{4} D^{*2} \quad (10.25)$$

In case incidence needs to be implemented to obtain passenger comfort as explained earlier, it can be simply added to Equation 10.24. It is important to stress that these formulas need to be calculated for each wing, while the propellers need to be the same size for each wing. Additionally, Vos only accounts for the lift coefficient change across the wings. However, the lift distribution change along the span still needs to be accounted for. Subsequently, this change in the lift distribution would decrease the Oswald efficiency factor, thus increasing induced drag. In order to not underestimate the induced drag, a model suggested by Patterson and Borer was used [26]. The effect of propellers on the Oswald efficiency factor is modelled as a parabolic function which can be seen in Equation 10.27.

$$e_{tan} = \frac{(\Delta V - \Delta V_{max})^2}{\Delta V_{max}^2} (e_{0,max} - e_{0,min}) + e_{0,min} \quad (10.27)$$

where ΔV is the average axial velocity created by the propellers, ΔV_{max} is the maximum possible average axial velocity created by the propellers, $e_{0,max}$ is the Oswald efficiency factor at 0 thrust, and $e_{0,min}$ is the minimum Oswald efficiency factor taken from literature [26]. It is important to note that the $e_{0,min}$ changes for different angles of attack, reaching lower values for low angles. Thus, a $e_{0,min}$ for low angles of attack was taken to give a conservative estimate.

With the defined parameters, Table 10.4 presents the influence of propellers on the aircraft under cruise conditions. The initial two rows detail varying thrust levels applied to the front and rear engines, with their combined thrust approximately equating to the required thrust for cruise. These thrust levels were adjusted to examine their impact on the Oswald efficiency factor, lift slope, and maximum lift coefficient.

Table 10.4: Effect of propellers on wing performance

Parameter	Value				Unit
T_f	0	1332	932	1732	[N]
T_r	0	1332	1732	932	[N]
$C_{L\alpha}$	0.0776	0.0796	0.0799	0.0791	[1/deg]
$C_{L_{max}}$	1.679	1.721	1.733	1.711	[-]
e_{tan}	0.737	0.702	0.705	0.699	[-]

The results indicate that increasing thrust on the rear wing leads to a higher Oswald efficiency factor, an enhanced lift slope, and a greater maximum lift coefficient. Consequently, to achieve a reduced cruise angle, the pilot can modify the thrust distribution between the front and rear engines. Additionally, the findings suggest that operating with higher rear thrust is more efficient with respect to induced drag, due to the elevated Oswald factor.

10.3.6. Extension of the Lift and Drag Curves Beyond Stall

To better understand the energy consumption in flight phases after stall such as the take-off and landing, or transition, a model predicting the lift and drag past the stall regions had to be implemented. To do so, a modified model created by Chauhan and Martins was used to predict the drag and lift beyond the stall region [27]. For the post stall lift, the following equations are used:

$$C_L = A_1 \sin(2\alpha) + A_2 \frac{\cos^2(\alpha)}{\sin(\alpha)} \quad (10.28)$$

$$A_1 = \frac{C_1}{2} \quad (10.29)$$

$$A_2 = (C_{L_s} - C_1 \sin(\alpha_s) \cos(\alpha_s)) \frac{\sin(\alpha_s)}{\cos^2(\alpha_s)} \quad (10.30) \quad C_1 = 1.1 + 0.018(AR) \quad (10.31)$$

where α_s is the stall angle, C_{L_s} is the lift coefficient at the stall angle, and AR is the aspect ratio of the wings combined. The post stall drag can be computed using the following formulas:

$$C_L = B_1 \sin(\alpha) + B_2 \cos(\alpha) \quad (10.32) \quad B_1 = C_{D_{max}} \quad (10.33)$$

$$B_2 = \frac{C_{D_s} - C_{D_{max}} \sin(\alpha_s)}{\cos(\alpha_s)} \quad (10.34) \quad C_{D_{max}} = \frac{1 + 0.065(AR)}{0.9 + t/c} \quad (10.35)$$

where C_{D_s} is the drag coefficient at stall angle, and t/c is the thickness of the wing divided by the chord which is defined by the airfoil. It is important to understand that the only the wings created lift. Thus, Equation 10.28 to Equation 10.31 are only used for the wings, while Equation 10.32 to Equation 10.34 are used for wings and fuselage. For the fuselage Equation 10.35 does not apply. Instead, to find the maximum drag coefficient of the fuselage, it was assumed that the fuselage is a cylinder. Thus, the drag coefficient of cylinders in cross-flow was obtained from literature using its cross-sectional area [28]. This equated to be approximately 1.2. However, this still needs to be turned into the aircraft coefficient by multiplying with the cross-sectional area of the fuselage and dividing by the area of the wings. Additionally, the cylinder assumption is naturally a conservative one due to the fuselage being a more elliptical shape. Thus, the fuselage will be more streamlined than a cylinder. Another thing that was neglected was the drag of the tail and the nacelles. However, they are believed to create significantly less drag in the post-stall regions. This is due to the tail not being greatly affected by the angle of attack but a sideslip angle. Nacelles are expected to have a bigger effect than the tail, but their effect should be relatively small when compared to the massive area of the fuselage and wings in cross-flow conditions.

With everything defined, Figure 10.3 and Figure 10.4 show the lift and drag coefficient respectively, for an angle of attack between -90° and 90° . It should be noted that the region near the stall angle was modelled to be parabolic using mathematical expression. Thus, introducing an error near the stall angle. Additionally, the parabolic curvature was not added at the negative stall angle due to the wings having a more abrupt stall for negative angles. This is due to the way airfoils are designed for aircraft.

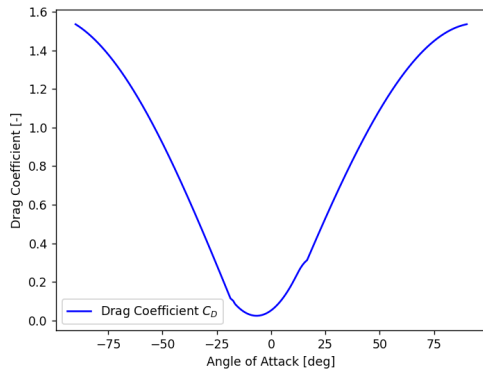


Figure 10.3: Drag coefficient vs angle of attack of the aircraft

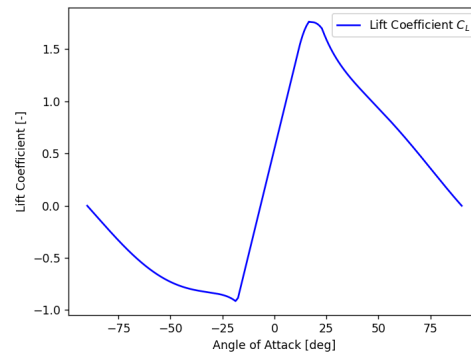


Figure 10.4: Lift coefficient vs angle of attack of the aircraft

10.4. Sensitivity Analysis

In the pursuit of optimising aerodynamic efficiency for aircraft design, the drag coefficient plays a pivotal role due to its direct impact on energy consumption and overall performance. Thus, a sensitivity analysis is performed for various parameters. Firstly, Section 10.4.1 analyses the zero drag coefficient C_{D_0} , which is followed by the induced drag coefficient sensitivity analysis in Section 10.4.2.

10.4.1. Zero Lift Drag

A Monte Carlo simulations was performed to analyse the sensitivity of C_{D_0} to various parameters. These parameters include: wing, fuselage and tail boundary layer transitions, aspect ratio, taper, Mach number, and interference factors for wings, fuselage, tail and nacelles. These parameters were chosen because they were obtained from literature or set as design points. Thus, it was deemed necessary to evaluate their impact.

The ranges for each parameter were obtained by taking the worst and best scenarios from literature. For example, the interference factor would start from 1 and go to 2, representing a very well designed and a badly

designed wing in terms of interference. For the design point parameters, a range accounting for a 50% change in both directions was chosen as seen in Table 10.5.

Table 10.5: Parameter ranges used in the sensitivity analysis

Parameter	Varied range
$BL_{transition_{wing}}$	0-0.75
$BL_{transition_{fus}}$	0-0.4
$BL_{transition_{tail}}$	0-0.75
AR	6-11
Taper	0.1-0.7
M	0.15-0.25
$IF_{FrontWing}$	1-2
$IF_{RearWing}$	1-1.6
IF_{fus}	1-1.4
IF_{nac}	1-1.2
IF_{tail}	1-1.2
$Upsweep_{fus}$	0°-30°

Additionally, each parameter was given a uniform distribution for the assigned ranges. Afterwards, an algorithm was used, taking random values from each parameter and computing the zero lift drag. This was repeated for a total of 10 000 times. The frequency of each C_{D_0} for randomly chosen input parameters can be seen in Figure 10.5, while the individual correlation factors of each input parameter can be seen in Figure 10.6.

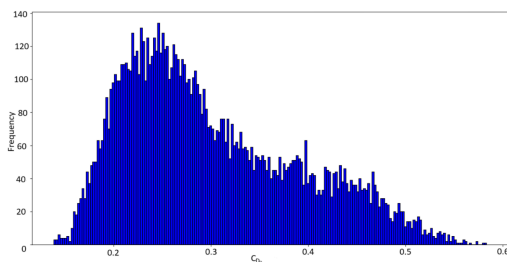


Figure 10.5: Zero Lift Drag Coefficient frequency

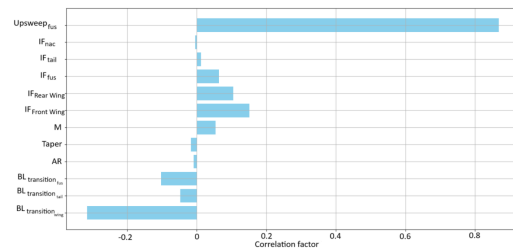


Figure 10.6: Correlation factor for Zero Lift Drag Coefficient input parameters

From the Monte Carlo simulations, the median C_{D_0} was calculated at 0.0278, with a mean value of 0.0299 and a standard deviation of 0.00886. These statistical metrics provide insights into the variability of the C_{D_0} under parameter uncertainties. In the end, the iteration model used the average value of the drag coefficients. As such, it slightly overdesigns the battery compared to the predicted values.

Correlation coefficients were computed to quantify the relationships between each input parameter and the drag. Notably, parameters such as upsweep of the fuselage, interference factor of the front wing, and interference factor of the rear wing exhibited the highest positive correlations with C_{D_0} of 0.868, 0.156 and 0.089 respectively, indicating an increase in C_{D_0} with higher values of these parameters. Conversely, transition of the boundary layer at the wing and fuselage showed a strong negative correlation of -0.32 and -0.0945 respectively, suggesting a decrease in C_{D_0} with increased values of this parameters. The findings underscore the critical influence of specific parameters on C_{D_0} variability. Parameters with higher correlation coefficients play significant roles in determining C_{D_0} , thus highlighting the more important parameters in aerodynamic design optimisation. Additionally, parameters demonstrating stronger correlation coefficients should be prioritised in manufacturing processes. For instance, ensuring a high quality surface finish on the wings or maintaining precise tolerances for the upsweep of the fuselage should take precedence over manufacturing considerations for the tail and its connections to the fuselage. However, these findings are specific to aerodynamics considerations. Other departments within the project may prioritise manufacturing processes for the tail, emphasising the importance of maintaining a balanced approach and fostering effective communication across different departments in projects of high complexity. Achieving this balance ensures that all aspects of the aircraft design, from aerodynamic efficiency to structural integrity, manufacturing feasibility and sustainability, are optimised to meet overall project goals.

10.4.2. Induced Drag Coefficient

A sensitivity analysis was conducted to investigate how key parameters affect the induced drag coefficient C_{D_i} of an aircraft in cruise conditions. The parameters that were investigated included aspect ratio, the wing tip effect, and the Oswald efficiency factor of the aircraft e_{tan} , due to them directly affecting the induced drag coefficient. Once again, these parameters used a uniform distribution within the predefined ranges, and 10 000 random combinations were performed. The frequency of each computed C_{D_i} for randomly chosen parameters can be seen Figure 10.7.

The resulting histogram illustrates that most configurations yield a C_{D_i} clustered around a mean value of 0.0420, while the median was 0.0398. One standard deviation computed for this simulation was 0.012. Once again, the average value for the induced drag was taken for the iteration loop. Similarly to Section 10.4.1, correlation coefficients were calculated to quantify the effectiveness of the input parameters on the induced drag Figure 10.8. It was observed that e_{tan} exhibited the highest negative correlation with C_{D_i} , indicating that more effort should be spent in optimising the lift distribution generated by the wings, and minimising the effect of the fuselage and propulsion system on the lift distribution. Nonetheless, the aspect ratio has a high influence on the induced drag. Thus, it should be as high as possible while keeping other departments in mind.

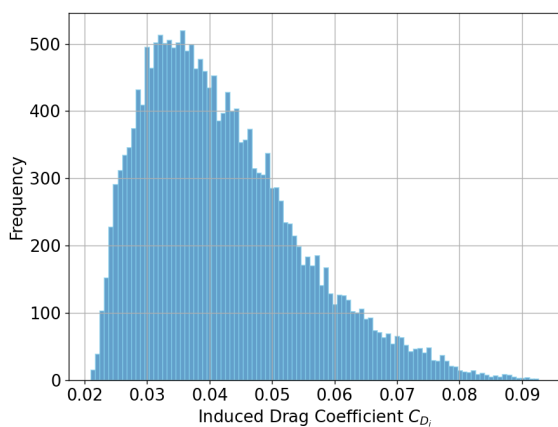


Figure 10.7: Induced Drag Coefficient frequency

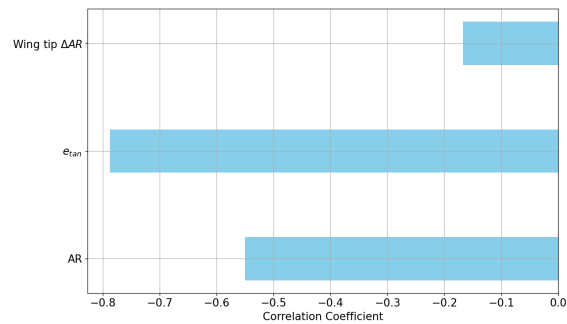


Figure 10.8: Correlation factor for Induced Drag Coefficient input parameters

In conclusion, optimising the induced drag coefficient hinges significantly on the Oswald efficiency factor and aspect ratio. These parameters emerged as pivotal factors influencing the induced drag coefficient during the sensitivity analysis. Hence, allocating greater research efforts and implementing stricter manufacturing tolerances for them are recommended to achieve a better aerodynamic efficiency, as well as a lower energy usage, thus more sustainable future. Conversely, while the analysis identified wing tips as moderate performance enhancers, their overall impact on reducing induced drag was found to be less substantial compared to the other two. As such, while optimising wing tips can provide marginal gains, it is advisable to prioritise resources and attention towards optimising the Oswald efficiency factor and the aspect ratio for more significant improvements in aircraft performance.

10.5. Verification of the Aerodynamic Model

Verification is a critical step in the development of an aircraft model to ensure its accuracy and reliability. The aim is to verify the accuracy of the model's lift and drag coefficient calculations.

Numerous unit tests were firstly performed during the making of the code. Each formula applied in the model was manually tested to ensure it computes the right value. Afterwards, a more general qualitative system test was performed, where values such as the aspect ratio, or the area of the components is changed, and its affect on the drag and lift coefficient is analysed to see if it changes in the expected way.

To further verify the model, a similar aircraft with known experimental data and measurements was used. The report where the experimental data and the sizing of the aircraft was presented by Kryvokhatko [29]. Firstly, all the inputs were changed to the aircraft used in the experiment. Afterwards, the experimental data for lift coefficient as a function of angle of attack, and drag coefficient as a function of lift coefficient were extracted from the graphs and directly compared to the predictions of the model. It is important to note that there is random error from estimating the plot given by Kryvokhatko due to not having the exact data points. This introduces a degree of uncertainty in the comparison process which could increase or decrease the error. The relative error, maximum error and minimum errors for the lift coefficients were 2.881%, 7.11% and 0.862% respectively,

while the same errors for the drag coefficients were 6.868%, 8.879% and 2.058% respectively. Additionally, the direct comparison of the experimental data and the model predictions was plotted in Figure 10.9.

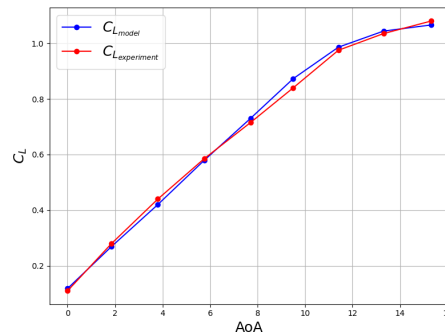


Figure 10.9: Comparison between the model predictions with the experimental data of another model.

It is important to note once again that there is random error from estimating the plot given instead of having exact data points. Efforts were made to take values more conservatively, thus promoting a higher error rather than accidentally reducing it. Despite this, the observed errors are relatively small compared to the 15% error that is accepted based on the design philosophy, suggesting that the model is accurate to an extent. The slightly higher error in the drag coefficient could be attributed to the complicated nature of predicting the Oswald efficiency factor or estimating the down wash effect. Additionally, the model is designed for aircraft utilising wings of equal size, while the aircraft in the experiment employs similar-sized wings. Nonetheless, the verification process confirms that the aircraft model is robust, with errors in the lift and drag coefficients being within acceptable ranges in this design philosophy. Future work should focus on further refining the drag coefficient calculation to enhance the model's accuracy and compare it to wider range of angles of attack.

10.6. Validation of the Aerodynamic Model

Computational Fluid Dynamics CFD is a branch of fluid mechanics that uses numerical analysis and algorithms to solve and analyse problems involving fluid flows. It allows a relatively accurate analysis before building costly prototypes, reducing material wastage and cost. Consequently, making the project more sustainable. To perform the CFD analysis, it was decided that Ansys Fluent, provided by TU Delft, will be utilised.

In this study, the $k - \omega$ model is employed for validation, having replaced the $k - \epsilon$ model as the most widely used two-equation model due to its several advantages. The $k - \omega$ model offers significantly greater accuracy for two-dimensional boundary layers under both adverse and favourable pressure gradients. These features make the $k - \omega$ model particularly advantageous for the CFD simulations of the aircraft, as it effectively handles the types of flows expected by the aircraft [30].

To accurately present the boundary layer, the y^+ parameter was analysed. Ideally, this parameter should be below 1 [30]. However, to achieve such a boundary layer representation, a computationally expensive mesh would need to be created. To reduce the computational efforts, a y^+ value below 30 was deemed sufficient. However, this implies that the flow at these points lies midway between being fully dominated by viscous effects and turbulence. Consequently, shear stresses due to viscous and turbulence stresses are of similar magnitude making it difficult to accurately predict the velocity profile of the boundary layer. Thus, it is recommended for future analysis, to obtain a value for y^+ lower than 1 by reducing the mesh's inflation layer. Additionally, the convergence criteria for the residuals were set to 10^{-5} except for the continuity residual which was set to 10^{-3} .

This report conducted 3 different CFD simulations where the aircraft was simulated at 0 angle of attack, the cruise angle and at vertical take-off. It is important to note that the simulation was conducted using only the wings, fuselage and the tail, while the nacelles, landing gear, wing tips and propellers were avoided due to limited power. The comparison between the developed aerodynamics model and the CFD results can be seen in Table 10.6, where the averaged y^+ value was found to be below 6.39.

Table 10.6: Comparison between the CFD and aerodynamic model predictions.

AoA	C_L_aircraft			C_D_aircraft			
	Model/CFD	Model	CFD	Error	Model	CFD	Error
0		0.504174302	0.501171	0.6%	0.048342	0.0372	29.95%
1.6		0.643971885	0.66561	3.25%	0.062005	0.04817	28.72%
-90		0	-0.19854	-	1.511461	2.033	25.65%

It is observed that the aerodynamic model generally provides conservative predictions when compared to CFD simulations in non-stall regions. The lift predictions from the aerodynamic model closely align with those from the CFD simulations. However, the aerodynamic model predicts higher drag values. This discrepancy arises due to the conservative estimation of zero lift drag, which dominates at low angles of attack. In contrast, during vertical take-off scenarios, the aerodynamic model underpredicts the drag force. Figure 10.10 illustrates the streamlines around the aircraft, highlighting clear interference between the wings and the fuselage. This interference is not accounted for in the aerodynamic model's predictions for vertical flight. Thus, the authors suspect this as the reason for the observed underprediction of drag.

As a result of this analysis, it is suggested to apply interference factors of 1.3 for both the wings and the fuselage in the aerodynamic model. Implementing these factors, a quick simulation of the aerodynamic model yielded a drag coefficient of 2.0534, demonstrating that the model can be accurate even for extreme angles of attack, such as -90° . However, further analysis should be done for a wider range of angle to ensure the accuracy.

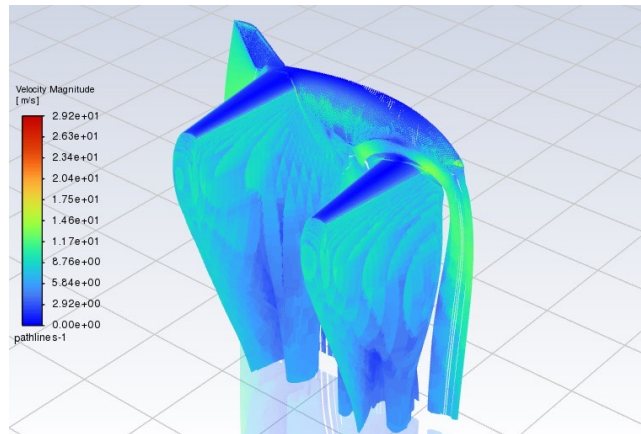


Figure 10.10: CFD model of the aircraft in vertical take-off showcasing the wing-fuselage interference.

For the validation of the aerodynamic performance, several future steps need to be undertaken post-project. Firstly, a down-scaled 3D model of the aircraft, including functioning propellers, nacelles and landing gear is required. This would allow to validate the aerodynamic coefficients of the aircraft by conducting wind tunnel experiments. In addition to quantitatively evaluating aerodynamic performance, a more qualitative experiment involving flow visualisation would be beneficial to determine whether the airflow behaves as expected around the aircraft's shape when it comes to separation and transition.

Performing wind tunnel testing will enable iterating the design which should pave the way for a subsequent flight test once the first prototype is built. This will allow for a direct comparison between the expected lift and drag performance of the aircraft and the actual results, providing a thorough validation of the design.

10.7. Aerodynamics Recommendations

There are several things that can be improved in the aerodynamic model. Firstly, the C_{D_0} could incorporate the propellers in the estimation to improve the accuracy. Furthermore, the interference between the fuselage and wings in vertical flight should be further investigated to improve the model beyond stall. This model also neglects the nacelles, landing gear, wing tips and propellers. Thus, for a more accurate representation, these should be included. Leading to the next point, by incorporating the aforementioned aspects, V&V can be repeated for the full aircraft, giving the most accurate representation of the aircraft in operating conditions, which can serve to further optimise other aspects of the aircraft such as the battery. When performing the CFD validation, a mesh convergence study should be performed, where the mesh is continually refined until the drag and lift coefficients do not experience a significant change. Lastly, the inflation layer representing the boundary layer should be sufficiently small so that the y^+ value is below giving an accurate representation of the boundary layer.

Chapter 11 | Propulsion System Design

This chapter covers the propulsion subsystem of the aircraft, responsible for the aircraft's thrust. It covers the requirements and the assumptions given in Section 11.1. Afterwards, the design process is explained in Section 11.2, followed by the results given in Section 11.3. Then, the sensitivity analysis and V&V are given in Section 11.4 and Section 11.5, respectively. Finally, a section regarding recommendations on the propulsion design is given in Section 11.6.

11.1. Propulsion Subsystem Requirements & Assumptions

Presented in Table 11.1 and Table 11.2 are the requirements and assumptions for the propulsion system design, respectively.

Table 11.1: Propulsion Subsystem Requirements.

Identifier	Requirement	Source(s)	Compliance	Method of verification
REQ-PRP-01	The propulsion subsystem shall provide the thrust required for vertical takeoff.	REQ-SYS-AC-09	✓	Analysis as given in Section 11.2, tests during production
REQ-PRP-02	The propulsion subsystem shall provide the thrust required for vertical landing.	REQ-SYS-AC-21	✓	Analysis as given in Section 11.2, tests during production
REQ-PRP-03	The propulsion subsystem shall be able to vary the thrust of individual rotors.	REQ-SYS-AC-23, REQ-SYS-AC-13	✗	Control interface and thrust settings designed at a later design stage
REQ-PRP-04	The propulsion subsystem shall be able to vary the thrust of the rotors equally.	REQ-SYS-AC-23, REQ-SYS-AC-13	✗	Control interface and thrust settings designed at a later design stage
REQ-PRP-05	The propulsion subsystem shall be able to provide the differential thrust required to control the aircraft position along all three axes in vertical flight.	REQ-SYS-AC-23	✗	Differential thrust follows from REQ-PRP-03
REQ-PRP-06	The propulsion subsystem shall be able to provide the thrust required to maintain all flight profile conditions.	REQ-SYS-AC-16, REQ-SYS-AC-07	✓	Analysis provided in Section 11.2
REQ-PRP-07	The propulsion system shall be able to induce a moment around the vertical axis in vertical flight.	REQ-SYS-AC-22	✓	Analysis provided in Section 11.2
REQ-PRP-08	The propulsion subsystem shall be able to operate at an altitude of 1000 m from sea level.	REQ-SYS-AC-08	✓	Analysis provided in Section 11.2
REQ-PRP-09	The propulsion subsystem shall be able to operate under the disturbance of 60 km/h wind gusts from all directions in vertical flight.	REQ-SYS-AC-24	✗	Testing will be performed at a later design stage
REQ-PRP-10	The propulsion subsystem shall be able to operate in rain, hail and snow conditions with an intensity of at least 4 mm/hour.	REQ-SYS-AC-90	✗	Testing of weather conditions will be performed at a later design stage
REQ-PRP-11	The propulsion subsystem shall be capable of transitioning from a vertical flight configuration to a climb configuration.	REQ-SYS-AC-12	✗	Aircraft transition provided in Section 7.6 & Rotational mechanism designed at a later design stage
REQ-PRP-12	The propulsion subsystem shall be capable of transitioning from a descent configuration to a vertical flight configuration.	REQ-SYS-AC-20	✗	Aircraft transition provided in Section 7.6 & Rotational mechanism designed at a later design stage & Section 11.6
REQ-PRP-13	The propulsion subsystem shall be placed more than 1.5m from the entrance of the aircraft.	REQ-SYS-AC-38	✓	Demonstrated in Section 11.2.1
REQ-PRP-14	The propulsion subsystem of the aircraft shall provide access for a pre-flight inspection.	REQ-SYS-AC-85	✓	Demonstrated in Section 11.2.1
REQ-PRP-15	The propulsion subsystem of the aircraft shall provide access for maintenance.	REQ-SYS-AC-84	✓	Demonstrated in Section 11.2.1
REQ-PRP-16	The propulsion subsystem shall not impose an unstable moment on the aircraft.	REQ-SYS-AC-17, REQ-SYS-AC-23, REQ-SYS-AC-46, REQ-SYS-AC-47	✓	Analysis provided in Section 11.2.1
REQ-PRP-17	The propulsion subsystem noise level in effective perceived noise in decibels (EPNdB) shall be lower than 92 EPNdB during takeoff.	REQ-SYS-AC-71	✗	Noise testing shall be performed at a later design stage
REQ-PRP-18	The propulsion subsystem overflight noise level shall be lower than 90 EPNdB.	REQ-SYS-AC-72	✗	Noise testing shall be performed at a later design stage
REQ-PRP-19	The propulsion subsystem approach noise level shall be lower than 95 EPNdB.	REQ-SYS-AC-73	✗	Noise testing shall be performed at a later design stage
REQ-PRP-20	The cost of the propulsion subsystem shall be less than 350,000 euros.	REQ-SYS-94	✗	Analysis provided in Section 11.2
REQ-PRP-21	The propulsion subsystem shall be capable of providing sufficient thrust for hovering after the loss of 1 motor.	REQ-SYS-AC-16, REQ-SYS-AC-86	✓	Analysis provided in Section 11.2.3
REQ-PRP-22	The propulsion subsystem shall be capable of providing sufficient thrust for hovering after the loss of 1 propeller.	REQ-SYS-AC-16	✓	Analysis provided in Section 11.2.3
REQ-PRP-23	The propulsion subsystem motors shall have a fire retarding subsystem.	REQ-SYS-AC-34	✗	Propulsion fire retarding system shall be designed at a later design stage
REQ-PRP-24	The propulsion subsystem motors shall self-contain a fire for a minimum of 5 minutes.	REQ-SYS-AC-34	✗	Propulsion fire retarding system shall be designed at a later design stage
REQ-PRP-25	The propulsion subsystem shall have an operational ambient air temperature range of -20 °C to 47 °C.	REQ-SYS-AC-31	✗	Testing of weather conditions shall be done at a later design stage

Table 11.2: Assumptions used for propulsion subsystem design.

Identifier	Assumption	Expected Effect
A-PRP-01	The effect of the vertical velocity of the aircraft during VTOL is neglected.	The vertical velocity imposes a downwash effect on the propeller blades, reducing the local angle of attack.
A-PRP-02	Transonic effects on wing tips appear when the Mach number reaches 0.7.	Transonic effects might appear earlier or later than 0.7. This will affect the RPM used, leading to different chord sizes.
A-PRP-03	A median C_L is applied over the whole propeller blade.	The C_L can vary based on propeller blade twist, causing for less accurate thrust estimations.
A-PRP-04	A median chord, $c_{\bar{r}}$, is applied over the whole propeller blade.	The chord can vary based on the propeller blade taper ratio, causing for less accurate thrust estimations.
A-PRP-05	The integral used for thrust estimations of the propeller blade has an upper limit of 0.97 blade radius to account for tip losses.	Tip losses could extend further or less than 0.97 blade radius, causing for less accurate thrust estimations.
A-PRP-06	The lift coefficient of the propeller blade, C_{L_i} , is assumed to vary linearly with angle of attack.	The lift coefficient might show nonlinear behaviour at various angles of attack, leading to a reduced accurate thrust estimation.
A-PRP-07	The moment of inertia of the propeller blades is assumed to be modelled by a rhombus placed within the propeller airfoil.	This reduces the moment of inertia of the propeller blade, leading to higher estimated stresses.
A-PRP-08	The density of the propeller blade material is assumed to be uniform within the entire volume of the propeller blade.	Inherent irregularities within the material might lead to a different density used, leading to less accurate mass estimations.
A-PRP-09	The volume of the propeller blades is assumed to be modelled by a rectangle of the chord length and maximum thickness.	This will overestimate the mass of the propeller blade.
A-PRP-10	Noise of motors is neglected.	This will reduce the estimated noise levels of the propulsion system.

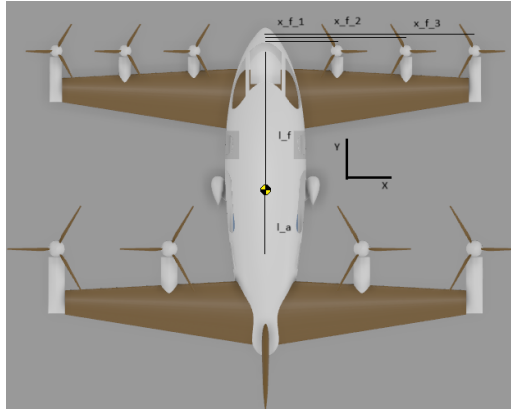


Figure 11.1: Layout of the propulsion system of the aircraft in VTOL configuration with corresponding XY locations (CG is shown for illustrative purposes and is not representative of the actual value).

11.2. Propulsion System Design Method

In this section the methods used for the sizing and design of the propulsion system is presented.

11.2.1. Configuration & Rotor Size

When designing an electrically powered aircraft, efficiency is a key factor as to keep battery weight low. For efficient thrust generation, propellers are the preferred option. Propellers are more efficient than their jet counterpart when flying slow and at low altitudes. They are also the ideal choice when powered by electric motors. Furthermore, accelerating a larger amount of mass is more efficient than imparting a larger velocity on a lower mass. With this in mind, the design strived for the maximum allowed rotor diameter. Furthermore, the propulsion system was primarily sized for the vertical takeoff and landing stage, as all lift would be generated by the propulsion system causing for this stage to be the most critical to design for.

Several factors needed to be kept in mind during the propulsion system design when operating in vertical takeoff and landing conditions. Firstly, the propulsion system will need to generate 1.3 times the weight to allow for a controllable takeoff, but also provide controllable differential thrust to account for wind disturbances. Secondly, the propulsion system should not impose an unbalancing moment on the aircraft. Thirdly, the propulsion system should provide enough thrust to safely land after one of the engines or rotors fail. It is thus necessary to achieve a compromise between rotor size and redundancy. A two rotor design would result in a dangerous unbalancing moment in case of failure. As symmetry is preferred, the decision was made to place four rotors on the aft wing. For the front wing, the rotor area is more limited. Firstly, the ground clearance is a factor to be kept mind when performing an emergency landing. Although it is not a requirement, it is preferred that a substantial amount of the front rotor blades do not break. Similarly for pilot safety, smaller rotor blades are less dangerous in case of failure than larger ones. Furthermore, the front rotors are more active during VTOL than cruise, meaning redundancy is a more important factor than efficiency. With this reasoning, the front wing will have six rotors instead of four. Furthermore, to ensure that the propulsion system does not impose an unbalancing moment on the aircraft, the left rotors will rotate clockwise when viewed from above, and the right rotors will rotate counterclockwise. In the following equations and symbols used, a denotes the aft propellers and f denotes the front ones.

With this configuration set in place, it is possible to determine the maximum allowed rotor diameter. This is done according to Equation 11.1.

$$d_{max} = \frac{b - w_f - N_{pr} \cdot c_{clear}}{N_{pr} - 1} \quad (11.1)$$

Here, b is the wing span, w_f is the fuselage width, N_{pr} is the number of propellers and c_{clear} is the clearance value, which has always been set at 0.2 m. The configuration of the propulsion system of the aircraft is illustrated in Figure 11.1. The parameters following the sizing process (number of rotors, diameters, total rotor area and positioning of rotors) are given in Table 11.3. Do note that locations are only given for half the wingspan of the motor, as they are placed symmetrically with respect to the longitudinal axis. Also, as all rotors and motors are placed outside of the wing or fuselage, access to maintenance and inspection has been kept facile.

11.2.2. Propulsion Motor Selection

With the placement and maximum diameters of the rotors known, a motor has been selected for the front and back wing rotors. For this, the required thrust during VTOL has been split up accordingly per rotor. Firstly, the total thrust is split up between front thrust, T_f and aft thrust, T_a . They are defined in Equation 11.2. This equation followed from a moment equilibrium, where l_a and l_f are the distance of the aft and front rotor to the CG in longitudinal position, respectively.

$$T_f = W \cdot T_r \quad \text{and} \quad T_a = W \cdot (1 - T_r) \quad \text{with} \quad T_r = \frac{l_a}{l_a + l_f} \quad (11.2)$$

Afterwards, the power consumption of each rotor was assumed to be described by momentum theory, also known as actuator disc theory [31]. The selection process eliminated thus the motors that could not meet the power required for vertical takeoff. From the remaining motors, a small trade-off on size and weight was performed. However, as all remaining motors had very similar sizes, or not did not have enough reliable data on this, only the weight played a factor in the trade-off. Thus, the lightest possible option for each rotor is the selected motor for that rotor.

The selected motor for the aft rotors is the *Siemens SP260D* [32], and the motor for the front rotors is the *YASA P400* [33]. Their parameters length l , diameter d and maximum power output P are given in Table 11.3 and are denoted with a subscript m .

11.2.3. Blade Properties

According to blade element theory during hovering flight, the thrust of a rotor can be estimated according to Equation 11.3. This equation assumes a constant chord and a median \bar{C}_L as stated in A-PRP-03 and -04. As \bar{C}_L is dependent on angle of attack, the variation in angle of attack can be accounted for by using blade twist. This \bar{C}_L was assumed to be equal to 1.1 and the airfoil chosen is the NACA 16-018. To increase the bending resistance of the airfoil, a thicker airfoil is preferred. Due to this, the NACA16-018 is chosen as the propeller airfoil. The lift and drag distributions of this airfoil have been analysed by Xfoil and are presented in Figure 11.2 and Figure 11.2¹ respectively, and a linear distribution of the lift coefficient over the angle of attack has been assumed from this prediction. As it follows from A-PRP-01, the effective angle of attack of the propeller blade is equal to its geometric angle of attack. Therefore during take-off, the pitch of the propeller blade is set at a maximum value of 17.5° at the root and decreases linearly to a value of 12.5° at the tip. During cruise, the effective angle of attack will be lower due to the incoming airflow, but as the thrust of the propulsion system is less critical at this stage, it was not sized for it. The solidity, σ_{sol} , is defined as the blade area divided by rotor area, the median chord used is the average of the tip and root chords.

$$C_T = \frac{T}{\rho \pi r^2 (\omega r)^2} = \frac{\sigma_{sol} \bar{C}_L}{6.6} \quad (11.3)$$

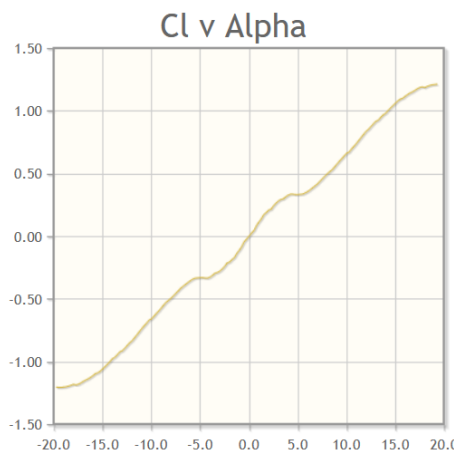


Figure 11.2: Lift distribution per angle of attack (dg) for NACA16-018.

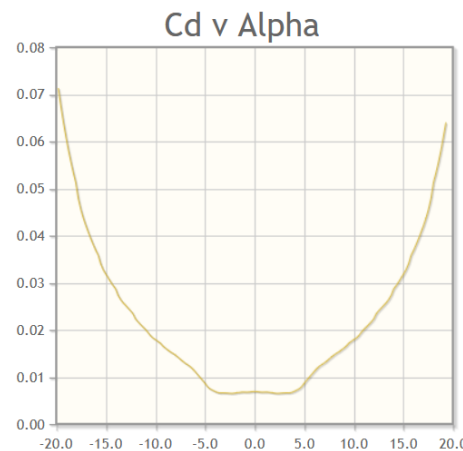


Figure 11.3: Drag distribution per angle of attack (dg) for NACA16-018.

¹<http://airfoiltools.com/airfoil/details?airfoil=naca16018-il> [cited 25.06.24]

The thrust coefficient can be related to the chord of the blade. The angular velocity was set at a value limited by a Mach number of 0.4 at the tip.

$$c_{pr_{med}} = \frac{T6.6}{N_{blades} C_L \rho \omega^2 r^3} = c_{pr_r} \frac{\lambda + 1}{2} \quad (11.4)$$

When calculating the thrust per propeller, if one aft engine fails, the total thrust is still more than the thrust required for hover. In case of an outboard aft engine failing, the RPM of the inboard rotor at the same side can be increased to keep balance whilst the outboard engine on the other side can be reduced by 40%. This is allowed, as the Mach number was kept at 0.4 at the tip and blade loading is equal to a maximum of 14.347 MPa, thus allowing for a Mach number increase of 0.1, which would result in a thrust sufficient for hover.

As a propeller blade acts like a wing, an estimation of the internal loads and stresses is necessary to see if the blade itself can withstand the loads without significant deformation or structural failure. Incorporating blade twist and taper, Equation 11.5 was derived from the lift equation. The twist was discussed prior. The taper ratio is 0.4.

$$dL = C_{L_\alpha} (\alpha_0 + \alpha_r r) (c_0 + c_r r) \frac{1}{2} \rho (\omega r)^2$$

$$\text{with : } \alpha_r = \frac{\alpha_t - \alpha_0}{r_t - r_0} \quad \text{and} \quad c_r = c_0 \frac{\lambda - 1}{r_t - r_0} \quad (11.5)$$

From the blade loading, the shear and moment loading can be found by integration. For simplicity, the airfoil was modelled as a rhombus placed inside the true airfoil geometry. This assumption will lead to an overestimation of the stresses as explained by A-PRP-07. Illustrations of the loads can be found in Figure 11.4 and Figure 11.5 and maximum estimated bending stresses are given in Table 11.3. With the bending stresses known, the material selected for the propeller is Sitka Spruce wood.

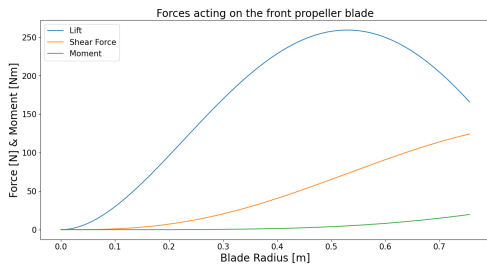


Figure 11.4: Front propeller blade loading.

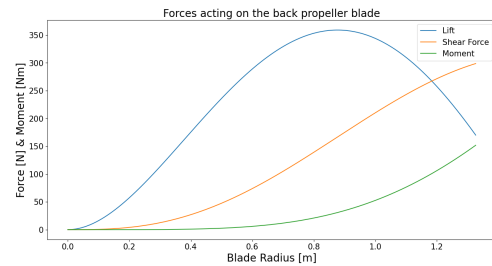


Figure 11.5: Aft propeller blade loading.

The mass of the propulsion subsystem is divided by motor mass and propeller mass. As motor mass is already known, only propeller mass will be estimated. From A-PRP-09, the chord used is the median chord found from Equation 11.4. The mass of a propeller blade is thus the volume of the rectangle multiplied by rotor radius. With the density known the mass of a single blade can be estimated. The mass of the propellers is thus the mass of a single blade multiplied by the number of blades and the number of rotors. Mass of the propulsion system is presented in Table 11.3.

11.2.4. Noise & Cost Estimation

Estimating noise levels produced by a propulsion system can be a complicated process. Due to time limitations, a simple estimation was selected. Firstly, the noise of the motors was neglected as per A-PRP-10. Thus only propeller noise was estimated. For this, the broad-band (vortex) noise was analysed per rotor individually according to *Marte & Kurtz* [34] and is given in Equation 11.6. $V_{0.7}$ represents the velocity of the blades at 0.7 radius length, also, this equation uses imperial units.

$$SPL = 10 \log \frac{6.1 \cdot 10^{-27} A_b (V_{0.7})^6}{10^{-16}} + 20 \log \frac{C_L}{0.4} \quad (11.6)$$

Using this, an SPL level of 79.21 dB for the front rotor and a value of 83.27 dB for the aft rotor was calculated. The noise on one side of a wing is then the summation of each rotor contribution. Summing these values again,

which is an overestimation, resulted in a total noise value of 91 dB. However, to check whether this satisfies REQ-PRP-17, -18, and -19, noise measuring and testing must be performed. The cost estimation followed from Braun [35]. This follows empirical equations regarding the price of the propellers and electric motors, although sized for hybrid-electric general aircraft. However, only the propellers and motors are estimated, thus this caveat was neglected. Furthermore, the authors were in contact with Siemens, leading to a higher confidence in the price estimation. The price of the electric motors is assumed to be equal to €650000. The price of the propellers is assumed to be equal to a total of €52600.

11.3. Results

Presented in Table 11.3 are the results of the propulsion design. Comparing to conventional aircraft, the propellers might appear very thick. As the HAROLD is VTOL capable, and furthermore made of wood, it is expected to have thicker propellers due to these reasons. It could be possible to rotate the propellers faster at VTOL stages in order to reduce the thickness. This would require thus further iterations in order to achieve a complete converged design.

Table 11.3: Values of propulsion subsystem sizing parameters and corresponding rationales.

Parameter	Value	Unit	Rationale
N_{prf}	6	-	As explained in Section 11.2.1.
N_{pra}	4	-	As explained in Section 11.2.1.
N_{blades}	5	-	As explained in Section 11.2.1.
d_f	1.633	m	As explained in Section 11.2.1.
d_a	2.60	m	As explained in Section 11.2.1.
A_{pr}	33.89	m ²	As explained in Section 11.2.1.
x_{f1}	0.98	m	As explained in Section 11.2.1.
x_{f2}	2.74	m	As explained in Section 11.2.1.
x_{f3}	4.5	m	As explained in Section 11.2.1.
x_{a1}	1.57	m	As explained in Section 11.2.1.
x_{a2}	4.5	m	As explained in Section 11.2.1.
l_f	2.856	m	As explained in Section 11.2.1.
l_a	2.368	m	As explained in Section 11.2.1.
d_{fm}	0.305	m	As explained in Section 11.2.2.
d_{am}	0.418	m	As explained in Section 11.2.2.
l_{fm}	0.107	m	As explained in Section 11.2.2.
l_{am}	0.3	m	As explained in Section 11.2.2.
P_{mf}	160	kW	As explained in Section 11.2.2.
P_{ma}	261	kW	As explained in Section 11.2.2.
c_{prf}	0.222	m	As explained in Section 11.2.3.
c_{pra}	0.25	m	As explained in Section 11.2.3.
RP_{Mf}	1660	r/min	As explained in Section 11.2.3.
RP_{Ma}	950	r/min	As explained in Section 11.2.3.
T_{fi}	3424.358	N	As explained in Section 11.2.3.
T_{aj}	6194.09	N	As explained in Section 11.2.3.
σ_f	2.738	MPa	As explained in Section 11.2.3.
σ_a	18.58	MPa	As explained in Section 11.2.3.
w_{pr}	518.24	kg	As explained in Section 11.2.3.
w_{prop}	174.24	kg	As explained in Section 11.2.3.

11.4. Sensitivity Analysis

In Section 11.2.3, the C_L values are assumed for Equation 11.3. This value might differ from reality as it is a median value assumed for the whole propeller blade. Furthermore, the maximum takeoff mass might differ from the ones calculated. A normal distribution was applied to these inputs, the outputs varied are the front and aft chords, and the propulsion system mass. A sample size of 100 was used in the normal distributions. From the results, it can be seen that a substantial amount of the output parameters is within the second deviation.

Table 11.4: Propulsion subsystem sensitivity parameters and results.

Parameter	m_{TO}	C_L	C_D	m_{prop}	c_{pf}	c_{pa}
μ	3349.6	1.1	0.031	503.124	0.221	0.25
σ	100	0.1	0.005	39	0.013	0.019
% in 1st deviation	68.49	67.77	68.77	23.4	43.11	53.05
% in 2nd deviation	95.46	95.64	95.56	72.19	73.14	88.15
% in 3rd deviation	99.69	99.76	99.80	99.18	88.19	98.5

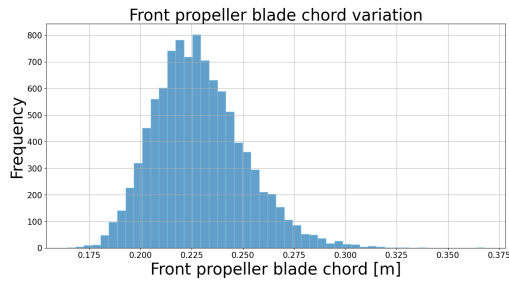


Figure 11.6: Variation of the front blade chord.

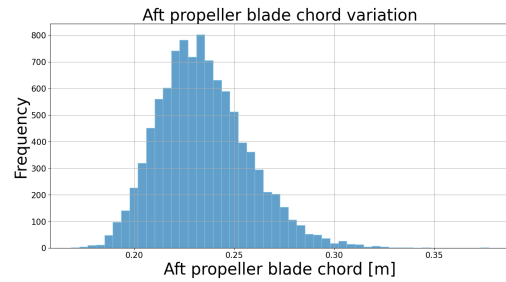


Figure 11.7: Variation of the aft blade chord.

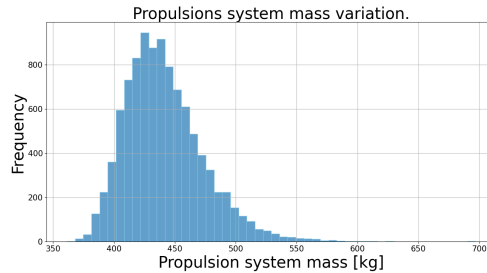


Figure 11.8: Variation of the propulsion system mass.

11.5. Verification and Validation

The scripts and code used for the propulsion subsystem have been verified by the use of unit tests, and the interactions between different pieces of code have been tested to see if the inputs and outputs have the correct units. Next, after code verification, the design process itself has been verified in the following way.

In *Lui* [36], a VTOL with an eight bladed vertical rotor configuration was analysed using CFD. With similar radius size and RPM, but differing solidity, the vertical rotors produced a maximum thrust of 3470 N. With a higher solidity, this value will be higher and thus closer to the estimated thrust of the back propellers of the HAROLD. Furthermore, in *Ilkko* [37], the thrust coefficient of a Sikorsky UH-60 Blackhawk was analysed. This value is close to a constant distribution of 0.025 over the blade radius. HAROLD achieves a thrust coefficient of 0.05, but as the solidity and median C_L values are higher, it can be expected to have a higher thrust coefficient.

For verifying the assumptions made in Table 11.2, the assumptions that are concerned with stress and weight, those being A-PRP-07 and -09, cause for those values to be overestimated. Therefore, the actual design will perform better in these areas than what is actually presented in Table 11.3.

11.6. Propulsion Recommendations

Due to time limitations, it was not possible to complete a fully detailed propulsion system design. In this section, the recommendations on how to achieve a better and more verified and validated design are given.

Firstly, a better analysis of the thrust per rotor can be estimated by the use of computational efforts, such as CFD. This will lead to a better distributed loading of the propeller blade and might result in a different blade twist than the current linear one. Secondly, the current airfoil might not be the optimal one, as a detailed analysis on propeller blade airfoil selection has not been performed. Thirdly, a fire retardation system has not been designed for the propulsion system, thus for safety and compliance with REQ-PRP-23 and -24, this is a matter that should be delved into deeper.

For compliance with the set requirements, a lot of testing could be performed for further confidence, or overall compliance in general. For example, the thrust of the propellers should be tested, as well as testing the limit loads the blade could carry to understand what angular velocity the maximum is. Secondly, testing of weather conditions could be done to test REQ-PRP-09, -10 and -25. Thirdly, the noise of the aircraft should be tested once the design is finished, to see if the design complies with REQ-PRP-17, -18 and -19.

Finally, the transition phases of the aircraft have been analysed on an aircraft level, in Section 7.6, the velocities, angles of propellers and forces acting on the aircraft have been analysed. However, the rotation mechanism has not been fully designed yet. With this, it is unknown whether the rotation system will be capable of carrying the loads introduced during the transitional phases.

Chapter 12 | Power

This chapter presents the detail design of the battery and thermal management system (TMS). With Chapter 11 covering the sizing of motors and propellers for the HAROLD, the logical next step is ensuring the power subsystem is capable of providing sufficient energy for operation. This is done with a more specific discharge analysis, considering non-linearities in battery behaviour. Following the standard for this work, Section 12.1 presents the subsystem requirements to be met by the design, including which ones have been fully met, and which are still to be verified in further design phases. This is followed by the main assumptions used in the sizing, together with their effect, in Section 12.2. The method used for the battery and TMS is presented in Section 12.3, followed by the results from the design, in Section 12.4. The results are followed by a sensitivity analysis in Section 12.5, which includes an analysis on the effect of battery technology on the design, among others. Lastly, Section 12.6 presents the verification and validation procedures conducted on the tools used for the power sizing.

12.1. Subsystem Requirements and Compliance Matrix

This section presents the power subsystem requirements, and whether they have been verified at this stage in the design. As can be seen in Table 12.1 at this point there are six requirements to be complied with, the reason for this is covered below.

Table 12.1: Power Subsystem Requirements Compliance Matrix.

Identifier	Requirement	Source(s)	Compliance	Method of verification
REQ-BAT-01	The battery shall fully power the aircraft's operations until battery end-of-life.	REQ-SYS-AC-06, R-TEC-13	✓	Analysis by battery evaluation in Section 12.3.1, testing during prototyping
REQ-BAT-02	The battery shall be rechargeable.	REQ-SYS-AC-33	✓	Inspection at the end of Section 12.3.1
REQ-BAT-03	The battery shall have a maximum degradation of 0.2 after 1460 cycles.	REQ-SYS-AC-77, REQ-SYS-AC-78, RAMS-06	✗	Testing during prototyping
REQ-BAT-04	The battery shall have an operational temperature range between 10°C and 35°C.	REQ-SYS-AC-78, RAMS-08	✓	Analysis by battery evaluation in Section 12.3.1, testing during prototyping
REQ-BAT-05	The battery pack must achieve an energy density of at least 300 Wh/kg.	REQ-SYS-AC-06	✓	Inspection at the end of Section 12.4
REQ-BAT-06	The battery shall be charged from 10% to 90% capacity in less than 100 minutes.	REQ-SYS-62, RAMS-04	✓	Analysis by battery evaluation in Section 12.3.1, testing during prototyping
REQ-BAT-07	The battery shall be protected from the environment as per IP67 standards.	REQ-SYS-AC-78, R-TEC-11	✗	Testing during prototyping
REQ-BAT-08	The battery shall be able to self-contain a fire for a minimum of 5 minutes.	REQ-SYS-AC-34, R-TEC-11	✗	Testing during prototyping
REQ-BAT-09	The battery shall use technology available from more than one provider.	REQ-SYS-AC-32, RAMS-03	✓	Analysis by battery sizing in Section 12.3.1
REQ-BAT-10	The cost of the battery subsystem shall be less than 100,000 €.	REQ-SYS-AC-94	✓	Analysis by budget estimation in Section 12.3.1
REQ-BAT-11	A battery inspection shall be possible by use of designated access points.	REQ-SYS-AC-84, REQ-SYS-AC-70	✗	Inspection at the end of the next design phase where this is implemented
REQ-BAT-12	The complete battery pack shall be removable as part of regular maintenance.	REQ-SYS-AC-78, REQ-SYS-AC-84	✓	Inspection at the end of Section 12.3.1
REQ-BAT-13	The battery system shall not have a single point of failure.	REQ-SYS-AC-1, R-TEC-03, R-TEC-13	✓	Inspection at the end of Section 12.3.1,
REQ-BAT-14	The battery capacity shall be designed with a safety factor of at least 10% of the design range.	REQ-SYS-AC-89	✓	Inspection at the end of Section 12.3.1
REQ-TMS-01	The thermal management system shall ensure a battery temperature lower than 35°C for a minimum of 90% of the operational time.	REQ-SYS-AC-33, RAMS-08	✓	Analysis by thermal analysis in Section 12.3.1
REQ-TMS-02	The thermal management system shall ensure a battery temperature lower than 50°C at all times.	REQ-SYS-AC-33, RAMS-08	✗	Demonstration during the prototyping stage
REQ-TMS-03	The thermal management system shall ensure a battery temperature of at least 15°C during operation.	REQ-SYS-AC-33	✓	Analysis by thermal analysis in Section 12.3.2
REQ-TMS-04	The thermal management system shall divert residual heat to the cabin.	REQ-SYS-AC-31	✓	Inspection in Section 12.3.2
REQ-TMS-05	The manufacturing/sourcing cost of the thermal management system shall be less than 30,000 €	REQ-SYS-AC-31	✓	Analysis by financial estimation in Section 12.3.2
REQ-TMS-06	The thermal management system shall have an operational ambient air temperature of -20°C to 47°C	REQ-SYS-AC-31	✗	Testing during the prototyping phase
REQ-TMS-07	The thermal management system shall be able to operate in rain conditions of at least 4 mm/hr	REQ-SYS-AC-31	✓	Inspection performed in Section 12.3.2

Requirements to be verified:

- **REQ-BAT-03:** A more detailed degradation analysis is required to estimate the cycle number, at this point degradation has been accounted for, but not the cycle life.
- **REQ-BAT-07:** To verify this requirement a physical model of the battery should be built, to then look at its isolating capabilities.
- **REQ-BAT-08:** Modelling of fire resistance requires a level of detail beyond what is possible at this phase. A prototype should also again be tested to validate the design.
- **REQ-BAT-11:** The encasing of the battery has not been defined yet, when done compliance should be verified.
- **REQ-TMS-02:** Although a temperature delta has been set a more detailed TMS model is needed to ensure performance at limit temperatures.
- **REQ-TMS-06:** Once the coolant is selected and the TMS structure further defined (coolant channel dimensions) this requirement shall be verified, probably during prototyping.

12.2. Assumptions

The assumptions for the battery and thermal managements system can be seen in Table 12.2.

Table 12.2: Assumptions used for subsystem.

Identifier	Assumption	Expected Effect
A-BAT-01	The battery is assumed to have a linear decrease in maximum voltage with depth of discharge (DoD)	Minor deviation in the available voltage .
A-BAT-02	All cells are assumed to discharge identically.	Cell performance could be lower, reducing lifetime of battery.
A-BAT-03	All cells are assumed to degrade at the same rate.	Asymmetries in degradation could limit the battery's lifetime.
A-BAT-04	The batteries are assumed to provide a maximum C-rate of 5	Part of the market is not suitable for the design.
A-BAT-05	Voltage available at each DoD is linearly interpolated between the two closest voltage values known from cell specifications.	Minor differences in voltage available for a certain current.
A-TMS-01	The mass of the TMS is proportional to the heat loss of the battery	Inaccuracies in the mass of the system.
A-TMS-02	The mass of the TMS is inversely proportional to the temperature difference between battery and airflow.	Neglecting non-linearities in mass behaviour with extreme values.

12.3. Method

This section covers the method used to size both the battery and thermal management system of the aircraft. The TMS design is highly dependent on the size and power output of the battery, while the battery itself depends on the power and energy requirements posed by the mission. For more detailed information on the mission see Chapter 13.

12.3.1. Battery Sizing

This subsection covers the different considerations taken when designing the battery pack.

Architecture The battery sizing is performed by analysing the battery pack at a cell level. The battery architecture is set to include n_{bat} batteries connected in parallel; with each battery being formed of n_{cell} cells connected in series. Figure 12.1 presents the battery architecture chosen.

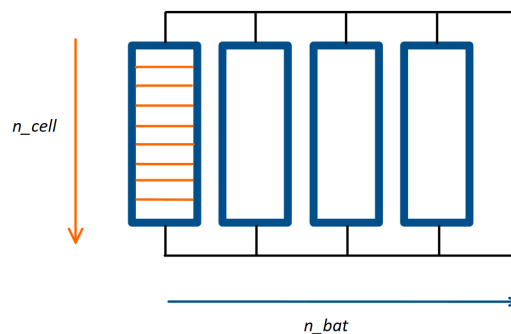


Figure 12.1: Battery pack geometry used in the sizing.

Discharge Model The battery discharge is modelled by looking at the discharge curve, a graph unique to each cell model that shows how its voltage drops along the discharge. This curve takes an almost linear shape for most of the discharge, the reason for assumption A-BAT-01 being used to simplify the sizing. Figure 12.2 and Figure 12.3 present the effect of this linearisation, showing the actual discharge curve for the cell used for this sizing and how it is linearised. The cell from which the discharge curve is obtained presents a maximum C-rate of 2, this value is unfeasible for eVTOL use, due to the higher peak power values required (see Chapter 13); due to this the battery is assumed to provide a maximum C-rate of 5, as seen in Section 12.2. This assumption still is coherent with the design philosophy of using currently available technology, with commercially available cells providing the aforementioned maximum C-rate ¹.

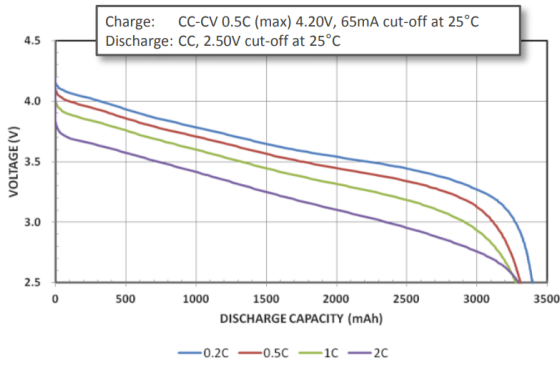


Figure 12.2: Original battery discharge curve.

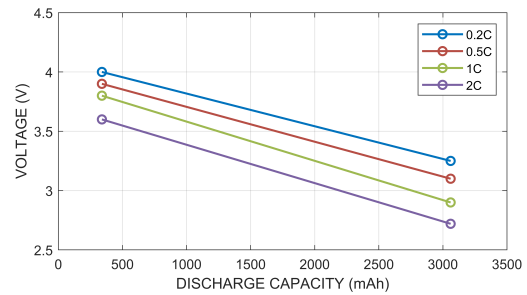


Figure 12.3: Linearised battery discharge curve.

With the linearised discharge curve being known it is possible to create an interpolant that finds, for a certain DoD and current I , the available voltage V . This interpolant is then used to find, for each time-step of length dt , the current required to generate the power required. It is important to note that the power required P_{req} is divided between the n_{bat} batteries; and the fact that this required power needs to include the efficiency of the transmission system η_{tr} . Once the required current is known for a certain moment, it is possible to update the depth of discharge of the battery using Equation 12.1, which is derived from the fact that DoD represents the ratio between current and starting capacity, and the increment of it can be found by integrating the discharge current, equal to $P_{req}/(V_{dis} \cdot n_{bat})$.

$$DoD_{i+1} = DoD_i + \frac{P_{req} \cdot dt}{V_{dis} \cdot C_{bat} \cdot n_{bat}} \quad (12.1)$$

The above process is repeated for every time-step in the mission until the mission is completed or the cell fails. The fail can fail in two modes, it can discharge to the maximum allowed DoD before finishing the mission, or it can fail to provide sufficient power at some point in the mission. In the first scenario the battery is said to be energy limited, while in the second it is power limited. After the discharge fails a number of $dbat$ batteries is added to the pack, with the discharge starting again. Once discharge is successfully conducted $dbat$ batteries are removed, if the discharge fails, the sizing is completed (with the result being the last functional solution).

The battery sizing is thus dependent on parameters like the DoD limits, the cells per battery n_{cell} and the battery increment $dbat$. Values for these parameters are presented together with the results from the sizing in Section 12.4. The discharge is limited between DoD values of 0.1 and 0.9, in order to ensure extreme discharge values are not reached, which could potentially damage the battery.

Energy Density While the original cells are modified to adapt to the eVTOL power intensive application, it is still essential to ensure the cells energy density is within what is currently attainable, something that links with the design philosophy of this work. With the battery type selected to be Lithium Ion due to their market availability and performance; the value is set at 400 Wh/kg for the energy density at pack level, and 700 Wh/L looking at the volumetric energy density. These values are possible with current technology [3], with the energy density requirement being more limiting, the values are selected to also account for a certain fraction of the battery pack being dedicated to insulation, fire protection, and battery removal. See in Section 12.5 the sensitivity of the battery design to the available energy density.

¹<https://amprius.com/products/> [accessed 17th June 2024]

Battery Division In order to house the battery inside the fuselage while controlling the longitudinal location of the centre of gravity of the aircraft, the battery is divided in two different packs: the main and auxiliary battery (see Chapter 8). The main battery has a limit volume, set in the final design to 0.293 m^3 , with the auxiliary battery housing the remaining volume of battery. In case the centre of gravity has to be shifted due to stability requirements the main battery may house a lower volume, making the auxiliary battery larger, and heavier. Table 12.3 presents the results of the sizing, including the battery division between both packs. The division of the battery in two packs also follows REQ-BAT-13, removing the single point of failure in the battery system. It must be noted that the aircraft would have enough power to perform a horizontal landing, but not nominally continue the mission.

Battery Cost Cost is an important part of the battery sizing analysis, since an overly expensive battery will not meet REQ-BAT-10, and could negatively affect the total cost of the aircraft. In order to estimate the battery cost a cost of 200 \$/kWh is used, although the cost is predicted to decrease, this value is taken to account for the increased cost a high power density cell could have [38]. The battery capacity used is not the capacity at end of life found in the sizing, but rather the beginning of life (BOL) capacity. This value is found by dividing the EOL capacity by $(1-\kappa)$, where κ is the allowed degradation. Next, the TMS sizing is presented in Section 12.3.2.

12.3.2. Thermal Management Sizing

Sizing of a thermal management system is tightly dependent on the power system to be cooled, and its efficiency. For this design the battery efficiency is assumed to be 90%, as presented before in Section 12.2; meaning 11% of the power value provided by the battery to the drive-train during the flight is lost in the form of heat. This heat \dot{Q} has to be dissipated by the TMS, and together with the temperature difference $\Delta T_{bat-air}$, is an input to Equation 12.2, an statistical relation used to calculate the mass of the system [39].

$$W_{TMS} = 0.05 \cdot \frac{\dot{Q}}{\Delta T} + 4.01 [kg] \quad (12.2)$$

The weight of the TMS can thus be decreased by increasing the operating temperature of the battery, but this worsens the discharge performance of the battery, a battery temperature of 30°C is selected, providing a difference in temperature of 21.5°C with the ISA temperature at the cruise altitude of 8.5°C [40], while not compromising the performance of the battery [41]. An accurate estimate of the TMS cost would require of a more detailed sizing, something outside the scope of this project, a preliminary estimate to ensure the system falls within budget is conducted, using the results from [42], where a TMS used to cool a 200 kW battery is estimated to have a cost of 200 \$, this value results in a TMS cost of 1\$/kW, to which a safety factor of 1.5 is applied due to the high uncertainty of the cost estimate. The TMS cost in euros is thus calculated with a mass cost of 0.93 €/kW.

Regarding the configuration of the TMS within the entire system, an air inlet under the aircraft's nose provides cool air to transfer heat to. Then, to meet REQ-TMS-04, and improve the aircraft's efficiency part of this airflow is diverted to heat the cabin, the details of this process are to be refined in a more detailed sizing of the TMS. In order to ensure the TMS and battery comply with REQ-TMS-07, the cooling circuit should be made water proof, to avoid damage to the battery.

12.4. Results

This section contains both the numerical results from the power sizing and the electrical diagram for the aircraft, which presents the main elements of the aircraft using, and providing, electric power.

12.4.1. Design Parameters and Discharge Graphs

After using the method specified above to size the battery and TMS of the aircraft, a total battery mass of 1032.0 kg was found. The TMS, on the other hand has an estimated mass of 96.4 kg. All other relevant parameters are presented in Table 12.3, with their unit and rationale. The main results from this sizing affecting the rest of the design are the system masses and the maximum power output from the battery. This last value is set so the battery meets the thrust to weight requirement of 1.3 during vertical flight, Chapter 13 covers this requirement in more detail. Figure 12.4 and Figure 12.5 present the discharge profile, it's specially relevant how the battery is optimised to discharge fully while also attaining power ratios close to 1.

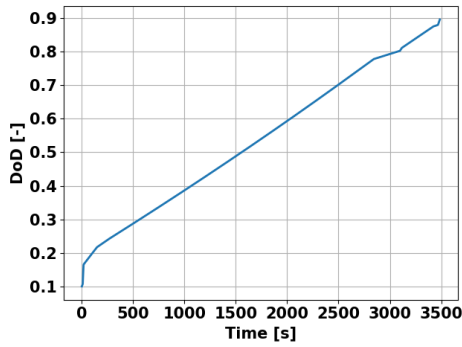


Figure 12.4: Battery depth of discharge throughout the mission.

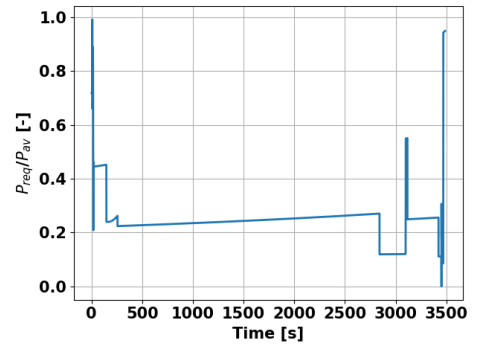


Figure 12.5: Ratio of power required to power available throughout the discharge.

Table 12.3: Battery and TMS sizing results and corresponding rationales.

Parameter	Value	Unit	Rationale
W_{pack}	1153.4	kg	Calculated using found n_{bat} and m_{bat} .
$W_{pack,main}$	586.0	kg	Depends on volumetric energy density and main battery volume.
$W_{pack,aux}$	567.4	kg	Pack mass not included in the main battery pack.
$V_{pack,main}$	0.293	m ³	Set as a design choice in Chapter 8
$V_{pack,aux}$	0.284	m ³	Found with the auxiliary pack mass and the volumetric energy density.
W_{TMS}	96.4	kg	Calculated using Equation 12.2
m_{cell}	0.022	kg	Defined to achieve a pack level BOL energy density of 400 Wh/kg
n_{cell}	40	-	As presented in Section 12.3.1.
n_{bat}	1290	-	Minimum number of batteries to complete the flight profile.
DoD_0	0.1	-	As presented in Section 12.3.1
DoD_f	0.896	-	DoD at the end of the discharge.
DoD_{lim}	0.9	-	As presented in Section 12.3.1
κ	0.2	-	Allowed degradation as presented in Section 12.3.1
C_{batBOL}	2.5	Ah	As presented in Section 12.3.1
C_{batEOL}	2	Ah	Found from the BOL capacity and allowed degradation.
e_{BOL}	400	Wh/kg	Set as a design choice.
e_{EOL}	320	Wh/kg	Derived from BOL energy density and the allowed degradation.
E_{pack}	370.0	kWh	Found from n_{bat} and e_{EOL} , accounting for discharge inefficiencies.

12.4.2. Electrical Block Diagram

Besides sizing the different elements of the power subsystem, it is also relevant to define the interactions between said elements, specially looking at how is the power transferred and transformed. Figure 12.6 below presents a electrical block diagram with the main elements in the system. In this diagram the DC-DC block refers to the stage where the current is adapted to be used in the cabin and by the flight instruments. Power connections to be used only in case of emergency are drawn with dashed lines, and feedback from the flight instruments to the power control unit (PCU) is not shown, for more detail on flight control see Chapter 14.

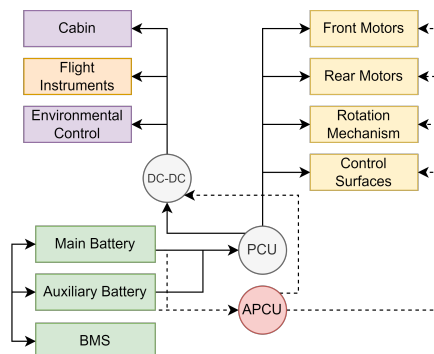


Figure 12.6: Electric block diagram of the aircraft.

12.5. Sensitivity Analysis

A sensitivity analysis was performed on several design parameters with a significant effect on the sizing. The results of the analysis can be found below, starting with the relevance of energy density, which following the design philosophy of this project has been selected to be attainable with current technology, as seen in Table 12.3. The results of this analysis do not include iteration of the aircraft's battery mass, since that falls outside the scope of the tool, thus high battery masses do not include the "snowball" penalty of having to carry a heavier pack.

12.5.1. Battery Energy Density

The battery energy density has a significant influence on the resulting battery mass required for the design in general aircraft, and as such is an interesting element to analyse. Figure 12.7 presents the resulting battery mass for different energy densities.

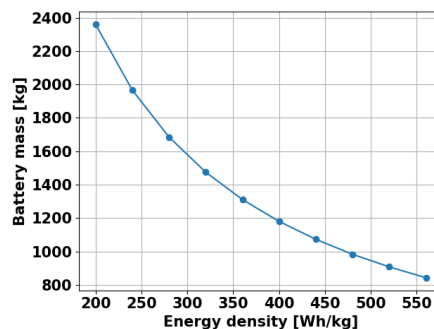


Figure 12.7: Resulting battery mass for varying pack-level energy density.

As can be seen in Figure 12.7, the relationship between energy density and battery mass is as expected, increasing the density reduces the total battery mass.

12.5.2. Cruise Speed

While the selected cruise speed comes from a user requirement, it is still relevant to look at the effect varying the cruise speed has on the required battery size. Figure 12.8 presents the resulting battery mass for different cruise speeds.



Figure 12.8: Resulting battery mass for varying cruise speeds.

As can be observed from the figure, the battery mass requirement finds a minimum for velocities between 250 and 270 km/h, with the peak at 260 km/h most likely due to the discretised discharge analysis. There is not an absolute minimum due to the discretisation of the battery pack into batteries, which means several aircraft may need a battery of the same size. This is also due to the fact that the battery has a minimum mass requirement imposed by power, and not energy requirements, as can be seen in the next section.

12.5.3. Range

The range requirement, set to 200 km, is one of the design parameters that affect the energy requirement and thus the total battery mass. Figure 12.9 presents the effect of modifying the mission range on the total battery weight.

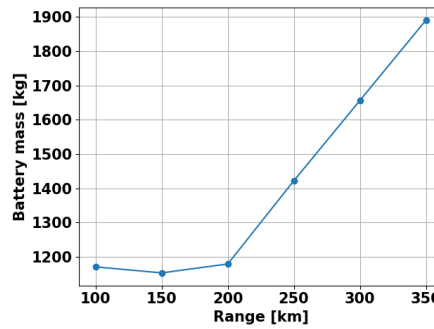


Figure 12.9: Resulting battery mass for varying range.

As presented above, the range has a big impact on the battery mass, with flights above 200 km becoming increasingly difficult with current battery technology. It can be seen, however, how the battery mass is similar when doubling the range from 100 to 200 km, this is due to the battery being power limited in that range; with the VTOL phases of the mission dictating the required number of batteries.

12.5.4. Temperature Difference

Lastly, the temperature difference between the cells and airflow has a significant effect on the overall mass of the TMS, this behaviour is presented in Figure 12.10.

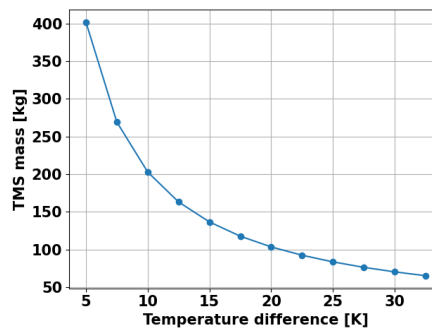


Figure 12.10: Resulting thermal management system mass for varying temperature difference.

As can be expected, a lower temperature difference slows conduction, requiring a heavier, more powerful, thermal management system. The selected design delta of 21.5°C allows for a significantly low TMS mass without requiring high discharge temperatures. In the case of extremely high temperatures within the aircraft's operating range (see REQ-SYS-AC-31), the TMS would perform poorly, making it essential to climb to its cruise altitude in order to cool the batteries.

12.6. Verification and Validation

In order to ensure the sizing process for the power subsystem is correctly conducted several verification and validation activities have been conducted. First the validity of the assumptions used has to be checked, after which the individual sizing tools have to be verified.

12.6.1. Assumptions

Table 12.4: Validation of the assumptions used for the preliminary structural model.

Identifier	Validation
A-BAT-01	For the cell in question (Figure 12.2 and Figure 12.3) linearising between $DoD=0.1$ and $DoD=0.9$ results in slightly (<5%) underestimating the available voltage.
A-BAT-02	With regards to the analysis this assumption is required, realistically cells will have variation in performance, however, as long as the average performance is as specified this assumption holds.
A-BAT-03	Cell degradation is not uniform, as with the capacity, asymmetries in degradation happen however in higher degradation regimes, where the battery would have to be replaced for safety in any case [43].
A-BAT-04	There are existing cells with the desired energy and power density (see footnote on second page of the chapter)
A-BAT-05	The presence of 4 data points for voltage with monotonic behaviour reduces the likelihood of significant error in the sizing. In further stages a detailed cell analysis should be conducted to better estimate the discharge behaviour.
A-TMS-01	This assumption is grounded on the need for larger amounts of coolant to dissipate higher heat values [44]; this assumption is only valid to get an estimate on the size of the TMS, but should be discarded for a detailed analysis in next design iterations.
A-TMS-02	With conduction being key for cooling, and Fourier's law dictating the rate of conduction being proportional to the temperature gradient, this assumption is correct in the general behaviour [45], it is however recommended to detail the TMS to better quantify this relationship.

12.6.2. Battery Sizing Tool

In order to verify the battery sizing tool a parallel tool was developed that could discharge a defined battery pack with a predetermined power required vector. This function then found all the discharge parameters found by the original sizing tool, which could then be compared. Table 12.5 presents for several output parameters values found by both tools and their relative error, as can be observed, both tools arrived at equal results, thus completing the verification. As for validation of the battery sizing, it is not possible to conduct it for the specific use case (eVTOL vehicles), due to the lack of available data on the subject. The tool was however validated for general electric aircraft by repeating the sizing conducted in [46]. The results from the validation resulted in a difference in MTOM of 3%, leading to the battery sizing tool passing its validation.

Table 12.5: Validation of the assumptions used for the preliminary structural model.

Parameter	Battery Sizing Tool Result	Battery Discharging Tool Result	Error %
DOD_f	0.897	0.897	0.0%
$C-rate_{avg}$	3.37	3.37	0.0%
$C-rate_{max}$	3.37	3.37	0.0%

12.6.3. Thermal Management System

Since at this stage in the design the TMS sizing is conducted by means of a statistical relation obtained from [42]; the verification of the tool consists in a unit test where the the TMS mass is calculated and compared with the tool output. The unit test was successfully completed, with an identical result being obtained in both cases. Regarding validation, TMS specifications for eVTOL aircraft designs are not readily available, complicating this task. As with the rest of the TMS design, a more detailed analysis should be performed with the results from the detail design of the aircraft.

12.7. Recommendations

Although the power analysis has covered the main limiting factors affecting battery sizing, giving a more accurate insight into the power requirements of the battery, there is still further analysis to be conducted. The main points of action at this stage are a detailed thermal management system, essential to know whether any substantial configuration changes are required (regarding battery location); and a degradation model that takes into account DoD and C -rate to estimate the lifetime of the aircraft. Such a degradation model would allow to devise an accurate schedule for battery replacement, giving more detail to the life cycle assessment of the HAROLD.

Chapter 13 | Flight Performance Analysis

This chapter covers the performance of the detailed aircraft design. First Section 13.1 presents the assumptions used for the analysis, with their validation presented in Section 13.5.1. The first two analyses revise the performance analysis conducted on the preliminary design [1]; while the last one, on headwind performance studies the possible range with different constant wind values. This performance analysis is conducted on the finalised design, and is used to check whether the aircraft complies with some of its requirements.

13.1. Assumptions

The main assumptions made in the flight performance analysis are presented below in Table 13.1 together with their expected effect.

Table 13.1: Assumptions used for the flight performance analysis.

Identifier	Assumption	Expected Effect
A-PF-01	Changing payload mass is assumed to not change the aerodynamic properties of the aircraft.	Change in drag and power requirements.
A-PF-02	Headwind is assumed to not alter the aerodynamic properties of the aircraft.	Deviation in lift and drag calculations.
A-PF-03	The aircraft is assumed to have a full battery in the rate of climb analysis.	Overestimation of ROC performance in normal operation.

13.2. Payload-Range Performance

While the HAROLD is optimised to fly at its design payload of 480 kg, the maximum payload is set at 600 kg. The payload-range analysis is thus conducted for payloads between 600 and 0 kg, with this last value requiring of the aircraft being configured for autonomous mode, since the pilot mass is included in the payload. Figure 13.1 below presents the payload range diagram, with indicators for the number of passengers, assuming a passenger mass of 80 kg. For this analysis the design flight profile presented above was used, with a lower T/W constraint of 1.2 to allow for higher payloads than the design value. When comparing the current payload-range performance to the analysis done in the preliminary design [1], a decrease of 15 km is seen for the 0 kg payload point, this is due to the preliminary analysis having less accurate assumptions on the power requirements for the battery pack. With the current analysis it is evident that at a range of 215 km the battery starts being limited by power, and not energy requirements. For this analysis the discharge model presented in Chapter 12 was also used.

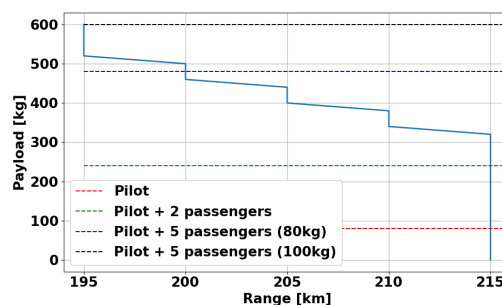


Figure 13.1: HAROLD's maximum range for its entire payload range.

13.3. Rate of Climb Performance

Due to the aircraft being sized for VTOL flight, its propulsion and powertrain are oversized for horizontal flight, resulting in very large rate of climb (ROC) values, as can be seen below in Figure 13.2. For this analysis the design weight of the aircraft, with a payload of 480 kg was used. When compared with the preliminary performance analysis [1], the maximum ROC is 7.5 m/s lower, while the maximum cruise speed, found at ROC=0 m/s is also 10 m/s lower. This is again due to overestimating the power available from the battery pack in previous stages of the design.

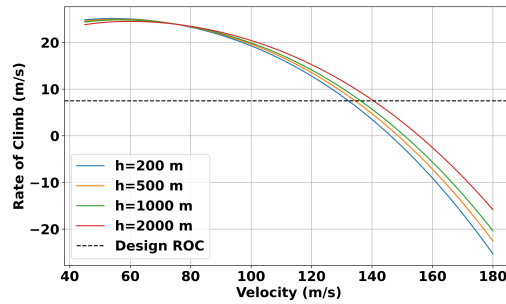


Figure 13.2: HAROLD's maximum rate of climb for varying velocity and altitude.

13.4. Headwind Performance

As a last performance analysis, the range achievable with different values of headwind is analysed. This analysis is conducted to ensure the aircraft is capable of flying with a wind of at least 60 km/h, as stated in the user requirements in Chapter 5. The maximum range achievable for the aircraft carrying its design payload of 480 kg is presented in Figure 13.3. Equation 13.1 presents the equation derived for this analysis, which applies a relative velocity change to the ground track of the aircraft using the headwind velocity w . Just the cruise phase of the mission was analysed, due to most of the range being covered in this phase.

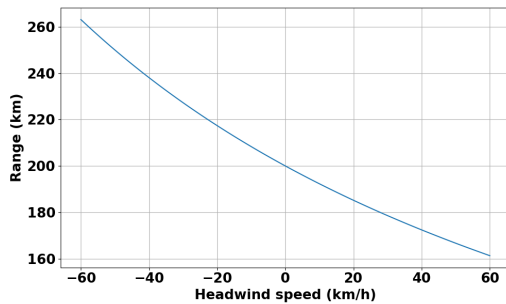


Figure 13.3: Maximum range for varying headwind.

$$R_{gr} = \frac{R}{1 - \frac{w}{v_{cr}}} \tag{13.1}$$

13.5. Verification and Validation

In this section the steps taken to verify and validate the assumptions and tools used during the performance analysis of the aircraft are presented. First the assumptions' validity is covered, followed by the performance analysis tools.

13.5.1. Assumption Validation

In Table 13.2 below the validation for the assumptions used in this analysis is presented. Note the assumptions applied for the flight profile analysis, covered in Chapter 7, also apply for this analysis.

Table 13.2: Validation of the assumptions used for the flight performance analysis.

Identifier	Validation
A-PF-01	Shift in CG due to payload could affect performance, but due to the small excursion the accuracy of the drag model can be considered limiting instead of the mass variation.
A-PF-02	The analysis is only valid for pure headwind with this assumption, but since it is a performance measure, it is valid as long as the wind considered is clear.
A-PF-03	As for A-PF-03 the assumption is valid, it just means the performance measure is done with an aircraft battery state that is slightly more powerful due to not being discharged at all.

13.5.2. Performance Analysis Tools

The first two performance analyses use tools developed and verified in previous design stages, although the payload-range diagram tool has to integrate the new battery discharge tool, verified in Chapter 12. The overall functioning of the tool is ensured by confirming the range possible for the design payload is indeed the design range. Verification of the wind analysis tool is simple, since it consists in applying an equation linking wind velocity with ground track Range (Equation 13.1). Validation of the equation involves validation of the assumptions

related with it, presented above (A-FP-03 and A-FP-05).

13.6. Recommendations

Although the performance analysis has covered the main performance characteristics relevant for the design, there are still some areas where more detail is recommended. The control scheme for the VTOL configuration, based for this analysis on a PID controller, results in large thrust oscillations in order to achieve a system stiffness capable of maintaining an attitude. A more complex controller that dynamically adjusts gains to the current state should be implemented to arrive at a more optimal solution to the control problem. The results from the performance analysis show that, while the current design is technically feasible, its design space is significantly constrained, with slight deviations in the operating conditions greatly affecting performance.

Chapter 14 | Avionics & Software

In this chapter, the design of the avionics systems is described. Next to an explanation of all the separate systems also their relations are described. These relations will be shown in three different ways. These three forms involve their hardware, their software and the communication between the different systems

14.1. Subsystem Requirements and Compliance Matrix

In Table 14.1 the subsystem requirements and their compliance are shown.

Table 14.1: Avionics Subsystem Requirements Compliance Matrix.

Identifier	Requirement	Source(s)	Compliance	Method of Verification
REQ-AVI-01	The aircraft shall be able to be trimmed in cruise conditions from the cockpit controls.	REQ-SYS-AC-18	✓	Inspection shows that the trim surface is present and powered by actuators as written in Section 14.3.1
REQ-AVI-02	The cockpit controls shall allow switching from manual to autonomous flight.	REQ-SYS-AC-29	✗	The initial avionics design assumes a pilot in control, later iterations can include the transition between manual and autonomous flight (since the sensors are present).
REQ-AVI-03	The cockpit controls shall allow switching from autonomous to manual flight.	REQ-SYS-AC-30	✗	The initial avionics design assumes a pilot in control, later iterations can include the transition between manual and autonomous flight (since the sensors are present)
REQ-AVI-04	The cockpit shall allow the pilot to reach all the controls in the cockpit from a single	REQ-SYS-AC-42	✗	The cockpit layout has not yet been designed, in the future this is recommended.
REQ-AVI-05	The aircraft shall have conventional responses to pilot inputs from the cockpit.	REQ-SYS-AC-45	✓	Analysis shows that the controls are comparable to the V-22 Osprey (Section 14.3.1)
REQ-AVI-06	The cockpit shall provide the pilot with the conventional flight information.	REQ-SYS-AC-91, REQ-SYS-AC-92, REQ-SYS-AC-93	✓	Inspection shows that all the conventional flight instruments are present as stated in Section 14.4
REQ-AVI-07	The cockpit shall indicate the aircraft's battery charge level.	REQ-SYS-AC-52	✓	Inspection of the engine data system shows that it can provide this data (Section 14.4)
REQ-AVI-08	The avionics shall allow for an autonomous landing procedure at the nearest ground station in case of an emergency	REQ-SYS-AC-55	✗	The initial avionics design assumes a pilot in control, later iterations can include the transition between manual and autonomous flight (since the sensors are present).
REQ-AVI-09	The pilot shall be able to control the elevator deflection from the cockpit.	REQ-SYS-AC-14, REQ-SYS-AC-48	✓	Inspection shows that the system is present to control the elevator (Section 14.3.1)
REQ-AVI-10	The pilot shall be able to control the rudder deflection from the cockpit.	REQ-SYS-AC-49	✓	Inspection shows that the system is present to control the rudder (Section 14.3.1)
REQ-AVI-11	The pilot shall be able to control the aileron deflection from the cockpit.	REQ-SYS-AC-50	✓	Inspection shows that the system is present to control the aileron (Section 14.3.1)
REQ-AVI-12	The pilot shall be able to control the thrust level from the cockpit.	REQ-SYS-AC-13	✓	Inspection shows that the system is present to control the thrust of the engine (Section 14.3.1)
REQ-AVI-13	The pilot shall be able to control the rotation around the vertical axis in vertical flight from the cockpit.	REQ-SYS-AC-22	✓	Inspection shows that the system is present to control the rotation of the aircraft (Section 14.3.3)
REQ-AVI-14	The pilot shall be able to control position of the aircraft along all three axes in vertical flight from the cockpit.	REQ-SYS-AC-23	✓	Inspection shows that the system is present to control the position of the aircraft (Section 14.3.3)
REQ-AVI-15	The avionics subsystem shall include the required sensors for autonomous flight.	REQ-SYS-AC-28	✓	Analysis shows that all the avionic systems together provide the required sensors for autonomous flight (Section 14.3.1)
REQ-AVI-16	The avionics subsystem shall include a sensor capable of measuring flight loads with an accuracy of +0.1 G.	REQ-SYS-AC-28, REQ-SYS-AC-39, R-TEC-10	✓	Inspection shows that an accelerometer is present (Section 14.4).
REQ-AVI-17	The cockpit shall indicate the measured G loads in flight conditions.	REQ-SYS-AC-39, R-TEC-10	✓	Inspection shows that an accelerometer is present (Section 14.4).
REQ-AVI-18	The avionics subsystem shall include an Automatic Dependent Surveillance–Broadcast (ADS-B) system.	REQ-SYS-AC-53	✓	Inspection shows that ADS-B is present (Section 14.4).
REQ-AVI-19	The avionics subsystem shall include an EASA certified radio system onboard for communication with parties outside the aircraft.	REQ-SYS-AC-54	✓	Inspection shows that the radio system is present (Section 14.4)
REQ-AVI-20	The cost of the avionics subsystem shall be less than 100,000 euros.	REQ-SYS-AC-94	✓	Analysis shows that the costs are equal to 94471.57 euros (Section 14.4)
REQ-AVI-21	The avionics subsystem shall have an operational ambient air temperature range of -20 °C to 47 °C.	REQ-SYS-AC-31	✗	The analysis of the temperatures has not yet been conducted and is recommended for the future.
REQ-AVI-22	The avionics subsystem shall include detectors capable of detecting fires in the propulsion and battery subsystems and the cargo hold.	REQ-SYS-AC-86	✓	Inspection shows that a fire detection system is present (Section 14.3.1)

14.2. Assumptions

The assumptions used during the design of the avionics design are shown in Table 14.2. In A-AVI-05 and A-AVI-06 miscellaneous avionics are mentioned. These include possible revisions of the avionic systems, for example, the flight computer. For fully autonomous flight a different flight computer might be needed compared to the

current one. It also includes avionics that might be overlooked or changed during this preliminary estimation and to account for possible additions that will become mandatory between the time of this analysis and certification of the aircraft.

Table 14.2: Assumptions used for the avionics subsystem.

Identifier	Assumption	Expected Effect
A-AVI-01	The pilot needs a flight computer to assist him during the transition phase from horizontal flight to VTOL.	This will have an effect on the selected control system and the software.
A-AVI-02	The first aircraft will still be piloted by a pilot.	This makes it easier to certify the aircraft since an autonomous system is more complex. This also allows for gathering more flight data to improve the quality of the autonomous system.
A-AVI-03	The engine data system of an electric system will have approximately the same price and mass as those of turbo propellers	If the price or weight changes this might influence the cost and mass calculations of the avionics.
A-AVI-04	Heat from the thermal management system can be redirected to assist with the air conditioning of the cabin	This reduces the power required by the air conditioning system to heat the cabin.
A-AVI-05	The miscellaneous costs are assumed to be 18,610 euros (20,000 US dollars).	This gives an extra buffer before the budget has been exceeded and it allows for upgrades to be taken into account when changing the avionics for autonomous flight.
A-AVI-06	The miscellaneous mass is assumed to be 20 kg.	This gives an extra buffer before the budget has been exceeded and it allows for upgrades to be taken into account when changing the avionics for autonomous flight.

14.3. Method

In this section the design process of the avionics system is described. This is done by first analysing the hardware, followed by the communication links between these hardware systems. Finally the software is of the avionics will be discussed.

14.3.1. Hardware

Before the hardware can be analysed the required systems in the aircraft must be determined. The first choice that needed to be made was the type of control system. For this three solutions were determined, namely a cable system, a hydraulic system and a fly-by-wire system. During the analysis of the systems it was determined that some actuators (either hydraulic or electrical) were needed in order to rotate the engines since doing this manually would require a lot of force. It was also determined that the pilot would most likely need assistance from a flight computer during the transition period (A-AVI-01), since this would also require the pilot to transition to a new control system. For the flight control system inspiration was taken from the V-22 Osprey¹, where the flight controls during horizontal flight are the same as for airplanes and during VTOL operations the thrust lever determines the altitude and the control stick and the pedals the attitude (comparable to airplanes). Based on these conclusions it was determined that the cable system would not be a good fit, since this would require a separate system to connect the flight computer to the cable system. Between the hydraulic system and the fly-by-wire system, the choice went to the fly-by-wire system since the aircraft is already based a lot on electrical systems and integrating the flight computer into a electrical system is easier than integrating it into a hydraulic system. Next to that the fly-by-wire system also has a weight and corrosion advantage in comparison to the hydraulic system².

From the selection of the control system, the other systems could be analysed. For this stage of the design an avionics system was designed for the first batch of aircraft, which follows A-AVI-02. This means that the initial collection of avionics is meant to help the pilot with his or her decisions during flight. However, all the systems were installed with an eventual transition to autonomous flight. This means that the combination of all the avionics together would provide the flight computer with enough information in order to fly autonomously. This would require some minor adjustments to these systems since most of them are now designed to give information on an instrument, but these changes would be considered minor changes. In Table 14.3 (which can be found in Section 14.4) all the avionic systems implemented in the aircraft can be found together with their price, weight and function.

Next to the avionic systems described in Table 14.3 the aircraft also contains other hardware which are (in)directly linked to the avionic systems. A couple of these hardware components are for example the ailerons, elevators, flight control stick, flight pedals, etc. In Figure 14.1 the relations between these hardware components are depicted. In this diagram the measuring devices are taken in a broader sense, because there might be multiple gyros, sensors and antennae for the different systems but for the simplicity of the diagram these are all combined into a single block. From this diagram it can also be seen that the flight computer has a relation to a lot of other components, this is because of the choice for the fly-by-wire system in which the flight computer has to evaluate the inputs of the pilot and sent the correct signal to the other subsystems.

¹<https://www.spinningwing.com/v22-controls> cited[19.06.2024]

²<https://www.flyaeroguard.com/blog/cable-systems-vs-hydraulic-systems-vs-fly-by-wire-in-aircraft/> cited[19.06.2024]

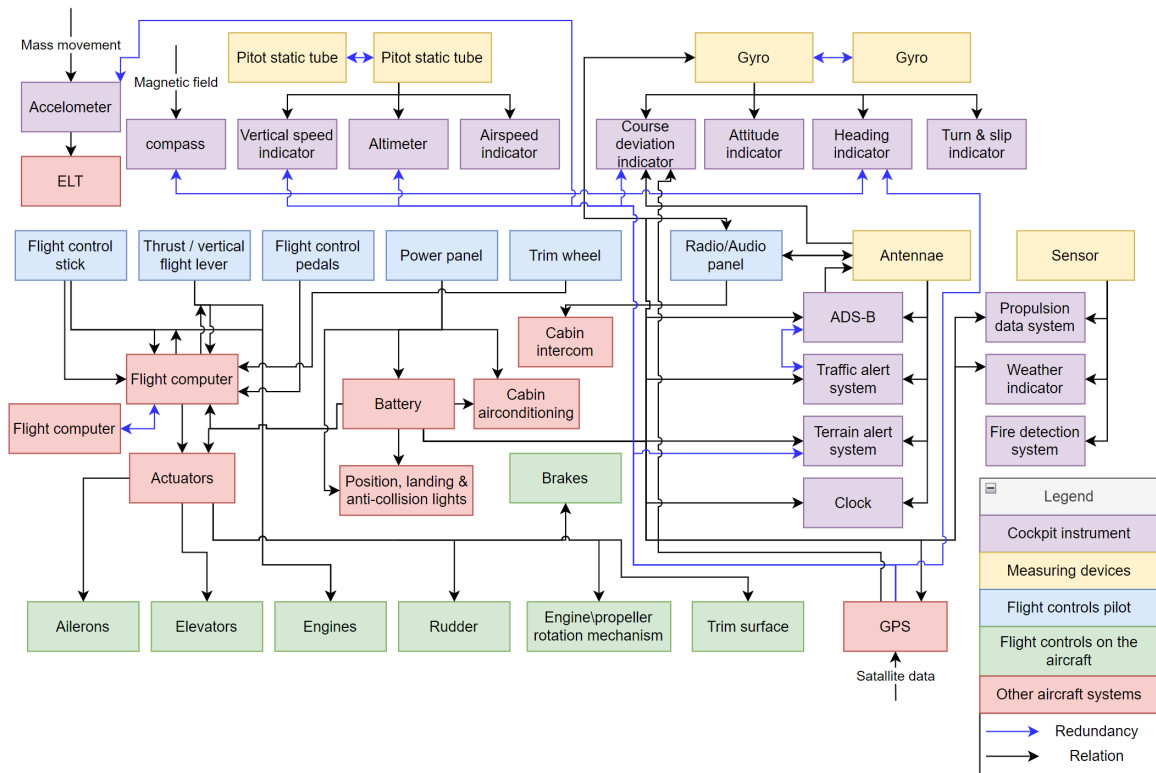


Figure 14.1: Diagram showing the relations of the hardware components of the aircraft.

14.3.2. Software

Next to hardware, there is also software included in the aircraft. The software used to give the pilot more information during flight is often incorporated in the cockpit instruments which can be found in Figure 14.1. Next to that there is also software that is included in the flight computer. For the initial stages (due to A-AVI-02), the flight computer will monitor the pilot and only assist the pilot in case of transition or in case the pilot flies into a dangerous situation. These dangerous situations can include a multitude of situations such as flying too close to terrain or traffic, but it can also include a situation in which the pilot flies the aircraft too close to the aircrafts absolute limits. These limits can for example include exceeding the designed load factor of 2 or surpassing the maximum allowed flight speeds. As explained in Section 14.3.1 this design is intended for piloted flight, so for autonomous flight some minor adjustments need to be made.

In Figure 14.2 the software relations are shown. The colours of the diagram are linked to the colours of Figure 14.1, these indicate in which type of hardware this software originated. The dotted boxes in Figure 14.2 indicate in which sections of hardware the software (depicted as the fully coloured boxes) will be implemented.

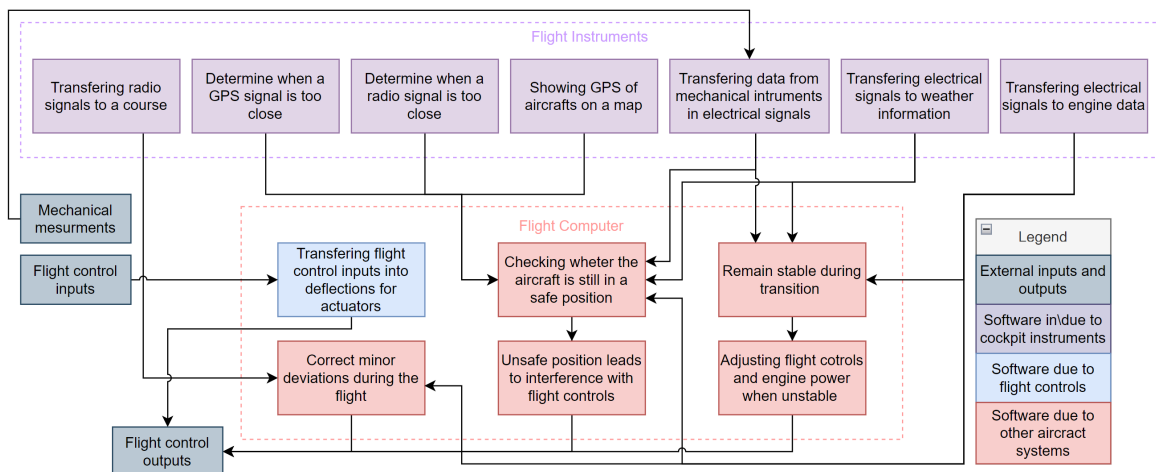


Figure 14.2: Diagram showing the relations of the software components of the aircraft.

a gyro as can be seen in Section 14.3.1 all have their own specific gyro, which can be used for redundancy of the other systems. Next to that the GPS system provides a lot of redundancy to the system of the aircraft, by providing backup data for the terrain warning system, altimeter, vertical speed indicator, heading indicator, course deviation indicator and accelerometer. Although this will require some calculations from the difference between the locations. It also only gives an indication about which value is correct (for some of the systems), for example the speed calculated via the GPS does not take the wind into account.

Table 14.3: Values of avionic components and corresponding rationales.

Component	Price [\$]	Mass [kg]	Rationale
ADS-B in/out (Automatic Dependent Surveillance-Broadcast)	4194	1.49	ADS-B shows other traffic to the pilot and tells the traffic where the aircraft is located.
Radio	3048	1.38	Radio is used to communicate with ATC, other aircraft and the ground station.
Pitot-static (2)	820	1.96	Pitot-static is used to measure the total and static pressure which is needed for multiple flight instruments.
Airspeed indicator	2299	0.23	The airspeed indicator provides information about the indicated airspeed.
Altimeter	3125	0.91	The altimeter provides information about the altitude of the aircraft.
Attitude indicator	2299	0.23	The attitude indicator provides information about the attitude of the aircraft in comparison to the aircraft.
Compass	295	0.45	The compass provides information about the heading (and is a back-up to the heading indicator).
Engine data system	8965	0.86	The engine data systems provides crucial information about the status of the engine and battery. A-AVI-03 is applicable here.
Vertical speed indicator	375	1.02	The vertical speed indicator gives information about the climb or descent rate of the aircraft.
Weather indicator	3580	1.86	The weather indicator provides the pilot with accurate weather data at that specific moment in time.
Position lights	1098	0.15	The position light indicates the orientation of the aircraft to traffic.
Anti-collision lights	139.75	0.05	The anti-collision lights visually indicate the location to traffic.
Landing lights (2)	498	0.64	The landing lights help to light the landing pad during landing operations.
Turn & slip indicator	2299	0.23	The turn & slip indicator indicates the turn rate and slip or skid of the turn.
Course deviation indicator	10796	2.31	The course deviation indicates how far and in which the aircraft has deviated from its assigned course or glide path.
Actuators	941	17	The actuators can move the engines and control surfaces to their correct angle.
Clock	389	0.31	The clock shows the pilot the time and its flight time such that he or she does not extends his or her flight dangerously
Heading indicator	2299	0.23	The heading indicator provides information about the heading of the aircraft.
ELT (Emergency Locator Transmitter)	1676	0.89	The ELT is activated when submerged in water or when experiencing an extreme G load. It than sends a signal for rescue services.
Power panel	820	1.25	The power panel allows the pilot to assign power to certain systems.
Safety Belts	6144	-	The safety belts keeps the passengers and the pilot safely in their seat.
GPS (Global Positioning System)	2299	0.23	The GPS system allows the pilot to navigate to his or her destiny.
Traffic warning system	779	0.31	The traffic warning system gives the pilot a warning for traffic that is too close. For autonomous flight, an automated avoiding action shall be paired with the warning.
Terrain warning system	3420	-	The terrain warning system gives the pilot a warning for terrain that is too close. For autonomous flight, an automated avoiding action shall be paired with the warning.
Audio panel	1998	0.81	The audio panel allows the pilot to select whether he is connected to the cabin or only to the ATC frequency.
Autopilot	6741	-	The autopilot allows the aircraft to fly itself in case the pilot selects this option.
Cabin air conditioning	450	0.68	The cabin air conditioning is used to provide a comfortable temperature in the cabin and can be assisted by A-AVI-04.
Flight computer (2)	10700	1.08	The flight computer stores and processes flight data, for autonomous flight an upgrade on this flight computer is likely required.
Accelerometer	239	0.07	The accelerometer shows the pilot the G loads on the aircraft such that he or she does not exceed the load factor.
Miscellaneous	20000	20	The miscellaneous costs and mass allows for unaccounted systems to be added (the fire detection system is for example included because of a lack of data). A-AVI-05 and A-AVI-06 are applicable.
Total	102725.75	56.63	The combined costs in US dollars and mass in kg.

14.5. Conclusion

In this chapter, the avionics of the HAROLD were discussed, this was done by means of hardware, software and communications after which a selection of the different systems was made (which can be found in Table 14.3). Initially, the avionics were selected with a piloted aircraft in mind. But extra systems were added to ensure all the sensors for autonomous flight would be present. These systems are not only implemented for the sensors but also provide additional information to the pilot to allow for better judgement of the situation. Next to that there is a redundancy system in place such that critical systems has a different system on which it can fall back. All these avionic systems in the aircraft together cost 102725.75 US dollars which is equivalent to 95586.31 euros and weights 56.63 kg.

14.6. Recommendations

For further development of the HAROLD it is recommended that further research is performed on autonomous flight. And more specifically how to combine the flight computer with all the sensors of the different avionics systems. More research should also be dedicated to the working of the software in a flight computer that is able to perform autonomous flight. A system that already exists such as Deckfinder⁶ from Airbus might be a valuable addition to such a system. It is also recommended to perform a power analysis for the different avionic systems in order to estimate their effect on the power of the entire aircraft.

⁶<https://www.airbus.com/en/products-services/defence/uas/deckfinder> cited[25.06.2024]

Chapter 15 | Material Analysis

Wood has historically been used in aircraft construction and is still in limited cases in hobby, glider and aerobatic aircraft. This, together with the fact that wood is regarded as a sustainable material (as it can be regrown within one human generation) indicates the potential for reintroducing wood into the aeronautical industry. In this chapter, the analysis of the materials in the aircraft structure is performed. The various aerospace-grade wood materials, their properties, and uses are analysed in Section 15.3. Subsequently, the considered wood materials are compared to some more common aerospace metal alloys and composites in Section 15.6.

15.1. Materials Requirements and Compliance Matrix

The materials used in the aircraft strongly influence the design of the aircraft and thus pose requirements to the design process. Additionally, aviation authorities regulate the material and structural specifications in aircraft to ensure standards for safe operations. All of these requirements for the materials are given in Table 15.1.

Table 15.1: Materials requirements compliance matrix.

Identifier	Requirement	Source(s)	Compliance	Method of verification
REQ-MAT-01	All wooden components shall be treated to Euro Class B.	REQ-SYS-AC-74, R-TEC-12	✓	Inspection in Section 15.3.4
REQ-MAT-02	Outward facing surfaces have to have an electrical resistance of max $2.5m\Omega$ ¹ .	REQ-SYS-AC-87, R-TEC-09	✓	Inspection in Section 15.3.4
REQ-MAT-03	There shall be at least two qualified suppliers for the wood used in the eVTOL structure.	REQ-SYS-AC-74, RAMS-02	✓	Verified by inspection in the supply chain analysis in Section 21.2.1
REQ-MAT-04	The aircraft shall be designed using material property values approved by EASA.	REQ-SYS-AC-86	✓	Inspection of the correspondence of ANC-18 material properties [47] to the material values given in the analysis
REQ-MAT-05	All wooden components outside the interior cabin shall reach EN 335 Use Class 3 specifications.	REQ-SYS-AC-74, REQ-SYS-AC-78, R-TEC-07	✗	Demonstration at a further design stage

Although not all of these requirements can be ensured at this stage of the design, they will have to comply with all of the safety regulations when the aircraft is to be certified for production and eventual use.

15.2. Assumptions

All of the assumptions used in analysing the materials used in the aircraft are provided in Table 15.2.

Table 15.2: Assumptions used for material analysis.

Identifier	Assumption	Expected Effect
A-MAT-01	All wood materials have a moisture percentage of 15%	Standard material properties for moderate climates, equivalent to the continental US can be used [47].
A-MAT-02	The wood moisture percentage does not change during the operational life with the help of coatings and adequate storage	The wooden structure has constant strength throughout its lifetime. The material properties would be overestimated if the moisture content rose in real application.
A-MAT-03	All wood materials are maintained within the operational temperature range of -20 - +47°C	No temperature degradation effects are taken into account. However, the material properties of wood are still reduced by around 20% at 47°C [47]
A-MAT-04	All wood materials have a grain slope of no more than 1 in 15 units, equivalent to 3.8° in longitudinal direction	The material properties of the wood elements are not affected due to defects in the grain structure [47]
A-MAT-05	The fatigue life of wood is longer than the operational lifetime of the aircraft [48]	The fatigue effect on the material properties is neglected.

15.3. Analysis of Wood as a Structural Material

This section analyses the use of wood as a material, which will later be implemented in different elements of the aircraft and the ground station. To do that feasibly, however, the material properties of wood have to be investigated thoroughly.

15.3.1. Main Material Aspects of Wood

Wood is a natural composite material - the alignment of the tree cells and the growth rings give the wood orthotropic behaviour [49] and as such, the mechanical properties of wood depend on the grain direction. The anisotropy can be fully described by 3 different directions: the longitudinal direction (parallel to the grain), the radial direction (normal to the growth rings) and lastly the tangential direction (perpendicular to the grain and tangent to the growth rings) [49].

Wood is also classified as a viscoelastic material [50], which means that it shows elastic as well as plastic

behaviour at the same time. Because wood is orthotropic, 12 constants are required to describe its elastic behaviour. These include 3 moduli of elasticity, 3 moduli of rigidity and 6 Poisson's ratios due to the previously identified three anisotropic directions. The most commonly used properties to describe the strength of wood are the modulus of rupture in bending, the maximum stresses in compression parallel and perpendicular to the grain, and shear strength parallel and perpendicular to the grain. Lastly, an important material property for aircraft design is the density. For comparing various wood species, the specific gravity (the ratio of densities of the wood and water), is most often used.

15.3.2. Available Wood Options

Historically, wood has been used in aircraft production when metallic materials were not as prevalent in the industry (start of the 20th century) or when other aerospace materials were in shortage (2nd World War). Nowadays, in light of increasing concern for sustainability, however, wood could be used as an alternative to modern aerospace materials to incorporate more sustainable materials and production techniques into aircraft design processes. Although wood is generally a widely available material, aerospace-grade wood is less accessible since the availability of wood depends on the species: some species are not grown on farms and could be rare, limiting their usefulness for commercial production. Most lumber trees are often grown in dedicated forests with a growth period of 35-45 years [51].

Furthermore, wood is an organic material; thus, each wood piece differs slightly in its fibre structure. Not all characteristics can be predicted before the tree is sawn into planks and sometimes are hard to evaluate from the outside, even when using high-grade lumber. Additionally, lumber elements with complicated dimensions and features could be impossible to create from a single piece of wood, because of the way the tree is shaped.

Finding wood that is durable enough for aerospace use while being easy to manufacture and that is easy to grow without many defects in the grain has historically been a difficult task. Although many wood species such as Sitka spruce, birch, ash, and Douglas Fir have the necessary strength in ideal grain conditions to sustain the necessary loads, the intricacies of degradation resistance, harvestability, and workability are most often the deciding factors². In previous aerospace use, Sitka spruce and Douglas fir have been preferred due to their resistance to degradation and the fact that they grow as large straight trees, minimising the defects in the grain structure and allowing the processing of long straight beam elements [49].

In some cases, also lighter and structurally weaker wooden materials have been used in aerospace applications. The Mosquito - perhaps the most famous wooden aircraft to have been manufactured, for example, made use of Balsa wood in its wing structure as a middle layer between two spruce plates for achieving a honeycomb-like wing structure. The de Havilland Aircraft Museum, Salisbury Hall, London Colney, Hertfordshire was contacted in order to learn more about such structures in the Mosquito based on their available records from restorations, but no answer was received during the time of this project.

15.3.3. Factors influencing Mechanical Properties of Wood

The properties of wood depend on factors such as moisture content and temperature [52]. Furthermore, degradation and fatigue can also appear over time. A good understanding of these mechanisms is required to be able to design a lasting vehicle with wood. This section contains a selection of graphs and information about the specific mechanical properties of wood.

Moisture Content

Moisture content (expressed in percentages) is an important factor for various wood properties. The moisture content starts affecting the material properties once the amount of water in the wood declines below the fibre saturation point, having a positive impact on most mechanical properties due to the inverse relation between the moisture content and the mechanical properties [49]. Many resulting material properties of dry (often referred to as oven-dry) wood can be estimated using a function where an increase in temperature leads to a percentage decrease in the estimated parameter. However, properties such as maximum load, impact bending, and tension perpendicular to the wood grain cannot be estimated with this method and behave erratically under changing moisture content. In Figure 15.1 graphs for several wood properties with changing moisture content have been plotted.

Temperature

Another factor in the properties of wood is temperature. In general, the mechanical properties of wood decrease with increasing temperature. Generally, this relation is linear until a temperature of around 150°C is reached [49]. The changes in mechanical properties during a quick change in temperature are called an immediate effect, and for temperatures below 100°C, these immediate effects of temperature are reversible. The change

²<https://woodenaviation.com/types%20of%20wood%20used.html> [cited 13.06.2024]

in the compressive strength of wood for a reversible immediate temperature change is shown in Figure 15.2. Additionally, as can be seen in Figure 15.2 it holds true that the more humid the wood, the larger the effect of temperature on the properties of wood is.

For temperatures outside of the 100°C range, irreversible degradation is likely to occur, which has lasting effects on the wood's properties. The severity of the degradation depends on moisture content, heating medium, temperature, exposure period, wood species, and the size of the timber part. Furthermore, the permanent effect of heating is cumulative - each subsequent heating cycle adds to the degradation.

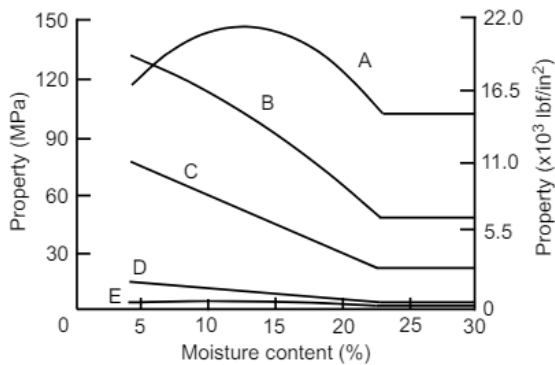


Figure 15.1: Compressive strength of wood (Sitka Spruce and Douglas Fir) under the influence of temperature for two moisture contents. The shaded area denotes the uncertainty in results from different studies. [49]

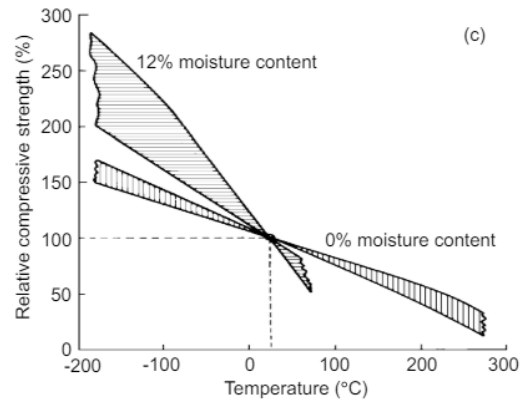


Figure 15.2: Wood properties with changing moisture content. A - tension strength parallel to strain, B - maximum bending stress, C - compression parallel to grain, D - compression perpendicular to grain, E - tensile strength of wood perpendicular to grain. [49]

Creep, Loading Duration, and Fatigue

When wood is loaded for a long period, creep is introduced to the material with the creep rate increasing at increasing load, temperature and moisture content [49]. Furthermore, when stressed wood is unloaded, approximately half of the creep is recovered after a time, usually in the order of a few months [49]. Similarly to the temperature effects mentioned before, the duration of the load is cumulative. The process of failure under continuous or intermittent loading is regarded as a creep-rupture process.

There is conflicting evidence for wooden elements subjected to a cyclic load resulting in failure. According to research from Karr et al., the element can fail due to fatigue with the fatigue life depending on the magnitude of the cyclic load. This relation is approximately exponential; a linear decrease in the cyclic load causes an exponential increase in the fatigue life. This relation for birch was obtained from experiments and is shown in Figure 15.3. The figure shows that at 50% relative stress amplitude, the fatigue life is approximately $2.5 \cdot 10^6$ cycles. Other factors that influence the fatigue life are the frequency of cycling, the type of loading, temperature, moisture content, element size and the range factor. On the other hand, the Civil Aviation Safety Authority of the Australian Government suggests that in general, upon proper maintenance and storage, wooden structures could last indefinitely [48]. The wooden structures in the designed aircraft will be assumed to have a fatigue life of longer than the operational period of the aircraft as per REQ-MAT-05.

Biological Degradation

Like other organic materials, wood is susceptible to degradation due to mould, fungi and insects [49]. Mould is generally of the least concern, as mould does not affect the cell walls but only the interior of the cell. Fungi, on the other hand, also metabolise cell walls, which are important to the strength of the wood. Fungi decay of wood could also be hard to detect from the outside. To prevent decay due to fungi and mould from starting or

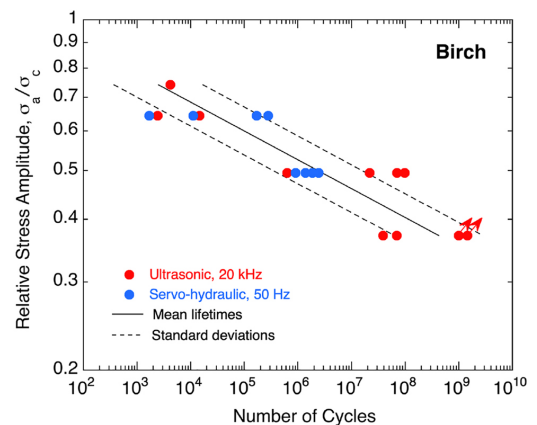


Figure 15.3: Fatigue life of Birch wood under cyclic load. [53]

progressing, the moisture content of the wood should be less than 20% [49]. Lastly, insects can also degrade lumber. Damage in wood that contains insects is dependent on the species of insect and the number of insects in the lumber. A common example would be termites which, although more common in tropical and subtropical regions of the world, present a threat to wooden structures on all continents on Earth³. Damage by biological degradation can be controlled by inspection of the wood element, and the risk of such damage can be proactively minimised through the use of protective chemicals which increase the wood's resistance to decay.

15.3.4. Wood Treatment

As was explained in the previous subsection, there are many factors that influence the properties of wood as a structural material, ranging from moisture to biological degradation. Thus, in order for wood to retain its material properties, it has to be treated prior to use in an aircraft structure.

One of the more effective treatments is to coat the structural wood with a protective coating [47]. Modern wood coatings are designed to practically eliminate the change of moisture levels in the wood as well as repel various biological factors such as fungi from entering the wood. Additionally, it was decided that the wood was to be treated with a flame-retardant which also offers the compliance with the previously set REQ-MAT-01 for wood treatment against fire according to EURO Class B. Further, it was decided that, in order to comply with REQ-MAT-02, all wood surfaces were to be coated with a thin layer of a conducting material.

15.4. Sustainability of Materials

Wood is often regarded as more sustainable compared to conventional aerospace materials such as Aluminium, Stainless Steel and Carbon-Fibre-Reinforced Polymer (CFRP) [54]. The main reasons for this are the low emissions during manufacturing and recycling, the ability to store CO₂ and wood being a renewable material.

One of the reasons why wood is sustainable is the low amount of energy needed to prepare raw wood into workable lumber [55]. Despite the travel distance between forest and sawmill being large in some cases, this process is still more environmentally friendly than the production of other aerospace materials at 0.55 kilograms of CO₂ per kilogram of wood [54]. In comparison, the carbon embodied in CFRP is 24.0 kg carbon per kg material⁴, aluminium embodies 16.1 kg carbon⁵ and lastly the production of stainless steel was estimated to cost 6.15 kg CO₂ per kg material⁶.

Additionally, trees sequester carbon inside the wood during growth by absorbing carbon dioxide from the atmosphere. The exact amount of carbon stored in the wood per kilogram depends on the species. On average, the carbon sequestration is 1.72 kg CO₂ per kg of dry wood⁷. This value can be deducted from the carbon footprint of the production of lumber if the lumber is not combusted at end-of-life, resulting in a negative carbon footprint of -1.17 kilogram CO₂ per kilogram wood.

Another advantage of wood as a building material is that wood is easy to down into new products. Recycling wood does not as much energy as other materials like metals because of remelting, however, this also comes with a disadvantage for recycling: wooden elements cannot be reformed into other elements of the same size and small defects such as drilling holes cannot be removed. Previous wood treatment also hinders the recycling process. Thus, the new wooden products have a lower recycling potential than the original material and the wood can only be downcycled. However, the carbon emissions of the recycling process for wood are still only a fraction of that of other materials. Recycled wood has a carbon footprint of 0.03 kgCO₂/kg⁸, whereas recycled steel embodies 0.88 kgCO₂/kg⁹, the carbon footprint of recycled aluminium is 0.5 kgCO₂/kg¹⁰ and lastly recycled CFRP has a carbon footprint of 11.73 kgCO₂/kg [56] when using the high-voltage fragmentation process (HVF). The carbon cost of this recycling process is substantially higher than the other aerospace materials because it enables the extraction of long carbon fibres. When the fibres are allowed to break into smaller pieces during recycling, other recycling techniques can be used and the carbon cost is considerably lower.

Because trees can be grown to create new wood, wood is a renewable building material. This means that no finite resource on earth is used up to create wood, which is the case for steel, aluminium and CFRP.

³<https://www.wolman.de/en/infocenter-wood/about-wood-pests/termites> [cited 15.06.2024]

⁴<https://dexmat.com/blog/carbon-fiber-alternative/> [cited 15.06.2024]

⁵<https://european-aluminium.eu/projets/a-low-carbon-footprint/> [cited 15.06.2024]

⁶<https://8billiontrees.com/carbon-offsets-credits/carbon-footprint-of-steel/> [cited 15.06.2024]

⁷<https://www.ecocostsvalue.com/lca/wood-lca-issues/> [cited 15.06.2024]

⁸<https://communitywoodrecycling.org.uk/our-measures/> [cited 15.06.2024]

⁹<https://8billiontrees.com/carbon-offsets-credits/carbon-footprint-of-steel/> [cited 15.06.2024]

¹⁰https://european-aluminium.eu/wp-content/uploads/2022/08/2020-05-13_european-aluminium_circular-aluminium-action-plan_executive-summary.pdf [cited 15.06.2024]

15.5. Engineering Lumber

Engineering lumber is a specifically modified wood material that has improved material properties compared to raw wood. The glueing of thin wood sheets in different grain directions also has the added benefit of being able to achieve a quasi-isotropic material, which is not true for wood in its natural form.

Laminated Wood Laminated wood construction involves assembling two or more wood layers, glued with their grains in parallel. These laminates can be made from either lumber or veneer. A well-laminated wood member matches the strength of a solid wood member of the same size. Factors like grain slope, density, and defects impact both laminated and solid wood similarly. However, lamination accommodates the use of thinner, clearer pieces of wood which can be inspected easier such that stronger wood sheets can be identified prior to assembling the layers. The potential for stronger members is therefore higher, especially in larger sizes [57].

Plywood Similarly to laminated wood, plywood is a composite wood product made from layers of thin veneers glued together. However, conventionally, the grain of each layer is oriented at a 90° angle to the adjacent layers. The outer layers are called "faces" while the inner layers are the "core" layers. Dimensional changes with differences in moisture are comparable to solid wood [57].

For the structural design, a variation of plywood was chosen in the design process. This was done to reduce the directional dependencies of the material properties of raw wood, resulting in a quasi-isotropic wood material. In order to estimate the final properties of the designed plywood, the fibre volume fraction method was used to estimate the properties of the laminate material. It was found that the optimal balance between longitudinal and transverse strength in the structure was achieved for a fibre volume fraction of 0.667 in the longitudinal direction. This result was obtained by comparing the properties of various plywood variations with different amounts of layers and fibre orientations. The strength of this laminate was evaluated to be 44.06 MPa in the longitudinal direction and 20.24 MPa in the transverse (shear) direction when using Sitka spruce wood in all layers. For Douglas fir, the same properties are 50.1 MPa and 20.7 MPa for the same failure stresses respectively. The number of layers in the ply laminate was not specified before the structural analysis since the thickness of the final plywood is a function of the loading condition in the aircraft. The number of plies will therefore be determined later as thicker material would require more plies in order to retain the material strength¹¹. In this analysis, only odd numbers of plies were considered since plywood with odd numbers of plies is less prone to warping and deformations¹¹.

15.6. Comparison of Wood With Other Aerospace Materials

In modern aerospace applications, the most common high-performance materials are various aluminium and steel alloys as well as fibre-reinforced composites. These materials have established themselves as reliable options in all parts of modern aircraft structural applications.

In terms of aluminium alloys, the more commonly used ones in aerospace are the 2xxx and 7xxx series¹². In terms of this project, the alloys of AL2024 and AL7075 are investigated in more depth. AL2024 was chosen since it is the most commonly used Al alloy in aerospace applications and is well-known for its fatigue resistance and high yield strength¹². The second alloy, AL7075, was chosen for its high strength and more specifically the high strength-to-weight ratio¹².

With the ever-growing interest in the aircraft industry towards fibre-reinforced polymer composites the designed eVTOL aircraft will also consider FRPs as a potential material. More specifically, the use of carbon fibre reinforced composites are considered for the structural elements of the aircraft. The main opportunity of using CFRPs is the potential for weight saving for structures that have mainly unidirectional loading. Although such composite materials have extremely high specific strengths, they are less than ideal in terms of greenhouse gas emissions. Moreover, CFRPs performs the worst in end-of-life treatment compared to the other mentioned materials^{13 14 15}. With sustainability being an important aspect of the design, CFRPs will only be considered as a last option in case the performance of the previously mentioned material options is evaluated to be insufficient.

Moreover, during discussions with the TU Delft Aerospace Materials and Structures department staff Julie Teuwen and Jos Sinke, it became apparent that wood will be a difficult material to join with other types of considered materials, especially thermoplastic polymers. In order to ease the manufacturing process as much as possible, metal alloys should be further preferred over composites due to the possibility of mechanical

¹¹<https://www.plywood.cc/no-of-plies-thickness-of-commercial-plywood/> [cited 26.06.2024]

¹²<https://www.thyssenkrupp-materials.co.uk/aerospace-grade-aluminum> [cited 15.06.2024]

¹³<https://european-aluminium.eu/projets/a-low-carbon-footprint/> [cited 15.06.2024]

¹⁴<https://dexmat.com/blog/carbon-fiber-alternative/> [cited 15.06.2024]

¹⁵<https://www.ecocostsvalue.com/lca/wood-lca-issues/> [cited 15.06.2024]

fastening.

15.7. Resulting Materials for Use in the HAROLD

As a result of the material analysis, the materials used in the production of the HAROLD were chosen. Since investigating the feasibility of using wood in modern aerospace applications is one of the aims of this project, wood is a material that will certainly be in the HAROLD's structure. The analysis yielded two potential candidates for the structural lumber. These were **Sitka spruce** and **Douglas fir**, as mentioned previously in this chapter due to their strength and (relative) availability as well as their use in historical wooden aircraft and the subsequent research that has been performed on them in this field of application.

As for the non-wood materials that make up the more critically loaded part of the aircraft structure, the main structural material is chosen to be **AL2024-T3**. This aluminium was preferred to AL7075-T6 despite its slightly inferior performance in yield strength (290 vs 460MPa respectively). However, according to the Granta material library in Ansys, the price of AL2024-T3 is much lower than for the latter option with the price ranges given as 3-4€/kg and 5.5-7.5€/kg for each material respectively [58]. As mentioned in this chapter previously, the CFRP option has opted to be kept as a reserve solution in case higher yield strengths are needed within the final resulting structure to prioritise design for higher sustainability in the aircraft using the other materials as described in Section 15.4.

Additionally, the minimum practical thicknesses of the materials have to be found in order for them to resist small impacts and handling without failure of the material. For wood plywood panels, this value was found to be 1.6mm according to the Wood Handbook [47][p.202]. For aluminium alloys, this value of minimum thickness is 0.4mm¹⁶.

15.8. Material Properties of the Selected Materials

The material properties of the materials considered in this chapter are given in Table 15.3.

Table 15.3: Material properties of the mentioned materials.

Material	Young's modulus (GPa)	Yield strength (MPa)	Shear strength (MPa)	density (kg/m ³)
Sitka spruce (l)	9.51	41.5	8.7	448.5
Sitka spruce (t)	0.930	1.3	26.0	448.5
Douglas fir (l)	10.2	42.8	9.1	528.6
Douglas fir (t)	0.95	1.44	26.5	528.6
AL2024-T3	73.1	290.0	264.0	2750
AL7075-T6	69.0	460.0	318.0	2830
CFRP (QI layup)	44.2	600	-	1610

The material properties of the wood materials are given for both the longitudinal and transverse grain directions since they vary by large margins. the CFRP properties are shown for a quasi-isotropic layup with the material fibre fraction amounting to 65% and the properties specified in the Granta library [58].

As for the designed plywood described in Section 15.5, the resulting material properties of both of the considered wood species are provided in Table 15.4. All of the provided values are the results of 0.667 fibre fraction in the longitudinal direction. The values used to calculate these

Wood species	Rupture strength (failure in bending) [MPa]	Shear strength [MPa]	Yield strength [MPa]
Sitka spruce plywood (l)	44.06	14.47	28.1
Sitka spruce plywood (t)	23.26	20.24	14.7
Douglas fir plywood (l)	50.10	14.83	29.01
Douglas fir plywood (t)	26.67	20.7	15.22

Table 15.4: Material parameters of the plywood

It can be seen that the Douglas fir plywood does have higher failure stresses. However, the specific strength ratio of the Sitka spruce is higher than for Douglas fir due to its lower density as seen in Table 15.3. As a result, the Sitka spruce was chosen as the preferred wood option going into the next step of structural analysis.

¹⁶<https://www.keytometals.com/Article95.htm> [cited 19.06.2024]

Chapter 16 | Structural Analysis & Design

In this chapter, the aircraft structure is detailed. First of all, the requirements for the aircraft structure and the assumptions used when analysing it are detailed in Section 16.1 and Section 16.2.1, respectively. For this analysis, a preliminary wing and fuselage structure was first designed, analysed and optimised in Section 16.2 so as to get an initial understanding of the structural loads acting on the aircraft. This information was then used to design and analyse a detailed wing and fuselage structure in Section 16.3, from which the final structural masses and dimensions were calculated. The landing gear was also designed and analysed; this can be found in Section 16.6.

16.1. Structures Subsystem Requirements and Compliance Matrix

In order to guide the design of the aircraft structure, the associated requirements need to be considered throughout the process. The subsystem requirements related to the aircraft structure can be found in the compliance matrix displayed in Table 16.1, along with a check to see whether the requirement has been complied with and where this compliance is demonstrated.

Table 16.1: Structures subsystem requirements compliance matrix.

Identifier	Requirement	Source(s)	Compliance	Method of verification
REQ-STR-01	As per the CS 25.303 regulations, a safety factor of 1.5 shall be applied to the prescribed limit loads which are considered external loads on the structure.	REQ-SYS-AC-39, REQ-SYS-AC-89, R-TEC-10	✓	Verified in the system tests of all systems
REQ-STR-02	All structural parts need to be inspectable using non-destructive methods.	REQ-SYS-AC-70, REQ-SYS-AC-84, R-TEC-05, RAMS-05	✗	Visual inspection at a later stage of the design
REQ-STR-03	All structural parts need to be maintainable using non-destructive methods.	REQ-SYS-AC-70, REQ-SYS-AC-84, R-TEC-05, RAMS-05	✗	Visual inspection at a later stage of the design
REQ-STR-04	The aircraft structure shall make up no more than 30% of the aircraft operating empty weight.	REQ-SYS-AC-03	✓	Analysis throughout the design process, as well as inspection by weighing when the aircraft is ready
REQ-STR-05	The structure shall not buckle when the aircraft is loaded at maximum take-off weight.	REQ-SYS-AC-97, R-TEC-04	✓	Analysis of the structure as given in this chapter
REQ-STR-06	The structure shall not yield when the aircraft is loaded at maximum take-off weight.	REQ-SYS-AC-97, R-TEC-03, R-TEC-04	✓	Analysis of the structure as given in this chapter
REQ-STR-07	The structure shall not fracture when the aircraft is loaded at maximum take-off weight.	REQ-SYS-AC-97, R-TEC-03, R-TEC-04	✓	Analysis of the structure as given in this chapter
REQ-STR-08	The structure shall not experience vibrations at its natural frequency.	REQ-SYS-AC-97, R-TEC-03, R-TEC-04	✓	Analysis by FEM in Section 16.4.
REQ-STR-09	At the end of its life, at least 20% of the aircraft structure shall be repurposed.	REQ-SYS-AC-76	✗	Analysis at a later stage of the design
REQ-STR-10	The manufacturing cost for the aircraft structure shall be less than 150,000 euros per vehicle.	Changed to REQ-STR-18	-	-
REQ-STR-11	The structure shall have an operational ambient air temperature range of -20 °C to 47 °C.	REQ-SYS-AC-31	✗	Testing at the prototyping phase
REQ-STR-12	The production process of the structure shall comply with AS 9100.	REQ-SYS-AC-89, R-TEC-2	✗	Compliance checked by inspection in the future
REQ-STR-13	The structure shall withstand all forces within the flight envelope and gust loads.	Changed into REQ-SYS-AC-97	-	-
REQ-STR-14	The aircraft shall have a max. positive load factor of no less than 2.0 and a negative load factor of no less than -0.5.	REQ-SYS-AC-86	✓	Analysis, taken into account throughout the design process
REQ-STR-15	Each part of the aircraft shall be free from excessive vibration throughout the limited flight envelope.	REQ-SYS-AC-86	✓	Analysis by FEM in Section 16.4.
REQ-STR-16	Fatigue behaviour of structural components shall comply with EASA MOC VTOL.2240 (a) and (b)	REQ-SYS-AC-86	✗	Testing at the prototyping stage.
REQ-STR-17	At least 25% of the structural weight of the aircraft shall consist of wood	REQ-SYS-AC-74	✓	Total percent of wood in the structural weight demonstrated in Table 16.11.
REQ-STR-18	The manufacturing cost for the aircraft structure shall be less than 300,000 euros per vehicle.	REQ-SYS-AC-95	✗	Analysis by financial analysis in the future

As can be seen in Table 16.1, REQ-STR-10 was removed and replaced with REQ-STR-18. This was done so as to keep the proportion of the aircraft structure manufacturing cost with the total manufacturing cost of the aircraft the same. Previously, the total manufacturing cost of the aircraft was 1,000,000 EUR (as per REQ-SYS-AC-79). However it was then doubled, reaching 2,000,000 EUR (as per REQ-SYS-AC-94). As such, the total cost of the manufacturing of the aircraft structure was thus also doubled.

16.2. Preliminary Structure

When designing the aircraft structure, tools can be built to analyse the structure and determine whether it is able to withstand the applied loads. Performing this analysis on the actual aircraft structure would be extremely time consuming and complicated, as such it is easier to use a simplified model of the structure in these calculations. To begin the analysis, a model which models the aircraft components as simple beams was built. The assumptions, method and results of this analysis are detailed in the subsequent subsections.

16.2.1. Assumptions

Before detailing the structural analysis, it is important to determine which assumptions will be used throughout the analysis, along with the expected effect that these will have on the analysis. This information can be found in Table 16.2.

Table 16.2: Assumptions used for the preliminary structural analysis.

Identifier	Assumption	Expected Effect
A-PS-01	The fuselage, wings and vertical tail are thin-walled.	The thin-walled assumption is used when $\frac{\text{width}}{\text{thickness}} > 10$ and $\frac{\text{height}}{\text{thickness}} > 10$, and it affects the calculation of the stress due to shear and torsion (as it assumes the shear flow is uniform throughout the beam cross-section) [59].
A-PS-02	The fuselage shape is assumed to be a cylindrical beam.	This assumption neglects the variation in fuselage diameter throughout the length of the fuselage. On the one hand, the beam does not take into account the reduction in the second moment of inertia of the fuselage in the sections with a smaller width; a smaller moment of inertia results in higher stresses, thus the predicted stresses at the front and back of the fuselage will be smaller than reality. On the other hand, the preliminary model will have a skin thickness that is higher than reality because the skin thickness was manually increased to artificially account for the airframe that should be inside the fuselage. If this increase was sufficient, the preliminary fuselage weight should correspond to reality. If it was not sufficient, it will be lighter than reality.
A-PS-03	The wing is assumed to be a rectangular beam.	This assumption neglects the change in beam width and height throughout the span of the wing. As per A-PS-11, the stress used for sizing corresponds to the maximal stress in the beam. With wings, the maximum loading is always found at the wing root since that is the connection point of the wing with the fuselage through which all of the wing loads are transmitted. In the case of the preliminary structure, the wing box is narrower at the root than in reality due to the fact that its dimensions do not vary. The smaller the cross section, the smaller the moment of inertia, the larger the stresses and thus the larger the skin thickness and beam weight. As such, the maximum stress of the preliminary model (and thus the skin thickness and weight) will be higher than the real values, resulting in a conservative estimate.
A-PS-04	The vertical tail shape is assumed to be a rectangular beam.	This assumption results in the same implications as A-PS-03.
A-PS-05	Joint failure is not considered as it is assumed that the adhesives and mechanical fasteners used in the structure do not fail before the material does.	The joints will have to be designed in such a manner that they are reinforced in cases where they risk failing before the material does. This will result in slightly heavier joints.
A-PS-06	Joints are assumed to be mass-less.	The total mass of the structure will be slightly lower due to these not being included in the mass calculation.
A-PS-07	The width of the beam modelling the aft wing, front wing and vertical tail wingbox is taken to be $0.5 \cdot c_{MAC}$, where c_{MAC} is the mean aerodynamic chord length of the modelled beam.	This assumption results in the wing size and thus the inertia being underestimated at the root of the wing and overestimated at the tip of the wing. Since higher inertia results in lower stresses, this assumption implies higher stresses than reality at the root and lower stresses than reality at the tip. Given that the bending moment is much higher at the wing root than at the tip, this assumption results in a conservative estimation of the critical stresses in the wing.
A-PS-08	The wing box height of the aft wing, front wing and vertical tail is taken to be the average thickness of the MAC of the part's airfoil.	The effect of this assumption is two-fold; it has implications for the stresses along the length and along the width of the wing. For the length, the effect follows that of A-PS-07. For the width, instead, it is necessary to compare the height of the wing box with the actual thickness of the airfoil. In the cases where the real thickness is larger than the wing box height, the model's stresses are overestimated (and as such are conservative). The opposite is true for when the real thickness is smaller than the wing box height. Almost all loads act in the front half of the wings (lift, thrust and engine weight when applicable), and for both the empennage airfoil (the NACA0012) and the wings airfoil (the LA203A), the front half of the airfoil has a thickness greater than average for more than 70% of the length for both cases. As such, it can be assumed that this assumption results in a conservative stress and subsequent weight calculation.
A-PS-09	The aircraft is instantaneously flying at cruise speed in horizontal flight or with $\frac{T}{W} = 1.3$ in VTOL flight.	With this assumption, the accelerations throughout the motion are neglected, as only two flying conditions are considered. This means that not the full range of loading cases present on the aircraft shall be analysed.
A-PS-10	The wooden beams (aft wing, front wing and vertical tail) are assumed to rupture before starting to cripple.	Even though buckling, and by extension crippling, are failure cases that do affect wooden beams, the wooden beams are assumed to be multiple centimetres thick and as such they should cripple at stresses higher than the rupture stress.
A-PS-11	The maximal stress acting in the beam is used to size each beam.	By applying this assumption, the stresses in the majority of the beam are overestimated. The higher the stress, the greater the required skin thickness and thus the heavier the beam. As such, this assumption results in a conservative estimation of the beam masses.
A-PS-12	The winglets are not taken into account when analysing the wings.	By neglecting the winglets, the front wing and aft wing beams are going to be slightly lighter than in reality. However, winglets reduce the drag acting on the wing (as explained in Section 10.3.3) resulting in an overall lower drag distribution over the wings.
A-PS-13	The loads acting on the aircraft wings are assumed to be symmetric, as such only one wing has to be modelled since it is assumed that the stresses, skin thickness and subsequent weight of the two wing halves are identical.	This assumption neglects cases in the flight profile where the right and left wings carry different loads (e.g. during turns or in cases of side wind). As such, there is the possibility that in some cases the loading on the wings will be higher than expected.

16.2.2. Method

In order to perform a well-rounded analysis of the aircraft structure, three failure modes were considered: failure due to an excess of normal stress (due to normal and bending loads), failure due to an excess of shear stress (due to shear and torsional loads), and failure due to crippling. The method and equations used for this analysis follow from Hibbler's book *Mechanics of Materials* [59] and from Megson's book *Aircraft Structures for Engineering Students* [60], however for clarity it is also summarised below.

First of all, the dimensions of each beam were specified. As per A-PS-07 and A-PS-08, the width and height of the wing boxes came from the preliminary estimates of the aircraft airfoil dimensions discussed in Chapter 10. For the fuselage, instead, the diameter is based off of the calculated value in Chapter 8. For convenience, these values are summarised again in Table 16.3.

Table 16.3: Dimensions of the beams modelling the aircraft in the preliminary structure.

Parameter	Aft wing	Front wing	Vertical tail	Fuselage	Unit
Beam width	0.598	0.598	0.451	1.75	[m]
Beam height	0.156	0.156	0.091	1.75	[m]
Beam length	5.330	5.405	1.526	8.725	[m]

For this analysis, the aircraft structure is analysed as four distinct beams: a thin-walled cylindrical beam for the fuselage, and a thin-walled rectangular beam with ribs and stringers for the vertical tail, right aft wing and right front wing respectively. A sketch of this layout can be found in Figure 16.1, along with the coordinate system used for each one of the beams (green for the wings, red for the fuselage and blue for the vertical tail); note that the drawing is not to scale. As explained by A-PS-13, the wings are assumed to have identical loading and thus results; as such, throughout the analysis only the right wings (from the pilot point of view) are modelled. Each beam is analysed one at a time. Since the wings and vertical tail are fixed to the fuselage, the resultant loads of the full aft wing, full front wing and the vertical tail are passed on to the fuselage and thus accounted for when analysing the fuselage structure.

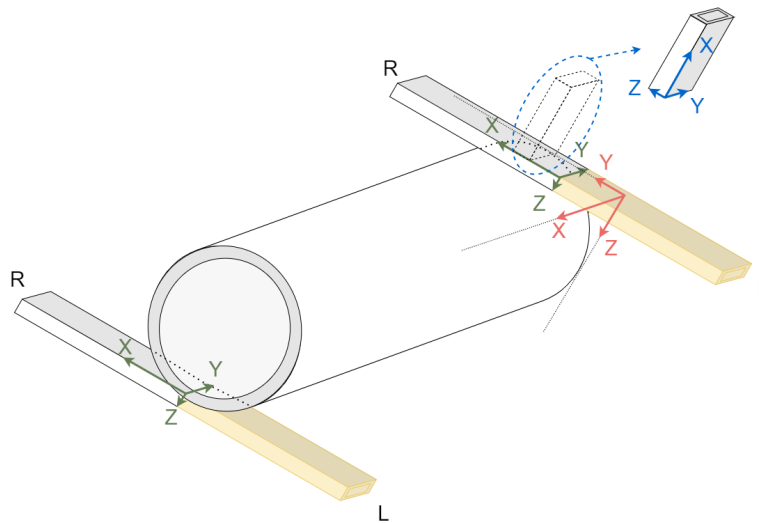


Figure 16.1: Preliminary structure layout

In order to maximise safety, a safety factor of 1.5 is applied to all of the loads. This ensures that, in case of unexpected situations loads or emergency situations, the aircraft structure will not fail and will keep the passengers safe. For horizontal flight, an additional load factor of 2 was then taken into account on top of the safety factor as per EASA regulations¹; this was done so as to account for the extreme loading cases of the flight envelope. This was not accounted for during VTOL flight because the aircraft engines do not have the capacity to accelerate the aircraft to such high accelerations. Overall, this resulted in the loads being multiplied by a factor of 3 for the structural analysis of the aircraft during horizontal flight and by a factor of 1.5 during vertical flight. In addition, in order to account for the effect of temperature changes on the material properties (as per REQ-STR-11), the maximum stress that the material is able to sustain is multiplied by 0.85 [49].

Next, the loads on the aircraft were analysed. A 3D figure with the loads acting along the fuselage, right aft

¹URL: https://www.easa.europa.eu/sites/default/files/dfu/proposed_moc_sc_vtol_issue_1.pdf [accessed: 19/06/2024]

wing and right front wing was generated so as to better visualise the loading of the structure. The loading case for vertical take-off is shown in Figure 16.2, while the loading case for horizontal cruise flight with maximum rudder deflection is shown in Figure 16.3. The name of the load is shown on the figure, where L corresponds to lift, T to thrust, D to drag and W to weight. Note that the load vectors are not to scale, and the locations of the loads are approximate. The axes for each beam are included in grey. Since the wings are separated from the fuselage in the model, the reaction forces are included in the modelling.

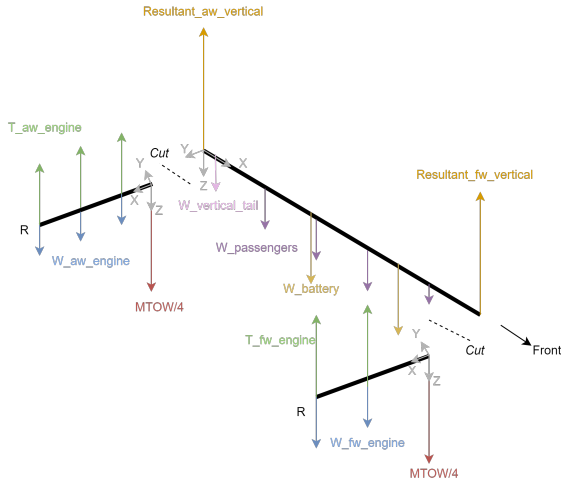


Figure 16.2: Loads during vertical take-off

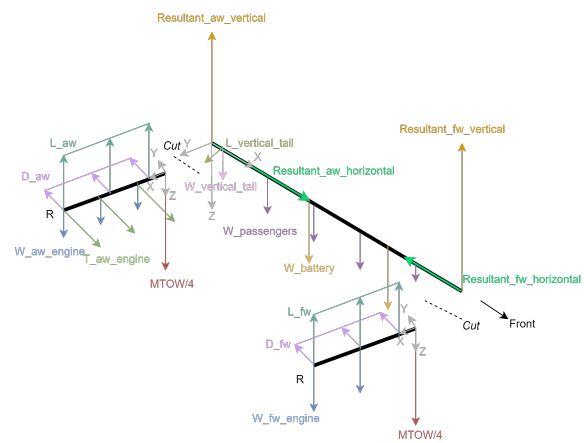


Figure 16.3: Loads during horizontal cruise flight with maximum rudder deflection

From the loads acting on each beam, the torsion of each beam could be calculated. Torsion is generated whenever a load does not act along the centre-line of the beam. For the wings, torsion was generated due to the engine weight, engine thrust and lift distribution. For the vertical tail, torque was only generated by the distributed lift. Finally, for the fuselage torque was generated by the passengers, the batteries and the landing gear.

In addition, the normal force, shear force and bending moment diagrams were also drawn and calculated. As an example, the diagrams for the aft wing during horizontal flight and vertical flight are shown in Figure 16.4. Due to the lack of loads in the X direction along the aft wing, there are only loads in the Y and Z direction. Note that the bending moment due to the loads in the Y direction acts around the Z axis, and the bending moment due to the loads in the Z direction acts around the Y axis.

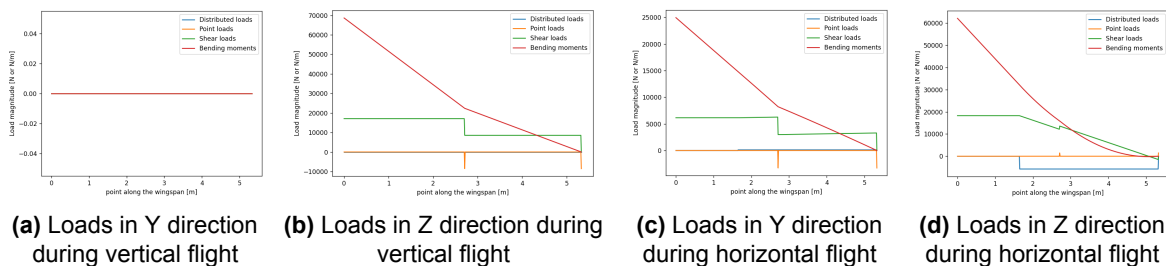


Figure 16.4: Aft wing shear and moment diagrams during horizontal and vertical take-off flight

With all of the loads found, the shear and normal stress of the beam were calculated, where the normal stress is due to the bending moment and the normal force, while the shear stress is due to the shear force and the torsion. In addition, the deflection of the beam was also calculated. In order to analyse the third and final failure mode (crippling), the critical load at which the beam will cripple had to be calculated. As explained by A-PS-10, crippling is not considered as a failure mode for wooden beams. For aluminium beams, instead, a semi-empirical method defined by Megson that uses aluminium’s properties is used [60].

The final step was to compare the stresses and critical buckling of the beam with the limits of the material to verify if the structure is able to safely withstand them. In order to minimise the aircraft weight, an iteration was performed. For the wings and vertical tail, the number of ribs, the number of stringers and the thickness of the beam were varied, whilst for the fuselage only the thickness was varied. Note that the stringers and ribs are made out of the same material as the rest of the beam. In addition, the material of the beams was iterated.

As explained in Section 15.7, two main materials are being considered for the aircraft: AL-2024-T3 and Sitka Spruce. As such, for each of the beams the calculations will be run using both of the materials so as to find which material is the best fit for each part of the aircraft. This iteration was repeated until the lowest mass at which the stresses and crippling could still be supported was found.

16.2.3. Results

When performing the method explained in Section 16.2.2, two considerations were driving the iteration: the need to minimise the aircraft structural weight, and the need to maximise the amount of wood used in the aircraft. It was found that making the whole aircraft structure out of wood would make the aircraft much too heavy, however having the fuselage made out of aluminium along with the wings and vertical tail made out of wood was the best option to maximise the amount of wood in the structure while keeping it at a reasonable weight.

The thickness, number of ribs and number of stringers which the iteration converged to for each of the four beams can be found in Table 16.4. These values were calculated for both horizontal and vertical flight, and the most critical ones were kept. The flight condition associated with these more critical values is also indicated per beam in Table 16.4. The mass, deflections and stresses, instead, can be found in Table 16.11, where they can be more easily compared with the results from the detailed design and the FEM analysis.

Table 16.4: Values of the preliminary structural sizing parameters.

Parameter	Aft wing	Front wing	Vertical tail	Fuselage	Unit
Beam thickness	32.4	30.3	61.7	1.5	mm
Number of ribs	8	9	3	NA	[-]
Number of stringers	28	28	22	NA	[-]
Most critical flight condition	Vertical	Horizontal	Horizontal	Vertical	[-]

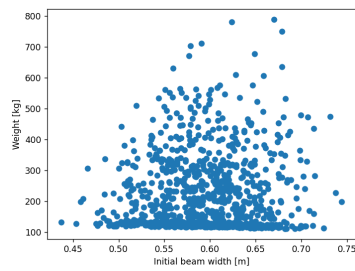
Note that in the case of the fuselage, even thicknesses as low as the minimum thickness for manufacturing (equal to 0.4 mm as per Section 15.7) could still support the loads applied to the fuselage without the structure failing. However, in reality such a thin skin is not practical as it would not be stiff enough to carry passengers and payload. Normally, this is resolved by adding an airframe inside the fuselage, however at this stage of the design this was deemed to be too complex. Instead, the thickness was manually increased to 1.5 mm such that the fuselage total mass was about 200 kg, a value that was considered reasonable for a fuselage of such dimensions.

As discussed in Section 16.5, the preliminary model was used for the aircraft-wide iteration detailed in Chapter 17. Since in the iteration the structure is not the only subsystem being optimised, the final sizing of the aircraft structure resulting from the optimisation will most certainly be slightly different to the values found in Table 16.4 and Table 16.11; the final result that the iteration converges to can be found in Table 17.3.

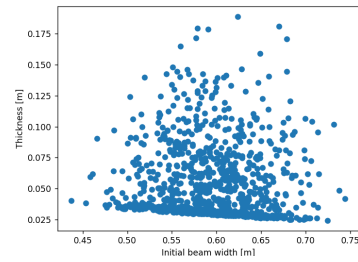
16.2.4. Sensitivity Analysis

In order to check that the results of the preliminary structure analysis are correct, it is important to perform a sensitivity analysis; this allows the confidence in the method to be measured. In this case, the sensitivity of the method against the geometric inputs it is initialised with was measured, as it is required that the analysis works for all kinds of inputs, not just the ones specific to the HAROLD. The main inputs in question are the width of the beam (in the case of the wings and vertical tail this corresponds to the wing box width, and in the case of the fuselage this corresponds to its diameter) and the initial beam skin thickness. Monte Carlo analysis was used so as to measure the impact that these two inputs have on the beam's structural weight and final skin thickness.

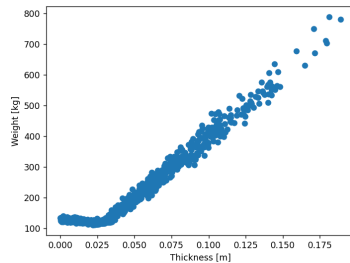
So as to run the analysis, a range of width and skin thickness variables had to be generated. These were generated using a normal distribution that is centred around the widths specified in Table 16.3 and the thicknesses specified in Table 16.11, and in both cases with a standard deviation of 0.05 m. Then, the preliminary analysis was run, resulting in a beam mass and new skin thickness for each point in the normally distributed list of width and initial thickness values. These results were compiled into scatter plots for easier visualisation; a very similar result was found for all four beam types, as such only the aft wing's scatter plots are provided as an example in Figure 16.5.



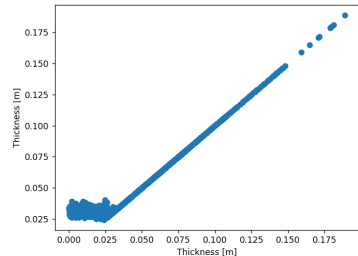
(a) Distribution of resulting beam weights from beam widths.



(b) Distribution of resulting skin thicknesses from beam widths.



(c) Distribution of resulting beam weights from skin thicknesses.



(d) Distribution of resulting skin thicknesses from skin thicknesses.

Figure 16.5: Monte Carlo analysis of relationship between a varying skin thickness and beam width and the resulting beam weight and skin thickness.

In order to fully understand these results, it is important to first understand how the calculations for the structural analysis were performed. A tool was built in Python to automate this process, and the tool required as inputs the loads acting on the beam and the geometry of the beam. After calculating the stresses in the beam due to the loads, if the failure stress of the material is below the stress level the structure is experiencing, the geometry is adapted to increase the failure stress. In the case of wing boxes (so for the front wing, aft wing and vertical tail), first of all S-stringers (with a width of 20 mm, a height of 40 mm and a thickness of 2 mm) were iteratively added to the wingbox to see if the failure stress can be increased to above the current stresses. If by the time the number of stringers has reached its maximum (determined by how many stringers can fit inside the wingbox), then the skin thickness is progressively increased until the beam does not fail under the applied loads. For the fuselage, the skin thickness is increased directly since no stringers are being considered in the preliminary design. The final geometric values and material properties of the beam are then used to calculate its mass. As such, even though the skin thickness is an input, it is also an output.

Looking at the subfigures in Figure 16.5, it can be seen that the relationship between the initial skin thickness and the final weight and final skin thickness is much clearer than the relationship with the initial beam width. Knowing the logic of the model, the shape of Figure 16.5c and Figure 16.5d can now be explained; if the initial skin thickness is too low to sustain the loads, it will be increased until it reaches an optimal value which minimises the weight while sustaining all of the stresses in the beam. The exact optimal value will depend on the width of the beam (which is also varying), hence why the flat part of the line slightly varies. However, if the initial skin thickness is already large enough to sustain the loads, it will not be increased and as such the final skin thickness will remain the same, as can clearly be seen in Figure 16.5d. The weight will, once again, vary slightly due to the width, however it follows the same relation. As such, it appears that the code is robust in its use of the skin thickness.

Looking at Figure 16.5a and Figure 16.5b, instead, it is apparent that when the width of the beam is varied, the results are much less coherent. There is a clear line on the bottom of the figure along which a large amount of points congregate, however above that line the points are distributed in what resembles a normal distribution. This result makes sense when thinking about the set-up of the code. As was explained above, the width of the beam is not iterated throughout the code, while the skin thickness is. In the cases where the initial skin thickness was too low to support all of the loads, the thickness was increased until it reached the optimal value. This is shown by the thick bottom line in Figure 16.5a and Figure 16.5b; the larger the wing box, the smaller the required thickness (due to the increased moment of inertia). For the weight, it remains fairly constant at one value due to the inverse relationship between the beam width and the skin thickness.

The distribution of the remaining points is due to the way that the code was set up; if the initial skin thickness was high enough to sustain the stresses in the beam, it was kept constant. As such, sometimes for a given beam

width the thickness (and subsequently the weight) is higher than the optimal value. The normal distribution looking shape of the points is in turn due to the fact that the input values were generated using a normal distribution. Very high initial skin thicknesses are rare (hence why very high final masses and skin thicknesses rarely occur in the plots), and these are most likely to occur at the mean value of the distribution simply due to the number of occurrences of that value. As such, these two figures serve as a demonstration of that the initial values were, in fact, distributed normally.

In conclusion, the sensitivity analysis demonstrates that, for each beam width, there is an optimal skin thickness and subsequent beam weight. It also shows the main drawback of the code; in order to converge to the correct values, the initial skin thickness must not be too high. This issue can be avoided by always initialising the analysis with the absolute minimum thickness that the beam can have for it to be manufactured (specified in Section 15.7), and then letting the code iterate this value until the optimal value was reached. This is the approach that was used when generating the results of the preliminary structure analysis.

16.2.5. Verification and Validation

In order to verify and validate the preliminary structure, it is important to first check the validity of the assumptions used when constructing the model (tabulated in Table 16.2). The validation of each assumption is detailed in Table 16.5.

Table 16.5: Validation of the assumptions used for the preliminary structural model.

Identifier	Validation
A-PS-01	As can be seen in Table 16.3 and Table 16.4, the $\frac{\text{width}}{\text{thickness}} > 10$ criterion holds for all the beams except for the vertical tail, while the $\frac{\text{height}}{\text{thickness}} > 10$ criterion only holds for the fuselage. As such, this assumption has no effect on the stress due to shear and torsion of the fuselage, but it does have some effect on the stress due to shear and torsion of the wings and a larger effect on the stress. In practice, the thin-walled assumption is often used as it simplifies calculations, however it is in nature a conservative assumption. This is because it assumes that the moment of inertia I and the polar moment of inertia J are lower than reality, and these are inversely proportional to the stress due to shear and torsion. As such, if the thin-walled assumption does not hold, the real stress values in the beam are actually lower than the ones calculated here, effectively resulting in a more conservative value. With such preliminary beam shapes, this is a positive thing as a margin is always good to have to account for any mismatches between the real and calculated values.
A-PS-02	In order to validate this assumption, it is important to compare the results of the preliminary structure model with that of the detailed structure model. As can be seen in Table 16.11, the overall mass of the detailed structure is higher than that of the preliminary structure by 16% due to the inclusion of an air frame inside the fuselage. In addition, the maximum normal stress is much higher in the detailed structure than the preliminary one. This is due to the tapering of the fuselage and the high loads introduced at the ends of the fuselage due to the wings. As such, the expected effect of increased stresses was correct. However, due to the extremely high strength of aluminium, this higher stress barely affects the resulting thickness since the minimum thickness of 0.4 mm is still able to sustain all of the loads (in this case, there is no need to increase the skin thickness since there is an air frame). As such, this indicates that with this assumption, the fuselage skin thickness increase in the preliminary structure estimation to account for the fuselage air frame was a bit under-conservative.
A-PS-03	When comparing the results of the front wing and aft wing from the preliminary structure model and the detailed structure model, it can be seen that, as expected, the maximum stresses are lower in the detailed structure. This is due to the wing box being wider at the root of the wing in the detailed design. When looking at the mass of the models, it can be seen that the detailed models have a higher overall mass than the preliminary model. This is most likely due to the larger skin thickness of the detailed model. This increased thickness is due to the loads at the wing tip; for both wings, there is an engine placed at the wing tip that generates large loads due to its mass and thrust. With the detailed model, the wing tip is very small and thus has a very small moment of inertia compared to the preliminary model. As such, a higher skin thickness is required to sustain the stresses. Since a constant skin thickness is assumed, this skin thickness is carried over to the rest of the wing. As such, this assumption results in a slight under estimation of the wing parameters.
A-PS-04	The exact same reasoning and validation can be applied to this assumption as with A-PS-03; the maximum stress is much lower with the detailed model, however with this assumption the mass and thickness is higher than what is calculated with the preliminary model.
A-PS-05	In the aerospace industry, mechanical fasteners used in the structure are usually made of aluminium or steel due to their high strength. For example, looking at AL-2024-T3 (the material from which the fuselage is made), the Granta library indicates that its yield strength is 246.5 MPa and its shear strength is 224.4 MPa [58]. However, as can be seen in Table 16.11, the stresses carried by the aircraft never surpass 19 MPa. As such, no mechanical fastener should fail at these stresses. In some cases, a glue may be used to glue wooden components together. As explained in Section 21.3.5 the only glue accepted by the FAA is Resorcinol glue. In order to be certified by the FAA, the glue must always fail after the wood does. As such, this assumption should not affect the results.
A-PS-06	This assumption is difficult to verify at this stage because the joints were overlooked throughout the analysis and thus it is not possible to quantify the effect of this assumption. A margin for the weight was accounted for by increasing the fuselage skin thickness to 1.5 mm (and thus increasing the total mass); this can at least in part account for the additional mass from the joints. However, a more detailed analysis should be performed in a later stage of the design.
A-PS-07	Comparing the maximum stresses calculated with the preliminary structure and the detailed structure for the aft wing, front wing and empennage, it can be seen that the expected effect was correct. Looking at Table 16.11, the maximal stresses acting in the preliminary wings is higher than in the detailed wings. This results in a more conservative stress analysis, which (as explained above for A-PS-01) is a positive result for a preliminary sizing.
A-PS-08	The same verification method and results as for A-PS-07 are found for this assumption.
A-PS-09	Even though not the full range of loading cases is analysed, the two cases analysed are actually the most critical ones. When the aircraft is flying vertically with a thrust to weight ratio of 1.3, the thrust loads are highest and thus result in the largest stresses during vertical flight. When the aircraft is flying at maximum cruise speed with maximum rudder deflection, it is experiencing the largest possible thrust load, lift loads and drag loads, resulting in the largest stresses that occur during horizontal flight. As such, this assumption does not affect the outcome of the analysis.
A-PS-10	As was found in Table 16.3, the thickness of the wooden beams is at least 3 cm every time. As explained by the War Department of the United States of America, a thickness of 0.125 inch, which is equivalent to 0.3175 cm, is sufficient in most woods to avoid buckling (and by extension, crippling) [57]. As such, this assumption does not affect the results of the analysis.
A-PS-11	Looking at Table 16.11, it can be seen that the stresses in the preliminary structure are indeed overestimated when comparing them with the stresses of the detailed structure and with the FEM (where applicable). This means that the preliminary model is estimating the stresses in a conservative manner, which (as explained above for A-PS-01) is a positive result for a preliminary sizing.
A-PS-12	The effect of this assumption is difficult to fully quantify at this stage without a more detailed analysis. However, when looking at the analysis performed in Section 10.3.3, it was found that including the wingtips reduces the overall energy usage of the aircraft. As such, by not including them in this analysis, the result is most likely more conservative.
A-PS-13	Due to the nature of this analysis, only two flight modes were analysed: horizontal flight at maximum cruise speed and vertical flight at maximum thrust. In both cases, loading is considered to be asymmetric. As such, it is difficult to quantify the effect of asymmetric loading without further and more detailed analysis.

In addition to the validation mentioned above, the code for the preliminary analysis was verified through hand calculation of simple beam loading cases where point and distributed loads were combined. All of the tested cases resulted in similar results when comparing the manual calculations to the automated ones. Finally, the model itself is validated in Section 16.5.

16.3. Detailed Structure

In order to get a second estimate of the structural design and its performance in terms of stresses and masses, an idealised boom section method [60] was performed. This was applied to all the previously identified structural components of the forward wing, back wing, fuselage and empennage.

16.3.1. Assumptions

Here, the assumptions used in analysing the structure using an idealised boom section are given.

Table 16.6: Assumptions used for the detailed structural analysis.

Identifier	Assumption	Expected Effect
A-DS-01	For the fuselage, the cross-sectional area of the structure is distributed evenly into booms around the cross-section	The stresses in the top and bottom parts of the fuselage are higher since the inertia is not optimised to resist bending due to lifting forces.
A-DS-02	The skin panels making up the wing box sections have a uniform thickness between two consecutive observed cross-sections.	The mass of the wing is going to be lower than it would be for uniform panel thickness along the wing span.
A-DS-03	The wood materials are resistant to impact buckling at a thickness of more than 1.6mm	Increase in wing weight in sections where the required thickness for carrying shear flow is lower, resulting in higher total weight.
A-DS-04	The used metals are resistant to impact buckling at a thickness of more than 1.5mm	Same as for A-DS-03.
A-DS-05	The wing box of the forward and back wings follow the contour of the spars and the airfoil	The wing box shape becomes more complicated and now has inertias in the I_{xy} and I_{yx} directions.

All of the assumptions given here will be verified in Section 16.3.5.

16.3.2. Method

The detailed structural analysis is based on the simplification of idealised booms where the cross-sectional area is concentrated into booms around the cross-section. The cross-section profile was made to follow the airfoil or circular fuselage shape at the specified lengthwise location along the analysed beam. The strength of this model is a better estimation of the moment inertia along the analysed structures since the cross-sections can be modelled more accurately than was done in the preliminary analysis. On the other hand, the structure is still idealised and the initialised boom areas influence the magnitude of the stresses within the structure on which the stress analysis is conducted. Therefore, the structure is expected to be more sensitive to the initialised values.

For all beams, the boom areas were initialised with the dimensional values found in the primary structural estimations. For the fuselage, the total cross-sectional area was then distributed equally between all booms in the cross-section as per assumption A-DS-01. For the wing beams however, the total area was divided between the booms such that 3/4 of the total area was in the top and bottom sides of the beam and the remaining 1/4 in the sides as was provided in assumption A-DS-02. This was done to simulate the effect of stringers (in the top and bottom of the wing box) in the wing box and to reach a higher wing box stiffness against lifting loads that result in moments around the Y-axis (as shown in Figure 16.1).

Subsequently, all normal forces and shear flows were calculated in the booms and cross-sections respectively. In case the initialised boom area resulted in a stress that was over the failure stress of the material, the boom area was increased until the stress was below the critical value. This was done for all booms of each cross-section. The resulting shear forces were then compared to the failure strength of the appropriate materials in shear, which resulted in the required minimum thickness of the structure between each boom. As the forces applied to the structure in this analysis already had a safety factor of 1.5 applied to them, this minimum thickness did not have to be increased further to account for a safety margin. However, in order to account for the risk of the material buckling due to too thin thicknesses, a minimum thickness of the material was set for all considered materials.

For both of the wood materials, the Sitka spruce and the Douglas fir, a minimum thickness of 1.6 mm was set since that is referenced to be the minimum thickness to avoid buckling due to impact loads [47]. For metals, the minimum thickness was set to 1.5 mm as a guideline from sheet metal manufacturing point of view² In case the skin thickness was evaluated to be below the minimum thickness, the thickness was automatically set to be the specified minimum thickness of the material. However, this method resulted in cross-sections with many varying thicknesses. This would, however, lead to a structure that is very difficult to manufacture. In order to increase the manufacturability of the structural elements, the thicknesses were made to be uniform along each "side" of the cross-sections (top, left, bottom, and right sides) such that one cross-section had a maximum of four thicknesses. The thickness of each of these "sides" was chosen based on the most critical value (the thickest section across the observed "side").

Consequently, the effect of the added thicknesses was evaluated on the original boom section based on the idealised boom theory [60]. The stresses were then reevaluated using the updated boom areas and the final results in terms of stresses and the structural element mass were recorded. All relevant detailed structure sizing parameters are provided in Table 16.7.

² <https://geomiq.com/sheet-metal-design-guide/> [cited 17.06.2024]

16.3.3. Results

Table 16.7: Values of detailed structure sizing parameters and corresponding rationales.

Parameter	Value	Unit
t_{min} (metals)	1.5	m
t_{min} (woods)	1.6	m
Number of evaluated cross-sections	10	[-]
Wing box front spar location	0.25	m
Wing box aft spar location	0.75	m
wing box height at the root	0.21	m
wing box height at the tip	0.126	m
Loading cases	[Varying]	N
Safety factor	1.5	[-]
Material failure stresses	[dependent on the material]	MPa
radius of the fuselage	1.2	m
the initialisation of the structural thickness (metals)	0.002	m
the initialisation of the structural thickness (woods)	0.03	m

As the inputs were given for all possible load cases, not all of them are used in every beam analysis; examples of such values are the wing box dimensions or the fuselage radius. All of the different beams and their load cases are then analysed with the input values. Outputs of the detailed analysis are given in Table 16.8 for the example calculation of the front wing.

Table 16.8: Outputs of the detailed structural analysis of the front wing

maximum thickness of the structural element	0.0522	[m]
mass of the structural element	159.07	[kg]
maximum normal stress within the structure	14.65	[MPa]
maximum shear stress within the structure	7.5	[MPa]

It can be seen that all of the maximum stress values stay below the failure stresses of the appropriate materials as were given in the Chapter 15 for material analysis. The maximum stress value presented in Table 16.8 is the stress in the wing root where the implied bending moment is the highest of the wing. The values obtained in this analysis will be compared to the results of the preliminary analysis in Section 16.5.

16.3.4. Sensitivity Analysis

In order to know the confidence in this method of detailed analysis, a Monte Carlo simulation of the model was performed. The sensitivity analysis was performed in two phases. In the first phase, the variables of the function such as the number of booms, spar locations, number of analysed cross-sections, etc. were altered whereas in the second phase, the input parameters of the preliminary design phase were varied.

For the first sensitivity analysis phase: the number of booms in the cross-section was modelled by a discrete uniform distribution with the booms in the flanges and the webs of the cross-section varying independently. The flange booms' uniform distribution function spanned values from 4 to 20 while the number of booms in the spars ranged from 1 to 12. These variations were chosen due to the smaller size of the spars compared to the flanges and to take the effect of the stringers into account. Simultaneously, the front and back spar locations were changed according to a random normal distribution with the centres of the normal curve located at their initialised values of 0.25 and 0.75 (as a fraction of the chord) respectively; the standard deviation was set to 0.05 to get a wider spread of values. These values were then analysed for all critical load cases of all of the structural elements. In Figure 16.6, an example sensitivity analysis is shown for the front wing in a VTOL configuration.

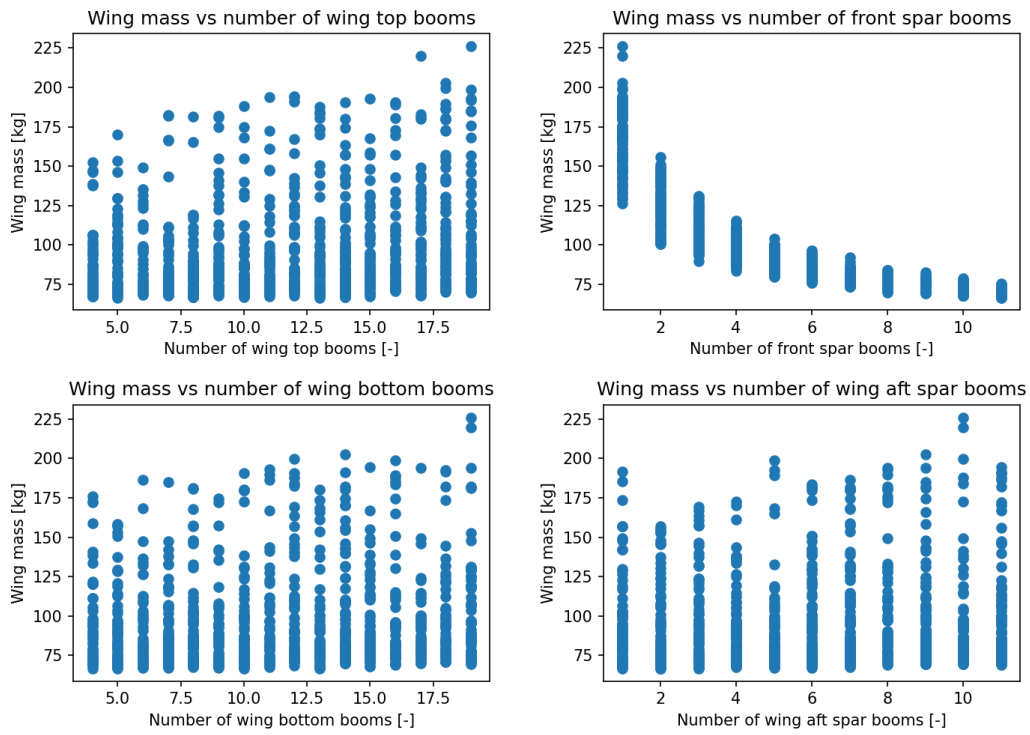


Figure 16.6: Sensitivity of the detailed structure analysis.

It was observed that the number of back spar or top and bottom flange booms did not affect the results of the mass calculation by a significant amount, if at all. The number of the front spar booms, however, had a non-negligible effect on the mass calculation. Increasing the number of front spar booms tended to result in lower masses and in a narrower range of mass values, meaning that the uncertainty of the function decreased.

Secondly, the effect of varying the inputs of the preliminary estimation in the form of the initial skin thickness and varying spar locations was investigated. For this purpose, the number of booms was set to 15 for the wing box flanges and to 6 for the wing box spars based on the previous analysis once again, a result of this analysis for the front wing is provided in Figure 16.7.

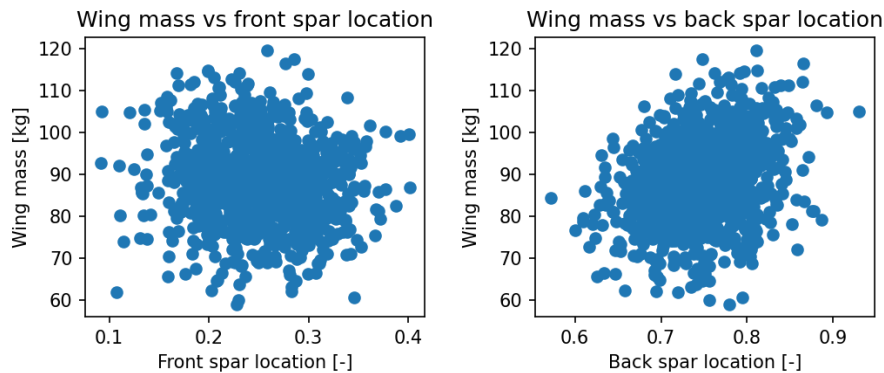


Figure 16.7: Detailed structural analysis sensitivity to the chosen parameters.

In Figure 16.7, the spar locations are given as a fraction of the chord. In this instance, it is seen that the variability in the results is high and the correlation between the obtained mass and spar locations has a considerable amount of noise. However, it can still be identified that moving the aft spar forward along the chord seems to result in a reduction of the wing's total mass whereas no such conclusion can be made for the front spar. This is a slightly surprising result since reducing the dimensions of the wing box seems to lead to a decrease in weight. However, this would mean an increase in stresses and thus an increase in the thickness between the booms which was previously anticipated to result in higher masses in the end.

Going further, the influence of the material area in the initialised cross-section and the initial wing-box thickness

as provided by the preliminary analysis are considered. Example analysis for the forward wing is displayed in Figure 16.8.

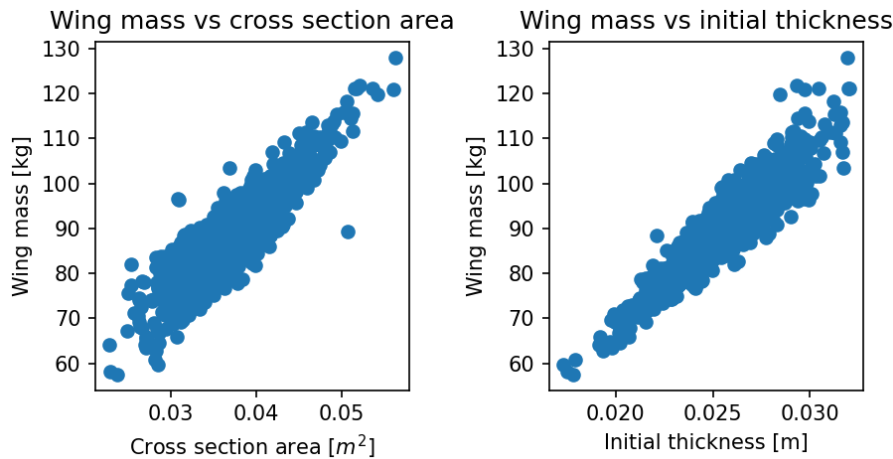


Figure 16.8: Detailed structural analysis sensitivity to the input parameters.

Firstly, it should be mentioned that the cross-section area referenced on the left is the area of the material in the cross-section and not the area that the cross-section encloses. A clear linear dependency between the wing mass and the initialised area is identified based on the performed analysis. Additionally, the initial thickness of the cross-section elements also influences the total mass by a linear relationship, albeit with a larger uncertainty in terms of the final mass result.

As the other beams and load cases not shown here presented similar relationships to the examples presented above, the code is deemed to be robust for its intended purpose.

16.3.5. Verification and Validation

In this section, the verification and validation process of the detailed structural code is performed. The assumptions and the model are verified by the end of this section.

Table 16.9: Validation of the assumptions used for the detailed structural model.

Identifier	Validation
A-DS-01	This is the basis of the idealised boom theory [60]
A-DS-02	The stresses in the wing are overestimated when compared to the option of having uniform thickness panels along the cross-section. However, the mass is underestimated when using this method.
A-DS-03	The thickness of some sections had to be increased to meet the minimum thickness requirement, increasing the structural mass. Assuming that the minimum thickness is sufficient for impact buckling as per the assumption will have to be verified at a later stage through material testing, however.
A-DS-04	Same as for A-DS-03
A-DS-05	The wing shape results in low values of I_{xy} and I_{yx} , when compared to I_{xx} and I_{yy} , resulting in a negligible effect on the structural analysis

To verify the detailed structural analysis code, a system test was performed by comparing the results of hand calculations of different load cases and cross-sections and the results of the design tool. It was found that the design tool matches the solutions of the hand calculations of similar conditions closely. An example of a simplified load case of the aft wing with a point load and its resulting shear flow in the root chord cross-section is shown in Figure 16.9.

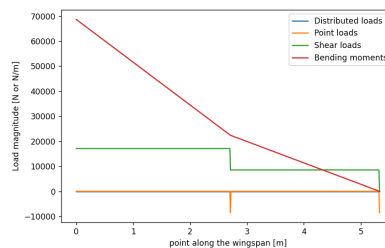


Figure 16.9: Example structural calculation of the design tool for a cantilever beam and a point load.

In combination with the previously conducted sensitivity analysis, the verification process was completed and the model was deemed to respond to variations in the input and design values in a relatively expected manner.

16.4. FEM Structure

To do modal analysis and validate the code for the structural analysis, Ansys software has been used to model the front wing under loads. This is widely used software containing multiple analysis programs that has proven itself and has regular quality control ³. The geometric model includes the skin, spars and stiffeners and was made in Ansys Discovery, Figure 16.10 shows the model. The model also takes into account sweep, the dihedral and the taper. The thickness gained from the detailed analysis was used to construct the wing box. The stringers were assumed to be square and have to same area as in the code. To fit the wing box better in the airfoil, the wingbox was moved more to the front of the wing. The material properties were assumed to be orthotropic for wood and the wing was modelled as made from solid Sitka Spruce instead of laminated, using the values found in source [49].

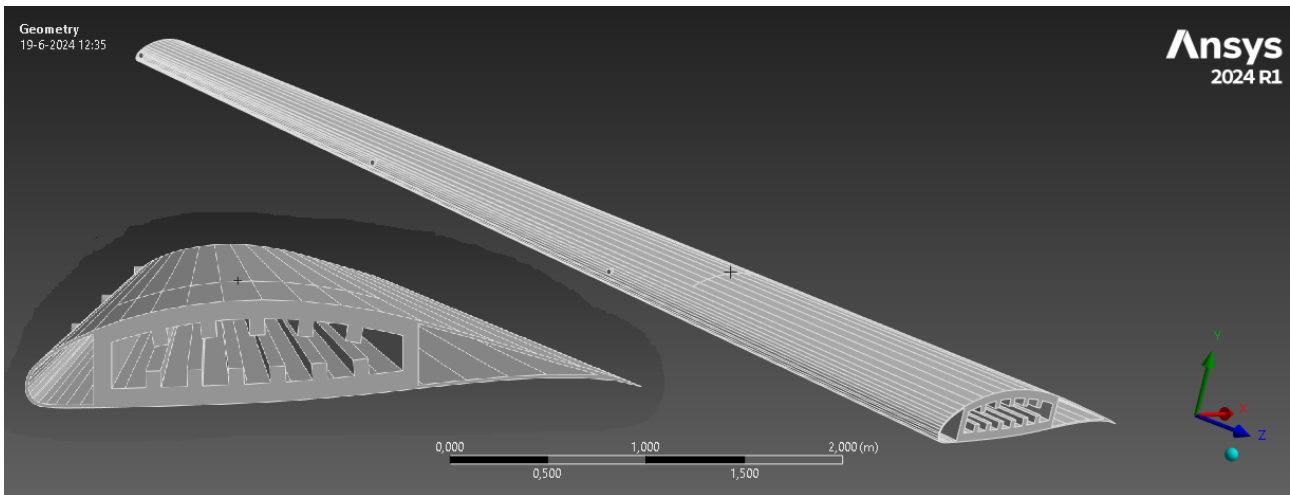


Figure 16.10: Geometry of the wing model in Ansys.

16.4.1. Modal Analysis

With the complete model constructed, Ansys could be used to compute the natural frequencies of the wing. The wing had a fixed support at the cross section area of the root and the first 6 natural frequencies were chosen for analysis. Table 16.10 shows the natural frequencies of the wing. The thin skin area at the trailing edge of the wing deforms the most under influence of all 6 modes. This can be seen in Figure 16.11 where the mode shape induced under mode 2 is shown.

Table 16.10: Frequencies of the first 6 modes.

Mode	Frequency [HZ]
1	11.551
2	34.42
3	40.077
4	41.455
5	46.736
6	52.119

³<https://www.ansys.com/company-information/quality-assurance>

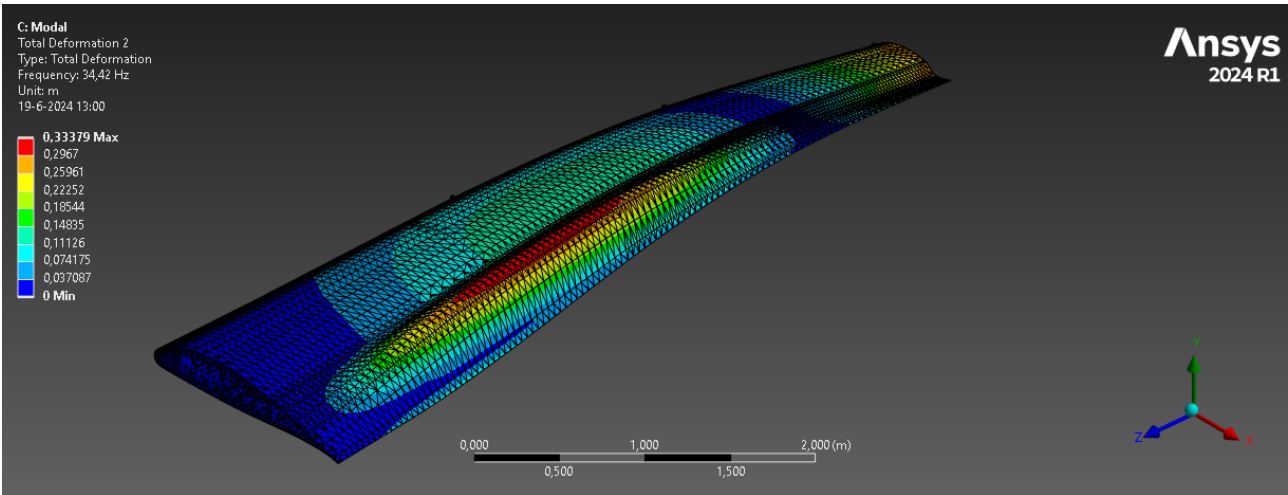


Figure 16.11: Total deformation of the wing under Mode 2.

16.4.2. Structural Model Validation process

To validate the structural model the design was compared with the results obtained from analysis using FEM of the wing model in Ansys. For this, the same forces were applied to the front wing as the detailed study in cruise flight, with a load factor of 3. The lift was modelled as a distributed load located at quarter-cord of the airfoil. The gravity acceleration was also applied to the model. In the model, the engines are not present but the thrust and weight are represented by point forces acting on booms connected with the front spar. Table 16.11 shows the results of the analysis. The deflection of the wing under the loads is shown in Figure 16.12. The stresses can be observed in Figure 16.13, here it can be seen that the highest stresses are located at the top part of the wingbox at the root of the wing.

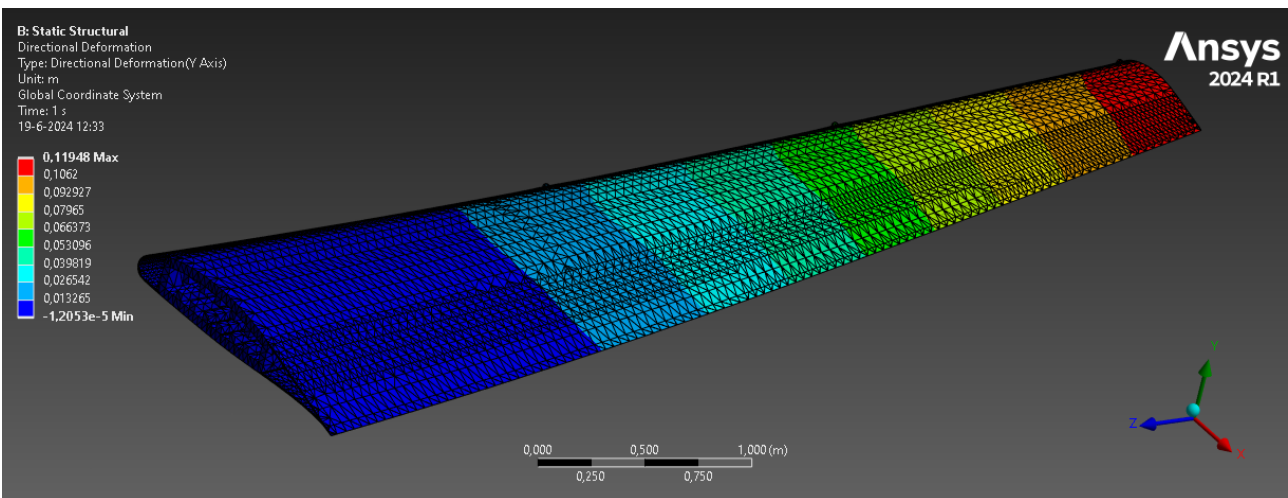


Figure 16.12: Deflection of the wing under loads during cruise.

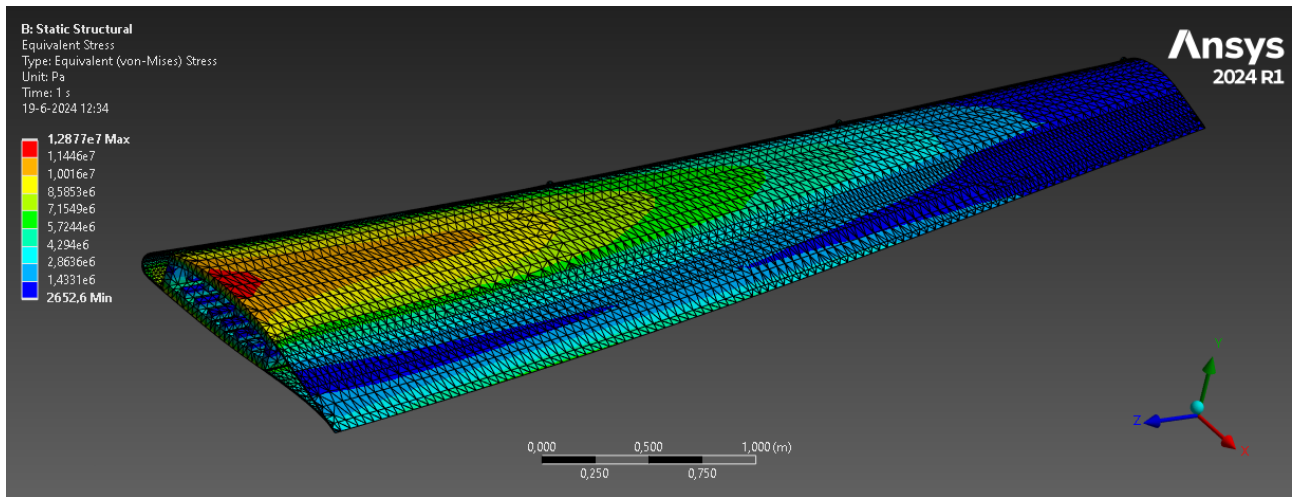


Figure 16.13: Stresses of the wing under loads during cruise.

16.5. Structure Model Comparison

In order to facilitate the comparison of all three of the models that were generated to analyse the aircraft structure, the mass, thickness, deflections and stresses of each beam analysis was compiled into Table 16.11.

Table 16.11: Results of each analysis method for each part.

Parameter	Preliminary structure (PS)	Detailed structure (DS)	FEM	Unit
Aft Half Wing				
Total part mass	130.73	132.37	-	[kg]
Skin thickness	0.0324	0.0383	-	[m]
Deflection in Y direction	0	0.0232	-	[m]
Deflection in Z direction	-0.2188	-0.0724	-	[m]
Maximum normal stress	18.9153	18.727	-	[MPa]
Maximum shear stress	9.4577	17.203	-	[MPa]
Front Half Wing				
Total part mass	124.15	103.41	109.85	[kg]
Skin thickness	0.0303	0.03733	-	[m]
Deflection in Y direction	0.0012	0.00165	0.006494	[m]
Deflection in Z direction	-0.1853	-0.1012	-0.1195	[m]
Maximum normal stress	18.9187	18.733	4.67	[MPa]
Maximum shear stress	9.4594	17.203	1.37	[MPa]
Vertical tail				
Total part mass	38.66	48.6	-	[kg]
Skin thickness	0.0617	0.0642	-	[m]
Deflection in Y direction	0	0.0	-	[m]
Deflection in Z direction	-0.5065	-0.89	-	[m]
Maximum normal stress	18.9713	0.586	-	[MPa]
Maximum shear stress	9.4856	0.366	-	[MPa]
Fuselage				
Total part mass	197.7	178.95	-	[kg]
Skin thickness	0.0015	0.0004	-	[m]
Deflection in Y direction	0	0	-	[m]
Deflection in Z direction	-0.0092	-0.0324	-	[m]
Maximum normal stress	0.2826	61.68	-	[MPa]
Maximum shear stress	0.1413	88.48	-	[MPa]
Materials in the structure				
Total structural mass of the aircraft	746.12	699.11	-	[kg]
Total mass of Sitka Spruce in the aircraft	548.42	520.16	-	[kg]
Total percentage of Sitka Spruce in the aircraft	73.50	74.40	-	[%]
Total mass of AL-2024-T3 in the aircraft	197.7	178.95	-	[kg]
Total percentage of AL-2024-T3 in the aircraft	26.50	25.60	-	[%]
Material Properties				
Rupture modulus (aka yield strength) of Sitka Spruce [58]		18.9753		[MPa]
Shear strength of Sitka Spruce [58]		17.2032		[MPa]
Yield strength of AL-2024-T3 [58]		246.5		[MPa]
Shear strength of AL-2024-T3 [58]		224.4		[MPa]
Crippling stress of AL-2024-T3 [58]		259.5123		[MPa]

In order to compare the three models, the front wing data will be looked at since that is the part for which the FEM model was generated. Even though the beam modelling each part is different, the PS and the DS tools work purely based on the geometric and load inputs that are specific to each beam but the calculation method is identical irrespective of what beam is analysed. Thus, if the front wing model is verified and validated, the whole tool can also be considered to be verified and validated.

When looking at the total beam mass and skin thickness, the DS is the most erratically performing beam analysis tool of the three. This is a bit strange as the increased level of detail of the DS with respect to the PS

was expected to yield less conservative geometric values, resulting in a lower skin thickness and mass in all beams. Moreover, when analysing the deflections of the beams in the Y and Z direction, the results of the DS were expected to fall in between the PS and the FEM analyses. However, that is not the case here, as the DS has the middle deflection in the Y direction and the smallest in the Z direction. However, the results of the DS are closer to the FEM analysis and therefore it is thought to be more accurate in this loading case. Furthermore, the maximum stresses of the DS make sense, as they are optimised to be right under the failure stresses. Due to the comparison with the PS, the results of the DS are believed to have a larger uncertainty and thus not preferred to be used in the iterative analysis.

As for the comparison between the preliminary structural tool and the FEM analysis, more anticipated results were achieved. As expected, the total beam mass of the PS is greater than the FEM, as whilst the FEM accurately models the front wing the PS is only a rough estimation of it, and as such the conservative estimates described in Table 16.5 result in a higher mass than reality. When looking at the stresses, instead, they are also quite a lot higher in the PS than in the FEM. This also meets the expectations, as the FEM has a much larger surface area (since the whole wing is modelled) while only the wing box is being modelled for the PS. This means that the moments of inertia are much higher for the FEM model, resulting in lower stresses throughout the structure. Finally, when looking at the deflection, the deflection in the Z direction is lower for the FEM than the PS due to the increased area over which the stresses are distributed. The only discrepancy occurs for the deflection in the Y direction (which is greater for the FEM than for the PS), however, a possible explanation for this comes from considering the nature of the wing. It is important to remember that not all of the lift is generated in the negative Z direction; the curvature of the airfoil results in some of the lift being produced in the positive Y direction, thus increasing the total load in the Y direction of the FEM (and thus its deflection) with respect to the PS.

In conclusion, the comparison of the three models showed that the detailed structure analysis came close to the results of the FEM analysis although it had a higher uncertainty compared to the preliminary design tool. The DS should therefore be tested further to reduce the uncertainty of its outputs. The preliminary structure analysis produces expected results that are comparable to the FEM model, and in the cases of discrepancies, the difference in the values is logical. As such, it is assumed that the preliminary structure model is validated.

16.6. Landing Gear Design

In this section the design of the landing gear is discussed. First the requirements and the assumptions are treated after which the calculation method is discussed and finally the sensitivity analysis of the calculations with the verification and validation methods are discussed.

16.6.1. Landing Gear Subsystem Requirements and Compliance Matrix

In Table 16.12 the subsystem requirements and their compliance are shown.

Table 16.12: Landing gear Subsystem Requirements Compliance Matrix.

Identifier	Requirement	Source(s)	Compliance	Method of verification
REQ-LDG-01	The landing gear shall be able to support the aircraft's maximum take-off weight.	REQ-SYS-AC-21	✓	Analysis by structural analysis, demonstration during prototyping stage in the future
REQ-LDG-02	The landing gear shall be able to sustain a horizontal landing in emergency situations.	REQ-SYS-AC-88, RAMS-10	✓	Analysis of the extreme loading case, testing during flight tests
REQ-LDG-03	The landing gear shall be able to withstand a landing load factor of 2	REQ-SYS-AC-21	✓	Analysis of the loading case, demonstration during flight tests
REQ-LDG-04	The landing gear shall be sized such that the aircraft does not tip over during ground operations	REQ-SYS-AC-62	✓	Analysis by means of cg analysis, demonstration of ground handling when prototyping
REQ-LDG-05	The landing gear shall have an operational temperature range of -20°C to 47°C.	REQ-SYS-AC-31	✗	Testing during prototyping stage
REQ-LDG-06	The landing gear shall be able to land on asphalt without impairing its functioning for subsequent flights.	REQ-SYS-AC-21, R-TEC-15	✓	Analysis by design load case, demonstration during flight tests in the future
REQ-LDG-07	The landing gear shall be able to be disassembled for maintenance.	REQ-SYS-AC-70	✗	Demonstration during prototyping
REQ-LDG-08	The manufacturing cost of the landing gear subsystem shall be less than 45000 euros.	REQ-SYS-AC-94	✗	Analysis by financial analysis at a later design stage
REQ-LDG-09	The Landing gear shall comply with EASA MOC VTOL.2220	REQ-SYS-AC-86	✗	A more detailed design is needed to confirm the compliance with the regulations
REQ-LDG-10	As per the CS 25.303 regulations, a safety factor of 1.5 shall be applied to the prescribed limit loads which are considered external loads on the structure.	REQ-SYS-AC-39, REQ-SYS-AC-89, R-TEC-10	✓	The safety factor of 1.5 was used in the stress calculations.

16.6.2. Assumptions

Before detailing the structural analysis, it is important to know what the assumptions used throughout the analysis are. These can be found in Table 16.13.

Table 16.13: Assumptions used for the preliminary structural analysis.

Identifier	Assumption	Expected Effect
A-LDG-01	In case of a horizontal emergency landing the front engines will be turned off and placed with the propeller blades parallel to the ground.	The wing tip of the front wing will be the limiting factor for ground clearance. In case the propellers can not be placed in the specified position a horizontal emergency landing may still be possible but the propellers will be heavily damaged.
A-LDG-02	The overturn angle is assumed to be 55°.	A further increase in the turnover angle might cause the aircraft to have a tendency to tip over during manoeuvring on the ground.
A-LDG-03	The wing-tip strike angle is assumed to be 5°.	The roll angle of the aircraft may not exceed the 5° during landing or take-off otherwise the front wing tip will strike the ground
A-LDG-04	The friction coefficient during braking was assumed to be 0.25 during braking.	The friction coefficient determines what part of the normal force is experienced during braking the higher the friction coefficient the higher the braking force
A-LDG-05	The angle of attack during a horizontal emergency landing is 12° or smaller.	This influences the angle under which the main landing gear is placed with respect to the most aft CG location. And thus influences the location of the main landing gear on the aircraft.
A-LDG-06	The landing gear can be modelled as a solid cylinder	This will give an first-order estimate of the weight but it might not be fully accurate.

The reasoning behind the assumptions in Table 16.13 is as follows: A-LDG-01 has been implemented because VTOL operations will be the standard for the aircraft and in case of an emergency landing the primary objective is to make sure the passengers and pilot land safely. Therefore damage to the propellers is allowable, which will only happen if the propellers can not be rotated in the vertical position in that specific emergency case.

The values of 55° for A-LDG-02 and 5° for A-LDG-03 were set to this value since they are the maximum and minimum recommended values respectively [17]. These are deemed sufficient since their influence on the VTOL operations is minimal.

The value of A-LDG-04 has been based on research into aircraft braking performance[61]. For A-LDG-05 the value of 12° was set because this is the angle under which the rear wing will start being influenced by the wake of the front wing.

16.6.3. Method

In the initial phase of the landing gear design consisted of determining the possible options for the landing gear. The considered landing gear configurations were a skid, a bicycle, a taildragger, and a tricycle landing gear. The skid landing gear was discarded because REQ-LDG-02 states that a horizontal landing must be performed in case of an emergency. The skid configuration does not comply with this requirement since the skids do not offer control when the landing gear touches the ground in case of a horizontal landing, making it unsafe to perform such an emergency landing.

Further analysis of the bicycle configuration was also discontinued. This was done because the bicycle landing gear is unstable, it is difficult for the pilot to handle during the landing phase and it does not allow for higher angles of attack. The allowance for a high angle of attack is not problematic for vertical landing or take-off, since the aircraft is in horizontal configuration during this procedure, however it will be a problem during the horizontal emergency landing [62]. The bicycle configuration is more difficult for the pilot during landing since the aircraft needs to perform a landing with a very low roll angle in comparison to other configurations⁴ since the stabilizing wheels on the edge of the wings are not meant to endure the initial impact of the landing. This means that a landing with the required 60 km/h winds (according to REQ-SYS-AC-25) will be very challenging. The last reason why the bicycle configuration was discarded, was its ground instability making it difficult to handle during ground operations [62].

The taildragger and tricycle configurations were analysed further to determine the optimal configuration. For this analysis, A-LDG-01 was used to determine the length and position of both configurations. The analysis is based on a lateral tip-over (Equation 16.1), tip clearance (Equation 16.2) and engine clearance (Equation 16.3) formula [17] using A-LDG-02 and A-LDG-03. This analysis showed that the main landing gear of the taildragger would be approximately twice as long as the tricycle landing gear, in order to facilitate a landing with an angle of attack around stall. The increased length means an increased weight, therefore the tricycle configuration was chosen in favour of the taildragger.

$$Y_{MLG} > \frac{l_{nose} + l_{main}}{\sqrt{\frac{l_{nose}^2 \tan^2(\psi)}{z^2} - 1}} \quad (16.1) \quad Y_{MLG} > \frac{b}{2} - \frac{z_t}{\tan(\phi)} \quad (16.2) \quad Y_{MLG} > y_e - \frac{z_n}{\tan(\varphi)} \quad (16.3)$$

The size of the landing gear was then determined via the formulas explained above and cooperation between the structures, aerodynamics and fuselage departments. Where the ground clearance, entrance height and structural weight of the landing gear were the most important discussion factors. In Section 16.6.4 the results in the dimensions can be found. The mass of the landing gear was calculated by combining the tyre mass with a

⁴<https://aerospaceweb.org/question/design/q0200.shtml> cited[13.06.2024]

first-order model of the landing gear. This first-order model consists of a solid cylinder made of 4340 steel alloys⁵ [63]. The loads and stresses on the modelled cylinder were calculated using the maximum take-off weight, REQ-LDG-03, REQ-LDG-10 and A-LGD-04. The tyre was selected by using the graph of Torenbeek which depends on the inflation pressure and the static load on the wheel [64]. The inflation pressure is determined by the landing surface, for which an overlapping pressure between hard grass and a small tarmac runway was chosen such that an emergency landing can be performed on grass but it is still able to operate from a tarmac landing pad.

16.6.4. Results

The calculations described were included in the iteration process and Table 16.14 shows the final results of the landing gear after the iteration process. For the masses of the nose⁶ and main⁷ landing gear a comparable tyre was selected and its weight was used as the input weight.

Table 16.14: Values of landing gear sizing parameters and corresponding rationales.

Parameter	Value	Unit	Rationale
Nose landing gear			
Tyre size	4.00-3.5	[]	The tyre size was derived from the graph from Torenbeek [64] as described in Section 16.6.3
Mass tyre	2.93	[kg]	Weight from a comparable tyre to the selected one.
Mass strut	3.69	[kg]	Modeled as a solid 4340 steel cylinder and calculated via its density
Radius strut	0.0158	[m]	Calculated from the maximum allowable stress after the application of safety factors
Height landing gear	0.6	[m]	Measured from the bottom of the front airfoil and calculated using tip clearance.
Location	1.20	[m]	Measured from the nose of the aircraft along the fuselage length
Main landing gear			
Tyre size	21x6.75-9	[]	The tyre size was derived from the graph from Torenbeek [64] as described in Section 16.6.3
Mass tyre	8.72	[kg]	Weight from a comparable tyre to the selected one
Mass strut	10.95	[kg]	Modeled as a solid 4340 steel cylinder and calculated via its density
Radius strut	0.0272	[m]	Calculated from the maximum allowable stress after the application of safety factors
Height landing gear	0.6	[m]	Measured from the bottom of the front airfoil and calculated using tip clearance.
Location	3.95	[m]	Measured from the nose of the aircraft along the fuselage length

16.6.5. Landing Gear Sensitivity Analysis

For the sensitivity analysis of the landing gear some of the input parameters have been given a normal distribution around their final value. The inputs that were given a normal distribution are the most aft CG location, the height of the most aft CG location, the maximum take-off weight, the overturn angle, the tip strike angle and the scraping angle. At first, only one of the inputs was given a normal distribution to check the influence they had on different outputs. It turned out that the aft CG location, height of the CG and the scrape angle of the aircraft have an influence on the location of the main and nose landing along the length of the aircraft. The outboard location of the main landing gear is influenced by the overturn angle and the tip strike angle and the weights of both the nose and main landing gears are only influenced by the maximum take-off weight.

The initial analysis described above is used to determine which inter-dependencies needed to be investigated in the final sensitivity analysis where all the previously described inputs were assigned to a normal distribution at the same time. The results of this analysis can be seen in Figure 16.14 and Figure 16.15.

In Figure 16.14 the influence of the different inputs on the main landing gear location can be seen in the top row and their influence on the nose landing gear can be seen in the bottom row. The leading influence on the location of the main landing gear is the location of the most aft CG (depicted in blue). This strong influence means that the influence of the height of the CG (depicted in green) and scrape angle (depicted in black) are very small and therefore do not show a clear relation. However the initial analysis showed that there was a dependency on these inputs. For the nose landing gear there is no clear leading input. The aft CG location and scrape angle are slightly more clustered together, thereby implying that their relation with the nose gear location is stronger than the relation of the height of the CG. But there is much more equally influenced by the different inputs as the main landing gear.

⁵<https://www.voestalpine.com/highperformancemetals/australia/app/uploads/sites/72/2018/03/4340.pdf> cited[13.06.2024]

⁶<https://shop.boeing.com/aviation-supply/p/505C66-5=0T> cited[14.06.2024]

⁷<https://shop.boeing.com/aviation-supply/p/217K22-1=0T> cited[14.06.2024]

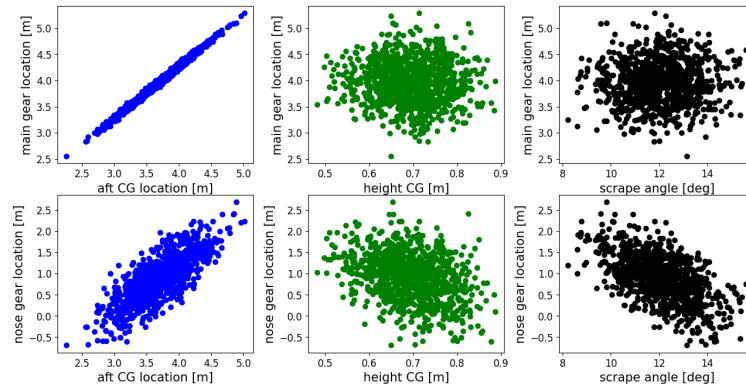


Figure 16.14: Sensitivity results for the locations of the landing gear along the length of the aircraft.

In Figure 16.15 the sensitivity of the outboard location (from the centre line of the aircraft) due to the tip strike angle (depicted in orange) and the overturn angle (depicted in purple) are shown in the top row and the influence of the maximum take-off weight (depicted in red) on the mass of the main (in the bottom left graph) and nose gear (in the bottom right graph) are shown in the bottom row. It can be seen that the mass of both types of landing gear is dependent on the maximum take-off weight and therefore has a very clear relation. For the outboard location, it is more complex. For these normal distributions, all the values of the tip strike angle that were below 5° were resigned the value of 5° since this is the minimum angle [17]. The same holds for angles above 55° of the overturn angle since this is the maximum angle [17]. For the outboard location of the main landing gear, it can be seen that the tip strike angle is most often the leading influence since most sample points follow a distinct relation. However, for certain combinations, the overturn angle can be the limiting case. However, the minimum outboard location of the main landing gear is achieved at a tip strike angle of 5° with the right overturn angle.

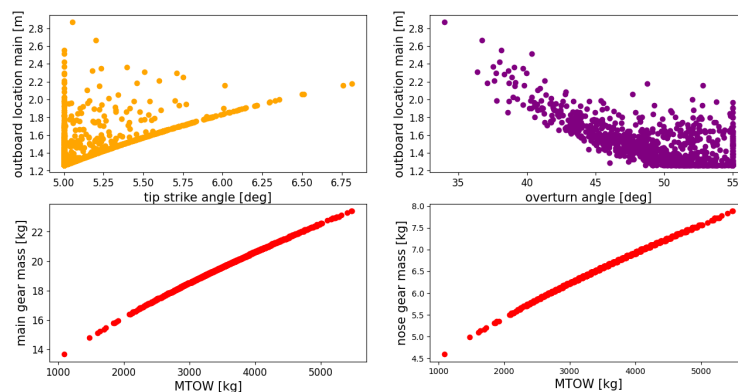


Figure 16.15: Sensitivity results for the outboard location and weights of the landing gear.

16.6.6. Landing Gear Verification and Validation

To verify the calculations of the landing gear the calculations were manually repeated for a select number of different input values. When comparing the results of the manual calculations to the results of the program, they turned out to be identical except for some rounding errors. This verified the calculations in the program.

For the validation of the results, another method was used. An employee of an aircraft maintenance company (EVW Maintenance⁸) was contacted. This employee measured the mass of the main landing gear of an aircraft with a comparable passenger count and landing gear size. This mass turned out to be 18 kg, which is close to the value generated by the calculations in Section 16.6.4 thereby validating the results of the calculations.

The assumptions are verified in Table 16.15.

⁸<https://www.atn-aircraft-division.nl/> cited[14.06.2024]

Table 16.15: Validation of the assumptions used for the landing gear.

Identifier	Validation
A-LDG-01	In case the actuators fail this might not always be true, but since propeller failure during an emergency landing is accepted the assumption is still valid.
A-LDG-02	Based on the method of calculation it is the maximum allowed [17] and the sensitivity analysis showed that in reality it is probably lower.
A-LDG-03	Based on the method of calculation it is the minimum allowed [17]
A-LDG-04	This is required according to the EASA regulations [65]
A-LDG-05	This is required according to the EASA regulations [65]
A-LDG-06	This is validated by research [61]
A-LDG-07	This is because otherwise, the rear wing will be in the wake of the front wing thereby stalling the aircraft.
A-LDG-08	It slightly underestimates the weight of the landing gear since the spring and deformation mechanisms are ignored together with the fairings.

16.7. Recommendations

In order to better the findings of this chapter, some recommendations are presented here below. For the aircraft structural models, it is recommended to repeat the analysis while also including an estimation of the effect of adhesives and mechanical fasteners on the total mass and stress of the part; this would allow for more complete results from the analysis. In addition, it would be beneficial for the models to be expanded to analysing non-symmetric loading too, such that even more loading cases can be modelled. Furthermore, it is recommended that the detailed model is further tested to understand why it has a more uncertain nature than the preliminary model. A more detailed sensitivity analysis is recommended to investigate the various parameters individually. Should the detailed model be fixed and perform better than the preliminary model, the detailed model should then be used in the full aircraft iteration detailed in Chapter 17 (rather than using the preliminary model) as it allow for the iteration to be even more accurate. In order to fully verify the structural models, it would be helpful to make a FEM model of all four structural parts (the front wing, aft wing, fuselage and vertical tail). This would improve the confidence of the models. Next, when considering the failure modes of the structures, the crippling and buckling of wooden beams should also be considered to ensure that that is not the failure mode of the part. Finally, for the landing gear design, it is recommended to model the landing gear more accurately this will not only improve the weight estimation of the landing gear but also improve the accuracy of the force calculations.

Chapter 17 | Design Integration & Results

In order to achieve a functioning aircraft system that complies with all requirements, the developed subsystems must be integrated together and the placement of components has to be optimised. In this chapter, the methods and results of the design integration and optimisation are discussed. The integration method itself is explained in Section 17.1. The aircraft weight and centre of gravity estimation, which is an important aspect of checking whether the aircraft meets its system requirements, is discussed in Section 17.2. The effects the design integration and weight and CG estimation have had on the subsystem design are covered by Section 17.3. Finally, in Section 17.4, the final results of the aircraft system design are presented.

17.1. Integration Method

The aircraft system consists of interlinked subsystems. That is, the design parameters of a certain subsystem can influence those of other subsystems. Therefore, iterations need to be performed in order to reach converged design parameters. These iterations were performed in Python, where the files corresponding to the design tools developed for each subsystem were run sequentially. The values of all output parameters which are inputs to other subsystems were stored in a CSV file, and were updated each time a file is run.

The iterative process was aided by a CAD model of the aircraft, in which the exact placement of components was determined. All components were placed such that they can form an assembly in which there are no conflicts between each other. The determination of the CG of certain components was also aided by the CAD model, as is discussed in more detail in Section 17.2. In order to reduce the time required for the iterations, the CAD model was not updated in each iterative cycle, but rather each time convergence of the outputs from the Python files was reached. This process is illustrated by Figure 17.1. In Figure 17.2, an N2 chart is shown that contains the various subsystem design tools and their respective inputs and outputs. Note that only inputs and outputs which link two or more subsystems are shown, and that some are grouped together in order to save space in the chart (e.g. the coordinates of the empennage position are grouped together as 'empennage positioning'). Also note that only the subsystems are shown that were included in the iterations. For example, since the fuselage design was mostly independent of other subsystems and the design was made in CAD software for the most part, it was excluded from numerical iterations. A block representing the CAD model construction has also been added to the chart in order to show the inputs and outputs. However, the dotted lines are used to indicate that updating the CAD model was not done in each iterative cycle of the Python codes. Whenever conflicts between subsystems or requirement violations were found during the iteration process, these were communicated to the responsible departments in order to find a solution. After a solution was proposed, the design parameters were updated and a new iteration was started. Iterations of the design were stopped as soon as the difference between the maximum take-off weight values was less than 1%.

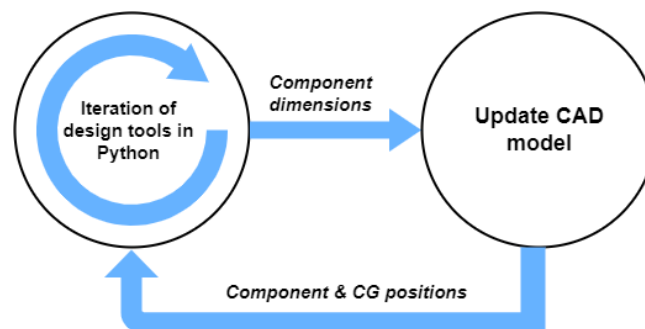


Figure 17.1: Aircraft design integration process.

Wings Sizing	Wing dimensions	$b_{real,front}$ $b_{real,aft}$	S		b	$b_{real,front}$ $b_{real,aft}$	$b_{real,front}$ $b_{real,aft}$		S
	Aerodynamic Analysis		C_{D0} $C_{L\alpha}$ $C_{D\alpha}$					Downwash gradient $C_{L\alpha}$	
		Propulsion System Sizing	A_{pr}		Motor Y-positions		Motor Y-positions	Motor Y-positions $W_{motor,front}$ $W_{motor,aft}$ $W_{prop,front}$ $W_{prop,aft}$	Motor dimensions Propeller dimensions
			Flight Profile & Transition Analysis	P_{req}	$T_{front, failure}$ $T_{aft, failure}$				
				Battery & TMS Sizing				$W_{pack,main}$ $W_{pack,aux}$ W_{TMS}	$V_{pack,main}$ $V_{pack,aux}$
	Empennage dimensions				Empennage Sizing				S_{emp} C_{rudder}
	Landing gear dimensions					Landing Gear Design		$W_{lg,main}$ $W_{lg,nose}$ $CG_{lg,main}$ $CG_{lg,nose}$	Landing gear dimensions
							Structural Analysis & Sizing	W_{fus} W_{fw} W_{aw} W_{emp}	
W_{MTO}		W_{MTO} $CG_{X,MTO}$	W_{DTO}		$CG_{X,max}$	W_{MTO} $CG_{X,max}$ $CG_{Z,max}$	W_{MTO}	Weight & C.G. Estimation	
	Wings positioning Nacelle dimensions	Motor X-positions			Empennage positioning		Wings positioning Empennage positioning Motor X-positions	CG_{fus} , CG_{fw} , CG_{aw} , CG_{emp} , $CG_{pack,main}$, $CG_{pack,aux}$, Motor X- positions, Motor Z- positions	CAD Model Construction

Figure 17.2: Design tool integration N2 chart.

17.2. Weight and Centre of Gravity Estimation

Following the completion of the design of the subsystems, the total weight and centres of gravity values could be estimated. The empty weight of the aircraft is defined as the sum of all components, except for the passengers, luggage and battery packs, and can therefore be obtained using Equation 17.1. Adding the total battery pack weight to the empty weight yields the operational empty weight, expressed by Equation 17.2. The design take-off weight was defined to be the operational empty weight plus the design payload weight as defined by requirement REQ-SYS-AC-02-A. However, the maximum payload weight with which the aircraft must be able to operate was set to be higher, as defined by requirement REQ-SYS-AC-02-B. As a consequence, the maximum take-off weight is higher than the design take-off weight, and is given by Equation 17.4. The final weight values are presented in Table 17.1.

$$W_E = W_{struc} + W_{prop} + W_{lg} + W_{av} + W_{int} + W_{TMS} + W_{add} \tag{17.1}$$

$$W_{OE} = W_E + W_{pack} \tag{17.2}$$

$$W_{DTO} = W_{OE} + W_{pay,des} \tag{17.3}$$

$$W_{MTO} = W_{OE} + W_{pay,max} \tag{17.4}$$

In order to calculate the total centre of gravity of the aircraft, the centres of gravity of the individual subsystems were estimated with the aid of CAD software. Then, the total CG was calculated using Equation 17.5. The CG location of the operational empty weight configuration is fixed, as the components constituting the operational empty weight are fixed in location. However, when the passengers, pilot and luggage are included, the CG is defined by a certain range. This is due to the fact that amount, location and weights of individual passengers

and luggage items can vary. The CG range in nominal operations was estimated by calculating the variation of the CG when the aircraft is loaded starting from the front and when it is loaded starting from the aft. For this calculation, the weight per person was taken to be 90 kg and the weight per luggage item was taken to be 10 kg, as this is what the maximum payload weight from requirement REQ-SYS-AC-02-B was based on. In Table 17.1, the estimated CG coordinates of the operational empty weight CG and the calculated CG range in nominal operations are presented.

The datum for the CG calculations was set as the tip of the nose of the aircraft, with the X-axis defined as the longitudinal direction and pointing to the tail, the Y-axis defined as the lateral direction and pointing to the right (as from the pilot's perspective) and the Z-axis defined as the vertical direction and pointing upwards.

$$CG = \frac{\sum CG_i \cdot W_i}{\sum W_i} \quad (17.5)$$

In order to check whether the aircraft is longitudinally stable, the neutral point, which is the most aft allowed CG position, is calculated using Equation 17.6. The equation is derived from setting up the moment equation of the aircraft around the CG and differentiating it with respect to the angle of attack, after which the derivative of the moment is set to zero in order to find the most aft CG point for which the aircraft is still statically stable. It is assumed that both wings are identical (Chapter 9) and that the contribution of drag to the moment is negligible. Furthermore, it is assumed that the dynamic pressure is the same at both wings. The parameters in Equation 17.6 are results obtained from the aerodynamic analysis described in Chapter 10.

$$CG_{X,allowed} = \frac{X_{ac,f} \cdot C_{L\alpha} + X_{ac,a} \cdot C_{L\alpha} \cdot \left(1 - \frac{d\epsilon}{d\alpha}\right)}{C_{L\alpha} + C_{L\alpha} \cdot \left(1 - \frac{d\epsilon}{d\alpha}\right)} \quad (17.6)$$

It is important that the X-coordinate of the CG never falls behind the neutral point, as this would result in static instability. In order to check what the most extreme X-position of the CG could be, this CG coordinate was calculated for the case in which the luggage has a maximum weight of 60 kg and all of the maximum passenger weight (6 times 90 kg) is concentrated in the last row of seats. In practice, this is not possible as 6 people cannot physically fit on the last row, and two people that are able to sit in the aircraft will not have a combined weight of 540 kg. Furthermore, the pilot is not likely to move to the aft row for whatever reason. Still, it is calculated as a conservative extreme scenario. As can be observed in Table 17.1, this extreme CG X-position still lies in front of the neutral point. It is thus confirmed that the aircraft is longitudinally statically stable in all conditions, meaning requirement REQ-SYS-AC-46 is complied with. It can also be seen that the operational empty weight is lower than 3000 kg, meaning requirement REQ-SYS-AC-03 is also complied with.

Table 17.1: Results of the weight and centre of gravity estimation.

Parameter	Value	Unit	Rationale
W_{struc}	740.0	[kg]	Result from the preliminary structures design tool discussed in Chapter 16
W_{prop}	518.3	[kg]	Value taken from Table 11.3
W_{lg}	46.0	[kg]	Total landing gear weight calculated from the strut and tire weights from Table 16.14
W_{av}	56.6	[kg]	Obtained in Section 14.4
W_{int}	120	[kg]	It assumed that the interior weight consists only of the combined weight of the seats. Each individual seat is assumed to have a weight of 20 kg, which is based on premium economy seat weight values from various airlines.
W_{TMS}	96.4	[kg]	Value taken from Table 12.3
W_{pack}	1153.4	[kg]	Value taken from Table 12.3
W_{add}	223.2	[kg]	During the iterations, the additional weight was set to 12.5% of the operational empty weight. The final value differs a bit from this percentage due to the fact that the iterations were stopped as soon as the maximum take-off weight was converged within 1%.
$W_{pay,des}$	480	[kg]	Set equal to the value from requirement REQ-SYS-AC-02-A
$W_{pay,max}$	600	[kg]	Set equal to the value from requirement REQ-SYS-AC-02-B
W_E	1800.5	[kg]	Calculated using Equation 17.1
W_{OE}	2953.9	[kg]	Calculated using Equation 17.2
W_{DTO}	3433.9	[kg]	Calculated using Equation 17.3
W_{MTO}	3553.9	[kg]	Calculated using Equation 17.4
$CG_{X,OEW}$	3.513	[m]	Calculated using Equation 17.5
$CG_{Y,OEW}$	0.005	[m]	Calculated using Equation 17.5
$CG_{Z,OEW}$	0.231	[m]	Calculated using Equation 17.5
$CG_{X,min}$	3.454	[m]	Calculated using Equation 17.5
$CG_{X,max}$	3.679	[m]	Calculated using Equation 17.5
$CG_{Y,min}$	0.004	[m]	Calculated using Equation 17.5
$CG_{Y,max}$	0.020	[m]	Calculated using Equation 17.5
$CG_{Z,min}$	0.231	[m]	Calculated using Equation 17.5
$CG_{Z,max}$	0.269	[m]	Calculated using Equation 17.5

Continued on next page

Parameter	Value	Unit	Rationale
$CG_{X,extreme}$	3.781	[m]	Calculated using Equation 17.5
$CG_{X,allowed}$	3.800	[m]	Calculated using Equation 17.6

17.3. Effects on Subsystem Design

During the integration of the design and the construction and updating of the CAD model, several conflicts between subsystems have been encountered that have led to certain design choices for the respective subsystems. These subsystem design choices have been discussed in the corresponding chapters, but the ones with the most impact on the design are summarised below.

17.3.1. Battery Placement

Initially, the desired location for the main battery pack was between the passenger cabin and the luggage hold. The auxiliary battery pack was initially placed below a lowered cabin aisle. However, once the first results of the CG estimation and stability analysis were obtained, it was observed that the CG was relatively far aft of the neutral point. Thus, significant changes in the configuration had to be made. As the battery pack is a relatively dense component and its placement is more flexible than the other subsystems, it was decided to change its location. Changing the ratio between the surfaces areas of the wings was also considered. Increasing the surface area of the aft wing would shift the neutral point more aft, but it was chosen to keep the area ratio as 1 in order not to constrain the diameter of the front propellers further and to keep the ground profile of the aircraft at a minimum.

After the passenger seats were designed, it was found that they could be shifted aft by 300 mm without changing the fuselage design, as discussed in Section 8.3.3. This allowed the main battery pack to be placed in a closed off compartment between the cockpit and passenger cabin. Still, the resulting shift in CG was not sufficient, so a larger portion of the auxiliary battery pack had to be concentrated in the front of the volume underneath the passenger cabin. In order to achieve this, it was chosen not to lower the aisle. It was also decided not to have an aisle lowering after the end of the auxiliary battery pack, as a margin is desired in case it turns out in a future design stage that the auxiliary battery pack volume is larger than estimated. Also, the auxiliary battery pack could not be shifted all the way to the front of the passenger cabin since space had to be kept available for the thermal management system, as discussed in Section 12.3.2.

17.3.2. Wing Placement

During construction of the CAD model, it was found that the position of the forward wing is highly constrained. With the required size of the root chord, there is only a very small range in longitudinal and vertical positions for which the wing surface does not fall outside of the fuselage at the centerline and for which the wingbox does not obstruct the feet of the pilot and intersect the main battery pack compartment. With the position of the forward wing relatively fixed, it was decided to move the aft wing as far aft as possible in order to keep the neutral point aft of the CG. Still, some margin had to be taken into account for empennage wake considerations, as explained in Section 17.3.3 below. The vertical position of the aft wing was set as high as possible in order to minimise wake effects from the front wing at high angles of attack and to maximise the ground clearance of the aft propellers in horizontal flight mode, while still keeping some margin for proper structural attachment to the fuselage.

17.3.3. Empennage Placement

As mentioned in Section 9.2.3, a third of the rudder area is required to lie outside the wake of the aft wing in order to allow for spin recovery. Initially, it was opted to place the empennage near the fuselage aft end on top of the fuselage, which is the conventional vertical tail position. However, due the wake of the aft wing in spin conditions, the empennage had to be placed more aft. The relatively large rudder size and small fuselage height at the aft end led to the design choice of extending the empennage below the fuselage. This design choice allows for a more robust structural empennage attachment to the fuselage and it ensures that a sufficient portion of the rudder area is located outside the aft wing wake in spin conditions.

17.3.4. Propeller Sizing

As discussed in Section 11.2.1, the propeller diameter must be maximised in order to maximise the propulsive efficiency. However, their diameter is constrained by the fuselage, as it covers a portion of the total wingspan. Therefore, the fuselage width is taken as a constraint in the propeller sizing, with a minimum clearance taken into account. For the front propellers, the fuselage width is most constraining in VTOL mode, whereas it is most constraining in horizontal mode for the aft propellers.

17.3.5. Landing Gear Configuration

As discussed in Section 16.6.3, several landing gear configurations have been considered. In a tail wheel configuration, the aircraft belly would make contact with the ground before the tail wheel. Combined with the fact that a tail wheel configuration causes the aircraft to be tilted backwards at all times when on the ground, it was chosen to implement a tricycle-type landing gear configuration. In order to minimise the aircraft drag, a retractable landing gear would be optimum. However, a retractable main landing was found to be unfeasible due to the limited volume underneath the cabin floor due to the placement of the auxiliary battery pack. A forward retraction of the nose gear was found to be unfeasible as flight control systems are present in the nose and windows are present for the pilot to look down during vertical landings. A backward retraction was also found to be unfeasible, as the volume aft of the nose gear is insufficient for the nose gear and the thermal management system was chosen to be placed there.

In Figure 17.3 below, a side view is provided in which the aircraft is cut through the centre line in order to illustrate the component positions mentioned in the previous subsections.

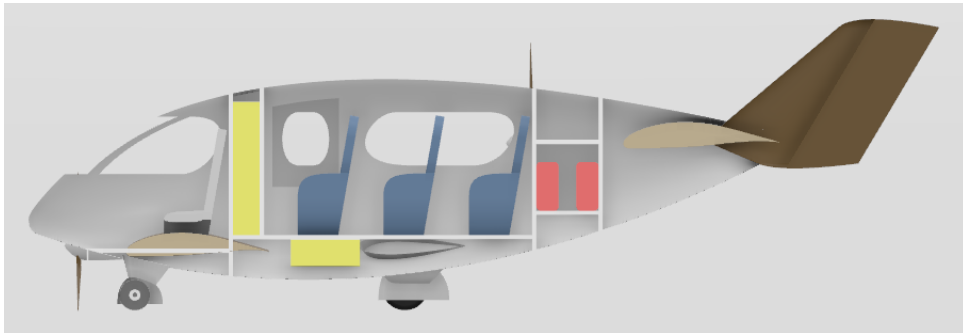


Figure 17.3: Section side view of the aircraft, where the battery packs are represented by yellow blocks and the luggage is represented by red blocks.

17.4. Design Results

After convergence was reached in the iterative process, the final design parameters were stored and the CAD model was updated one last time. In Figure 17.4, the convergence behaviour of the aircraft weight values is shown. In Table 17.3, the main final design parameters are presented. In Figure 17.5 through Figure 17.11, multiple views of the final CAD model of the aircraft are shown.

Table 17.3: Main parameters of the final aircraft design.

Parameter description	Parameter symbol	Value	Unit
Maximum take-off weight	W_{MTO}	3554	[kg]
Design take-off weight	W_{DTO}	3434	[kg]
Operational empty weight	W_{OE}	2954	[kg]
Total battery pack weight	W_{pack}	1153	[kg]
Most forward longitudinal CG position	$CG_{X,min}$	3.454	[m]
Most aft longitudinal CG position	$CG_{X,max}$	3.679	[m]
Most aft allowed longitudinal CG position	$CG_{X,allowed}$	3.800	[m]
Fuselage length	-	8.725	[m]
Wing surface area	S	20.298	[m ²]
Maximum wingspan		10.812	[m]
Maximum span including propellers		13.718	[m]
Maximum lift coefficient	CL_{max}	1.679	[-]
Percentage wood in the structure by mass	-	70	[-]
Maximum range at design payload	R	200	[km]

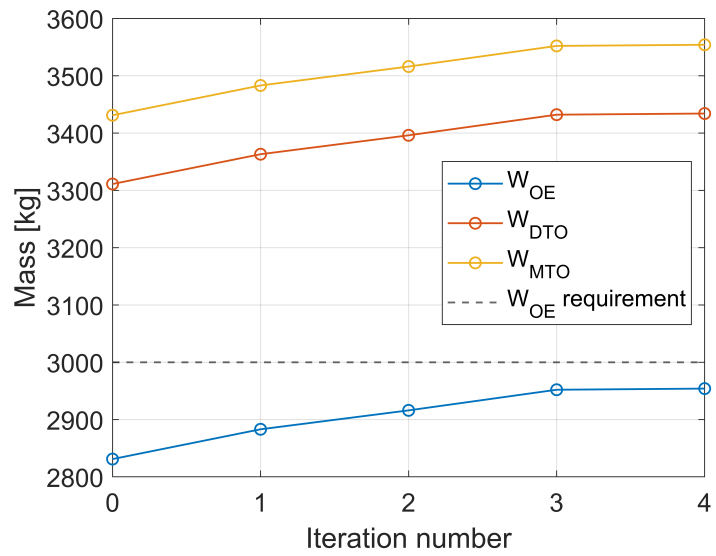


Figure 17.4: Convergence behaviour of the aircraft mass.



Figure 17.5: Isometric view of the final aircraft assembly in horizontal flight mode, including passengers and pilot.



Figure 17.6: Side view of the final aircraft assembly in horizontal flight mode.



Figure 17.7: Front view of the final aircraft assembly in horizontal flight mode.

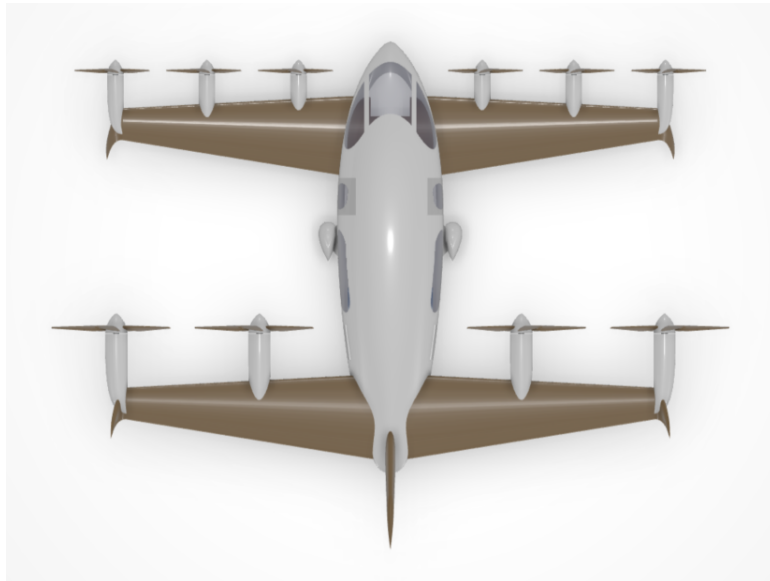


Figure 17.8: Top view of the final aircraft assembly in horizontal flight mode.

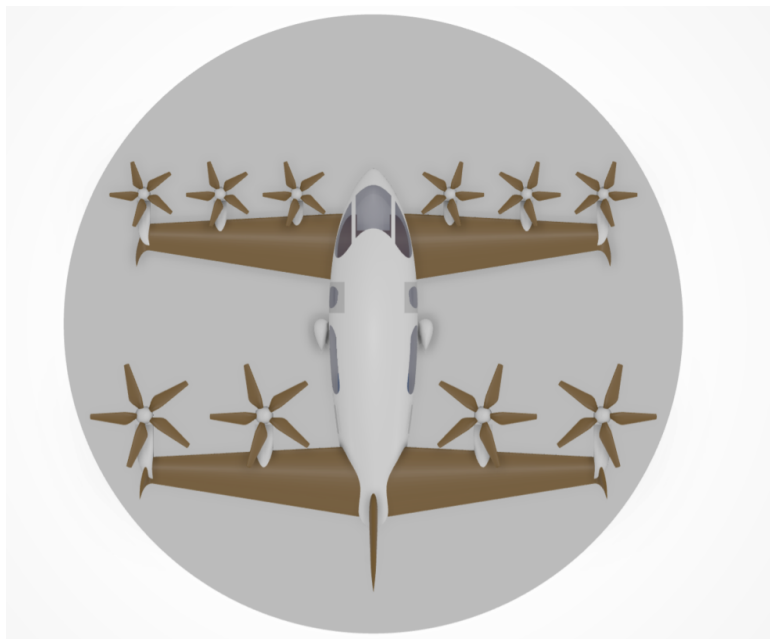


Figure 17.9: Top view of the final aircraft assembly in VTOL flight mode, with an H1 landing pad circumference as reference.



Figure 17.10: Perspective view of the final aircraft in VTOL flight mode with the entrance door and left luggage hatch opened, while the pilot is placing the luggage.



Figure 17.11: Perspective view of the final aircraft in cruise conditions, including passengers and pilot.

Chapter 18 | Ground Station Design

Now that the aircraft model is complete, it is time to take a look at the ground station that will service the craft during its lifetime. This was done, just like with the aircraft, while following a set of requirements associated with the system, as can be seen in Table 18.1. The ground station consists of three major components - a lobby for passengers to wait in, a storage area for the hydrogen fuel and the fuel cells required for the energy generation, and the landing pad.

18.1. Ground Station Subsystem Requirements and Compliance Matrix

This section lists the the requirements that are related to the ground station design.

Table 18.1: Ground station subsystem requirements compliance matrix.

Identifier	Requirement	Source(s)	Compliance	Method of verification
REQ-LAN-01	The landing pad shall have a safety area* with a diameter of at least 2 times the HAROLD maximum dimension.	REQ-SYS-GS-01, REQ-SYS-GS-03, R-TEC-16	✓	Inspection of the design by the end of the chapter
REQ-LAN-02	The landing pad shall have a fire extinguishing system	REQ-SYS-GS-10	✓	Inspection of the design by the end of the chapter
REQ-LAN-03	The boundaries of the landing pad shall be made visible to the pilot(s) by means of illumination.	REQ-SYS-GS-04	✓	Inspection of the design by the end of the chapter
REQ-LAN-04	The manufacturing cost of the landing pad shall be no more than 5% of the total ground station manufacturing budget.	REQ-SYS-GS-16	✓	Analysis by financial analysis in Section 18.3.2
REQ-CHA-01	The ground station charging units shall be able to recharge the aircraft battery.	REQ-SYS-GS-02, REQ-SYS-GS-06	✓	Inspection of the charging infrastructure design
REQ-CHA-02	The charging unit shall be able to be connected to the electricity grid with alternating current voltage levels ranging from 1-36 kV.	REQ-SYS-GS-07	✓	Inspection of the charging infrastructure design
REQ-CHA-03	The charging unit shall operate with an alternating current frequency of 50 Hz.	REQ-SYS-GS-08	✓	Inspection of the charging infrastructure design
REQ-CHA-04	The charging unit shall indicate the charging status to the pilot(s).	REQ-SYS-GS-09	✓	Inspection of the charging infrastructure design
REQ-CHA-05	The charging unit shall be capable of fully charging the eVTOL within 100 minutes.	REQ-SYS-GS-02, RAMS-04	✓	Analysis of the charging infrastructure, demonstration during prototyping
REQ-CHA-07	A standard maintenance routine of the charging unit shall not take longer than 4 hours per unit by one mechanic.	REQ-SYS-GS-14, R-TEC-05	✗	Demonstration when a full prototype is built
REQ-CHA-08	The manufacturing cost of the charging unit shall be no more than 10% of the total ground station manufacturing budget.	REQ-SYS-GS-16	✓	Analysis by financial analysis in Section 18.3.2
REQ-OPG-01	The ground station shall be able to communicate with the aircraft.	REQ-SYS-GS-05	✓	Inspection of the GS design by the end of the chapter
REQ-OPG-02	The ground station operations shall be powered by green hydrogen.	REQ-SYS-GS-12	✓	Inspection of the GS design by the end of the chapter
REQ-HYD-01	The hydrogen storage tanks shall have a service life of at least 20 years.	REQ-SYS-GS-15	✗	Analysis of the hydrogen tanks at a later design stage
REQ-HYD-02	The manufacturing cost of the hydrogen storage shall be no more than 70% of the total ground station manufacturing budget.	REQ-SYS-GS-16	✓	Analysis by financial analysis in Section 18.3.3
REQ-FAC-01	The ground station shall to able to accommodate at least 6 people in a waiting room.	REQ-SYS-GS-20	✓	Inspection of the GS design by the end of the chapter
REQ-FAC-02	The waiting room shall be equipped with at least one bathroom.	REQ-SYS-GS-20	✓	Inspection of the GS design by the end of the chapter
REQ-FAC-03	The manufacturing cost of the facilities shall be no more than 20% of the total ground station manufacturing budget.	REQ-SYS-GS-16	✓	Analysis by financial analysis in Section 18.3.1

18.2. Method

The Ground station design was carried out in large during the midterm phase of the report, as a great detail was required in order to carry out a fair trade-off. Following the concept selection as detailed in Section 6.1.2, the main design aspects left to be finalised were the percentage of wood used in the construction and the exact layout of the station.

18.2.1. Wood Selection & Amount

As with every asset of the aircraft design, the ground station structure is also partially made of wood. While in the United States up to 90% of residential houses still employ a wooden frame, this number is far lower as Europe, with around 20% of residential buildings in Germany utilising timber as its main construction material [66]. This is, for one, due to the unavailability of wood in comparison with other resources throughout parts of Europe (such as the Netherlands), the lower longevity of the resource when compared to stone and brick, as well as the steel-and-concrete tendencies of the Cold War era in the East of the continent. Nevertheless, construction with wood is not something unheard of in Europe, and is included in the curriculum of many architectural and civil engineering programs. As such, finding an architect and overseeing engineer with the relevant knowledge would likely not be an issue.

The wood type was selected by looking at the local availability of different species throughout Europe and their use in construction. As geographic position is one of the main factors when deciding on the wood species, it was decided that the wood type used would vary based on location to both minimise transportation distance for the raw material, as well as procure materials from smaller companies in the interest of sustainability. The species were evaluated on their historical use in buildings, their availability, and their strength.

As for the amount used, the goal was to maximise the wood percentage in the structure. Of the three main buildings present in the ground station, only the visitor lobby can incorporate wood as main construction element, as the landing platform is designed as per road regulations, and the hydrogen storage requires stronger reinforced walls in case of an emergency. Although not used as a structural element, wood can be utilised as a decorative lining on the outside of the fuel storage facility. As for the lobby, the architectural design of the station was considered when determining the amount of wood in the structure.

18.2.2. Layout and Interior Design

The layout of the ground station was done in compliance with REQ-LAN-01, REQ-OPG-01, REQ-FAC-01, and REQ-FAC-02. REQ-LAN-01 affected the positioning of the sizing and construction of the landing pad, for which the CEO of the road construction company Patishta Ltd. eng. Tsvetanka Radoslavova¹. Eng. Radoslavova quoted a cost per square meter, as well as a recommended thickness and material for the landing pad. As for the facilities, the communications are carried out via an antenna mounted on a the lobby connected to a computer inside it.

The interior design of the ground station was carried out over the course of several days and coordinated with Bulgarian architect and interior designer archt. Katerina Valkova who has designed modern interiors, yet still incorporates wood as a major stylistic element. In consultations with archt. Valkova, the main furnishing elements were picked among high quality sustainable pieces. This process was conducted over a day, with similar, dimensionally equivalent pieces being used in the 3D render of the ground station.

18.2.3. Power Supply

The power supply of the ground station is based on the design picked during the concept trade-off, namely a hydrogen-fuelled fuel cell stack. When designing the station, the power output requirement for the station was determined after obtaining the final battery capacity, considering that the station has to service 12 aircraft per day. After that, hydrogen efficiency was found, and thus the required amount of hydrogen for one day was found. After that, the hydrogen deliveries were considered, and based on the cost, environmental impact, and reserves left after a cycle of use, a delivery schedule was determined. After that, operational costs for sourcing green hydrogen were computed.

18.3. Results

As mentioned earlier, the ground station consists of three major elements - the lobby, the hydrogen fuel storage area, and the landing pad. This section delves deeper in the design of each of those elements.

¹<https://ksb.bg/member/patishta-ood/> [cited 19 June 2024]

18.3.1. The Lobby

The lobby consists of two identical modules with a capacity of 6 people excluding personnel, each with one 3-stall bathroom. The hospitality section of the module takes the shape of a square with a side of 6.1 m, and the bathroom is shaped like a one-eighth of a circle with a radius, equal to the side of the main lobby. In total, the lobby takes up an area of 102.5 m². The outer lobby walls consist of a wooden frame and a glass covering, providing a sleek and modern look, combined with the more traditional style of the wood framing. As for the interior walls, the wooden frame still persists, but the walls also have a wooden wall cladding instead of utilising glass. Overall, the lobby would utilise 6.75 m³ of wood, which would be either cedar in Southern Europe, oak in Central Europe, and pine in Northern Europe. All three tree species are often used in construction and are easily found in the aforementioned geographical regions. Furthermore, the ground station has a slanted roof in order to take into consideration weather conditions in the majority of Europe. Additionally, the ground station is connected to the electrical grid as a back-up plan in case the power issues with the hydrogen system. The lobby furnishings consist of four armchairs², one couch³, 2 coffee tables^{4 5}, and one reception desk⁶ per module, as well as three toilets and two sinks. Each unit is additionally equipped with an air conditioning unit to keep the temperature in the lobby comfortable both during the winter and the summer. A 3D model showing the ground station lobby can be seen in Figure 18.1, and the station's floor plan is available in Figure 18.2.



Figure 18.1: 3D render of the ground station lobby

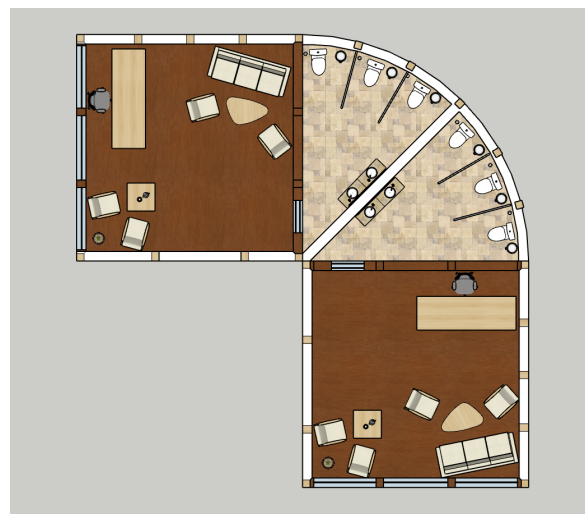


Figure 18.2: Floor plan of the ground station lobby

Overall construction is expected to cost around 1490 €/m² (150\$/ft²)⁷, or 152,725€ for the building in total, with an additional 45,000€ for the furniture, and another 20,000€ for connection to the grid. Lastly, the antenna and computer are anticipated to cost another 10,000€⁸.

18.3.2. The Landing Pad

The landing pad is equivalent to an H2 type helipad with a diameter of 24 metres inscribed into a square with the same side, with a charger installed that can be considered and equivalent to the Tesla Supercharger V4. This is in accordance with REQ-LAN-01, as this way the landing pad has a diameter larger than twice the HAROLD's largest dimension. According to the quote given by eng. Radoslavova, the cost per square meter for a 12 cm thick asphalt top layer, supported by 50 cm gravel base would be 91.6 €/m², amounting to a total cost for the construction of the landing pad of 52,760€. An additional 10,000€ are considered for costs of installing the charging port and navigational lighting as per REQ-LAN-03. The cost for the charger itself is considered to be 100,000€⁹. Additionally, since this is an equivalent to an already established product, it can be seen that it

²<https://kavehome.com/nl/en/p/turqueta-armchair-made-from-solid-teak-wood-100-fsc> [cited 22.05.2024]

³<https://kavehome.com/nl/en/p/turqueta-3-seater-sofa-made-from-solid-teak-wood-230-cm-100-fsc> [cited 22.05.2024]

⁴<https://kavehome.com/nl/en/p/turqueta-coffee-table-made-from-solid-teak-wood-70-x-70-cm-100-fsc> [cited 22.05.2024]

⁵<https://www.robustetafels.nl/tafels/eettafels/organische-eettafels/eettafel-constance/> [cited 22.05.2024]

⁶<https://mywoodream.com/> [cited 22.05.2024]

⁷<https://www.forbes.com/home-improvement/contractor/cost-to-build-a-house/> [cited 22.05.2024]

⁸https://www.eleshop.nl/aaronia-hyperlog-20300-emi-antenne-20mhz-3ghz.html?gad_source=1&gclid=CjwKCAjwg8qzBhAoEiwAWagLrNkeX4rXH3MjF2T89tLzp8cPct9UP1ERD3s0wPxbCr1qSw5wcNCEqxCuhQQAvD_BwE [cited 19 June 2024]

⁹https://techcrunch.com/2013/07/26/inside-teslas-supercharger-partner-program-the-costs-and-commitments-of-electrifying-road/?guccounter=1&guce_referrer=aHR0cHM6Ly91bi53aWtpcGVkaWEub3JnLw&guce_referrer_sig=AQAAAG3FTjPwQ-078dopE_d9_

fulfils REQ-CHA-03 and REQ-CHA-02¹⁰. Lastly, the charger is able to provide a power output of 250 kW, which would be able to charge the aircraft in 90 minutes, with a near-future upgrade that would allow them to provide up to 350 kW¹¹. Finally, an extra feature the charger used will have over the Tesla Supercharger V4 is going to be a screen that displays the charge amount. A render of the landing pad can be seen in Figure 18.3.

18.3.3. The Hydrogen Fuel System

The power system is designed to withstand the theoretical maximum power it may need to provide, namely in the case that the station has to service 12 aircraft in one 24 hour period. This working condition considers charging all 12 crafts to their full capacity, or a desired power output of twelve times the HAROLD's maximum battery capacity, amounting to 4.44 MWh. Considering that the HAROLD charges in 100 minutes, the power generated during additional 20 minutes per ground cycle is used for powering the machinery in the ground station and the lobby. The hydrogen fuel system consists of two stacked hydrogen cells, each capable of providing 110 kW of power developed by Horizon Educational¹², and 7 sets of the Multiple Element Hydrogen Gas Containers (MEGC) developed by VÍTKOVICE CYLINDERS [67]. These components take up an area of 105 m² and are to be stored in a concrete building away from the main lobby. The construction of this building would cost 32,760€¹³. Additionally, as per a quote from Horizon Educational, the price per fuel cell is 220,000€, and the price of a hydrogen storage system, similar to the MEGC is 350,000€. A compressor to regulate the pressure going into the fuel cell must be installed to raise the pressure to the required level for the fuel cell. This compressor costs a further 6,000€¹⁴. An additional 20,000€ are considered to provide all the piping and wiring to transport the hydrogen from the fuel tanks to the compressor and fuel cells. A 3D render of the outside of the hydrogen storage facility can be seen in Figure 18.4.



Figure 18.3: 3D render of the ground station landing pad



Figure 18.4: Floor plan of the ground station hydrogen storage building

18.4. Overview & Recommendations

As mentioned in the previous chapters, the ground station consists of three main components - the waiting lobby for passengers of the HAROLD, the landing platform for the eVTOL, and the hydrogen storage area. The lobby can accommodate 12 passengers, plus two staff members, and provides basic amenities, such as temperature control and two bathrooms. The landing pad is the equivalent of an H₂ helipad, with a diameter of 24 metres, and is equipped with one 250 kW charger. The hydrogen storage area contains 7 fuel tank stacks, each with the capacity to hold 315 kg of H₂ gas, as well as two 110 kW fuel cells. The total construction cost of the ground station amounts to 1,239,245€.

As for recommendations, one of the aspects not considered in this design was the construction of a special building for operators and pilots. The development and exact equipment to be in this building is to be decided, but a deeper dive into regulations and precedents on this topic is recommended. Additionally, the matter of security may be looked into, with different options for reinforced materials, personnel, and monitoring technology being examples of possible elements to be considered. Finally, further hospitality options may be explored in the future, such as larger or smaller lobby designs, food and drink options such as vending or coffee machines, and possibly even separate storage facilities for both commercial and private use.

sYqx1bmMjn3tYS0EWhfZ4x1SSR05tdwMGNwdrCM2yeuxP9gUX0ABc6RC0_UD_jUSQfw-H-5NDjZQ5S7uyWIDT7SH72DrRZUy31nmngxmH5J4rky6FpzVAqi5ENv1oC [cited 19 June 2024]

¹⁰<https://teslatap.com/articles/supercharger-superguide/> [cited 19 June 2024]

¹¹<https://www.notateslaapp.com/news/1535/tesla-confirms-v4-superchargers-will-charge-at-350kw-or-115-miles-in-5-minutes> [cited 19 June 2024]

¹²<https://www.horizoneducational.com/110kw-liquid-cooled-fuel-cell-v1-series/p1572> [cited 19 June 2024]

¹³<https://www.storable.com/resources/learn/storage-facility-construction-cost/> [cited 22.05.2024]

¹⁴<https://piston-compressor.en.made-in-china.com/product/OGxRsJXuqEca/China-Reliable-and-Versatile-Hydrogen-Silent-Air-Compressor.html> [cited 19 June 2024]

Chapter 19 | Sustainability Analysis

Because of the current climate crisis in the world, sustainability is becoming a more important criteria for a successful product. To increase sustainability, goals should be set early in the design and sustainability should be an important factor for design choices. This chapter starts with introducing the goals and requirements for the sustainability of the HAROLD. This is followed by an explanation of the measures and choices made during the design to comply with these in Section 19.1. After this in Section 19.2, an Life Cycle Assessment has been performed of the design to quantify its sustainability. Lastly, several end-of-life options to minimise the waste generation of the HAROLD are explained in Section 19.3.

19.1. Sustainability Aspects

Several system requirements were set to assure that the sustainability of the design and operations are at certain level. These are: REQ-SYS-AC-74, REQ-SYS-AC-76, REQ-SYS-AC-77 and REQ-SYS-GS-12. The two most important of these are REQ-SYS-AC-74, this states that at least 25% of the aircraft structure should be made out of wood. This is beneficial to sustainability because wood is a renewable material and stores carbon from the atmosphere. Second, REQ-SYS-GS-12 requires the carbon neutral operations of the ground station excluding charging.

Besides the requirements, sustainability was also taken into account for several trade-offs. In the concept trade-off for the eVTOL, the energy consumption was the most important criteria as this not only affects the electricity usage, but also the size of the battery which is the most polluting part of the aircraft.

In the ground station trade-off the most important criteria was the CO_2 emissions of the energy source. In contrast to REQ-SYS-GS-12, this energy source is used to charge the aircraft and the ground station.

For the materials trade-off, embedded CO_2 was one of the criteria with the highest weights. This is the amount of carbon that is emitted during the sourcing and production of the material.

The requirements and trade-off criteria resulted in many sustainable aspects of the HAROLD. The most notable aspect of sustainability in the design is the usage of wood as a structural element. Trees absorb CO_2 , the captured amount of CO_2 per kg of wood is roughly 1.72 kg^1 . Furthermore, the harvesting and refining of wood requires significantly less energy than that of current conventional aerospace materials, such as polymer composites, etc². Additionally, manufacturing products from wood causes for less carbon emissions than producing them for conventional aerospace materials³. In addition, other materials used in the aircraft are chosen in a way it minimises the carbon footprint, such as using aluminium instead of CFRP.

In order to operate in a sustainable way, the design shall incorporate batteries as power storage. There is a caveat, however, the manufacturing phase of batteries can release a significant amount of CO_2 . For reference, an 80 kWh lithium-ion battery will release between 2400 - 16000 kg CO_2 ⁴. The battery weight depends on the MTOW of the HAROLD. Because wood has a lower specific strength than conventional aerospace materials, a compromise between the amount of wood in the structure and battery size has been made. In addition, the lifetime of the battery shall be increased by reusing it for less demanding applications.

Lastly, the batteries of the HAROLD will be charged and the ground station will be powered using fuel cells running on green hydrogen. This allows the ground station to efficiently store its own green energy to not be reliant on the grid which is not fully green. This enables the HAROLD and the ground station to operate in a carbon neutral way.

19.2. Life Cycle Assessment

To quantify the sustainability of the final design, the carbon costs of the acquisition and production of the materials will be assessed for the HAROLD and ground station. The impact category that will be used in this assessment is the CO_2 emitted, as CO_2 has a large effect on climate change. The ground station will be fully powered by hydrogen, this hydrogen is sourced from green producers and because of this the only operational emissions comes from the delivery by truck of the hydrogen.

For material sourcing, the amount of CO_2 emitted per kg of material was found in several sources. With this value, the amount of CO_2 emitted can be calculated per material mass fraction of the aircraft and ground station. For the aircraft, emissions values are presented in Table 19.1. Values for the ground station are presented in Table 19.2.

¹<https://www.ecocostsvalue.com/lca/wood-lca-issues/> [cited 17.05.2024]

²http://www-materials.eng.cam.ac.uk/mpsite/interactive_charts/energy-cost/NS6Chart.html [cited 16.05.2024]

³<https://sustainability.mit.edu/article/timber-or-steel-study-helps-builders-reduce-carbon-footprint-truss-structures> [cited 16.05.2024]

⁴<https://climate.mit.edu/ask-mit/how-much-co2-emitted-manufacturing-batteries> [cited 16.05.2024]

The production of wood costs around 0.55 CO_2 per kg of wood [54]. Thus wooden planks sequester 1.17 kg CO_2 per kg. Furthermore, 1 kg aluminium emits 16.1 kg of CO_2 ⁵. Steel was estimated to have 1.63 kg CO_2 per kg embodied⁶.

For the battery and the engine of the aircraft, values for the inherent CO_2 per kg are assumed to be 25⁷ and 13 [68] respectively. For the engine, a slotless electrical motor is assumed, because of their use in eVTOLs. The values for concrete was retrieved from website⁸ and the carbon cost of asphalt was found in source⁹.

Table 19.1: LCA for the HAROLD.

Material	Weight [kg]	kg/kg CO_2	Carbon Costs [kg CO_2]
Wood	716.47	-1.17	-838.27
Aluminium	197.7	16.1	3182.97
Battery	1153.39	25	28834.75
Engine	344	13	4472
Steel	26.49	1.63	43.2
Total	2438	-	35694.7

The total mass that is accounted for in the LCA of the HAROLD is lower than its OEW, about 82.5%. Thus part of the aircraft is not accounted for in the LCA, and in real life the carbon cost per eVTOL will be higher. From Table 19.1 it can be noted that the carbon cost for the materials and manufacturing of the battery account for more than 80% of the total carbon cost. This implies that innovative battery technologies could substantially lower the carbon cost per eVTOL. Furthermore, the sequestering ability of wood has decreased the carbon cost of the eVTOL by 2.4%, whereas an other material like aluminium or CFRP would have only added to the emitted carbon.

Table 19.2: LCA for the Ground Station.

Material	Weight [kg]	kg/kg CO_2	Carbon Costs [kg CO_2]
Wood	2227.5	-1.17	-2606.2
Concrete	171543.7	0.18	30877.9
Asphalt	158976	1.37	217797.1
Steel	185605	1.63	302536.2
Total	518352.2	-	548605

The production of the hydrogen should not have any emissions. However, it must be noted that the stations are not expected to be connected to a supply line. As such, delivering the hydrogen fuel would still generate some emissions. Hydrogen delivery is usually done by truck, which emits 57 grams of CO_2 per km¹⁰ and 10 grams of CO_2 per km of shipping¹¹. It was assumed that the average truck delivery distance would be around 500 km, with an additional 13,280 km in shipping¹² that is assumed to be done every 3 months. This amounts to 28.5 kg of CO_2 per weekly delivery, and another 132.8 kg for the shipping, or 11.1 kg/week. Since the station is expected to be refuelled once a week, one can calculate that the average daily emission would be about 5.65 kg/day. As can be seen in Table 19.2 the emissions of steel are very high due to the large amounts used. In order to offset this value, hydrogen must be utilised for a prolonged time.

From Table 19.2 it can be seen that the asphalt and steel are the most polluting aspects of the ground station design. To combat this, it might be possible to utilise existing infrastructure in order to negate the use of more asphalt. Recycled asphalt can also be used to achieve this, and asphalt can be recycled many times¹³. Steel can be recycled well too and to lower the carbon cost of the steel, recycled steel can be used for the hydrogen tanks.

⁵<https://european-aluminium.eu/projets/a-low-carbon-footprint/> [cited 16.05.2024]

⁶<https://www.sustainable-ships.org/stories/2022/carbon-footprint-steel> [cited 16.05.2024]

⁷<https://fourksystems.co.uk/advice/lithium/lithiums-carbon-footprint/> [cited 19.06.2024]

⁸https://en.wikipedia.org/wiki/Environmental_impact_of_concrete [cited 19.06.2024]

⁹https://www.e3s-conferences.org/articles/e3sconf/pdf/2018/06/e3sconf_icenis2018_07001.pdf [cited 19.06.2024]

¹⁰<https://theicct.org/publication/co2-emissions-from-trucks-in-the-eu-an-analysis-of-the-heavy-duty-co2-standards-baseline-2024> [cited 20.05.2024]

¹¹<https://www.freightos.com/freight-resources/air-sea-freight-co2-emissions-calculator/> [cited 29.05.2024]

¹²<http://ports.com/sea-route/port-of-mumbai,india/port-of-rotterdam,netherlands/> [cited 29.05.2024]

¹³<https://americanasphalt.com/how-is-asphalt-paving-recycled/> [cited 24.06.2024]

19.3. End-of-Life

In order to ensure carbon emission neutrality, a plan for the aircraft parts at end-of-life (EOL) of the aircraft must be made. Various sustainable options exist for EOL, such as reusing or recycling of parts for other applications. If a part cannot be recycled, burning for energy or landfill are options, but these are undesired.

In the case of the eVTOL, the batteries and the electrical motors could be recycled for spare parts or reused in the aftermarket for applications that are less demanding in terms of performance. For this purpose, a material passport should be made for these parts. A material passport contains information about the carbon footprint, the working conditions for the extraction of raw materials, hazardous substances, and instructions for disassembly to facilitate recycling, among other details¹⁴. This is mandatory to have for batteries in the EU starting from February 2027 because of the EU Batteries Act. An effective end-of-life plan is especially important for the batteries as they have to be replaced approximately every 4 years as mentioned in Chapter 12.

All metal parts should be aimed to be recycled or reused. The metals used in the HAROLD can be fully recycled by remelting. To increase the probability of recycling parts of the eVTOL, the materials used should be easy to separate from each other. In case of the HAROLD, this was achieved by manufacturing the wings out of wood and the fuselage out of aluminium.

The chance that the wooden wings of the aircraft can be reused in aircraft is smaller, because of degradation over their lifespan. EOL options for the airframe could be downcycling to other less demanding applications. For example, the wooden structural elements could be used in the interior design industry for furniture and flooring, which do not require high-material performance. Although the production numbers of the aircraft are not expected to be high enough to supply a constant flow of wooden scrap parts, a number of unique design elements for aviation enthusiasts can still be made. Burning for energy without carbon capturing is not a suitable option, as this releases the CO_2 stored in the wood back into the atmosphere. Storing the unrecyclable parts of the aircraft in a landfill could be a viable option for the wooden structure, as the CO_2 is stored in the ground and the wood biodegrades over a period of 50 years¹⁵. Furthermore, the treatments that are used for wood are not detrimental to the environment [49].

As for the ground station, the same principles as the eVTOL apply. The ground station should be designed in a way that parts can easily be detached and used in other buildings. Wood from the ground station can be used again as a sustainable building material. The use of asphalt and steel should be minimised as the production of these materials has a higher impact on the climate, but these can be recycled too.

¹⁴<https://www.fraunhofer.de/en/press/research-news/2024/april-2024/circular-economy-a-digital-eu-product-passport-for-batteries.html> [cited 24.06.2024]

¹⁵<https://twinenviro.com/2019/10/11/how-long-does-it-take-to-decompose/> [cited 01.05.24]

Chapter 20 | Operations & Logistics

In order to render the designed aircraft and ground station functional, it is important to determine the functioning of both systems (both individually and together) and the logistics involved in their operation. This will be discussed in this chapter, with the aircraft-specific tasks found in Section 20.1 and the ground station-specific tasks found in Section 20.4.

20.1. Aircraft Operations & Logistics

In this first section, the operations and logistics that the aircraft must follow are found. This will be discussed in this chapter over three distinct mission phases: the pre-flight phase (discussed in Section 20.1.1), the in-flight phase (discussed in Section 20.2) and the post-flight phase (discussed in Section 20.3).

20.1.1. Pre-flight Phase

Before any mission can begin, it is necessary to conduct several activities to ensure that it is successful. First of all, a flight plan must be conducted by the pilot. This is required so as to verify that the destination is within the flying range of the aircraft and to check whether the weather conditions are compatible with flying. Once this step has been completed, coordination with air traffic control (ATC) is required so as to receive the clearance to fly. This is especially important for the WUAV since a large part of its missions phases will take place inside urban areas. In addition, for the parts of the flight that occur within urban areas it is necessary to also plan the take-off, climb, descent, and landing phases of the mission so as to ensure that they are compatible with the urban environment. For example, it is necessary to ensure that the aircraft does not fly too close to tall buildings or those with special security relevance.

While the pilot is busy completing the aforementioned activities, the aircraft batteries should be put to charge. Due to the high mass of the batteries (with the auxiliary one weighing 567.4 kg and the main one weighing 586 kg, as indicated in Table 12.3), it is not beneficial for the aircraft to have a removable battery design, as even though the charging process would be faster there would be many complications related to removing, replacing and storing such a battery that would balance out the potential benefits of this model. Since the turn-around time is 2 hours (as indicated by REQ-USR-08), the aircraft should be put to charge briefly after landing to ensure that the battery is sufficiently charged for the upcoming flight. Since the battery energy capacity (specified in Table 12.3) is equal to 305.5 kWh, a battery charging time of 1 hour and 30 minutes is possible if the charger specified in Section 18.3.2, which has a power of 250 kW, is used. This charging power requirement will generally be lower though, since the battery is not fully charged on each cycle to minimise degradation. As such, as long as the battery charging begins shortly after landing the charging time should not be an operational limitation to the turnaround time.

Once the charging of the battery and the coordination of activities with ATC have been completed, the final three steps of the pre-flight operations can be completed: the pre-flight checks, the passenger boarding and the platform clearance. The pre-flight checks are conducted by the pilot before any of the passengers board the plane; these involve checking the aircraft for any issues that might have been missed and checking the passengers. Due to the flight being operated privately, security activities are limited to identity checks for cross-border flights and the screening activities the operator desires to implement. Once the checks have been completed, the passengers can board the aircraft following the instructions from the pilot and any ground station crew that may be present. Finally, the ground station should be cleared for take-off whilst the pilot briefs the passengers on emergency procedures for the aircraft. With all of these pre-flight activities complete, the next phase of the mission may begin.

20.2. In-flight Phase

The second phase of the mission is the in-flight phase, which lasts from take-off until landing. As the aircraft makes its way through the previously established flight plan, the pilot must stay in contact with ATC as to avoid potential dangerous situations with other urban aerial vehicles (UAVs). In case the pre-planned flight cannot be followed due to unexpected circumstances that require deviations, the pilot must immediately contact the ATC to coordinate further actions. In order to account for any potential deviations, the aircraft is able to fly an additional 20 km beyond its maximal flight range of 200 km.

Once the aircraft is approaching its final destination, the pilot must contact the ATC for landing clearance. Upon confirmation, the aircraft may begin its vertical descent, performing a landing at the desired ground station or standard helipad. In the case where a standardised helipad is chosen for landing, the pilot must ensure that the pad is large enough to fit the aircraft. In addition, she must ensure that the platform has charging capability

that is suitable for the aircraft battery or that the aircraft has sufficient charge remaining to allow it to perform an additional flight to a charging station where charging can be handled.

20.3. Post-flight Phase

Once the aircraft has landed, the post-flight phase begins. First of all, the passengers are disembarked, and then the aircraft battery is put to charge. The pilot must then conduct a post-flight check of the aircraft and complete the post-flight documentation, reporting on the completed flight as well as the status of the aircraft. If another flight is scheduled to start at the end of the turnaround period, the ending of one flight is tied to the beginning of the following one, and all of the steps provided in the pre-flight operations discussed in Section 20.1.1 are followed once more.

20.4. Ground Station Operations & Logistics

In this section, the operations and logistics procedures that are specific to the ground station shall be discussed. Two main facets are covered: in Section 20.4.1 the power supply of the ground station is explained, and in Section 20.4.2 the amenities found at the ground station are described.

20.4.1. Power Supply

After the trade-off that was conducted in Section 6.2.4, it was decided that the ground station power supply would be sourced from hydrogen fuel cells. As such, the ground station must therefore receive a weekly supply of gaseous hydrogen. This is done by finding an external contractor that is able to provide the ground station with hydrogen that was generated using green energy; this is important as it ensures that the carbon footprint of the ground station is minimised. In order to improve the availability of green hydrogen for as many ground stations around Europe as possible, the hydrogen will be imported to major European ports (such as Rotterdam) and subsequently distributed across the continent via trucking networks. A weekly delivery of green hydrogen would cost 9,750€ due to its higher cost compared to other hydrogen varieties.

20.4.2. Amenities

The ground station's main purpose is to facilitate the landing, charging and take-off of aircraft. However, it also serves as the location in which passengers are boarded and disembarked, and as such it is necessary to ensure an adequate level of passenger comfort to incentive passengers to use the HAROLD as a transportation method. The ground station is equipped with a waiting room in which passengers can be protected from the elements while waiting to board their aircraft. In order to maximise passenger comfort, the waiting room is heated, supplied with electricity and supplied with basic amenities such as a water fountain and a vending machine. The heat, electricity and water required for this are obtained through the local energy grid of the ground station. As for the vending machine, a contract will be signed with a local contractor to refill the machine as frequently as needed.

The ground station would also require personnel to staff it, including security and a receptionist. These people would be hired via a standard working contract at a salary 33% above the minimum wage in the given country, or a salary, enough to cover the average cost of living in the given city the station is operational in - whichever is higher. This would amount to variable costs depending on the country, but for the Netherlands, this would amount to 6,526€ paid out in employee salaries.

Chapter 21 | Production Plan

The following Production plan will cover the major assembly process as well as the manufacturing of the wing and fuselage sub assemblies. Greater emphasis was placed on the the manufacturing processes involving wood as they are currently not commonly used in aerospace manufacturing. Manufacturing methods will greatly depend on exact part geometry, volume and requirements. At the current design stage part design is not available therefore the production processes selected should be understood only as a possible manufacturing route.

21.1. Production Requirements and Compliance Matrix

Table 21.1: Materials requirements compliance matrix.

Identifier	Requirement	Source(s)	Compliance	Method of verification
REQ-PRO-01	The production process of the structure shall comply with AS 9100.	REQ-SYS-AC-89, R-TEC-2	✗	Demonstration at a further design stage, see Section 21.6
REQ-PRO-02	All wooden components shall be sealed with a epoxy or polyurethane varnish	REQ-SYS-AC-74, REQ-SYS-AC-78, R-TEC-07	✓	Inspection in Section 21.3.7
REQ-PRO-03	The manufacturing cost per vehicle shall be less than 2,000,000 euros.	REQ-SYS-AC-94	✓	Inspection in Chapter 23
REQ-PRO-04	The wings shall be manufactured out of wood	REQ-SYS-AC-97	✓	Inspection in Section 21.3

21.2. Supply Chain

The following Section will discuss supply chain aspects for Wood as well as Batteries. These are the materials that we expect to pose the largest challenge for the supply chain

21.2.1. Wood Supply Chain

NACA wrote in their report about Aircraft wood "Of all the requirements of wood in aircraft, the procurement of suitable, clear, straight-grained lumber presents the most important problem" [69]. Furthermore to meet FAA guidelines selected wood has to meet MIL-S-6073 specification.[70]. Sitka spruce which is the most common aircraft wood is becoming scarce and expensive ¹. However, at the moment, a variety of suppliers are available, satisfying the material requirement of REQ-MAT-03. It takes about 40 years for Sitka spruce trees to mature for harvest, and only a fraction of them achieve the higher-grade quality necessary to meet regulatory specification². For the aforementioned reason an alternative wood species might be needed. This wood must be readily available, meet mechanical and dimensional requirements, and comply with specifications. During the detail design phase smaller and and shorter components should be preferably considered to be made out of wood as they allow for more flexibility in wood selection.

21.2.2. Battery Supply Chain

The use of a battery into the design presents supply chain challenges that could impact the overall design. The concentrated and geographically specific nature of battery material supply chains, especially for critical minerals like lithium, cobalt, and nickel, could lead to supply instability and price volatility. This situation is increased by the dominance of China in processing these materials, which adds a geopolitical risk factor. Additionally, the long lead times required for mining and refining these materials could delay production schedules. Furthermore many materials used in batteries such as cobalt, presents challenges due to ethical concerns such as child labor and conflict mining.[71]

21.3. Manufacturing of wooden wings

The wing assembly mainly consists of the skin, spars, ribs, and ailerons. The skin is typically made of flat, bent, or moulded plywood, depending on its specific location on the wing. Spars are crafted from either straight or curved laminated wood, based on their position within the wing. Ribs combine flat plywood and laminated wood. Ailerons, essentially miniature wings, adhere to the same design principles as the entire wing. The following subsections will explain how different types of plywood and laminated wood, as well as ribs, are manufactured. Additionally, the process of assembling these parts into a wing and connecting them to the fuselage will be detailed.

¹<https://www.eaa.org/aaa/aircraft-building/builderresources/while-youre-building/building-articles/wood-for-wings>. [cited 21.05.2024]

²<https://www.ox.ac.uk/news/2017-07-19-growing-better-trees-faster> [cited 21.05.2024]

21.3.1. Production of Plywood Parts

Flat plywood panels can be produced using established plywood manufacturing methods for which full solutions are commercially available. For flat skin sections, these plywood panels can be used as is, also for panels with small curvature, provided the face panels have grain orientation parallel to the bending axis. Higher curvatures can be reached by softening the wood, for instance by hot steam, and then bending it to the desired shape. To achieve very complex shapes, such as double-curved shapes, the plywood can be created in a mould so that the finished plywood panel already has the desired shape. [57]

Flat plywood panels

The main production steps of producing flat plywood panels are as follows: First, the veneers are peeled from a log; then, the veneers are inspected for defects and selected based on quality standards. Next, the veneers are dried. After drying, glue is applied, and the panels are first cold and then hot pressed. Afterwards, they are sanded down and cut to size. Before being used, the plywood must undergo a quality inspection. For this process, entire production machines are available, such as the "Full Range of Plywood Making Machine" from Shandong Gaotong Machinery Co., Ltd., priced at 300,000 USD ³

Bend Plywood

Flat plywood can be bent into a the desired shape. For this the moisture content and temperature of the plywood is increased and pressure is used to bent it to the desired shape. This can be done by for instance by soaking the veneers in water or steaming them with water vapor before bending . Small curvatures can be also achieved without softening the wood but that is only possible to relatively small curvatures. [57]

Moulded plywood

Instead of creating flat plywood, the plywood can be already created in the desired shape using a mould. This is more labour intensive but allow especially complex shapes like large radii as well as double curved parts. The moulding is mostly done using bag moulding techniques such as vacuum bag moulding. [57]. Figure 21.1 shows a schematic of a bag moulding process, the mould covered with thin veneers with glue in between them and then placed in a bag. An air tight steel shell is placed over the bag and heat and pressure is applied to shape the veneers to the mould while the glue cures. Figure 21.2 Show an moulded plywood engine faring.

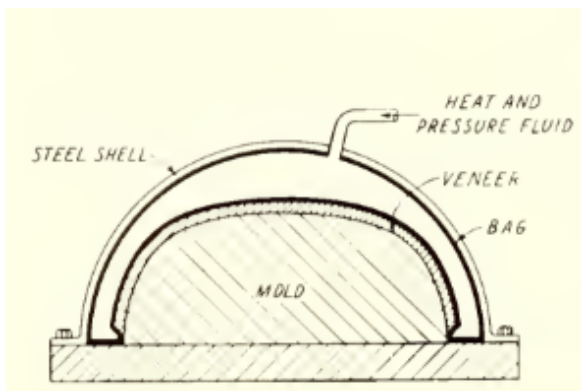


Figure 21.1: Bag moulding[57]

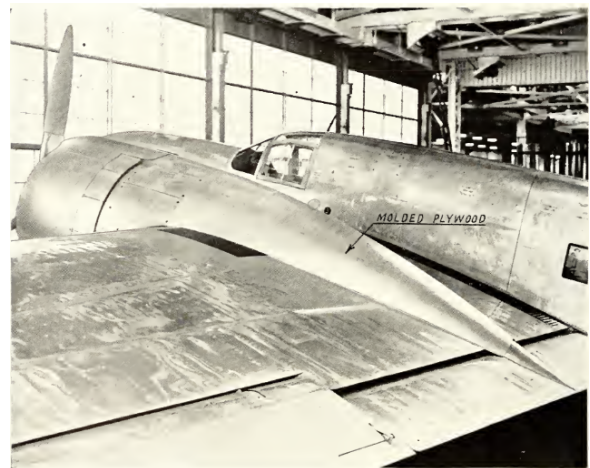


Figure 21.2: Example of moulded plywood [57]

21.3.2. Production of Laminated Wood

Laminated wood is mostly used where forces act mostly in one direction. Laminated wood can be made from veneers like plywood, but also it can be made from thicker lumber. The main reason for using laminated wood over stolid wood beams is because it is easier to guarantee the quality as inspection is simplified. Furthermore it is also easier to bend it into the desired shape. [57]

Straight Laminated members

Creating laminated wood from lumber or veneer is similar to the process used when creating plywood. The main difference is that laminated members such as spars tend to be very long requiring a unusually long press.

³<https://gtcomachinery.en.made-in-china.com/product/odPAHWECryrs/China-Full-Range-of-Plywood-Making-Machine-for-Plywood-Factory.html>

Furthermore laminated wood is usually cured without additional heat because of its increased thickness and length compared to plywood [57]. Figure 21.3 shows the gluing process for flat, long laminated stock. The veneer layers are placed upon each other with glue in between and pressure is applied through evenly spaced screw clamps.

Curved Laminated members

Creating curved laminated is similar to creating straight members. The main difficulty is in applying the pressure for gluing. Dedicate forms are required to achieve an evenly distributed gluing pressure of sufficient magnitude[57]. Figure 21.4 shows how even pressure can be evenly applied using a form.



Figure 21.3: Gluing of flat laminated stock [57]

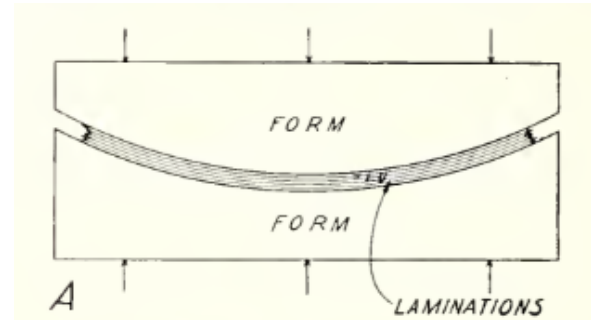


Figure 21.4: Production of curved laminated members [57]

21.3.3. Ribs

Wooden ribs are usually manufactured out of a continuous rib cap, braces and gussets. Rib caps strips and braces are placed in a jig and subsequently Gussets are spread with glue and then nailed in place. This process is called nail gluing. after completing one side the rib is flipped and the gussets are also glued on the other side [57]. Figure 21.5 shows how gussets are nail glued to the ribs with the assistance of a simple jig.



Figure 21.5: Manufacturing of wooden aircraft ribs using nail gluing [57]

21.3.4. Scarf Joints

Often the length and width of available lumber is not sufficient to create large enough veneers and lumber for the creation of plywood and laminated wood [57]. In this case Scarf joints have to be used, an example of a simple scarf joint can be seen in Figure 21.6. Furthermore Figure 21.7 shows how multiple scarf joints can be glued simultaneously, allowing for faster process times.

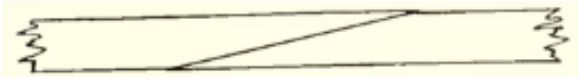


Figure 21.6: Example of a classic scarf joint [57]

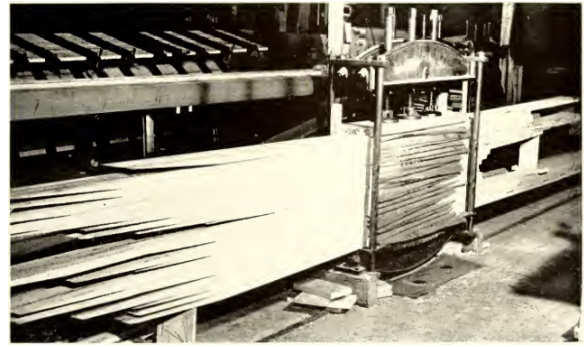


Figure 21.7: Multiple scarf joints glued at the same time [57]

21.3.5. Glue

Adhesives are widely used in the manufacturing of wooden aircraft. Not only are they essential for the creation of Plywood and Laminated wood components but also they are the most common technique used for joining wood components during assembly. Historically many different types of glues were used but now only resorcinol-formaldehyde resin is approved by the FAA for use in wooden aircraft structures [70]. It is a two-part synthetic resin adhesive consisting of resin and a hardener. Resorcinol is a costly adhesive, produced only in a few locations globally [72]. Furthermore, resorcinol requires precise joints and high clamping pressure, making it difficult to work with.

21.3.6. Assembly

Once the sub components are finished the wooden wing can be assembled. The wing can be divided into three sections: The leading edge, the section between front and back spar and the trailing edge. Elaborate jigs will be necessary to attach the ribs at correct position and angle. First the ribs of the leading edge are nail glued to the front spar. In the same jig the bend plywood leading edge skin is also attached to the ribs. Afterwards the spar with the leading attach ribs is transferred into another jig where the centre section ribs and the back spar are attached. Positioning of the trailing edge ribs can be performed in a more simple jig as the ribs are more lightweight. [57] Figure 21.8 shows a jig that allows the correct positioning of the leading edge rib section. Furthermore Figure 21.9 shows an assembly of the middle rib section to leading and trailing edge.

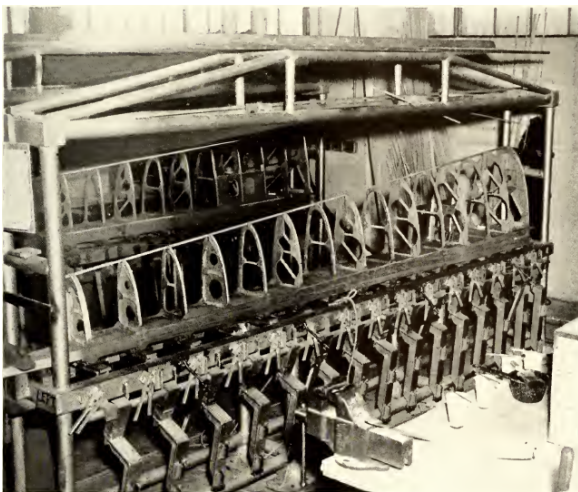


Figure 21.8: Assembly jig for attaching leading edge rib

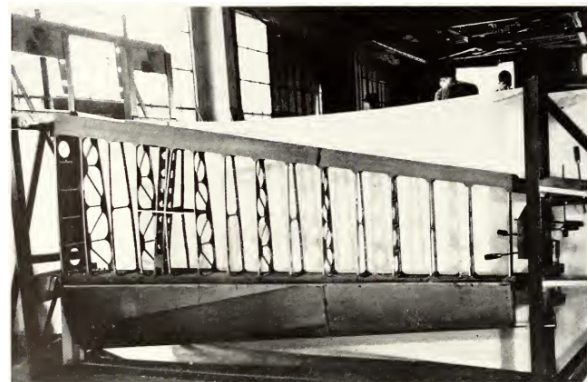


Figure 21.9: Leading and trailing edge attached with a centre section rib

21.3.7. Surface Finishing

To protect the wood from moisture, sealer has to be applied to all wooden components. For this epoxy varnishes and polyurethane varnishes can be used ⁴. To rapidly apply sealer to both inside and outside, dipping will be

⁴<https://eaavintage.org/tech-tip-wood-glues/>

used. For this the entire assembly is dipped into a large tank containing the sealer. After every dip excessive sealer is wiped off using rags. Figure 21.10 shows a wing section being dipped to sealer.

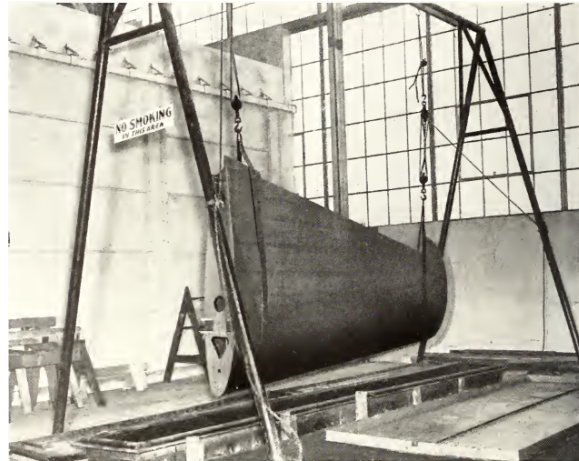


Figure 21.10: Dipping of a wing section [57]

21.4. Fuselage Production

The fuselage will be created from shaped aluminium panels which are reinforced with stiffening elements. As only conventional aerospace manufacturing methods are used, the methods will not be explained in detail. An in depth explanations of the methods used can be found in reference [73].

Skin panels The manufacturing of the skin panels from sheet metal stock largely depends on skin geometry and features. For flat sections simple shearing and cutting operations can be sufficient. While more complex double curved skin section will have to be manufactured using stretch forming. Furthermore chemical milling can be used to create more weight optimised skins.

Stiffeners For the stiffening elements various methods are available depending on geometry, features, volume and design requirements. Rubber forming is a common method for more complex stiffeners made from while simple stringers can be extruded.

Assembly Assembly will require large and riding jigs to allow the fuselage to be assembled. Most likely rivets will be used for the connecting sheet metal parts. If mechanically countersunk rivets need to be used the minimal skin thickness will be 0.8 mm⁵

21.5. Assembly Sequence

The assembly sequence of the major parts can be found in Figure A.6 . The Assembly process is separated in 4 major stages. First the main structural sub assemblies are assembled and painted, secondly they are put together from the main assembly, then electrical components are integrated, lastly interior components and miscellaneous parts are installed. For now it will be assumed that painting will be conducted before the main structure is assembled as the wooden wings and metal fuselage will need different painting methods. Furthermore it will simplify the painting process because of the smaller size of the sub assemblies.

21.6. AS9100

AS9100 is a quality management system standard specifically designed for the aerospace sector, derived from ISO 9001 and incorporating additional aerospace-specific requirements[74]. This standard is based on the the Seven Quality Management Principles, which are central to guiding organisations towards improved performance. These principles are: Customer Focus, Leadership, Engagement of People, Process Approach, Improvement, Evidence-Based Decision Making, and Relationship Management [75]. Implementing AS9100 affects manufacturing systems by enforcing rigorous quality controls, ensuring consistent production quality, and fostering a culture of continuous improvement, which are vital for aerospace manufacturing reliability and safety. Nevertheless it is premature to fully integrate AS9100 at this design stage. The current manufacturing system is based on rough planning and feasibility analysis rather than detailed process controls and company wide implementations that AS9100 requires. Full integration of AS9100 is more appropriate at later stages

⁵<https://www.eaa.org/aaa/aircraft-building/buildresources/while-youre-building/building-articles/metal/flush-riveting-tips>

when the detailed design and manufacturing processes are more defined.

21.7. Volume

Company	Production Volume
Joby Aviation ⁶	500
Archer Aviation ⁷	650
Volocopter ⁸	50+
Lilium Jet ⁹	400

Table 21.2: Production volume of promising eVTOL companies per year.

Because the eVTOL market is small at the moment and has to be established yet, it is hard to determine the demand for eVTOLs in the future. However, for the planning of the production it is important to estimate how many aircraft have to be produced every year. To estimate this, it is assumed that the demand for the HAROLD is comparable to other eVTOL designs that already have determined their production volume. The plan should account for production at full scale, which will only be reached after a few years. The numbers given for the other eVTOLS are also for full-scale production. The production volumes per year of four competing companies is given in Table 21.2. From this it is estimated that the first production plant for the HAROLD should have a capacity of approximately 500 aircraft per year. This number will be used for sizing the production system in the detail design stage.

21.8. Sustainable Manufacturing

The manufacturing process plays a crucial role in the sustainability of the HAROLD. Achieving net-zero emissions throughout our entire supply chain remains a challenging goal, yet it is critical when selecting our suppliers. It is entirely feasible for our own production plant to achieve net-zero emissions, a possibility already demonstrated by BMW with their successful establishment of a net-zero carbon emission production facility in Hungary¹⁰. To realise this, our factory will harness renewable energy sources like solar panels and wind turbines. We will prioritise energy-efficient processes and machinery to enhance our operational efficiency. Furthermore, we aim to minimise waste through recycling programs and by repurposing scrap materials where possible. Furthermore, through the process of lean manufacturing, waste will be inherently reduced as well. Additionally, we will focus on water conservation, implementing strategies such as rainwater harvesting and recycling water from process such as soaking of wood veneers or cleaning or cleaning of the exterior.

¹⁰<https://balkangreenenergynews.com/bmw-building-worlds-first-carbon-free-car-plant-in-hungary/>

Chapter 22 | Project Design and Development Logic

In order to get a complete understanding of this project, it is important to look at what the subsequent phases of the project development would be. This is shown using two tools: a project design and development logic diagram and a Gantt chart. These are discussed in Section 22.1 and Section 22.2, respectively.

22.1. Project Design and Development Logic Diagram

Should the WUAV project be continued beyond the point presented in this report, it is important to lay out a road map for what the future tasks will be. This is shown in the Project Design and Development Logic diagram, which covers all of the future phases of the project (including manufacturing, AIT, operations and EOL). The diagram can be found in Chapter A.

22.2. Gantt Chart

A Gantt chart was generated to complement the information in the Project Design and Development Logic diagram. It displays a timeline of main processes and major milestones, giving an overview of the project until the production of the first customer HAROLD. The chart can be found in Chapter A.

Chapter 23 | Financial Analysis

23.1. R&D, Manufacturing and Sales Price

To estimate the Research and Development ($R\&D$) as well as for cost the methods Explained in Part 8 of Roskams Aircraft Design [76] were selected. This method is primarily based on statistics and uses mainly systems level design parameters such as the max speed, the take off weight and number of parameters. After consultation with aerospace manufacturing technologies expert Ir. Jos Sinke A system level approach for estimating cost was determined to be the most appropriate at this design stage. Methods for determining manufacturing cost based on parts, require exact part geometry or extensive data on Part manufacturing cost. Precise geometry is not available at this stage of the design process and data about part manufacturing cost is not published by manufactures.

23.1.1. Assumptions

Table 23.1 Shows the assumptions that were used when performing the Cost analysis for R&D, Manufacturing and Sales price. Assumption A-FIN-01 is crucial as it allows us to use Roskams design methods for air planes. A-FIN-02, A-FIN-03, A-FIN-05 are based on standards assumption that can be used in case no exact values are known yet. A-FIN-04 was assumed because of the wealthy target audience. A-FIN-07 was set based on the recommendation of Dr. Baris Kumru.

Table 23.1: Assumptions used for financial analysis.

Identifier	Assumption	Effect
A-FIN-01	Harold can be assumed to be a complex airplane design	Roskam's Airplane Design method Can be used; $F_{diff} = 1.5 - 2$ (moderate to aggressive use of advanced technology)
A-FIN-02	CAD will be used in the design	$F_{cad} = 0.8$
A-FIN-03	During R&D every 3 months a Test aircraft will be produced	$N_{rr} = 0.33$
A-FIN-04	Aircraft interior is of a similar quality as the interior of a Private Jet	$F_{int} = 3000$
A-FIN-05	10% Profit will be earned on the R&D program as well as for every build Harold aircraft	$F_{pro} = 0.1$
A-FIN-06	Cost for flight test during manufacturing programme is negligible	$C_{ftom} = 0$
A-FIN-07	The Manufacturing program will last 20 years	$M_{len} = 20$

Table 23.2 shows all input parameters that were used for the Cost analysis. Values are given in SI units and EUR values but were converted into the appropriate units when applying Roskams design method. W_{MTO} , V_{cruise} , N_{pax} , $C_{Propulsion}$, $C_{Battery}$, $C_{Avionics}$ are design Values taken form the current iteration. For N_{rdte} , N_{st} , F_{fin} the recommended ranges from Roskam were taken, for the Baseline the mean values were Assumed. The hourly rates for Engineering, Manufacturing and Tooling R_e , R_m , R_t were taken from Roskam and converted to current rates using cost escalation factors as described in Roskams airplane design method [76]. To account for local variation, rates were varied by $\pm 25\%$, as recommended by Roskam [76]. The judgement factor F_{diff} greatly affects the cost estimation. It judges the difficulty of the design on a scale from 1 (Conventional air plane) to two (very aggressive use of advance technology). For the baseline $F_{diff} = 2$ was assumed because of the combination of electrical propulsion and VTOL capabilities. It can be argued that because of the maturing eVTOL market and advances in eVTOL research the technology can be classified as less advanced and therefore $F_{diff} = 1.5$ was used as the lower bound for the range. Similarly F_{mat} is a correction factor for the used material, ranging from conventional aluminium alloys ($F_{mat} = 1$) to carbon composites ($F_{mat} = 3$). For the base line was assumed $F_{mat} = 2$ was chosen. Wood has similar difficulty to carbon fibre composites in design and manufacture but the Fuselage is mainly created from conventional alloys. It can be argued that because of the simplicity of manufacturing with wood in small series offsets the added design difficulty. On the other side it can be also argued that because of less information and research being available for wood usage in aerospace application the design is more difficult than that of carbon fibre composites. For large-scale production, fully automated processes capable of producing high-quality wooden components are not available. Therefore achieving the desired quality for mass production of wooden parts might prove more challenging compared to manufacturing with composites. For the aforementioned reasons the full range of 1 to 3 will be considered.

Table 23.2: Input parameters used for calculating cost.

Name	Description	Baseline	Range	Unit
W_{MTO}	Max take off weight	3553.90	3553.90	Kg
V_{cruise}	Max speed	250	250	Km/h
N_{pax}	Number of Passengers	6	6	-
$C_{Propulsion}$	Cost propulsion system	702,000.00	702,000.00	EUR
$C_{Battery}$	Cost Battery	60,000.00	60,000.00	EUR
$C_{Avionics}$	Cost avionics	93,000.00	93,000.00	EUR
N_{rdte}	Number of Test aircraft	4	2 - 8	-
N_{st}	Number of static test	2	2 - 0	-
N_{rr}	Test aircraft production rate	0.33	0.33	-
F_{diff}	Judgement factor for complexity	2	1.5 - 2	-
F_{cad}	Judgement factor for usage of computer assisted design	0.8	0.8	-
F_{mat}	Correction factor for material	2	1 - 3	-
F_{int}	Factor for interior cost	3000	3000	USD (1990)
F_{pro}	Factor for profit	10%	10%	-
F_{fin}	Factor for financing cost	0.15	0.1 - 0.2	-
R_e	Rate for hour engineering	118.36	88.77 - 147.95	EUR
R_m	Rate for hour manufacturing	69.04	51.78 - 86.31	EUR
R_t	Rate for hour tooling	88.77	66.58 - 110.97	EUR
USD to EUR	USD to EUR exchange rate [†]	0.93	0.93	-
M_{len}	Length of manufacturing programme	20	20	years

Figure 23.1 shows how the unit cost changes depending on the production volume per year assuming a total production program length of 20 years. We can see that as the volume increases the sales price per unit degrees. This is because the R&D cost can be distributed over a larger amount of sales.

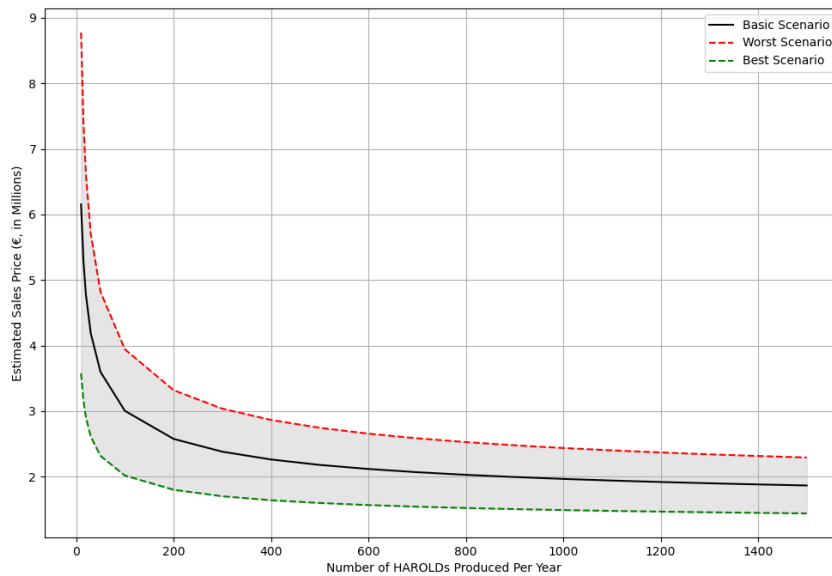


Figure 23.1: Estimated Sales Price of eVTOLs Production per Year

23.1.2. Cost Breakdown

This subsection shows the cost breakdown for the assumed yearly production volume of 500 HAROLD's per year as determined in Chapter 21. Table 23.3 shows the cost break down for the Research, Development, Testing and Evaluation cost. Table 23.4 Shows the cost breakdown for the manufacturing program. Table 23.3 shows the cost break down for the research, development, testing and evaluation cost .Table 23.6 shows the sales price breakdown for a single HAROLD. Finally Figure 23.2 shows the break even point assuming the baseline sales price and a production volume of 500 units for 20 years.

Table 23.3: RDTE cost analysis (values in thousands of Euros).

Name	Description	Baseline (€, in thousands)	Range (€, in thousands)
C_{aed_r}	Airframe Engineering and Design Cost	10,469	5,187 - 14,856
C_{dst_r}	Development Support and Testing Cost	2,176	1,284 - 2,766
C_{fta_r}	Flight Test Aircraft Cost	101,663	42,783 - 179,981
C_{fto_r}	Flight Test Operation Cost	413	128 - 2,442
C_{tsf_r}	Test and Simulation Facilities Cost	17,649	0 - 80,018
C_{fin_r}	Cost to Finance the RDTE Phases	26,474	6,173 - 80,018
C_{RDTE}	Total Cost for RDTE	158,844	55,555 - 360,079

Table 23.4: Manufacturing cost analysis manufacturing (values in millions of Euros).

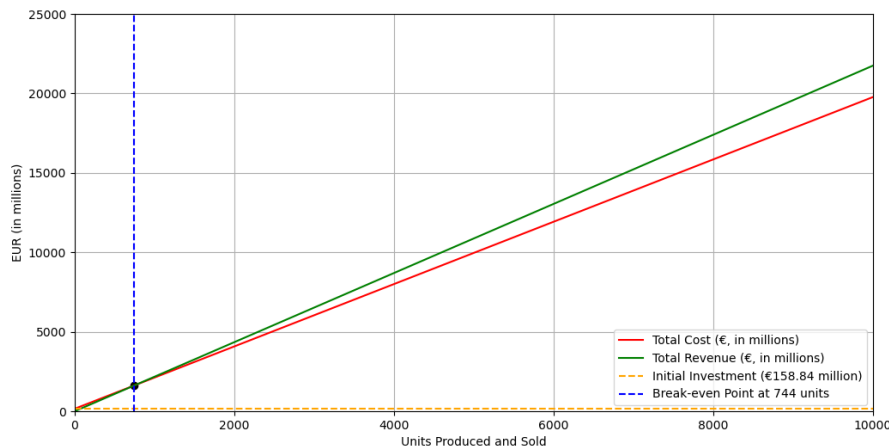
Name	Description	Baseline (€, in thousands)	Range (€, in millions)
C_{aed_m}	Additional Engineering and Design Cost	43,830	24,650 - 54,790
C_{apc_m}	Aircraft Production Cost	16,626,160	12,992,410 - 19,573,640
C_{fin_m}	Cost of Financing the Manufacturing Program	2,941,760	1,446,340 - 4,907,110
C_{man}	Cost of Manufacturing	19,611,750	14,463,400 - 24,535,540

Table 23.5: Production cost breakdown per unit (values in thousands of Euros).

Name	Description	Baseline (€, in thousands)	Range (€, in thousands)
C_{eam}	Cost for Propulsion, Battery and Avionics	855	855 - 855
C_{intm}	Interior Cost	34.46	34.46 - 34.46
C_{manm}	Manufacturing Labour Cost	295.72	167.18 - 367.00
C_{matm}	Material Cost	423.09	211.69 - 633.89
C_{toolm}	Tooling Cost	15.90	9.17 - 19.30
C_{qcm}	Quality Control Cost	38.44	21.73 - 47.71
C_{apcm}	Aircraft Production Cost	1,662.62	1,299.24 - 1,957.36

Table 23.6: Sales price per unit.

Name	Description	Baseline (€, in thousands)	Range (€)
C_{RDTE_u}	RDTE Cost per Unit	15.88	5.55 - 36.00
C_{man_u}	Manufacturing Cost per Unit	1,961	1,446 - 1,957
C_{Pro_u}	Profit per Unit	197.70	145.18 - 199.33
AEP	Sales Price Per Unit	2,174	1,597 - 2,738

**Figure 23.2:** Break even point and total cost/revenue

23.1.3. Validity

Carugo compares Roskam's method with the sales prices reported by eVTOL manufacturers. He shows that Roskam's method deviated between +7.42% and -8.58% compared to the reported price estimates [77]. The estimated prices from eVTOL manufacturers must be approached with caution. For instance, while Lilium initially indicated a sales price of 2.5 million for their 7-seater in 2021², it ultimately announced that its first jets at a price tag of 10 million³, quadrupling their initial estimated price.

²<https://www.flightglobal.com/aerospace/lilium-puts-25-million-price-tag-on-initial-jets/143724.article>

³<https://www.flyingmag.com/liliums-pioneer-edition-jet-hits-u-s-market-with-launch-of-private-sales/>

Chapter 24 | Conclusion

In this report, the design process and results regarding the electrically powered VTOL aircraft named **HAROLD** (Hovering Aerial paRtially wOoden Lift-off Device) is presented. Due to the current increase in interest of VTOL aircraft, along with increased concern for sustainability, a new sustainable design can enter the market. As current VTOL aircraft are already mostly electrically powered, it is with the structural elements of the design where the sustainability can be further increased. With this, the **HAROLD** represents a groundbreaking advancement in the VTOL market, seamlessly integrating sustainability with cutting-edge aviation technology by utilising wood as its main structural element. This not only significantly reduces the environmental impact during production but also ensures a superior end-of-life process, making **HAROLD** a more sustainable alternative compared to its current eVTOL contenders. In the end, the design was able to achieve a wooden structural mass fraction of 73%.

The inclusion of a hydrogen-powered ground station further enhances the **HAROLD**'s green credentials. By utilising hydrogen fuel cells and incorporating efficient hydrogen storage solutions, the ground station exemplifies a commitment to renewable energy sources and operational efficiency. Not only that, but the ground station infrastructure incorporates wood to a maximum possible amount as well.

From the design process, the **HAROLD** is capable of carrying 6 passengers including pilot over a maximum range of 200 km. Furthermore, the cruise speed can reach velocities of 900 km/h. Therefore, the **HAROLD** is a strong competitor to current short range private jets and is expected to perform well in corporate and private luxury markets where people prioritise the sustainability aspects of their products. Not only that, but safety has been a main concern during the design process. Even with one engine inoperative can the **HAROLD** still operate and hover to ensure the safety of its passengers.

Due to time limitations, the design of the **HAROLD** has yet to be fully detailed. In order to achieve a fully detailed design, the following recommendations have been made. Firstly, some subsystems need to be incorporated into the complete design. These are for example, the rotational mechanism operating during the transitional phases, or the fire retarding system incorporating within electrical subsystems. The thermal management system should also be sized in more detail, since it could become limiting for such a power intensive application.

Secondly, more detailed design tools can be used in order to achieve a better design. With these design tools, complex interactions between subsystems and flow phenomena can be analysed and understood to a better degree. Recommendations in this area are: the influence of the propulsion system on wing performance and vice versa, the influence of the interaction of the propeller blade tips interference. For structural analysis, the mass from the mechanical fasteners can be included when calculating the total structural mass. Also the crippling of wooden beams is something to be analysed. Another point in this area if performing a thorough thermal analysis to see what points of the aircraft are critical. This links back to the fire retarding subsystem again as well. For this, coolant type and battery interaction could be considered.

Finally, rigorous testing of subsystems as specified in each chapter should be completed to verify each requirement. These should include testing of normal operations to see if they achieve the desired performance. Other than normal testing, extreme limit testing should be performed to better understand where the aircraft will fail.

HAROLD's design prioritises both environmental responsibility and high performance, positioning it as a formidable contender in the VTOL market. Its unique combination of sustainability, advanced engineering, and practical utility offers an unparalleled solution for eco-conscious air travel. As the industry moves towards greener technologies, **HAROLD** emerges as the best option for those seeking an environmentally friendly, efficient, and reliable VTOL aircraft.

References

- [1] del Cahno J., Cecelja I., van Egmond M., Hakk H., Lazzaroli E., Michielsen M., Radoslavova T., Rato A., Skrobisz F. and Wilbrink M. *WUAV: Wooden Urban Air Mobility Vehicle Midterm Report*. Version 2.0. Technische Universiteit Delft Faculty of Aerospace Engineering, May 2024.
- [2] Peter Jones. 'The evolution of urban mobility: The interplay of academic and policy perspectives'. In: *IATSS Research* 38.1 (2014), pp. 7–13. ISSN: 0386-1112. DOI: <https://doi.org/10.1016/j.iatssr.2014.06.001>. URL: <https://www.sciencedirect.com/science/article/pii/S038611121400017X>.
- [3] F.M. Nizam Uddin Khan, Mohammad G. Rasul, A.S.M. Sayem and Nirmal Mandal. 'Maximizing energy density of lithium-ion batteries for electric vehicles: A critical review'. In: *Energy Reports* 9 (2023). Proceedings of 2022 7th International Conference on Renewable Energy and Conservation, pp. 11–21. ISSN: 2352-4847. DOI: <https://doi.org/10.1016/j.egyrs.2023.08.069>. URL: <https://www.sciencedirect.com/science/article/pii/S2352484723012118>.
- [4] Sofia Pinheiro Melo, Felipe Cerdas, Alexander Barke, Christian Thies, Thomas S. Spengler and Christoph Herrmann. 'Life Cycle Engineering of future aircraft systems: the case of eVTOL vehicles'. In: *Procedia CIRP* 90 (2020). 27th CIRP Life Cycle Engineering Conference (LCE2020) Advancing Life Cycle Engineering : from technological eco-efficiency to technology that supports a world that meets the development goals and the absolute sustainability, pp. 297–302. ISSN: 2212-8271. DOI: <https://doi.org/10.1016/j.procir.2020.01.060>. URL: <https://www.sciencedirect.com/science/article/pii/S2212827120301062>.
- [5] S.R. Naqvi, H. Mysore Prabhakara, E.A. Bramer, W. Dierkes, R. Akkerman and G. Brem. 'A critical review on recycling of end-of-life carbon fibre/glass fibre reinforced composites waste using pyrolysis towards a circular economy'. In: *Resources, Conservation and Recycling* 136 (2018), pp. 118–129. ISSN: 0921-3449. DOI: <https://doi.org/10.1016/j.resconrec.2018.04.013>. URL: <https://www.sciencedirect.com/science/article/pii/S0921344918301502>.
- [6] Lloyd Watson. 'Zero emission future urban air transport – who has the lead?' In: (2023). URL: <https://www.hka.com/zero-emission-future-urban-air-transport-who-has-the-lead/>.
- [7] Carlos Collantes Rivero. 'The current state of the eVTOL industry'. In: *Medium* (2023). URL: <https://medium.com/@cecollantes/the-current-state-of-the-evtol-industry-a-personal-view-be3707db967e>.
- [8] European Union Aviation Safety Agency. *Special Condition for small-category VTOL-capable aircraft*. June 2024.
- [9] Rob E. Wolleswinkel, Reynard de Vries, Maurice Hoogreef and Roelof Vos. 'A New Perspective on Battery-Electric Aviation, Part I: Reassessment of Achievable Range'. In: *American Institute of Aeronautics and Astronautics (AIAA)*, Jan. 2024. DOI: 10.2514/6.2024-1489.
- [10] Roskam J. *Airplane Design Part I: Preliminary Sizing of Airplanes*. DARcorporation, 1985. ISBN: 9789993249603.
- [11] Yue Deng, Aaron J. Ridley and Wenbin Wang. 'Effect of the altitudinal variation of the gravitational acceleration on the thermosphere simulation'. In: *Journal of Geophysical Research: Space Physics* 113 (9 Sept. 2008). ISSN: 21699402. DOI: 10.1029/2008JA013081.
- [12] Tengfei (Tim) Zhang, Jinsong Dong and Sumei Liu. 'Modeling and Measuring the Leaked-Air Rate into the Insulation Layer of a Single-Aisle Aircraft Cabin'. In: *Buildings* 12.5 (2022). ISSN: 2075-5309. DOI: 10.3390/buildings12050652. URL: <https://www.mdpi.com/2075-5309/12/5/652>.
- [13] Schiktanz D. 'Conceptual Design of a Medium Range Box Wing Aircraft'. Hochschule für Angewandte Wissenschaften Hamburg, 2021.
- [14] Raymer D.P. *Aircraft Design: A Conceptual Approach*. American Institute of Aeronautics & Astronautics, 1992. ISBN: 978-0930403515.
- [15] Oliviero F. 'Aerospace Design and Systems Engineering Elements II AE2111-II aircraft part, Aircraft aerodynamic analysis–Estimation of Lift & Drag'. In: (2022).
- [16] Dieter Scholz. 'Empennage sizing with the tail volume complemented with a method for dorsal fin layout'. In: *INCAS BULLETIN* 13.3 (Sept. 2021), pp. 149–164. DOI: 10.13111/2066-8201.2021.13.3.13.
- [17] Vos R. and Hoogreef M. *Aerospace Design and Systems Engineering Elements I*. AE1222-II Aerospace Design & Systems Engineering Elements. 2022. URL: <https://brightspace.tudelft.nl/d21/le/content/407821/viewContent/2282380/View>.
- [18] Mohammad H. Sadraey. 'Design of Control Surfaces'. In: *Aircraft Design: A Systems Engineering Approach*. John Wiley & Sons, Ltd, 2013, pp. 685–713.

- [19] *Lift-curve slope and aerodynamic centre position of wings in inviscid subsonic flow*. Engineering Sciences Data Unit, 1977.
- [20] Fabrizio Nicolosi, Danilo Ciliberti, Pierluigi Vecchia, Salvatore Corcione and Vincenzo Cusati. 'A comprehensive review of vertical tail design'. In: Sept. 2016, p. 7. DOI: 10.13140/RG.2.2.12606.69448.
- [21] Irfan Nazir Wani, Balendra Bhaskar, Shourabh Singh Raghuwanshi, Nitesh Kushwah, Yogesh Agrawal, Abhinav Kumar, Anish Pandey and Bhavana Ayachit. 'Design & analysis of NACA 0012 airfoil with circular dent of 30 mm depth on upper surface'. In: *Materials Today: Proceedings* (2023). ISSN: 2214-7853. DOI: <https://doi.org/10.1016/j.matpr.2023.05.013>. URL: <https://www.sciencedirect.com/science/article/pii/S2214785323026342>.
- [22] Lai C. H. and N Kamaruddin. 'Effect of fuselage diameter on aerodynamic characteristics for straight wing at low and high aspect ratio'. In: *IOP Conference Series: Materials Science and Engineering* (2018). DOI: 10.1088/1757-899X/370/1/012055.
- [23] Mondher Yahyaoui. 'A New Method for the Prediction of the Downwash Angle Gradient'. In: *International Journal of Aviation, Aeronautics, and Aerospace* 46 (2019), p. 19.
- [24] D. Scholz M. Nita. 'Estimating the Oswald factor from basic aircraft geometrical parameters'. In: *Deutscher Luft- und Raumfahrtkongress 2012* (2012). DOI: 10.2514/6.2016-3522.
- [25] T Bouquet and R. Vos. 'Modeling the Propeller Slipstream Effect on Lift and Pitching Moment.' In: *55th AIAA Aerospace Sciences Meeting: Grapevine, Texas Article AIAA 2017-0236 American Institute of Aeronautics and Astronautics Inc. (AIAA)*. (2017). DOI: 10.2514/6.2017-0236.
- [26] Michael D. Patterson and Nicholas K. Borer. *Approach Considerations in Aircraft with High-Lift Propeller Systems*. American Institute of Aeronautics & Astronautics, 2017. DOI: 10.2514/6.2017-3782.
- [27] Shamsheer S. Chauhan and Joaquim R. R. A. Martins. 'Tilt-wing eVTOL takeoff trajectory optimization'. In: *Journal of Aircraft* 57 (2020). DOI: 10.2514/1.C035476..
- [28] R. T. Cliffe C. F. Heddleson D. L. Brown. *Summary of Drag Coefficients of Various Shaped Cylinders*. GENERAL ELECTRIC ATOMIC PRODUCTS DIVISION AIRCRAFT NUCLEAR PROPULSION DEPARTMENT, Apr. 1957.
- [29] Illia Kryvokhatko. *Kryvokhatko Aerodynamics of Tandem Wing Aircraft From Dinosaurs to UAVs and Supersonic Planes*. Springer, 2023.
- [30] David C. Wilcox. *Turbulence Modeling for CFD*. 3rd edition. DCW Industries, 2006. ISBN: 9978-1-928729-08-2.
- [31] Adelphi Terrace. *TRANSACTION SOF THE INSTITUTION OF NAVAL ARCHITECTS*. University of Michigan, 1865.
- [32] Frank Anton, Olaf Otto, Head Sales, Business Development, Thierry Olbrechts, Simcenter Aerospace, Julia Hetz and Marketing Manager. *Presentation on behalf of Siemens Next47 Digital Factory PLM Software Simulation & Testing Solutions*. 2018.
- [33] *P400 R Electric Motors Product Sheet*. URL: www.yasa.com.
- [34] Jack E Made and Donald W Kurtz. *N A Review of Aerodynamic Noise From Propellers, Rofors, and Liff Fans*. 1970.
- [35] Carsten Braun, D Felix Finger, Falk Goetten and Cees Bil. *Cost Estimation Methods for Hybrid-Electric General Aviation Aircraft*. 2019. URL: <https://www.researchgate.net/publication/337757069>.
- [36] Yi Liu, Cameron T Druyor and Li Wang. *High-Fidelity Analysis of Lift+Cruise VTOL Urban Air Mobility Concept Aircraft*. URL: <https://HighFidelityCFDVerificationWorkshop.github.io;>
- [37] Juho Ilkko, Elomatic / Finflo and Timo Siikonen. *Simulation of a helicopter rotor flow*. 2011. URL: <https://www.researchgate.net/publication/273961236>.
- [38] Lukas Mauler, Fabian Duffner, Wolfgang G. Zeier and Jens Leker. 'Battery cost forecasting: a review of methods and results with an outlook to 2050'. In: *Energy Environ. Sci.* 14 (9 2021), pp. 4712–4739. DOI: 10.1039/D1EE01530C. URL: <http://dx.doi.org/10.1039/D1EE01530C>.
- [39] Mehmet Efe Balli. 'eVTOL Aircraft Conceptual Design and Optimization'. MA thesis. 2020.
- [40] N.M. Kuprikov. 'International standard atmosphere - a tool for technological measurement sovereignty in the aerospace industry'. In: *E3S Web of Conferences* 460 (Dec. 2023). DOI: 10.1051/e3sconf/202346007022.
- [41] Daberechi David Agwu, Felix Opara, Nkwachukwu Chukwuchekwa, Damian Dike and Lazarus Uzoечи. 'Review Of Comparative Battery Energy Storage Systems (Bess) For Energy Storage Applications In Tropical Enviroments'. In: (Sept. 2018).

- [42] Ali Asef, Iman Chitsaz and Navid Madani. 'Modeling and total cost optimization of battery thermal management system in a hybrid electric vehicle'. In: *Journal of Energy Storage* 52 (2022), p. 104844. ISSN: 2352-152X. DOI: <https://doi.org/10.1016/j.est.2022.104844>. URL: <https://www.sciencedirect.com/science/article/pii/S2352152X22008519>.
- [43] Dongho Koo, Bomee Kwon, Jeonghyeop Lee and Kyu Lee. 'Asymmetric behaviour of Li/Li symmetric cells for Li metal batteries'. In: *Chemical Communications* 55 (July 2019). DOI: 10.1039/C9CC04082J.
- [44] Sina Lohrasbi, René Hammer, Werner Eßl, Georg Reiss, Stefan Defregger and Wolfgang Sanz. 'A Comprehensive Review on the Core Thermal Management Improvement Concepts in Power Electronics'. In: *IEEE Access* 8 (Sept. 2020). DOI: 10.1109/ACCESS.2020.3021946.
- [45] R. Kovács. 'Heat equations beyond Fourier: From heat waves to thermal metamaterials'. In: *Physics Reports* 1048 (2024). Heat equations beyond Fourier: From heat waves to thermal metamaterials, pp. 1–75. ISSN: 0370-1573. DOI: <https://doi.org/10.1016/j.physrep.2023.11.001>. URL: <https://www.sciencedirect.com/science/article/pii/S0370157323003770>.
- [46] Reynard de Vries, Rob E. Wolleswinkel, Maurice Hoogreef and Roelof Vos. 'A New Perspective on Battery-Electric Aviation, Part II: Conceptual Design of a 90-Seater'. In: American Institute of Aeronautics and Astronautics (AIAA), Jan. 2024. DOI: 10.2514/6.2024-1490.
- [47] Forest Products Laboratory (U.S.); United States. Army-Navy-Civil Committee on Aircraft Design Criteria.; United States. Aeronautical Board. *ANC-18 Design of Wood Aircraft Structures*. 1944. DOI: 0.5479/sil.1018746.39088017549809.
- [48] Civil Aviation Safety Authority, Australian Government. *AWB 02-011 Issue 2 - Timber, Plywood and Adhesives for Aircraft Use*. Mar. 2021. DOI: 0.5479/sil.1018746.39088017549809.
- [49] Gedeon G. *Wood Handbook*. Forest Products Laboratory, 1999.
- [50] Salim Hizoroglu. 'Strength Properties of Wood for Practical Applications'. In: (2016).
- [51] Ridley-Ellis D. *Rate of growth*. Napier University Centre for Wood Science & Technology Blog. Accessed: 2024-05-22. 2016. URL: <https://blogs.napier.ac.uk/cwst/speed-of-growth/>.
- [52] L.J. Markwardt. *aircraft woods: their properties, selection and characteristics*. Tech. rep. Forest Product Laboratory, 1931.
- [53] Karr U., Fitzka M., Schönbauer B.M., Krenke T., Müller U. and Mayer H. 'Fatigue testing of wood up to one billion load cycles'. In: *Holzforschung* 76.11-12 (2022), pp. 977–984. DOI: doi:10.1515/hf-2022-0111. URL: <https://doi.org/10.1515/hf-2022-0111>.
- [54] Richard Bergman, Maureen Puettmann, Adam Taylor and Kenneth E. Skog. 'The Carbon Impacts of Wood Products'. In: *Forest Products Journal* 64.7–8 (Dec. 2014), pp. 220–231. ISSN: 0015-7473. DOI: 10.13073/fpj-d-14-00047. URL: <http://dx.doi.org/10.13073/FPJ-D-14-00047>.
- [55] BNP Media. *The Embodied Energy in Wood Products*. https://continuingeducation.bnpmmedia.com/article_print.php?C=754&L=221. Accessed: 2024-05-22.
- [56] Paul Tarisai Mativenga Norshah Aizat Shuaib. 'Carbon Footprint Analysis of Fibre Reinforce Carbon Composite Recycling Processes'. In: *Elsevier* (2017).
- [57] *ANC Bulletin: Wood Aircraft Inspection and Fabrication*. Issued under the supervision of the Aeronautical Board. Washington, D.C.: United States Government Printing Office, Dec. 1944.
- [58] Ansys. *Granta materials library*. 2024. URL: <https://www.ansys.com/resource-center/brochure/granta-data-products-overview>.
- [59] Hibbeler R.C. *Mechanics of Materials*. 10th SI edition. Pearson Education, 2018.
- [60] Megson T.H.G. *Aircraft Structures for Engineering Students*. 6th edition. Elsevier Ltd, 2016.
- [61] Wang C. and Holzapfel F. 'EVALUATION OF AIRCRAFT BRAKING PERFORMANCE BASED ON OPERATIONAL FLIGHT DATA'. In: *31st Congress of the International Council of the Aeronautical Sciences* (2018).
- [62] Sadraey M. *Aircraft Design: A System Engineering Approach*. Wiley, 2012. Chap. Landing gear design, pp. 508–581.
- [63] Jeevanantham V., Vadivelu P. and Manigandan P. 'Material Based Structural Analysis of a Typical Landing Gear'. In: *IJISSET - International Journal of Innovative Science, Engineering & Technology* 4 (4 2017), pp. 295–300.
- [64] Torenbeek E. *Synthesis of Subsonic Airplane Design*. Springer-Science+Buisness Media B.V., 1982. ISBN: 978-90-481-8273-2. DOI: 10.1007/978-94-017-3202-4.

- [65] European Union Aviation Safety Agency. *Proposed Means of Compliance with the Special Condition VTOL*. EASA, 2020.
- [66] Christian Mergel, Klaus Menrad and Thomas Decker. 'Wood or not? An analysis of regional differences in wooden residential building permits in Germany'. In: *Journal of Cleaner Production* 376 (2022), p. 134328. ISSN: 0959-6526. DOI: <https://doi.org/10.1016/j.jclepro.2022.134328>. URL: <https://www.sciencedirect.com/science/article/pii/S0959652622039002>.
- [67] VÍTKOVICE CYLINDERS. 2024.
- [68] Nisarg Dave, Xuebei Zhang, Zeyuan Xu, David Gerada, He Zhang, Jing Li, Gaurang Vakil and Chris Gerada. *Carbon Emission Comparison of Slotted and Slotless Motors for eVTOL Application*. 2022. DOI: 10.1109/ITEC53557.2022.9813759.
- [69] L. J. Markwardt. *Aircraft Woods: Their Properties, Selection, and Characteristics*. Tech. rep. 354. National Advisory Committee for Aeronautics. United States Department of Agriculture, Madison, WI: Forest Products Laboratory, 1931.
- [70] Federal Aviation Administration. *Acceptable Methods, Techniques, and Practices: Aircraft Inspection and Repair*. Advisory Circular AC 43.13-1B. Change 1, Initiated by AFS-640. Washington, D.C.: U.S. Department of Transportation, Sept. 1998. URL: https://www.faa.gov/documentLibrary/media/Advisory_Circular/AC_43.13-1B.pdf.
- [71] *Global Supply Chains of EV Batteries*. Tech. rep. International Energy Agency, 2022.
- [72] Pizzi A. *Advanced Wood Adhesives Technology*. First edition. CRC Press, 1994. DOI: 10.1201/9781482293548.
- [73] Jos Sinke. *AE3211 II Production of Aerospace systems Reader*. 2023.
- [74] *AS9100D:2016, Quality Management Systems - Requirements for Aviation, Space, and Defense Organizations*. Executive Overview provided by Perry Johnson Consulting, Inc. Perry Johnson Consulting, Inc. Troy, Michigan, Apr. 2017. URL: www.pjcinc.com.
- [75] *Quality Management Principles*. Available from ISO, ISO Central Secretariat, Chemin de Blandonnet 8, Case Postale 401, CH-1214 Vernier. International Organization for Standardization. Geneva, Switzerland, 2015. URL: <http://www.iso.org>.
- [76] Jan Roskam. *Airplane Design Part VIII: Airplane Cost Estimation: Design, Development, Manufacturing and Operating*. Lawrence, KS: DAR Corporation, June 2018.
- [77] Daniele Carugo. 'Development and Production Costs Estimation Methodology for eVTOL'. Supervised by Davide Ferretto. Master's Thesis. Turin, Italy: Politecnico di Torino, Apr. 2024.

Appendix A | Large Diagrams

This appendix includes the large organisational diagrams. The Functional Breakdown Structure diagram is given by Figure A.1. The Functional Flow Diagram, instead, is covered by Figure A.2 and Figure A.3. In Figure A.4, the Project Design and Development Logic diagram is provided. Finally, the Gantt chart corresponding to the project design and development logic diagram is given in Figure A.5.

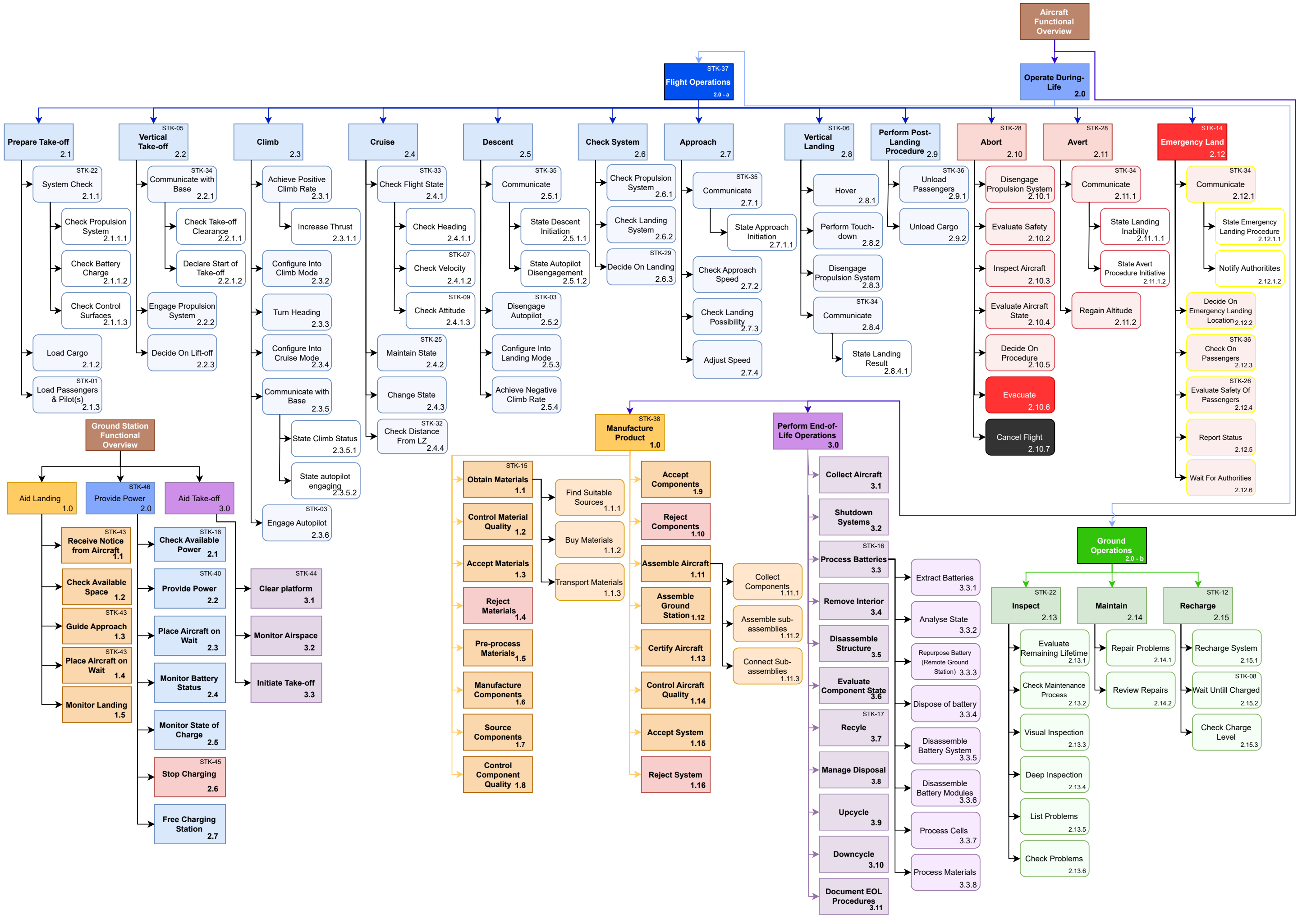


Figure A.1: The Functional Breakdown Structure diagram.

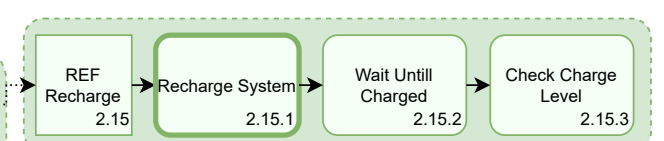
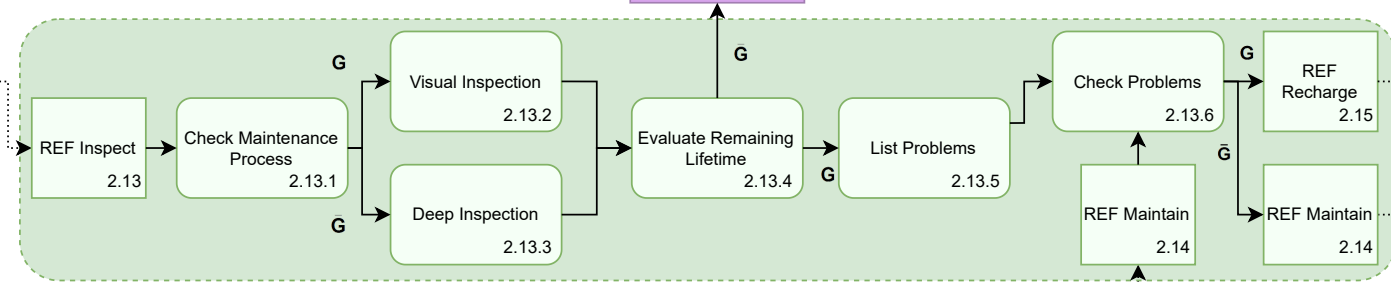
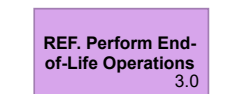
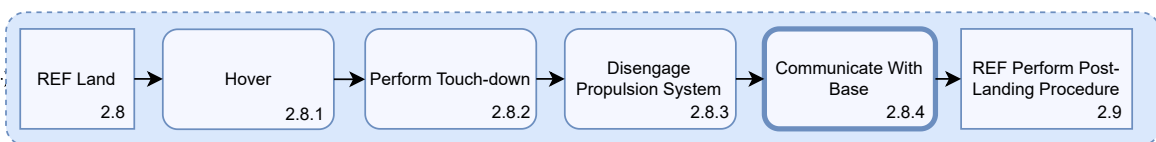
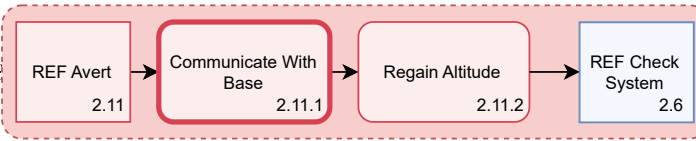
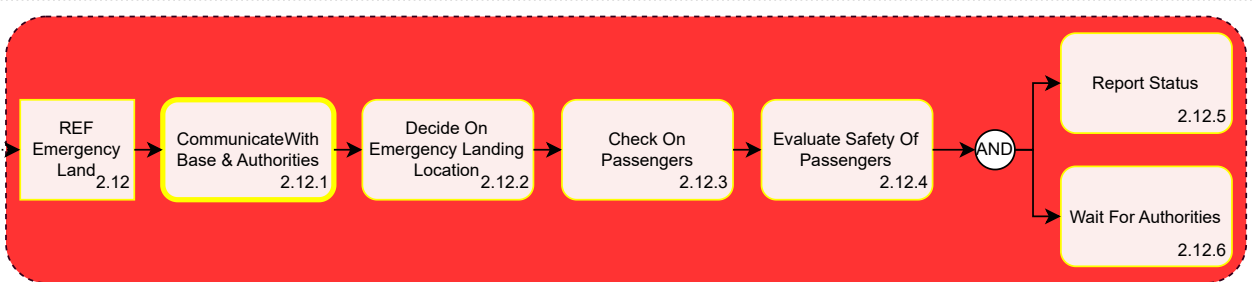
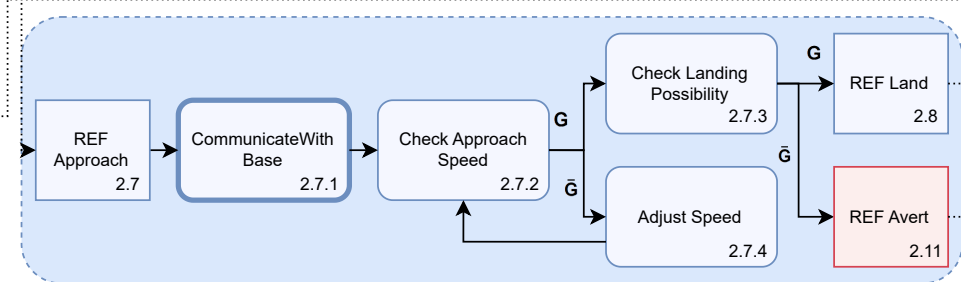
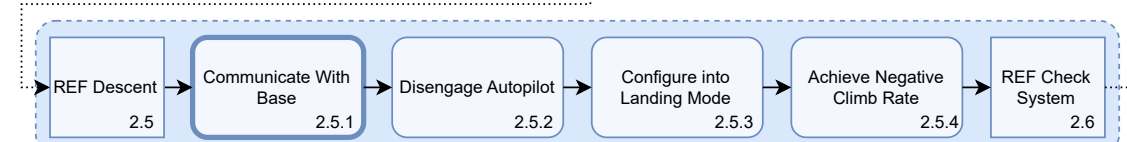
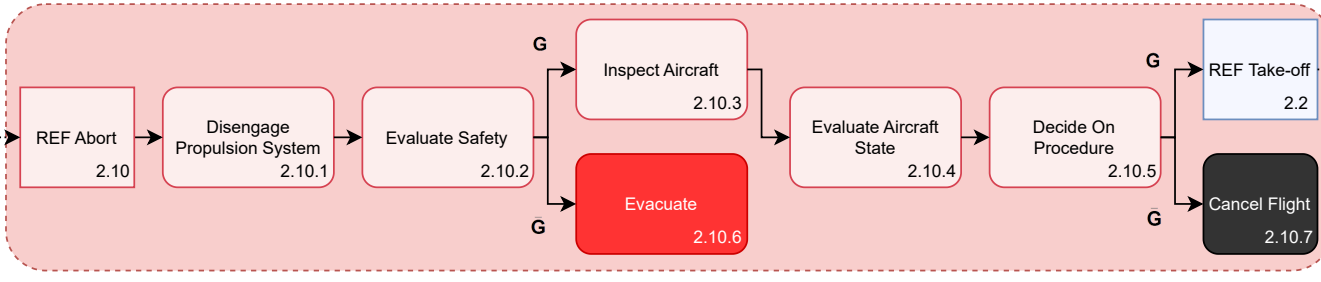
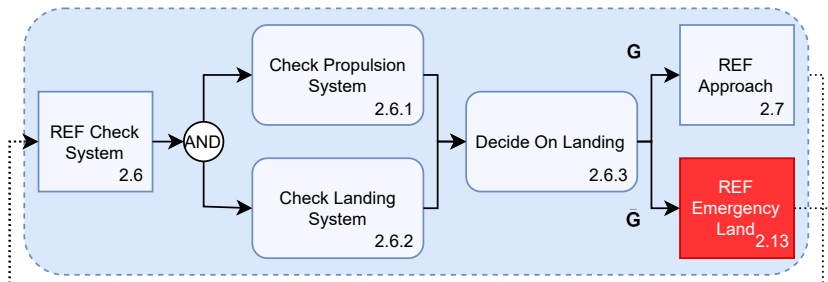
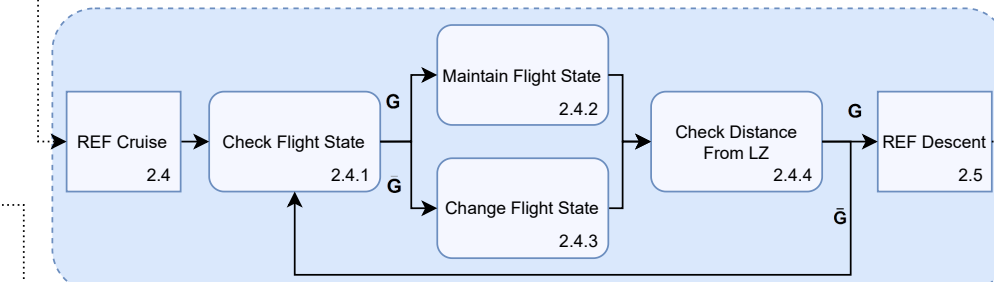
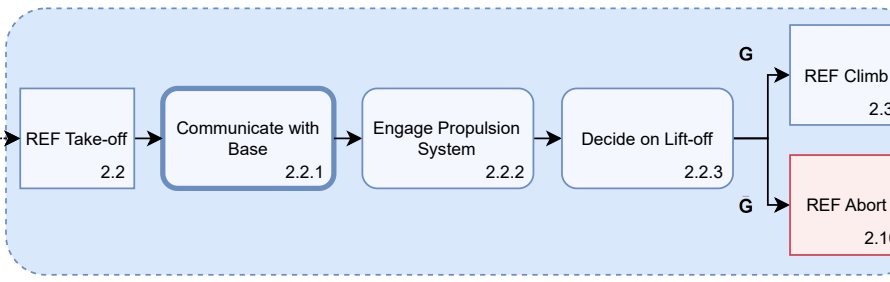
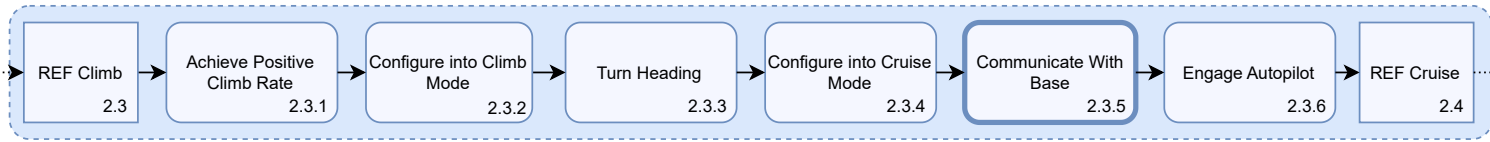
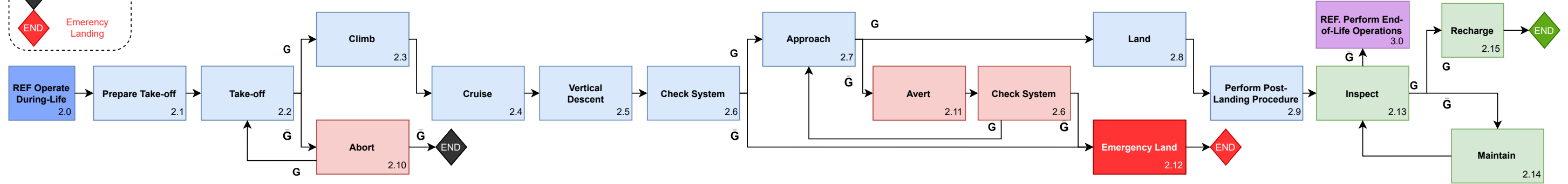
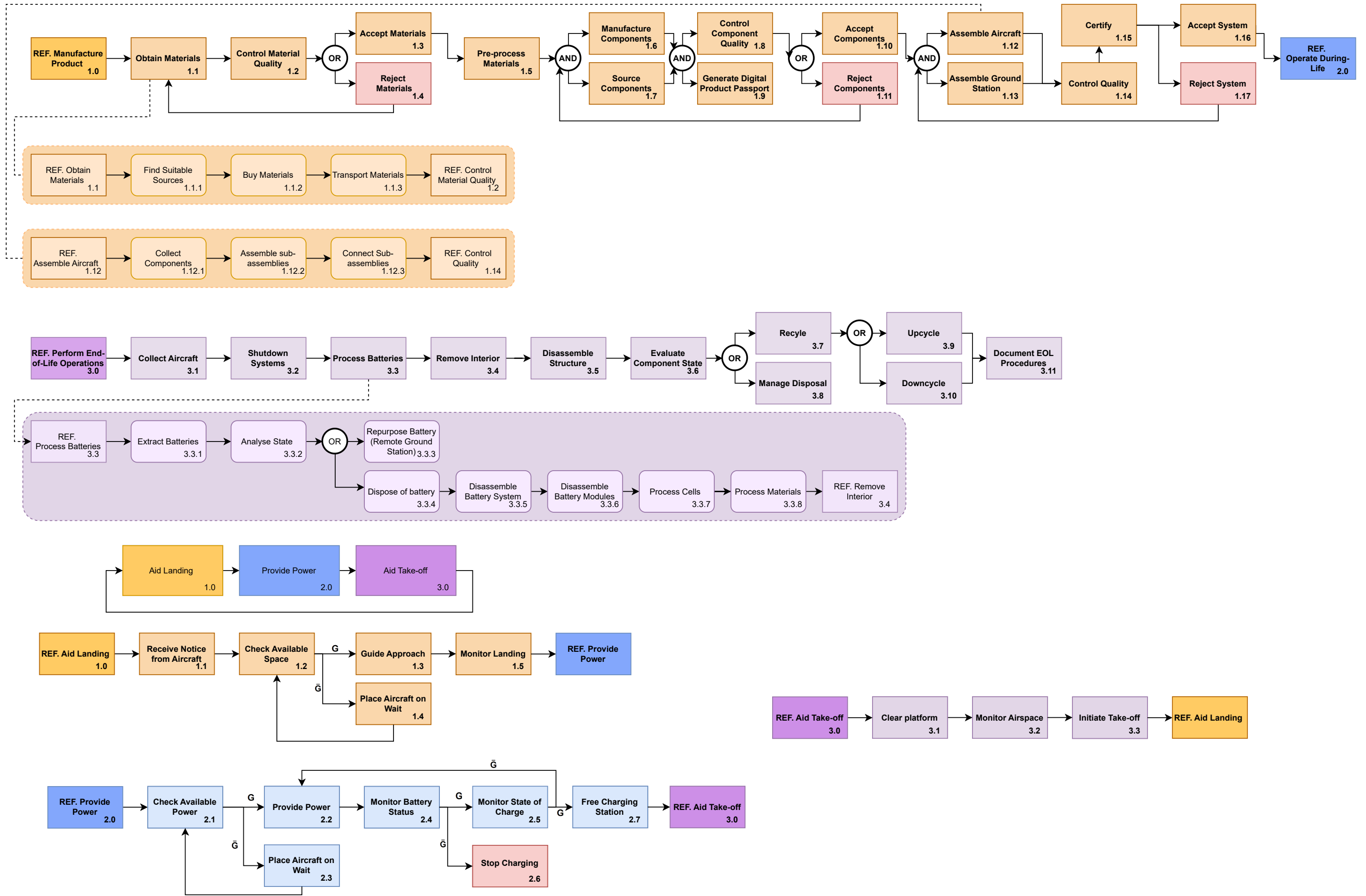


Figure A.2: The Functional Flow Diagram.

Figure A.3: The Functional Flow Diagram.



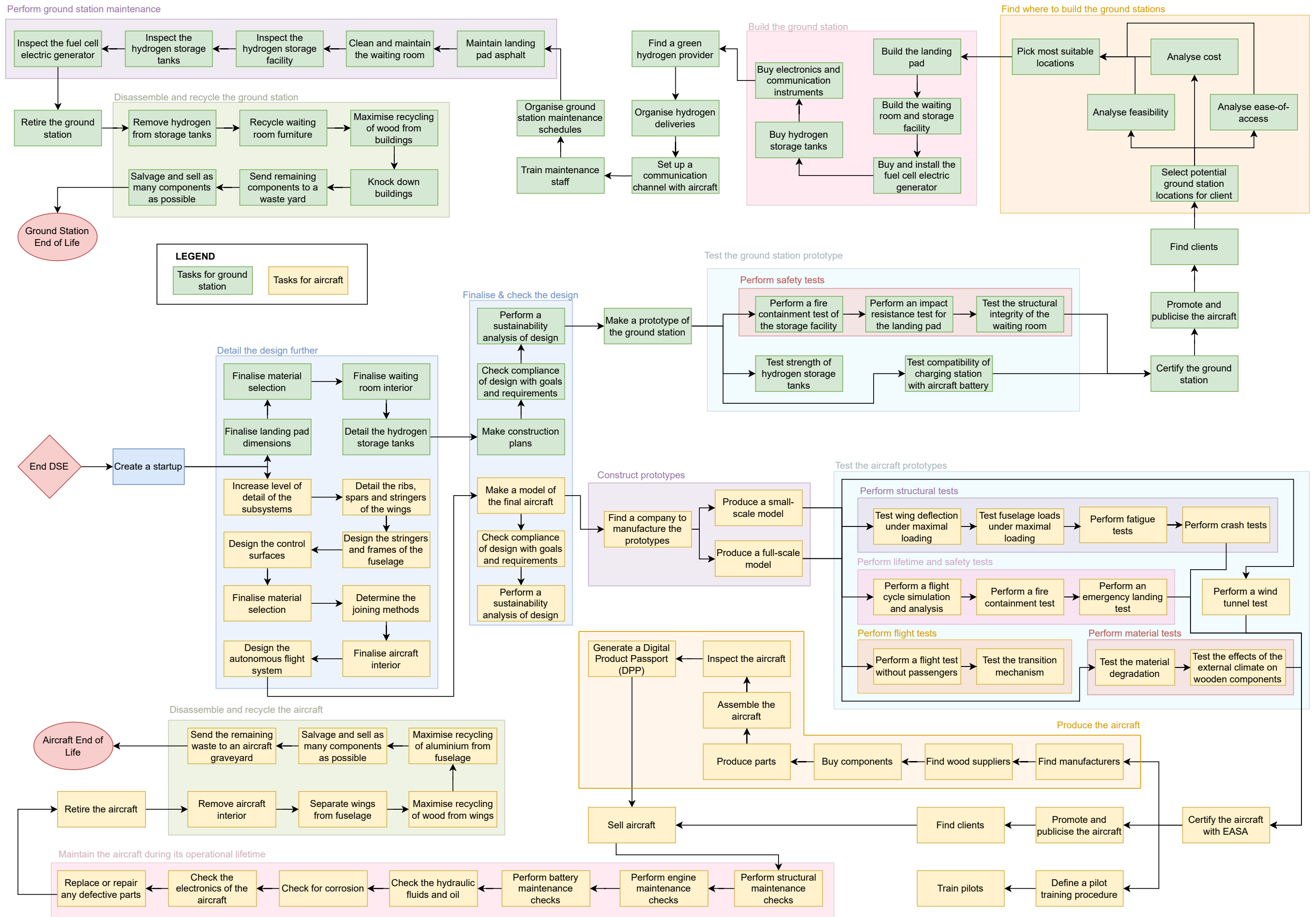
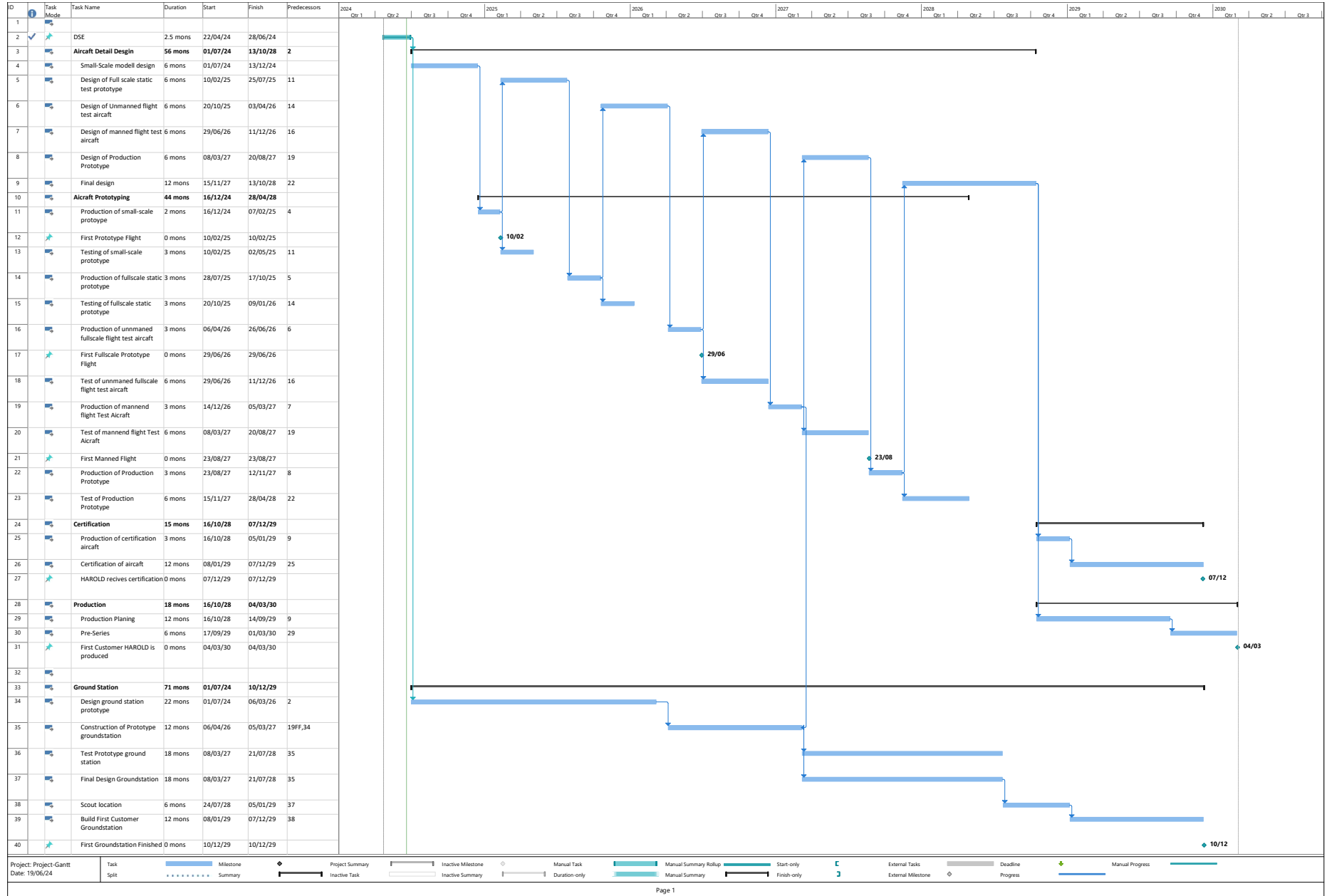


Figure A.4: The Project Design and Development Logic diagram.

Figure A.5: Project Gantt Chart.



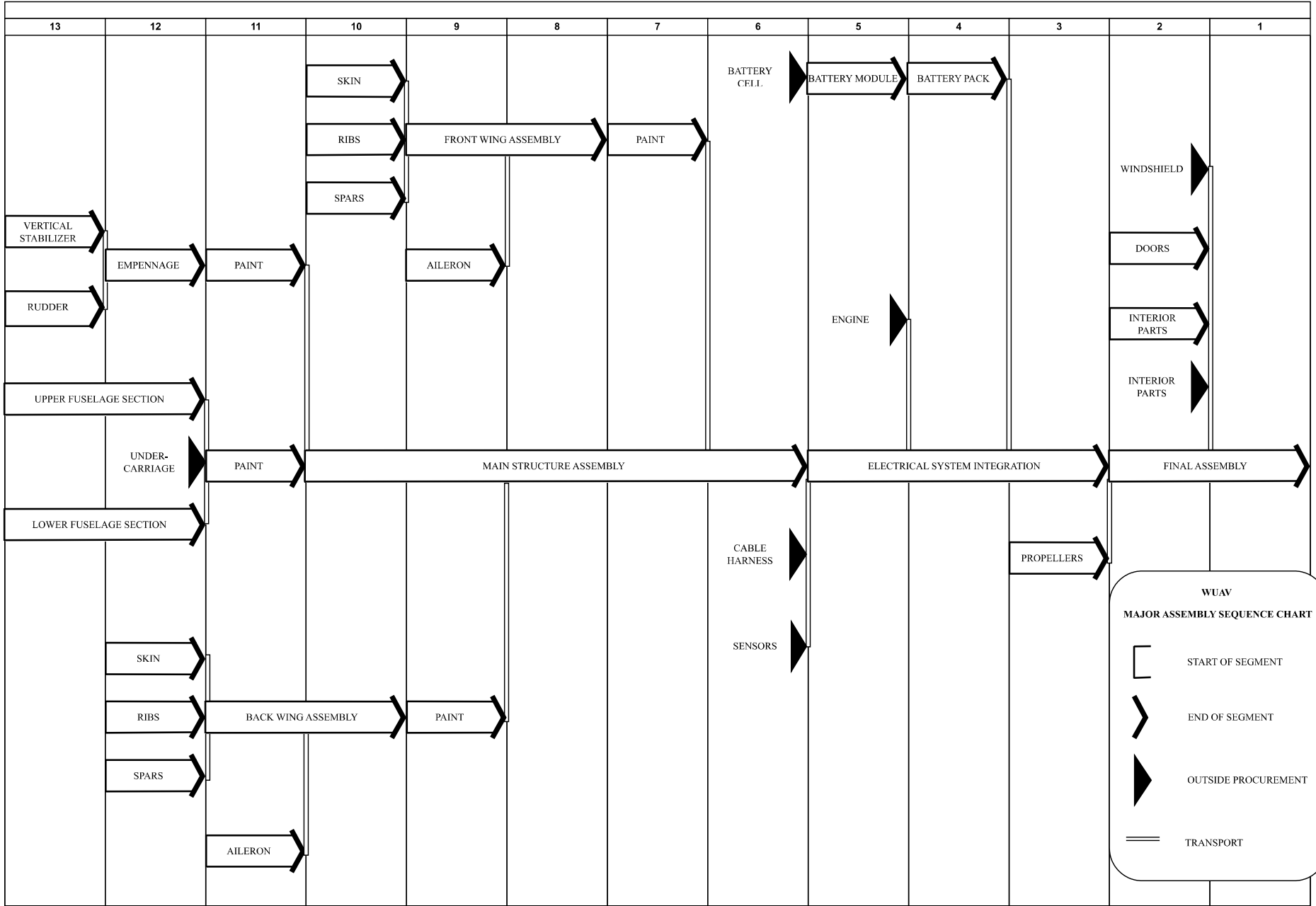


Figure A.6: Major Assembly Sequence Chart